University of Windsor
Scholarship at UWindsor

Electronic Theses and Dissertations | Theses, Dissertations, and Major Papers

2008

Experimental study on the bond behaviour of the concrete-CFRP interface

Wafaa El-Tawil
University of Windsor

Follow this and additional works at: https://scholar.uwindsor.ca/etd

Recommended Citation

El-Tawil, Wafaa, "Experimental study on the bond behaviour of the concrete-CFRP interface" (2008). *Electronic Theses and Dissertations*. 7929.
https://scholar.uwindsor.ca/etd/7929

This online database contains the full-text of PhD dissertations and Masters' theses of University of Windsor students from 1954 forward. These documents are made available for personal study and research purposes only, in accordance with the Canadian Copyright Act and the Creative Commons license—CC BY-NC-ND (Attribution, Non-Commercial, No Derivative Works). Under this license, works must always be attributed to the copyright holder (original author), cannot be used for any commercial purposes, and may not be altered. Any other use would require the permission of the copyright holder. Students may inquire about withdrawing their dissertation and/or thesis from this database. For additional inquiries, please contact the repository administrator via email (scholarship@uwindsor.ca) or by telephone at 519-253-3000ext. 3208.

VITA AUCTORIS

NAME:	Wafaa El-Tawil
PLACE OF BIRTH:	Beirut, Lebanon
YEAR OF BIRTH:	1979
EDUCATION:	W. D. Lowe Secondary School, Windsor 1995-1998 University of Windsor, Windsor, Ontario 1999-2003 BACHELOR OF APPLIED SCIENCE Co-op University of Windsor, Windsor, Ontario 2005-2008 MASTER OF APPLIED SCIENCE, Civil Engineering

Experimental study on the bond behaviour of the concrete-CFRP interface

By

WAFAA EL-TAWIL

A Thesis
Submitted to the Faculty of Graduate Studies
through the Department of Civil and Environmental Engineering
in Partial Fulfillment of the Requirements for
the Degree of Master of Applied Science at the
University of Windsor

Windsor, Ontario, Canada

2008

© 2008 WAFAA EL-TAWIL

Library and Archives Canada

Published Heritage Branch

395 Wellington Street
Ottawa ON K1A 0N4
Canada

Bibliothèque et Archives Canada

Direction du Patrimoine de l'édition

395, rue Wellington
Ottawa ON K1A 0N4
Canada

Your file Votre référence
ISBN: 978-0-494-47072-5
Our file Notre référence
ISBN: 978-0-494-47072-5

NOTICE:
The author has granted a non-exclusive license allowing Library and Archives Canada to reproduce, publish, archive, preserve, conserve, communicate to the public by telecommunication or on the Internet, loan, distribute and sell theses worldwide, for commercial or non-commercial purposes, in microform, paper, electronic and/or any other formats.

The author retains copyright ownership and moral rights in this thesis. Neither the thesis nor substantial extracts from it may be printed or otherwise reproduced without the author's permission.

AVIS:
L'auteur a accordé une licence non exclusive permettant à la Bibliothèque et Archives Canada de reproduire, publier, archiver, sauvegarder, conserver, transmettre au public par télécommunication ou par l'Internet, prêter, distribuer et vendre des thèses partout dans le monde, à des fins commerciales ou autres, sur support microforme, papier, électronique et/ou autres formats.

L'auteur conserve la propriété du droit d'auteur et des droits moraux qui protège cette thèse. Ni la thèse ni des extraits substantiels de celle-ci ne doivent être imprimés ou autrement reproduits sans son autorisation.

In compliance with the Canadian Privacy Act some supporting forms may have been removed from this thesis.

While these forms may be included in the document page count, their removal does not represent any loss of content from the thesis.

Conformément à la loi canadienne sur la protection de la vie privée, quelques formulaires secondaires ont été enlevés de cette thèse.

Bien que ces formulaires aient inclus dans la pagination, il n'y aura aucun contenu manquant.

Canada

AUTHOR'S DECLARATION OF ORIGINALITY

I hereby certify that I am the sole author of this thesis and that no part of this thesis has been published or submitted for publication.

I certify that, to the best of my knowledge, my thesis does not infringe upon anyone's copyright nor violate any proprietary rights and that any ideas, techniques, quotations, or any other material from the work of other people included in my thesis, published or otherwise, are fully acknowledged in accordance with the standard referencing practices. Furthermore, to the extent that I have included copyrighted material that surpasses the bounds of fair dealing within the meaning of the Canada Copyright Act, I certify that I have obtained a written permission from the copyright owner(s) to include such material(s) in my thesis and have included copies of such copyright clearances to my appendix.

I declare that this is a true copy of my thesis, including any final revisions, as approved by my thesis committee and the Graduate Studies office, and that this thesis has not been submitted for a higher degree to any other University or Institution.

ABSTRACT

FRP materials have been widely used to either strengthen or rehabilitate many concrete structures in numerous applications. Since epoxy is usually used for bonding, the tensile stresses are being transferred from the FRP to concrete by means of the bonding interface. Effort is still being made to fully understand the conditions at the concrete-FRP interface in order to improve the design of concrete structures externally strengthened with FRP. Various studies have been pursued to define and correlate the parameters that can influence the bond behaviour.

Another significant issue is that high shear stress concentrations are generated at the end of the externally bonded reinforcement where the forces have to be transferred between FRP and concrete. Therefore, it is of great importance to determine the effective bond length of FRP materials. Researchers have come up with a many estimations for the effective bond length needed to achieve the bond strength capacity. A reliable value must be achieved in order to have a safe design.

The present research was to study the effect of the parameters that are believed to influence the behaviour of the concrete-CFRP interface the most. The effective length required to achieve the bond strength capacity was also determined. The behaviour of thirty two specimens and two control specimens has been reported in details.

This study concludes that the maximum load carrying capacity and bond strength increases when cross wraps are located on both halves of the specimen, the specimen has rough surface, or the bond length increases. However, the maximum load carrying capacity increases but bond strength decreases when the bond width increases or CFRP stiffness increases. Finally, the effective length obtained was less than 100 mm in most cases.

DEDICATION

To the most caring couple

To my parents

(with love and lots of appreciation)

ACKNOWLEDGEMENTS

I would like to thank Dr. Das, who was always available and ready to assist. His continuous help, encouragement and valuable suggestions are much appreciated. Dr. Das devoted a lot of his valuable time to make this study a success.

I would also like to thank Dr. Ghrib for his assistance and encouragement. His vast knowledge and constructive comments were very helpful in improving this research.

I would like to express my gratitude to the committee members, Dr. Altenhof and Dr. Madugula for their beneficial comments to improve this thesis.

Many thanks to the technical staff, Bill Middleton, Lucian Pop, Patrick Seguin, and Matthew St. Louis for their enormous assistance in the laboratory.

I owe many thanks to my parents, my siblings, and my husband for their understanding and continuous help; especially my mom and my sister, Leila, and her husband who were always there for me.

Lastly, I would like to convey my appreciation to my friends, especially Sun Yuan for his immense aid and continuous presence in the laboratory. Many thanks also go to Meiling Chen, Laura Duncan and Wafa Polies for their help.

TABLE OF CONTENTS

LIST OF TABLES

LIST OF FIGURES

CHAPTER 1
INTRODUCTION

1.1 General

Even though steel, masonry, and concrete have served the civil engineering society satisfactorily for a long time, most of the existing infrastructure in Canada, the United States, Europe, and other developed countries are in urgent need of repair or replacement. The main cause to these problems is the corrosion of reinforcing steel inside the concrete, which results in delamination or concrete spalling, loss of steel reinforcement, and failure in some instances (ISIS Canada, 2004). Fiber Reinforced Polymers (FRP) materials have emerged as proficient alternative repair solution.

FRPs have already been used in the aerospace, aeronautical, and automotive industries for decades. They can be modified to take various forms and shapes. In addition, they are not permeable to electromagnetic waves and are very light in weight. They have a high strength-to-weight ratio, do not corrode, and have a tremendous fatigue resistance. Even though the initial cost of FRPs can be very high, they can be deemed to offer an economical solution in new construction projects when the cost of a structure is calculated over its entire life cycle because of their improved durability and significantly lower maintenance cost.

1.2 Statement of Problem

FRP materials have been widely used to either strengthen or rehabilitate many concrete columns, beams and slabs in numerous applications. Epoxy is usually used to bond any FRP material to concrete structures. Hence, the tensile stresses are being transferred from the FRP to concrete by means of the bonding interface. Effort is still being made to fully understand the conditions at the concrete-FRP interface in order to improve the design of concrete structures externally strengthened with FRP. Various studies have been pursued to define and correlate the parameters that can influence the bond behaviour. Most researchers (Bizindavyi and Neale (1999), De Lorenzis et *al.* (2001), and Sato et *al.* (2001)) agree that the CFRP's stiffness, the bond length, and the bond width are the principal parameters that would affect the concrete-CFRP interface behaviour. Less attention is drawn to the effect of surface preparation and the amount and location of cross wraps. It is important to observe the influence of the concrete surface preparation since it affects the load transfer mechanisms. Further, it is well known that the main task of cross wraps is to prevent debonding from taking place in a desired area. Therefore, the amount of cross wraps certainly plays an important role in the behaviour of the concrete-CFRP interface.

Another significant issue is that high shear stress concentrations are generated at the end of the externally bonded reinforcement where the forces have to be transferred between FRP and concrete. Therefore, it is of great importance to determine the effective bond length of FRP materials. Researchers have come up with a many estimations for the effective bond length needed to achieve the bond strength capacity. For instance, De Lorenzis et *al.* (2001) concluded that the effective bond length is 93 mm, whereas Horiguchi and Saeki (1997) obtained a value of 75 mm. Ueda et *al.* (1998), on the other hand, stated that the effective bond length is less than 100 mm. Sato et *al.* (2001) found that that value is between 100 mm and 200 mm. A reliable value must be achieved in order to have a safe design.

1.3 Objectives and Scopes

This study was conducted in order to identify the various parameters that play a major role in affecting the bond strength capacity. Consequently, the primary objectives of this research are:

(1) To determine the influence of CFRP's stiffness, CFRP length, CFRP width, surface preparation, and location of cross wraps on the concrete-CFRP interface.
(2) To determine the effective length required to achieve the bond strength capacity.
(3) To study shear transfer between concrete and CFRP.

The scope of this study was limited to concrete specimens that are 500 mm long, 150 mm wide, and 150 mm high. Thirty two specimens and two control specimens were tested under tensile load until debonding took place.

1.4 Contents and Organization

This thesis is divided into five chapters:

Chapter 1 is the introduction.

Chapter 2 summarizes findings accomplished by other researchers relevant to the topic studied, such as previous studies on the history of FRP's application, concrete-CFRP interface behaviour under different testing methods, and determination of the effective bond length.

Chapter 3 discusses the properties of all materials and instrumentation used. It also describes in details the experimental program that was performed in acquiring the required data.

Chapter 4 focuses on the analysis of the concrete-CFRP interface response. The effective bond length is also determined in that chapter.

Chapter 5 summarizes the results obtained and concludes the present work.

CHAPTER 2
LITERATURE REVIEW

2.1 General

FRPs can be defined as being a subgroup of composites. Composites, on the other hand, are obtained by combining two or more materials at a macroscopic level to form a new material that has different but better properties than the combined materials. For FRPs, the composite consists of high strength fibers entrenched in a polymer matrix (also known as resin).

Resin's Properties:

The resin is congruent with the fibers both chemically and thermally. Its major task is to bind the fibers together, protect them from harsh environments, and transmit load from one fiber to an adjacent fiber. If a fiber breaks, the resin will not only transfer the load to an adjacent fiber, but to several others as well. This will prohibit further fiber failure and weakening of the composite. There are three types of resins used in composites in infrastructure: polyesters, vinylesters, and epoxies. Polyesters are the most popular in the manufacture of infrastructure composites.

Fibers' Properties:

Fibers generally have a uniform diameter, are stable during handling and do not vary in strength tremendously between neighbouring fibers. Their main role is to strengthen and stiffen the composite. Therefore, they are usually chosen to have a high stiffness and strength. The most common types of FRP fibers available for use in infrastructure are: glass, carbon (graphite), and to a lesser extent, aramid. Even though glass fibers are the cheapest, carbon fibers are preferred in structural engineering applications.

2.2 Applications of FRPs

The use of FRP materials for structures has been increasing. To date, there are various infrastructure-related field applications of FRPs around the world. The ones that gained the most attention can be divided into the following categories:

- Externally bonded FRP used for maintenance and rehabilitation;
- FRP used for internal reinforcement of concrete;
- Structures made of FRP hybrid,
- Structures that are all-FRP; and
- FRP used in seismic retrofitting, especially in retrofitting hollow bridge piers.

2.2.1 Externally Bonded FRP

One of the earliest applications of FRP involved the repair of concrete structures externally with FRP composites. Since they have been very effective in improving the strength of already-built members with minor problems, thousands of installations of this type have been accomplished worldwide. External FRPs have also been used to increase the shear capacity of concrete structures. These composites were aimed at controlling cracks as well. During the last two decades, various repairs have appeared with concrete, metallic, masonry and timber structures.

Concrete Structures: Carbon FRP sheets can be applied to a circular concrete column that needs to be strengthened. In addition, concrete bridge girders are fortified in shear with externally bonded carbon FRP sheets (ISIS Canada, 2004). Commonly, FRP plates are attached to the tension face of flexural elements to enhance their bending capacity, or to their side to amplify their shear capacity.

Metallic Structures: FRP sheets or wraps are generally bonded to the exterior of metallic structures, such as cranes or overhead signs to significantly increase their flexural, shear, axial, and joint strengths. For example, welded joints can be repaired in an overhead tubular aluminum sign standard using glass FRP sheets.

Masonry Structures: Both the strength and ductility for in-plane and out-of-plane shear and flexural behaviour of masonry walls and columns can be enhanced by using external FRP reinforcements.

Timber Structures: Flexural capacity of a beam or girder is increased by externally bonding FRP to timber structures. In this case, FRP plates or sheets are connected to the exterior of the timber member using a structural adhesive.

One of the first implementations of this technique was performed in the county of Lacerne, Switzerland. The Ibach Bridge was erected in 1969. It spanned 228 m, and was designed as a continuous multi-span box beam (Meier, 1995). Due to the installation of new traffic signals, some of the prestressing was damaged. Although the unit weight price of CFRP exceeds that of steel significantly, it was chosen for the rehabilitations. Only 6.2 kg of CFRP was sufficient for rehabilitation rather than 175 kg that might be necessary of steel. Additionally, CFRP's lightweight precluded utilizing expensive falsework since all tasks were performed from a mobile platform.

2.2.2 Internal FRPs

The corrosion of steel reinforcement is the main cause of concrete bridge elements deterioration (i.e. girders, columns, piers, pier caps and decks). FRPs are resistant to corrosion making them a perfect candidate to replace steel reinforcement. FRP materials have been especially helpful as internal reinforcement of concrete in situations where high tensile strength, low mass density, resistance to chloride attack, and electromagnetic transparency are required. Currently, most forms of internal FRP reinforcements widely employed follow the form and function of available steel reinforcement. Several challenges have been resolved in dealing with internal FRPs. One major disadvantage in this application is that FRP composites behave linear elastically to failure when loaded in tension. Hence, concrete elements reinforced internally with FRP rebars will not demonstrate an identical failure mode as when reinforced with steel. FRP reinforcement's lower modulus is another important issue, since it can lead to more serviceability problems, such as increased deflections or wider cracks under service loads.

The Bishop Grandin Boulevard is a four-lane divided highway that was constructed in 1998. It represents the first Canadian experience of using FRP dowels in concrete pavements. Approximately 27,000 vehicles per day travel on this pavement section with 10% truck traffic (Shalaby and Murison, 2001), and so far no pavement crisis have been declared.

2.2.3 Hybrid Structures

Since FRP composites have a higher initial cost, a number of hybrid systems have been recently constructed. Hybrid systems have demonstrated to be very effective since they combine the high stiffness and high compression strength of conventional materials. Most of the structures being utilized are the hybrid FRP/concrete structural systems. These systems are best designed by placing the FRP composites where its high tensile strength can be exploited, while taking advantage of the high compressive strength of concrete. Moreover, FRP hybrids are very beneficial because they can be very light, and the fact that no corrosion is expected to take place makes them maintenance-free. These types can be used as stay-in-place formwork, concrete-filled FRP piles and/or girders for bridges, and as supporting elements in buildings.

In Canada, FRP was first utilized in the Beddington Trail Bridge located in Calgary, Alberta (Tennyson *et al.*, 2001). The bridge is composed of two spans containing 13 bulb-T girders each. Out of the twenty six girders, six were prestressed using FRP tendons. The bridge was open to traffic in 1993. A system of structurally integrated optical sensors was installed to monitor the behaviour of the bridge.

2.2.4 All-FRP Structures

Some structures are being fabricated entirely out of FRP. By using pultruted FRP structural sections that can be manufactured from glass FRP, this technique is classified as being the easiest but most inexpensive in the long run. All-FRP can be used to construct specific structural components like ground anchors, cable-stayed bridge support cables, glulams, signs, grates and drains, guardrails, bridge deck panels and space trusses. In addition, small-scale structures such as parking garage stairwells, pedestrian bridges, short-span road bridges and utility poles can be built purely from FRPs.

FRP prestressing tendons have been used in the Notsch Bridge in Austria, and the Ulenberg Bridge in Germany. In Ohio, FRP rods were employed in the re-decking of the Salem Avenue Bridge, and in the construction of the Pierce Street Bridge (Uomoto *et al.*, 2002).

2.2.5 Seismic Retrofitting

The primary application for seismic retrofitting is column wrapping. It can replace steel jackets and provide additional confinement for the column. That in turn, provides additional ductility to the column and allows rebar splices with inadequate laps to be more fully developed. Most masonry walls are not connected to each other correctly making them vulnerable under seismic events. The major problem is that most of the times, the walls orthogonal to the direction of earthquakes collapse following out-of-plane mechanism. Encasement of masonry structures of FRP shells may improve their strength and ductility tremendously hence solving this problem.

The Portage Creek Bridge in Victoria, British Columbia was built in 1982 prior to current seismic design codes and would not comply with the current standards' requirements with regards to potential earthquake forces (Mufti, 2002). It was decided that FRP wraps should be used to strengthen the short columns, which would potentially fail in catastrophic shear during a large earthquake.

2.3 Introduction to Carbon Fibers

Carbon fibers are formed by controlled pyrolysis, where one of the three main sources of fibers is treated by heat (i.e. carbonization, stabilization, and graphitization) to generate carbon filaments that are small in diameter. Ninety two percent of carbon fiber weight is carbon composition (Chung, 1994). They can either be short or continuous, and their structure can be crystalline, partly crystalline or amorphous. The properties of carbon fiber are manipulated by molecular composition. The carbon layers can smoothly slide pertaining to each other since the bonding between them is Van der Waal bonding (Chung, 1994). The properties of the carbon fibers vary broadly depending on the structure of the fibers.

Commercial carbon fibers are acquired from three sources:

(1) Pitch, a by-product of petroleum distillation that is passed through a thin nozzle and stabilized by heating,

(2) PAN (PolyAcroloNitrile), which is carbonized through burning, and

(3) Rayon.

Both rayon and isotropic pitch are useful for fabricating low modulus carbon fibers. PAN and liquid crystalline pitch are utilized in higher modulus carbon fibers.

Carbon fibers are classified as either high modulus Type I or high strength Type II. These types differ in properties due to the disparities in fiber microstructure. The arrangement of the hexagonal layer networks available in graphite is responsible for the differences. For instance, the material would be classified as graphite if those layers are organized in three-dimensional stacks. If, on the other hand, the layers are arranged two-dimensionally and the bonding is weak, the material would be defined as carbon.

Even though carbon fibers are more expensive than glass fibers, they are currently being preferred in structural engineering applications, especially for repair and strengthening of reinforced concrete beams, columns and slabs. Their attractiveness is derived from their low density, exceptional resistance to thermal (low thermal expansion coefficient), chemical and environmental effects, high tensile modulus and regularly decreasing cost.

2.3.1 CFRP Products

There are various forms of carbon fiber reinforced polymers. The most common ones are: Laminate sheets, LEADLINE bars, ISOROD-carbon-vinyl ester reinforcing bar, NEFMAC grids and plates. Physical properties of each are listed in Table 2.1.

Table 2.1 – Physical Properties of CFRP Products

PRODUCT	LAMINATE SHEETS	LEADLINE BAR	ISOROD – CARBON – VINYL ESTER	NEFMAC GRID	SIKA CARBODUR CFRP PLATES
MODULUS OF ELASTICITY (GPa)	240 / 640	147	111.1	100	225
MAX. TENSILE STRENGTH (MPa)	3800 / 2650	2550	1596	1200	2167
ELONGATION AT FAILURE	0.4 / 1.7%	1.8%	1.8%	0.7 / 1.5%	1.12%
THICKNESS (mm)	1.2 – 1.6	6 – 12	10 – 25	15 – 20	1.0 – 1.5

Laminate Sheets

Laminates, which are the most common forms of composites in structural applications, are created by stacking various thin layers of fibers and matrix and joining them. Several physical and mechanical properties can be achieved depending on the stacking layout and the fiber orientation in each layer.

Laminate sheets are high strength, pre-manufactured carbon/epoxy laminates. They are used for surface mounted or near surface mounted applications adding strength and stiffness to concrete or masonry structures. Both paste and liquid epoxy resins aid these laminates in bonding to concrete and providing a light weight, non-corrosive material that is easy to install (ISIS Canada, 2004).

LEADLINE Bar

It is a type of carbon FRP pre-stressing (pre and post-tensioning) bar fabricated by Mitsubishi Chemical with their coal tar pitch fiber materials. It has been used mainly in Japan for bridges and industrial building applications. LEADLINE bar has also been utilized in few bridges across Canada (ISIS Canada, 2004). It is manufactured by pultrusion. This process is explained in details later in this chapter.

ISOROD-Carbon-Vinyl Ester Reinforcing Bar

It is made of continuous longitudinal E-glass fibers joined together with a polyester resin. Pultrusion is again used here, and the outcome is a bar with a smooth surface that can be distorted with a helical twisting of identical fibers. The CFRP reinforcing bars behave elastically and linearly up to failure in tension. They demonstrate brittle tensile failure mode (ISIS Canada, 2004).

NEFMAC Grid

New Fiber Composite Material for Advanced Concrete grid is a two-dimensional reinforcement made of high performance fibers such as glass and carbon impregnated with resin. It is mostly used in offshore construction, bridge decks, tunnel lining applications, and light-weight curtain walls in buildings. Besides being corrosion resistant, NEFMAC facilitates good stress transfer since the intersections offer anchorage and mechanical interlock in the concrete. Pin-winding, which is a process similar to filament winding (explained later in this chapter) is performed in fabricating this grid as flat or curved (ISIS Canada, 2004).

CFRP Plates

CFRP Plates can be bonded to the exterior of concrete structures using high-strength adhesives to provide additional reinforcement to that provided by internal reinforcing steel. They have the advantage of being easy to handle because of their light-weight, corrosion resistance, and high strength. Their mechanical properties in the longitudinal direction are almost exclusively controlled by the fibers. What is really great about them is that they have long fatigue life. Commercially available CFRP plates consist of 60 to 70% by volume of unidirectional carbon fibers of approximately 10 μm diameter (Almakt *et al.*, 1998). The most popular manufacturer of CFRP plates in Canada is Sika Canada Inc.

2.3.2 CFRP Adhesives

Adhesives allow bonding structural elements without altering the physical appearance of the structure. The bond forces result from the molecular attraction generated between the adhesive and bonded materials. That bond can be weakened by the presence of dirt, oil, dust, or grease. Hence, it is of great importance to clean the surface of the structure thoroughly before applying the adhesive. It has been found that adhesion to exposed aggregates is better than to hardened cement paste (Sato *et al.*, 2001). The advantage of using adhesives rather than anchorages such as bolted connections is that the former generates distributed stress over the entire contact interface, whereas the latter produces concentrated stress.

Epoxies, the most popular adhesives in structural applications, are used mainly for producing high performance composites with advanced mechanical properties, corrosion resistance, good adhesion to a substrate and superior electrical properties. In general, epoxies cured with heat will be more heat-resistant than those cured at room temperature. Epoxy resins are utilized with various fibrous reinforcing materials, including glass, carbon, and aramid.

2.3.3 Carbon Fiber Processing Methods

There are various methods of composite processing that are utilized. Only three of them are relevant in fabricating structural components.

Hand Lay-up (Wet Lay-up)

This process is widely used in structural rehabilitation applications. In this technique, resins are impregnated by hand into fibers, which are in the form of unidirectional mats, fabric, or braid. This is usually achieved by rollers or brushes. The molding, called bag molding, is done by placing the tapes or fabrics in a die and introducing high-pressure gases or a vacuum via a bag to force the individual plies together. Any desired thickness of FRP is accomplished by adding the required number of layers on top of each other. This method produces laminates with low void contents and higher fiber volume fractions. Wet lay-up is easily and rapidly performed in the field, but quality control and skilled labour are very important in order to accomplish good results. There are three common types of wet lay-up systems:

- Dry unidirectional fiber sheets with the fiber running in one planar direction,
- Dry multidirectional fiber sheets or fabrics with fibers oriented in at least two planar directions, and
- Dry fiber tows wound or mechanically applied to the concrete surface. They are impregnated with resin during the winding operation.

The following steps illustrate the installation process (Figure 2.1)

- Prepare Substrate: The concrete must be properly prepared before bonding. No spalling or delamination should be present, and the corners must be ground to a minimum radius of 10 mm (Horiguchi and Saeki, 1997). Any unevenness in the concrete is usually removed with a mineral-based re-profiling mortar.
- Prime Concrete: Some systems require that the clean surface be coated with a primer.
- Apply Epoxy: The adhesive is applied to the front and back of the material using a roller or brush in order to saturate the sheet and ease installation. Once that is done, the material may be rolled to facilitate transport.
- Place FRP Sheet on Structure: Unfold the sheet rolls onto the structural element being strengthened. Placing one roll at a time, pressure should be applied to the wrap using a hard rubber roller with ridges.
- Apply Epoxy to Sheet Surface: To fully saturate the material, a topcoat of epoxy should be added on the surface.

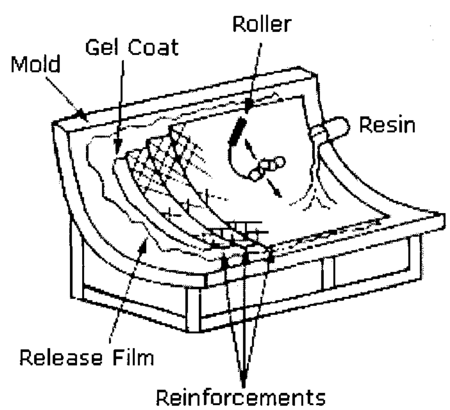

Figure 2.1 – Hand Lay-up Process
(U.S. Department of Labor, 2002)

Pultrusion

FRP bars, rods, tendons, plates, I-beams, prestressing strands and twisted cables are produced by using pultrusion. It is a technique that is fully automated and hence, very economical. This process is done by hauling untreated fibers through a resin bath and then through a heated die. At this stage, the polymer matrix takes the form of the die, and the structural component is produced (Figure 2.2)

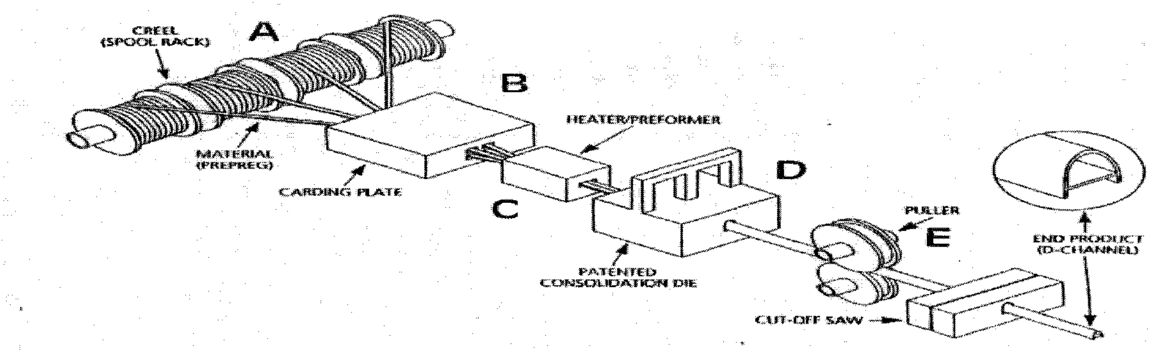

Figure 2.2 – Pultrusion Process
(Alma Memo Series, 1995)

Filament Winding

It is primarily used for hollow, circular or oval sectioned components like poles, pipes, and tubes. In this method, fibers are drawn off single or multiple continuous fiber spools through a resin bath before being wound into a rotating mandrel to produce the desired shape (Figure 2.3). The temperature of the mandrel, the impregnation temperature of the resin, the impregnation time, the tension of the fibers, and the pressure of the fiber winding are processing parameters that need to be controlled. The main advantage of filament winding is its high processing speed, which results in a low cost.

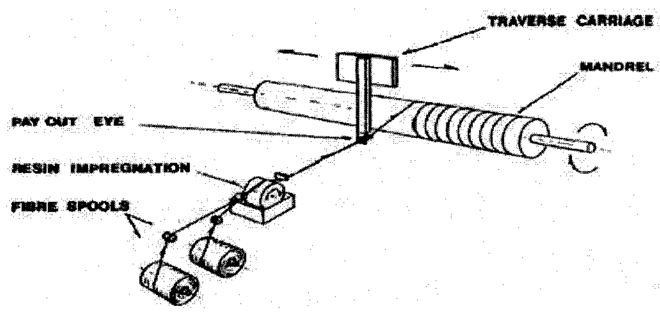

Figure 2.3 – Filament Winding Process
(TIFAC, 2004)

2.4 Behaviour of RC Beams Strengthened with CFRP Sheets

One of the most successful technologies for strengthening or stiffening reinforced concrete is the use of externally bonded CFRP material in the form of laminates (sheets) or plates. Plates are connected to the bottom surface of beams to add tensile reinforcement. CFRP sheets provide additional tensile resistance by being attached to the bottom surface or wrapped around the stem of RC rectangular or T-beams by applying epoxy adhesives. RC beams externally strengthened with CFRP laminates have a low overall installation cost because of their light weight, corrosion and alkali resistance and large tensile strength. In addition, this reinforcing technology provides great strength and an excellent fatigue resistance.

In most strengthening cases, the interface bond between CFRP composites and concrete substrates is vital in transmitting stresses from the RC structure to the externally bonded CFRP composites. Hence, a good understanding of that phenomenon is critical in achieving a more consistent design. Plate bonding and sheet bonding are the two interface bonding systems available. CFRP plate bonding systems allow more quality control than sheet bonding, whereas there is a greater potential for construction imperfections with sheet bonding since the curing of the CFRP composites and the mixing of resins are both carried out in the field. Sheet bonding systems' popularity originates from their high flexibility and convenience for construction. They are mostly utilized in flexural and shear strengthening where debonding of the CFRP from concrete substrate can lead to overall structural failures (Figures 2.4 and 2.5).

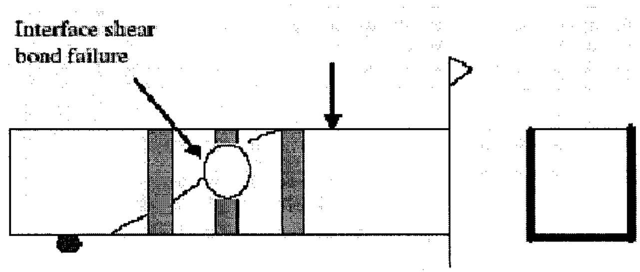

Figure 2.4 – Shear Strengthening Case for Interface Debonding Failure (Ueda and Dai, 2005)

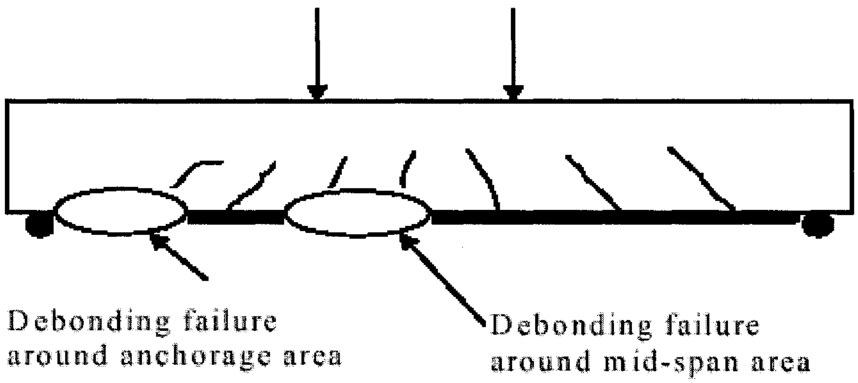

Figure 2.5 – Flexural Strengthening Case for Interface Debonding Failure (Ueda and Dai, 2005)

2.5 Ductility

Ductility is needed since it offers warning for any forthcoming failures. Usual design ensures that failure of RC beams initiates by some cracking of concrete in tension followed by yielding of steel reinforcement. After extensive deformation at no considerable loss of load carrying capacity, concrete cracking, and ultimate failure take place.

External strengthening analysis of RC beams with CFRP is based on Bernoulli's hypothesis of strain compatibility that plane sections remain plane. This necessitates absolute bonding between concrete and CFRP and the capability of stresses to be transmitted by the concrete to the CFRP laminate by shear. Absolute bonding assumption requires that:

1. Sufficient anchorage and development length is warranted for the CFRP reinforcement.
2. CFRPs are linear elastic up to failure
3. In most cases, initial strains in the section at the time of strengthening can be ignored
4. Concrete compressive stress-strain curve is parabolic. Furthermore, concrete is assumed to have no strength in tension.

Generally, when steel reinforcement yields in an RC beam externally strengthened with carbon fiber, there would be considerable reserve capacity (i.e. the beam can still carry increasing load after the steel reinforcement yields but at a lesser intensity with respect to deflections than before the steel yields). The CFRP retains its elastic behaviour until failure happens abruptly. Failure can be due to CFRP debonding, rupturing of CFRP sheets or concrete crushing. In the last two modes of failure, the ultimate strength of the structural member can be easily predicted by following conventional RC flexural theory. When it comes to CFRP debonding, however, the strengthened member is not able to reach its ultimate strength; hence, the prediction of that type of failure is not an easy task.

It might be difficult to fulfill ductility requirements, since if the design is controlled by the "Serviceability Limit State", the amount of FRP provided to a structure may be larger than that required by the "Ultimate Limit State" (Triantafillou *et al.*, 2001). The Canadian Highway Bridge Design Code (2000), based on the work of Jaeger *et al.* (1997), evaluates the deformation index of FRP strengthened beams with the following performance factor:

$$(M_u \Phi_u)/(M_{.001} \Phi_{.001}) \tag{2.1}$$

Where M is the beam's moment, Φ is the curvature. The subscript "u" refers to the ultimate state, whereas ".001" defines the service state that corresponds to a concrete maximum compressive strain of 0.001. This performance factor is usually greater than 4 for a rectangular beam and greater than 6 for a T-section.

2.6 Flexural Strengthening

Even though composite materials have been successfully used for strengthening, there are still various design problems that need to be dealt with. In most of the beams tested thus far, applying externally bonded laminates resulted in a disastrous brittle failure originating from a premature laminate peeling off prior to reaching the design load. The three most common types of failures associated with flexural strengthening are plate-end failure (subsection 2.6.1), anchorage failure (subsection 2.6.2), and mid-span debonding (subsection 2.6.3).

In Canada, the design of RC strengthened with FRP should be performed using the limit states present in the existing design codes. Steel is treated as elastic-perfectly plastic, with strain hardening neglected, and concrete is treated using the concept of an equivalent rectangular stress block as suggested in CSA A23.3 for reinforced concrete buildings, and in CSA S6 for concrete bridges (ISIS Canada, 2004). In addition, CSA S806-02 (2002) offers all design guidelines and test methods available for the design and construction of building components with FRP.

In Flexural strengthening applications, CFRP composites are connected to the tensile surface of the reinforced concrete beams. For this type of strengthening, it is assumed that CFRP materials are perfectly linear elastic. Hence, failure in such a situation would be due to CFRP rupture, concrete crushing, or delamination. To calculate the ultimate flexural strength in either of these modes, a similar technique as that used for steel reinforced sections is followed.

Meier (1987) reported the use of thin CFRP sheets as flexural strengthening reinforcement of concrete beams. He proved that steel plates can be replaced with CFRP with an overall cost savings as high as 25%.

Plevris (1995) investigated the flexure behaviour of concrete beams strengthened with CFRP sheets. The most significant variables affecting the member strength were found to be the concrete strength, CFRP failure strain, and CFRP's length to width ratio. Based on the results, it was concluded that, except for the cross section dimensions, the effects of the laminate's length, and the initial strain, all other variables including the ratio of live to dead load are equally important on reliability against flexural failure.

Alagusundaramoorthy *et al.* (2003) studied the flexural behaviour of RC beams strengthened with CFRP sheets. The objective of their investigation was to study the effectiveness of externally bonded CFRP sheets on carbon fiber fabric in increasing the flexural strength of concrete beams. Four-point bending flexural tests were conducted up to failure on nine concrete beams strengthened with different layouts of CFRP sheets and carbon fiber fabric, and on three beams with different layouts of anchored CFRP sheets. In order to predict the flexural behaviour of beams strengthened with CFRP sheets and carbon fiber fabric, they introduced an analytical procedure based on compatibility of deformations and equilibrium of forces. Comparisons between the test results and the analytical calculations showed that the flexural strength increased up to 58% on concrete beams strengthened with anchored CFRP sheets.

2.6.1 Plate-End Failure

Many studies have been performed on the mechanisms of the plate-end failure because of its catastrophic results (Sebastian, 2001). This type of failure is very brittle and is generated due to high concentrations of shear and normal stresses happening at the end of CFRP near supports. The main factors that influence this type of failure are the distance between the ends of the CFRP and the beam supports and the usage of fairly thick CFRP plates. Thus, this is not a concern for CFRP sheet bonding systems since they are usually extended to the support.

2.6.2 Anchorage Failure

Also known as debonding and is due to insufficient anchorage length of CFRP sheets. Anchorage failure of CFRP is usually noticed in beams strengthened for flexure with CFRP, which usually debonds at about half of its ultimate strain. That is most often caused by the weakness of the concrete substrate rather than in the epoxy.

Since the effective bond length has been reported in a wide range by different researchers, it becomes important to come up with some sort of approach where the anchorage length can be acquired based on the bond stress-slip relationship. By developing a model, the anchorage length of CFRP sheet-concrete interfaces can be determined by analyzing the strain distributions in CFRP sheets and the bond stress distributions along the interface. The effective bond length is defined as the active bond length, L_e, and is formulated as the following:

$$L_e = \frac{\sqrt{2 E_f t_f}}{B \sqrt{G_f}} \ln\left(\frac{1+\alpha}{1-\alpha}\right) \qquad (2.2)$$

where L_e is the effective bond length. It increases with the stiffness of CFRP, but decreases with the increase of interfacial fracture energy (G_f), and the interfacial ductility factor (B) (Ueda and Dai, 2005). The α is a factor that equals the bond force that the effective bond area can withstand (P_u) to the defined theoretical maximum bond strength (P_{max}) (Equations 2.3 and 2.4). Factor α is always less than 1 since no matter how big the interfacial slip becomes, there constantly exists an infinitesimal shear stress between the CFRP and concrete. Based on experiments, factor α can be taken as 0.96 for anchorage designs (Dai, 2003).

The bond strength for CFRP sheet-concrete interfaces can be expressed as follows:

$$P_u = \alpha P_{max} \tag{2.3}$$

$$\alpha = \frac{\exp\left(\dfrac{L_b B\sqrt{G_f}}{\sqrt{2E_f t_f}}\right) - 1}{\exp\left(\dfrac{L_b B\sqrt{G_f}}{\sqrt{2E_f t_f}}\right) + 1} \tag{2.4}$$

$$P_{\max} = \left(b_f + 2\Delta b_f\right)\sqrt{2E_f t_f G_f} \tag{2.5}$$

where P_u is the bond strength of CFRP sheet-concrete interface with a given bond length L_b, L_b is the bond length of CFRP sheets, Δb_f is an additional width that can be taken as 3.7 mm based on test results (Sato *et al.*, 2001).

The large distribution of bond strength is another concern. Even though a standard concrete surface treatment is followed, the bond strength of CFRP sheets-concrete interfaces is very sensitive to the condition of concrete surface preparation. That is because the bond failure takes place within a thin concrete layer just underneath the adhesive all the time, and the conditions are affected by the skills of the workers.

2.6.3 Mid-Span Debonding

In this case, the interface debonding starts from the tips of mid span flexural or flexural-shear cracks of RC members. This type of failure results from the interaction between the steel reinforcement, concrete cover, and the CFRP sheets. Hence, it is completely related to the interface slip and delamination behaviours between the CFRP sheets and the concrete substrate.

It is also connected to crack spacing, dowel action on the CFRP sheets, and the bond between the concrete and steel reinforcement. Mid-span debonding guidelines attempt to avoid it by recommending limits on the strains in the CFRP sheets.

2.7 Shear Strengthening

CFRP shear reinforcement may be continuous sheets or strips in finite width. Externally-bonded CFRP shear reinforcement's behaviour resembles the internal steel stirrups in that bridging shear cracks enhances the shear capacity of the concrete.

Since the height of the beam limits the length over which CFRP reinforcement can be anchored, the quality of the existing concrete is vital. Also, it is required in some cases to add a longitudinal CFRP shear anchorage strip to improve anchorage of the external shear reinforcement (Figure 2.6). In order for potential failure of CFRP sheets caused by stress concentrations at the corners of the beam to be prevented, corners should be rounded to a minimum radius of 1 5mm (ISIS, 2004).

(a)

(b)

Figure 2.6 – CFRP Anchor (a) before Installation & (b) after Installation (Kim, 2006)

Shear failures are brittle. Hence, they should be avoided. The two main shear failure modes are CFRP rupture and delamination or debonding of CFRP from the concrete surface. CFRP rupture occurs at an average stress level that is below the ultimate strength of CFRP due to stress concentration. Delamination of CFRP from the concrete surface, on the other hand, is related to the bond mechanism, and is more applicable to the CFRP systems that do not close around the entire cross section. The lower of the two results is taken as the shear strength contribution of the CFRP reinforcement.

2.8 Combination of Shear and Tension

The main attributing failure when a combination of shear and tension is considered is the "Block Shear" or "Cleavage Failure". It is associated with laminates having insufficient cross wraps or inadequate edge distance. For this type of failure, a crack parallel to the applied load starts at the edge of composite and propagates toward the bolt hole. This causes the commencement of other cracks across the net section due to the formation of in-plane stresses.

RC beams externally strengthened with CFRP in flexure can originate another mix-mode failure (combination of shear and tension). The interface debonding may commence from the tip of a shear-flexural crack. In that case, the peeling is generated by crack opening in longitudinal direction as well as crack sliding in the vertical direction. The latter is difficult to measure during experimental tests of RC beams flexurally strengthened with CFRP sheets. Shear strengthening with transverse strips limits the diagonal cracking, which may restrain this type of failure.

2.9 Bond of CFRP Sheet-Concrete Interfaces under Tension

Tensile tests of this nature are much easier than those performed for shear. The three types of tests that have been used are direct tensile test method, three-point bending and wedge splitting (Figures 2.7 – 2.9). The direct tensile test method was first suggested by Japan Society of Civil Engineering (JSCE) and the Architectural Institute of Japan (AIJ). This method is handy since it verifies the quality of the interface bond qualitatively. For instance, one can monitor if the concrete has fractured or not. The CFRP-concrete interface bond properties under tension can be examined parametrically and quantitatively using either the three-point bending or the wedge splitting method. In addition, the three-point bending test may be utilized for evaluating the bond degradation of CFRP sheet-concrete interfaces when exposed to harsh environment and fatigue loading. Since adhesives have a greater effect on the CFRP sheet-concrete interface in shear rather in tension, their selection does not play a major role here.

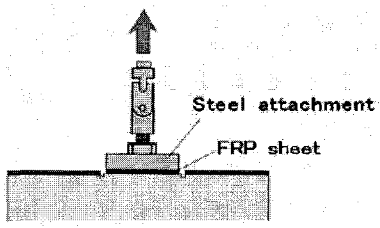

Figure 2.7 – Direct Tension Test (Ueda and Dai, 2005)

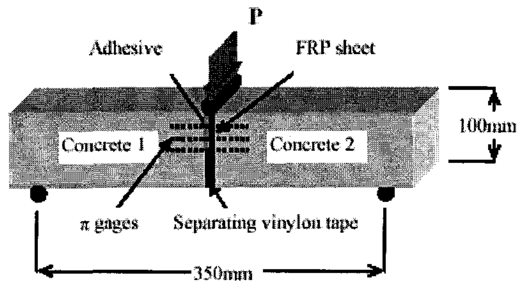

Figure 2.8 – Three-Point Bending Test (Ueda and Dai, 2005)

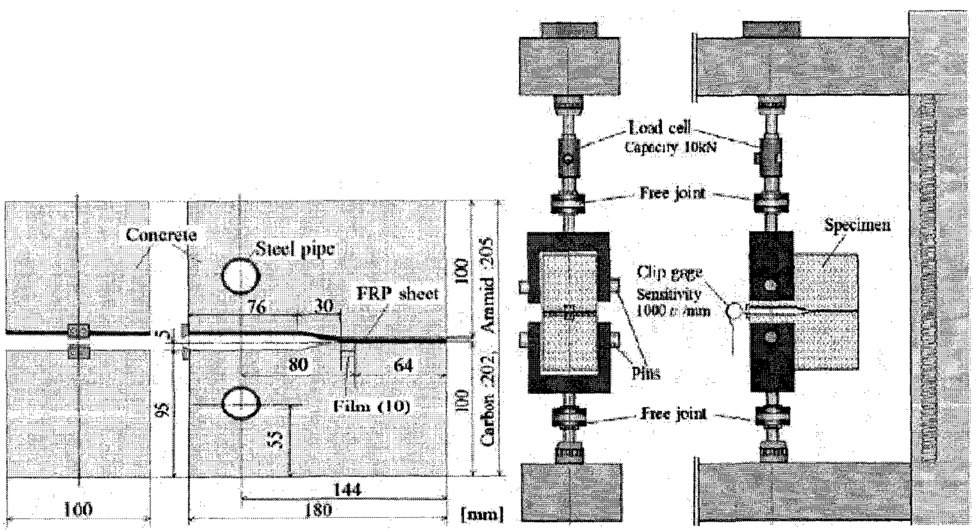

Figure 2.9 – Wedge Splitting Test (Ueda and Dai, 2005)

2.9.1 Anchorage Design for Tensile Force in CFRP Sheets

The bond of externally bonded CFRP sheets to concrete differs from that of reinforcing bars in concrete (Ueda and Dai, 2005). Usually, the anchorage design criteria for the bond of reinforcing bars in RC beams is to assure an adequate development length that would aid the reinforcing bar to resist a tensile force equivalent to its tensile strength. The externally bonded CFRP sheets, however, don't usually reach their material strength even over a very long bond length. This is due to the presence of premature debonding and effective bond length. Various models have been proposed up to date where only the effects of CFRP stiffness and concrete strength are considered. In most available models, the effective bond length is utilized to predict the bond strength of a CFRP sheet-concrete interface by determining if its bond length is longer than the effective bond length.

2.10 Bond of CFRP Sheet-Concrete Interfaces under Shear

The main task of the bond interface between CFRP sheets and concrete is the transfer of shear stresses from the concrete structure to externally bonded CFRP sheets for shear and flexural strengthening. Test methods include single-lap, double-lap, bending and inserted type (Figure 2.10). Using these methods, the strain distribution in the CFRP sheets have been studied to illustrate the local interfacial shear bond behaviour. Further, interface characteristic parameters such as the average shear bond strength, effective bond length, maximum shear bond stress, interfacial fracture energy, and the local bond stress-slip relationship have been evaluated (Ueda and Dai, 2005).

Numerous studies have been done in this area. The main factors that are expected to affect the bond are: CFRP bonded length, concrete strength, number of CFRP plies (stiffness), ply width, and surface preparation.

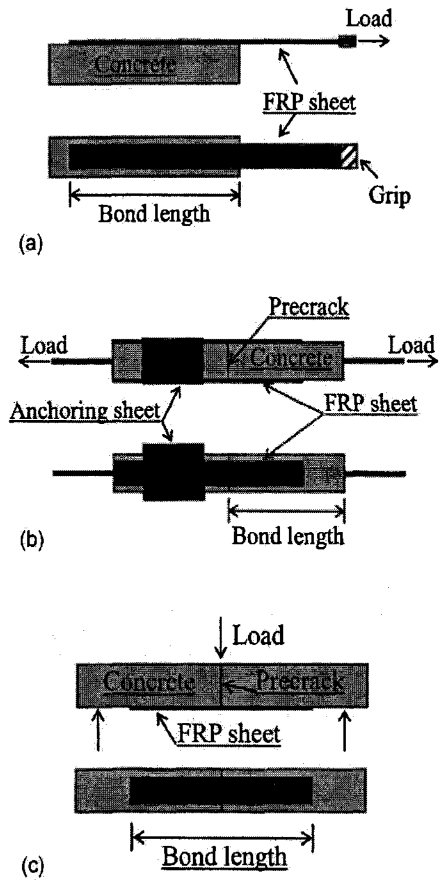

Figure 2.10 – Shear Bond Test Methods: (a) Single-Lap, (b) Double-Lap, and (c) Bending Type (Niu and Wu, 2006)

Yoshizawa *et al.* (1996) studied the effect of concrete surface preparation on the bond behaviour. The specimen was tested in tension producing direct shear on the sheets. Sandblasting and water jet were both used for surface preparation. It was reported that, in comparison to sandblasting, the water jet doubled the capacity of the specimen. The bonded length of the CFRP sheet, however, did not affect the ultimate load significantly.

Brosens and Van Gemert (1997) performed some preliminary shear experiments. Two concrete prisms (150 mm x 150 mm x 300 mm) were attached by gluing three layers of CFRP laminates at two opposite sides. Steel plates were bonded on the other sides to apply the tensile force. They stated that the failure load increases with the increase of bonded length, which does not agree with other researchers' findings. Nonetheless, they did mention that the effect of bonded length diminishes at longer lengths. It was found that the critical bond length is at least larger than 275 mm.

Horiguchi and Saeki (1997) studied the effect of test method and quality of concrete on the bond of CFRP sheets. They examined the outcome of three different test methods, shear test, flexural test, and direct tensile test.

For the shear test, two concrete specimens were used with rectangular cross-sections of 100 mm wide, 100 mm high, and 200 mm long. The specimens were bonded with carbon sheets on each side.

Two concrete specimens with rectangular cross-sections of 150 mm wide, 150 mm high, and 200 mm long were prepared for the bending test. A carbon sheet was attached on the tension side of these specimens.

For the tensile test, the bond strength between the CFRP sheet and the concrete surface was determined by the ultimate tensile force divided by the bonding area of 40 mm x 40 mm.

Out of the three tests, the tensile test generated the largest average bond strength, and the bending test ranged second. The lowest bond strength was obtained in the shear test. In instances of low compressive strength, however, the three test results were converged at certain level.

Maeda *et al.* (1997) examined the bond mechanism of CFRP sheets. Test results illustrated that the ultimate load increases as the stiffness of the fiber sheet increases. The maximum load did not vary for bonded lengths above approximately 100 mm. This outcome proved the existence of an effective bond length that is less than 100 mm.

Another group of researchers conducted an experimental study on bond strength of Continuous Fiber Sheets (CFS) (Ueda *et al.*, 1998). Several series of pull-out tests were carried out based on five different specimen layouts. In two types, tensile load was applied through the steel bar entrenched in the concrete block to which CFS was bonded. In another type, CFS was directly pulled at one end, and hydraulic jacks sandwiched between the concrete blocks to which CFS was glued were utilized to develop tensile force to CFS in the last two types. Based on the experimental results, it was concluded that the bond strength does not increase with bond length longer than 100 mm. As CFS stiffness increases, the maximum local and average bond stresses at delamination increase, and CFS strain gradient decreases. CFS with a narrower width has bond strength greater than a wider width. An equation to predict the maximum local bond stress was suggested based on the observed bond stress in CFS.

Bizindavyi and Neale (1999) presented a new experimental apparatus designed and constructed at the University of Sherbrooke, Canada. The test system consisted of an FRP laminate bonded to a concrete block, which is then placed into a tensile loading frame. The assembly was designed so that there is direct shear at the composite-to-concrete interface. From the tests, full tensile capacity of the bonded composites could develop for both one and two-ply CFRP and GFRP laminates. For a one and two-ply 25 mm wide CFRP-to-concrete joints, bond lengths of 80 mm and 220 mm, respectively, were adequate to reach the full capacity of the composites. However, these findings are only applicable for the composite systems used in this investigation.

Brozens and Van Gemert (1999) carried out a series of twenty four direct shear tests. The test specimens consisted of two concrete prisms (150 mm x 150 mm x 300 mm) bonded together with one, two, or three plies of CFRP sheets at two opposite sides. On the other two sides, steel plates were glued to initiate the tensile force. They tested two CFRP widths, 80 mm and 120 mm, and two bonded lengths (the length on one prism, which is half of the total CFRP length), 150 mm, and 200 mm. The main objective of their study was to verify the assumptions, and to check the validity of a non-linear fracture mechanics based design that was set up to describe the occurrences at the end of the externally bonded reinforcement. Results showed that the fracture load of the direct shear test specimens can be very well predicted.

Lorenzis *et al.* (2001) prepared flexural test specimens. The specimen used was a plain concrete beam with an inverted T-shape. A steel hinge at the top and a saw cut at the bottom, both located at midspan, were used to control the distribution of the internal forces. A 51 mm wide CFRP strip was glued to the tension face of the beam. A transverse sheet was placed on one side to force failure at the other end. Further, the sheet was left unbonded for approximately

51 mm on each side of midspan. This investigation illustrated that the maximum load is not affected by the bonded length and the concrete strength. Also, the sheet width did not influence the bond strength. The CFRP stiffness affected the bond failure load, but the average of the maximum loads of the two-ply series was only 1.5 times that of the one-ply series. Finally, roughening the surface by chiseling improved the performance of the specimen, and was much better than sandblasting. Failure occurred in the former by rupture of the FRP sheet at a remarkably higher load.

Nakaba *et al.* (2001) conducted a double-face shear type bond test. The specimen consisted of a prism with a notch at the center, reinforced with FRP laminates on both faces. This research studied the effect of CFRP stiffness, concrete strength (50 and 24 MPa), and influence of putty thickness. Thirty six specimens were tested where the bond length was taken as 300 mm, and the laminate width was 50 mm. Carbon (standard and high stiffness) and aramid fiber were used. To verify the influence of the quality of the substrate, the specimens were made by concrete and mortar. It was concluded that the maximum load increases as the stiffness of FRP increases. The maximum local bond stress was not found to be influenced by the type of FRP, but it increased as the compressive strength of concrete increased.

Yao *et al.* (2005) performed an experimental study on the bond shear strength between FRP and concrete using a Near-End Supported single-shear pull test. The specimens consisted of a concrete prism bonded with an FRP strip. The factors considered were the bond length, the width ratio between the FRP strip and the concrete prism, the height of the concrete free edge, and the offset in the load position. Based on the outcomes, it was recommended that the bond length in a standard test should be around two times the effective bond length specified by Chen and Teng's model (Chen and Teng, 2001). The height of the free concrete edge should be around 50 mm for a concrete prism 150 mm high. Further, the distance between the positioning frame preventing the uplifting to the concrete prism and the far end of the FRP strip should be suitable to avoid elevated flexural tensile stresses near the far end of the FRP strip, and the intrusion with interfacial behaviour as well.

Kamel *et al.* (2006) presented a study on the interfacial behaviour of CFRP sheets when applied to concrete members as external reinforcement. Two shear test methods were performed using separate test series to examine the bond behaviour and failure mechanism of CFRP sheets bonded to concrete. The first series used modified push-apart specimens, whereas the second series consisted of pull-apart specimens. In both series, the bond length, bond width, and strain distribution were investigated. The anchorage requirements were studied only in the pull-apart specimens.

Each specimen in the push-apart series was a rectangular concrete block with a rectangular empty core. Metal sheets were positioned along the width of the specimen arms in their center to force the crack to develop in that location. A rigid steel plate was fixed to the inner face of the specimen to create a flat surface for applying the load.

In the pull-apart test, on the other hand, each specimen was a concrete prism with two embedded concentric steel bars. Metal sheets were placed at mid height to initiate crack when the load was applied. Anchor sheets were bonded on both sides of specimens prepared for studying the anchor sheet effect. Spiral reinforcements were placed around the steel bars to reduce the possibility of any bond slip of the rebars that apply the load to the concrete. Each steel bar was 25 mm in diameter and 500 mm in length, with 250 mm inside the concrete prism.

It was found that anchor sheets placed at 90° to the primary test sheets and bonded underneath the tested sheet would show better or equivalent overall bond behaviour compared with those bonded on top of the tested sheet. The distance at which the anchor sheet was placed from the crack did not influence the bond behaviour. CFRP sheet widths ranged between 25 mm and 250 mm, while the bond length was varied from 50 mm to 250 mm. It was confirmed that an effective length beyond which no increase in the bond strength takes place. They also observed that the average bond strength decreases with an increase in width until an effective bond width is reached. Beyond that width, the average bond strength remained constant as the sheet width is increased. There did not seem to be any correlation between the effective bond length and effective bond width.

2.11 Bond of CFRP Sheet-Concrete Interface under Shear and Tension

Since the CFRP sheet-concrete interface experiences both shear and tension, it makes sense to study this combined mode more thoroughly. Karbhari and Engineer (1996) performed a bond test by producing different interface peeling angles. Their main goal was to be able to evaluate both Mode I and Mode II (tension and shear, respectively) components of interfacial fracture energy. They were also hoping to allow a quantitative comparison of interface adhesion mechanisms and energies.

In Japan, a new application of CFRP strengthening has been developed where the CFRP sheets are being bonded on the bottom surface of tunnel linings or elevating bridges (Ueda and Dai, 2005). This technology was created to prohibit weakened concrete blocks from falling. The two types of test methods applied in this case are the beam-type dowel test and the slab-type shear punching test. In the former, one-directional CFRP sheets are bonded on the bottom of a notched concrete beam (Figure 2.11). In the latter, however, bidirectional CFRP sheets are attached on the bottom of a concrete slab (Figure 2.12). The outcome from both test methods is similar. Under the dowel action, the two basic bond characteristics of CFRP sheet-concrete interface are acquired. During the interface debonding procedure,

(1) The peeling angle is constant, and
(2) The maximum vertical force per unit width for CFRP sheet-concrete interface is a constant value.

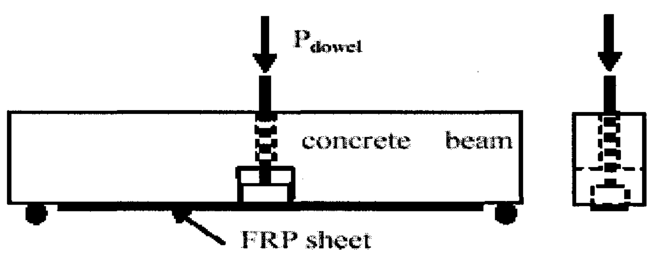

Figure 2.11 – Beam-Type Dowel Test (Ueda and Dai, 2005)

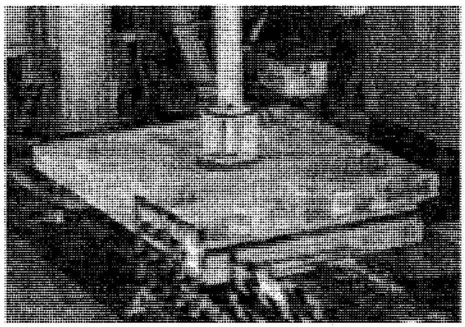

Figure 2.12 – Slab-Type Dowel Test (Ueda and Dai, 2005)

Some tests (Ueda and Dai, 2005) were performed to observe whether or not the flexural strengthening effectiveness of FRP sheets is influenced by the ratio of transverse reinforcements. Same amount of FRP sheets were used to flexurally strengthen two RC beams that were designed to fail in flexure. Steel stirrups were installed in both beams in distinct ratios. About 10% higher flexural capacity and better ductility were discovered in the strengthened RC beams having a larger amount of transverse reinforcments. Hence, the amount of transverse reinforcement does affect the mix-mode failure of CFRP sheet-concrete interface and should be taken into consideration during design.

CHAPTER 3

EXPERIMENTAL METHOD

3.1 Introduction

Various studies have been pursued to define and correlate the parameters that can influence the bond behaviour. It is still not clear what variables would affect the behaviour of the concrete-CFRP interface most. In this study, 32 reinforced concrete specimens and two control specimens were tested and test data were analyzed to study shear transfer between CFRP and concrete. The parameters studied included the bond length, bond width, surface preparation, presence of cross-wraps on one or both halves of the specimen, and the stiffness of CFRP. Table 3.1 shows the test matrix used for this study. The specimen designation followed to express the various possible combinations was:

LxxxWxxxLnXWx

where, **Lxxx** stands for the length of the CFRP sheet in mm. That value varied between 450 mm and 350 mm,

Wxxx stands for the width of the CFRP sheet in mm. Half the specimens had a CFRP width of 100 mm, whereas the other half had a CFRP width of 75 mm,

Ln stands for the number of CFRP layers, which was varied between one layer and two layers,

X stands for the surface preparation (either rough (R) or smooth (S)), and

Wx stands for the placement of cross wraps. They were either placed on one half or both halves of the specimens.

Table 3.1 – Parameters

SPECIMEN DESIGNATION	LENGTH (mm)	WIDTH (mm)	# OF CFRP LAYERS	SURFACE PREPARATION	X-WRAPS (sides)
L450W100L1SW1	450	100	1	smooth	1
L450W100L1SW2					2
L450W100L1RW1				rough	1
L450W100L1RW2					2
L450W100L2SW1			2	smooth	1
L450W100L2SW2					2
L450W100L2RW1				rough	1
L450W100L2RW2					2
L450W75L1SW1		75	1	smooth	1
L450W75L1SW2					2
L450W75L1RW1				rough	1
L450W75L1RW2					2
L450W75L2SW1			2	smooth	1
L450W75L2SW2					2
L450W75L2RW1				rough	1
L450W75L2RW2					2
L350W100L1SW1	350	100	1	smooth	1
L350W100L1SW2					2
L350W100L1RW1				rough	1
L350W100L1RW2					2
L350W100L2SW1			2	smooth	1
L350W100L2SW2					2
L350W100L2RW1				rough	1
L350W100L2RW2					2
L350W75L1SW1		75	1	smooth	1
L350W75L1SW2					2
L350W75L1RW1				rough	1
L350W75L1RW2					2
L350W75L2SW1			2	smooth	1
L350W75L2SW2					2
L350W75L2RW1				rough	1
L350W75L2RW2					2

This chapter discusses the properties of the materials used, the experimental procedure, and the instrumentations used for the experimental study.

3.2 Material Properties

The materials used in this study are concrete, steel bars, primer, saturant, and CFRP sheets. The properties of each material are given below. It should be noted that the concrete was designed so that it would have a fully flowing condition (a slump of equal to or greater than 200 mm)

3.2.1 Concrete

The slump chosen for this study was around 200 mm. The nominal maximum size of coarse aggregates was taken as 10 mm, and the 28 day compressive strength was selected to be 30 MPa. No water reducing agent was added. Hence, the by-weight composition of the concrete mixture was as follows:

Water : Cement : Coarse Aggregate : Fine Aggregate = 1 : 1.85 : 3.5 : 4.7

3.2.1.1 Sieve Analysis

The sieve analysis was performed according to the requirements of CSA A23.1-M90 (1990) and CSA-23.2-2A (1990).

Fine Aggregates

The CSA A23.1 M90 – Clause 5.3 specifies that the sizes of normal-density fine aggregate shall be according to Table 3.2:

Table 3.2 - Fine Aggregates Selection (CSA A23.1 M90 1990)

Sieve size	Total passing sieve, percentage by mass
10 mm	100
5 mm	95 – 100
2.5 mm	80 – 100
1.25 mm	50 – 90
630 μm	25 – 65
315 μm	10 – 35
160 μm	2 – 10

CSA A23.2-2A (1990) states the following:

Clause 3.1: "fine aggregate sampled by the quartering method shall be thoroughly mixed and shall be in moist condition."

Clause 3.2: "Samples of fine aggregate for sieve analysis shall have a mass, after drying, of approximately the amount indicated in Table 1". That table is reproduced as Table 3.2 in this chapter and specifies that for material at least 90% finer than a 5 mm sieve and more than 5% coarser than a 2.5 mm sieve, the sample mass should be 450 ± 50 g.

RESULTS

Based on requirements of CSA A23.2-2A (1990) – Table 1, three batches of sieve analysis were undertaken and results are shown below:

Batch #1

Total Mass = 500.00 g

Table 3.3 – Fine Aggregate Results (Batch #1)

Sieve Size	Weight (g)	Percent Passing
9.5 mm	0	100
4.76 mm	4.33	99.1
2.38 mm	94.66	80.2
1.19 mm	92.62	61.7
595 μm	88.52	44
297 μm	108.02	22.4
150 μm	80.91	6.2

Batch #2

Total Mass = 500.51 g

Table 3.4 – Fine Aggregate Results (Batch #2)

Sieve size	Weight (g)	Percent Passing
9.5 mm	0	100
4.76 mm	4.32	99.1
2.38 mm	112.19	76.7
1.19 mm	94.74	57.8
595 μm	89.17	40
297 μm	113.10	17.4
150 μm	86.56	0.2

Batch #3

Total Mass = 500.12 g

Table 3.5 - Fine Aggregate Results (Batch #3)

Sieve size	Weight (g)	Percent passing
9.5 mm	0	100
4.76 mm	4.21	99.2
2.38 mm	123.48	74.5
1.19 mm	98.35	54.9
595 μm	88.53	37.2
297 μm	107.39	15.7
150 μm	76.33	0.5

Coarse Aggregates

CSA A 23.1 M90 – Clause 5.4 – Normal-Density Coarse Aggregate states that the sizes of coarse aggregate shall be selected from the standard sizes given in Table 3.6, which shows the requirements for "Group I" of Table 2 of CSA A23.1 M90 (1990). Group 1 was selected since it includes combined aggregate gradings most commonly used in concrete production, whereas Group II provides for special requirements, i.e. gap grading, pumping, etc., and for blending two or more sizes to produce Group I gradings. The nominal size of aggregate selected was 14-5 mm.

Table 3.6 - Coarse Aggregates Selection (CSA A23.1 M90 1990)

Sieve size	Total passing sieve, percentage by mass
20 mm	100
14 mm	90 – 100
10 mm	45 – 75
5 mm	0 – 15
2.5 mm	0 – 5

According to CSA A23.2-2A, Clause 3.3: "Samples of coarse aggregate for sieve analysis shall have a mass, after drying, not less than the amount indicated in Table 2". That table states that for a nominal maximum size of aggregate of 10 mm, the minimum mass of sample should be 1 kg.

RESULTS

Based on requirements of CSA A23.2-2A (1990) – Table 2, three batches of sieve analysis were undertaken and results are shown below:

Batch #1

Total Mass = 1000.40 g

Table 3.7 - Coarse Aggregate Results (Batch #1)

Sieve size	Weight (g)	Percent passing
19.1 mm	0	100
12.7 mm	15.36	98.5
9.5 mm	414.03	57.5
4.76 mm	537.05	3.5
2.38 mm	23.42	1.0

Batch #2

Total Mass = 1000.32 g

Table 3.8 - Coarse Aggregate Results (Batch #2)

Sieve size	Weight (g)	Percent passing
19.1 mm	0	100
12.7 mm	18.92	98.1
9.5 mm	414.41	56.7
4.76 mm	521.92	4.5
2.38 mm	30.39	1.5

Batch #3

Total Mass = 1000.91 g

Table 3.9 - Coarse Aggregate Results (Batch #3)

Sieve size	Weight (g)	Percent passing
19.1 mm	0	100
12.7 mm	26.05	97.4
9.5 mm	420.98	55.3
4.76 mm	513.56	4.0
2.38 mm	26.42	1.4

The results acquired from the fine aggregates and coarse aggregates batches were satisfactory as they fulfilled the CSA A23.1 M90 (1990) requirements.

3.2.2 Steel Bars

Threaded steel bars of 15 mm diameter were chosen for this study. They were obtained from Windsor Factory Supply. Each bar had an original length of 800 mm. It was first cut in half, and later to the desired length using the steel saw available in the Structural Laboratory of the University of Windsor.

3.2.3 Primer

The primer, "Sikadur 330", was acquired from Sika Canada Inc. (Sika Canada Inc., 2007). It is a two-component impregnating resin for fabric reinforcement that has high strength, and high modulus. At a temperature of 10°C, it has a pot life of 90 minutes, whereas at 35°C, its pot life reduces to 30 minutes. The primer's tensile strength is 30 MPa. It has an elongation at rupture of 1.5%, and a flexural E-modulus of 3.8 GPa.

3.2.4 Saturant

Sikadur 300 was the saturant suggested by Sika Canada Inc. (Sika Canada Inc., 2007). It is a two-component impregnating resin that has high strength, and high modulus. It has a tensile strength of 55 MPa, a tensile modulus of 1.72 GPa, a flexural strength of 79 MPa, and a flexural modulus of 3.45 GPa. Its elongation at rupture is 3%.

3.2.5 CFRP Sheet

SikaWrap Hex 230C was also bought from Sika Canada Inc. (Sika Canada Inc., 2007). It is a unidirectional carbon fiber fabric especially manufactured for structural strengthening systems. This fabric is known for its light weight and high strength. According to the manufacturer, SikaWrap Hex 230C has a tensile strength of 3.45 GPa, an E-modulus of 230 GPa, and an elongation at rupture of 1.5%. When cured with Sikadur 330 saturant (standard cure at 21°C - 24°C after 5 days), its tensile strength and E-modulus become 894 MPa and 65.4 GPa, respectively. It has a Poisson's Ratio of 0.30.

3.2.5.1 Coupon Test

The coupon test was undertaken in accordance with ASTM-D3039/D3039M-00 (ASTM committee D30, 2006). This method determines the in-plane tensile properties of polymer matrix composite materials reinforced by high-modulus fibers. At least five specimens per test condition required testing. Since SikaWrap Hex 230C is 0° unidirectional, each coupon should have a minimum overall length of 250 mm, a minimum width of 15 mm, and a minimum thickness of 1.0 mm.

Every tab must have a length of 56 mm, and a thickness of 1.5 mm. The standard suggests that the most consistently used bonded tab material has been continuous E-glass fiber-reinforced polymer matrix materials (woven or unwoven) in a 0°/90° laminate configuration. The tab material selected was E-glass fiber reinforced polymer matrix board. It came in pieces that had dimensions of 114 mm x 165 mm (4.5 in x 6.5 in), and was later cut at the University of Windsor's laboratory to match the geometry recommended by ASTM-D3039/D3039M-00 (Figure 3.1).

Five coupons with a length of 350 mm and a width of 25 mm were prepared. After cutting the CFRP to the desired dimension, Sikadur 330 was applied on both sides of each piece and on the tabs using a small brush. Once the CFRP strips and tabs were well saturated, hand pressure was applied to affix the tabs on the strips (Figure 3.2).

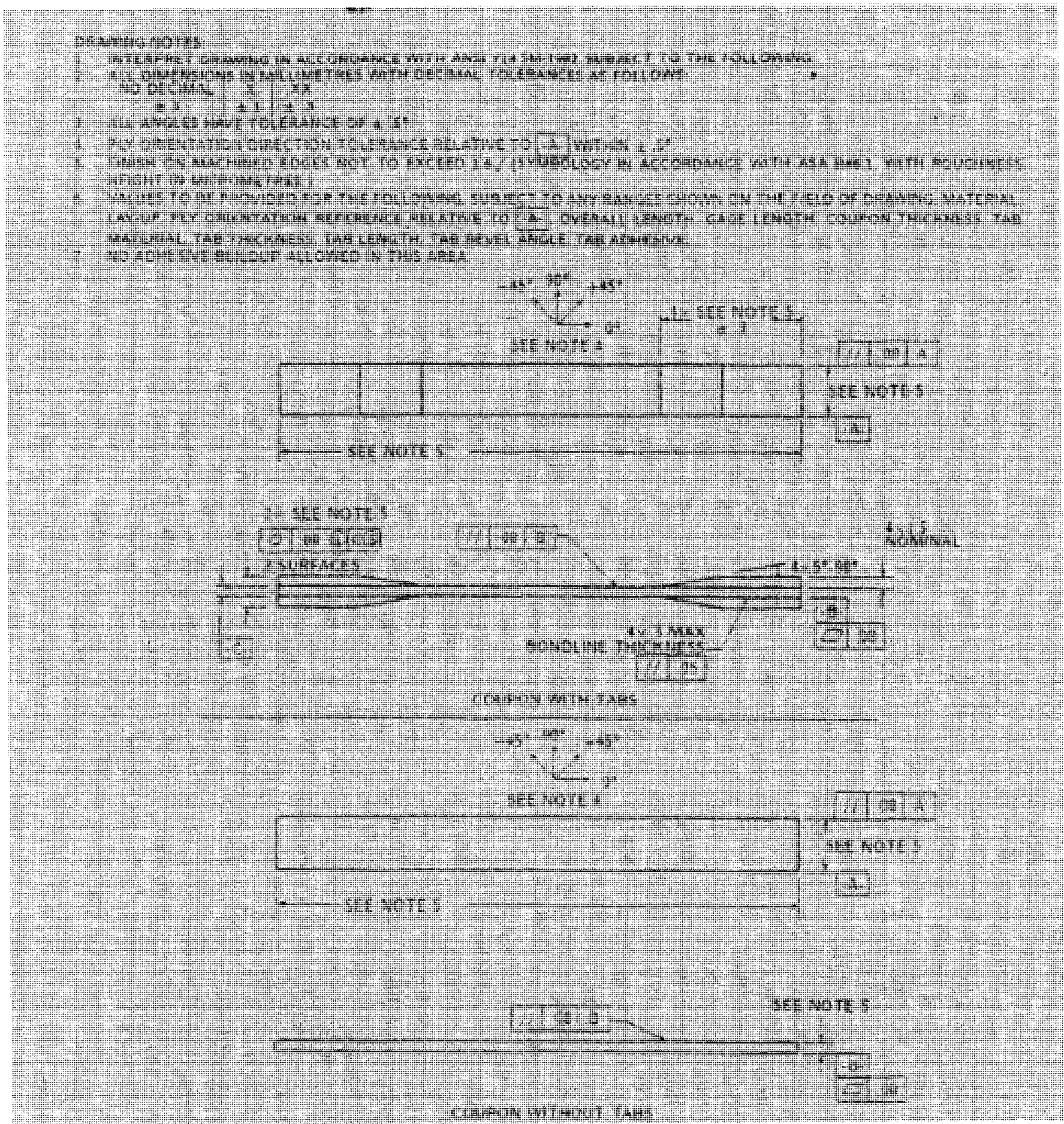

Figure 3.1 - Tension Test Specimen Drawing
(ASTM committee D30, 2006)

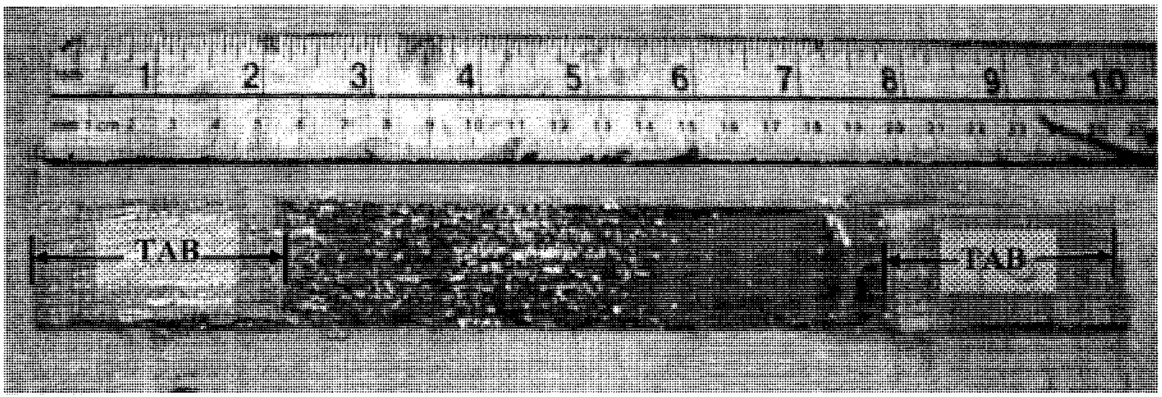

(a) - Coupon Length

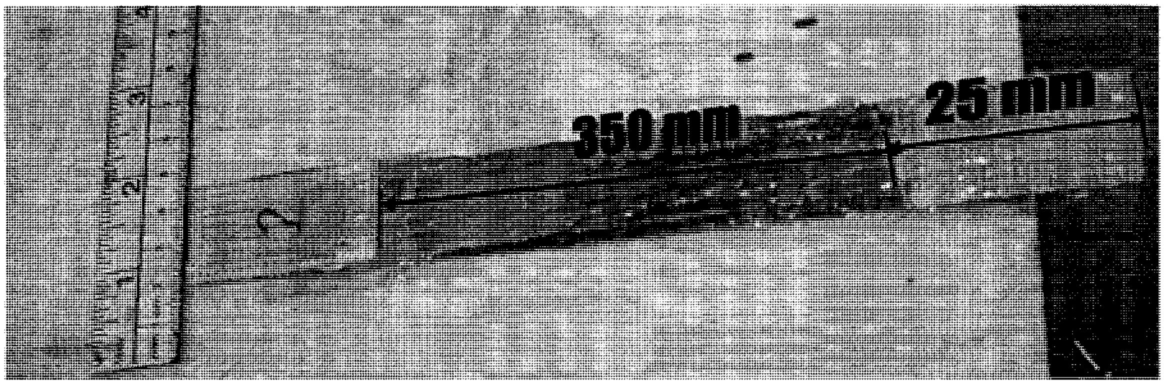

(b) - Coupon Width

Figure 3.2 - Coupon Dimensions

The coupons were allowed to cure for one week. Subsequently, their widths and thicknesses were recorded using a digital caliper. The results are shown in Table 3.10.

Table 3.10 - Coupon Dimensions

Coupon	Width (mm)	Thickness (mm)
1	25.74	0.38
2	25.05	0.33
3	26.31	0.32
4	25.14	0.34
5	25.22	0.33

The ASTM standard (ASTM committee D30, 2006) recommends that, for most purposes, the extensometer gage length should be in the range of 10 mm to 50 mm [0.5 in to 2.0 in]. The extensometer used in this study has a gauge length of 50 mm. It was calibrated on October 9, 2006 before the tests were conducted.

A Tinius Olsen universal testing machine (serial number 98336) was used for application of the load. Each coupon was placed in the grips of the test machine making sure that the long axis of the gripped specimen was aligned with the test direction (Figure 3.3). Then, the grips were tightened. On average, each test took about two and a half minutes until the specimen failure, and the maximum load was about 8 kN. The displacement that was obtained at the moment of rupture was 0.56 mm on average. The type of failure that was observed for all five coupons was SGM (Longitudinal Splitting Gage in the Middle), which is classified by the ASTM standard (ASTM committee D30, 2006) as a typical mode of failure (Figure 3.4).

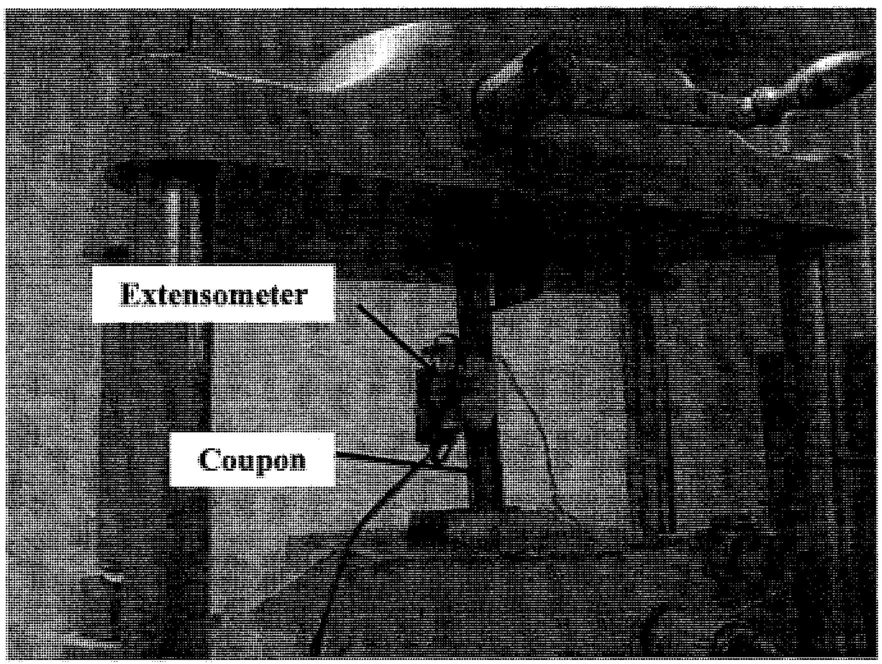

Figure 3.3 - Coupon Test Set-up

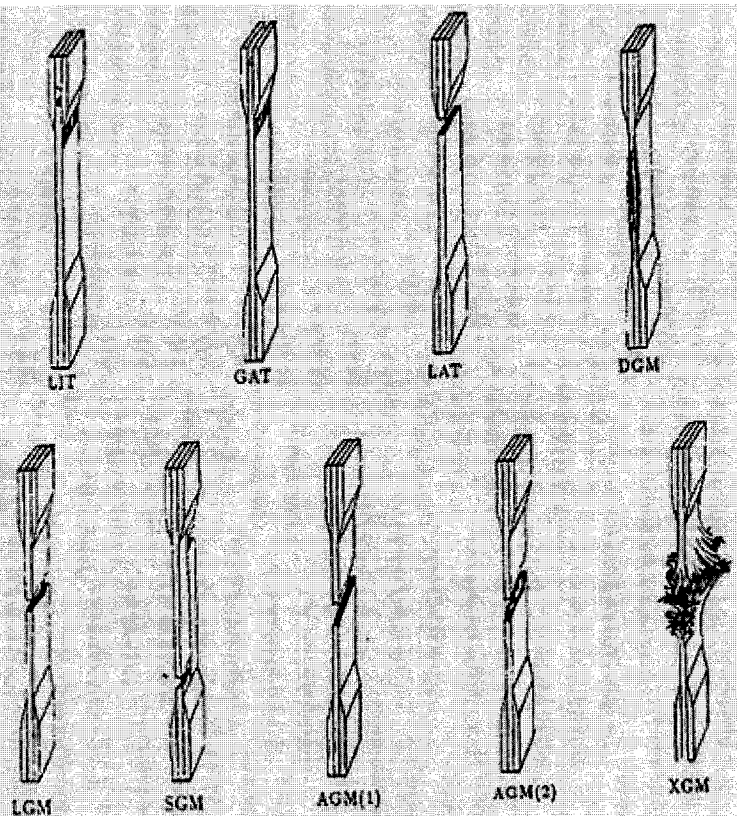

First Character

Failure Type	Code
Angled	A
edge Delamination	D
Grip/tab	G
Lateral	L
Multi-mode	M(xyz)
long. Splitting	S
eXplosive	X
Other	O

Second Character

Failure Area	Code
Inside grip/tab	I
At grip/tab	A
<1W from grip/tab	W
Gage	G
Multiple areas	M
Various	V
Unknown	U

Third Character

Failure Location	Code
Bottom	B
Top	T
Left	L
Right	R
Middle	M
Various	V
Unknown	U

(a) - Tensile Test Failure Codes/ Typical Modes (ASTM committee D30, 2006)

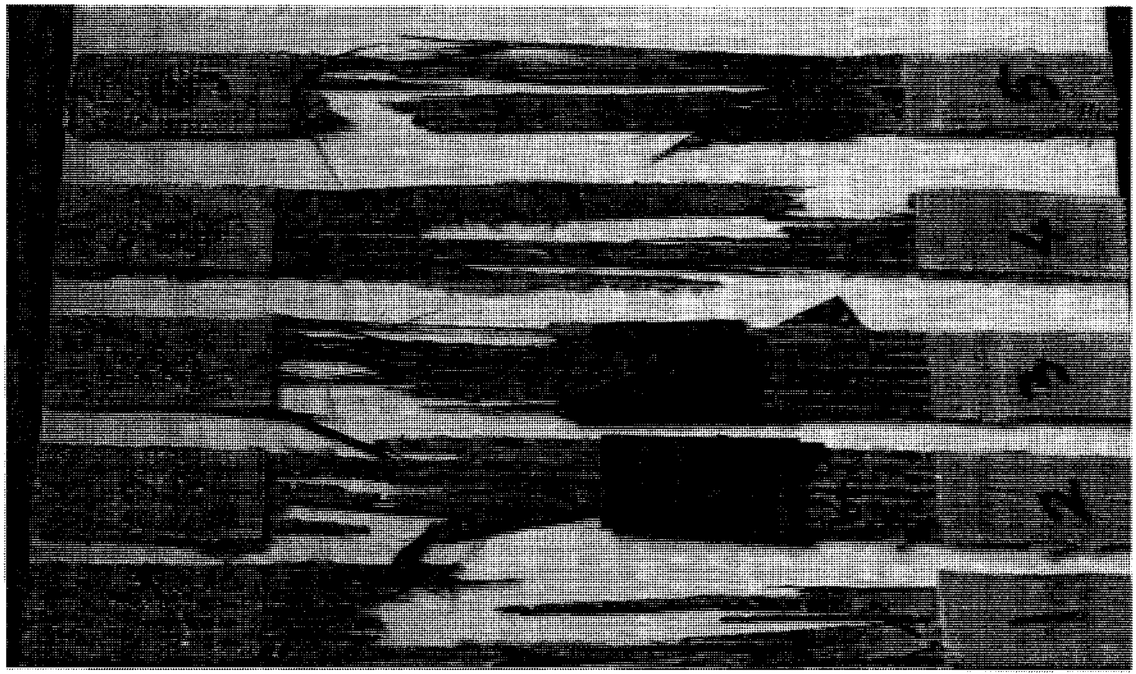

(b) - Failed Coupon Specimens

Figure 3.4 - Coupon Failure

Tensile Strength:

The tensile strength from the coupon specimens was calculated as recommended in ASTM-D3039/D3039M-00, which is shown in Equation 3.1:

$$F^{tu} = P^{max}/A \tag{3.1}$$

where, F^{tu} = ultimate tensile strength, MPa

P^{max} = maximum load before failure, N

A = average cross-sectional area = $w \times h$, mm^2

w = width of the coupon specimen, mm

h = thickness of the coupon specimen, mm

Based on the results of the five coupons, the average ultimate tensile strength was obtained as 889 MPa, which is very close to the manufacturer's value of 894 MPa.

Poisson's Ratio:

Poisson's Ratio was determined according to the specification of ASTM-E 132-04 (2004), which recommends plotting the average longitudinal strain, ε_l, and the average transverse strain, ε_t, against the axial tensile load, P. A straight line must be drawn through each set of points, and the slopes, $d\varepsilon_l/dP$ and $d\varepsilon_t/dP$ should be determined. Poisson's ratio is calculated as shown in Equation 3.2:

$$\nu = \frac{d\varepsilon_t / dP}{d\varepsilon_l / dP} \tag{3.2}$$

In order to verify this value, Coupons 2 and 3 were set up in such a way that each had two strain gauges, one at the center in longitudinal direction, and the other one in transverse direction installed just under the first one. The specifications of the strain gauges used will be discussed later in this chapter. Based on the results (Figure 3.5), the Poisson's Ratio was 0.27, which agrees to a degree to the manufacturer's value of 0.30.

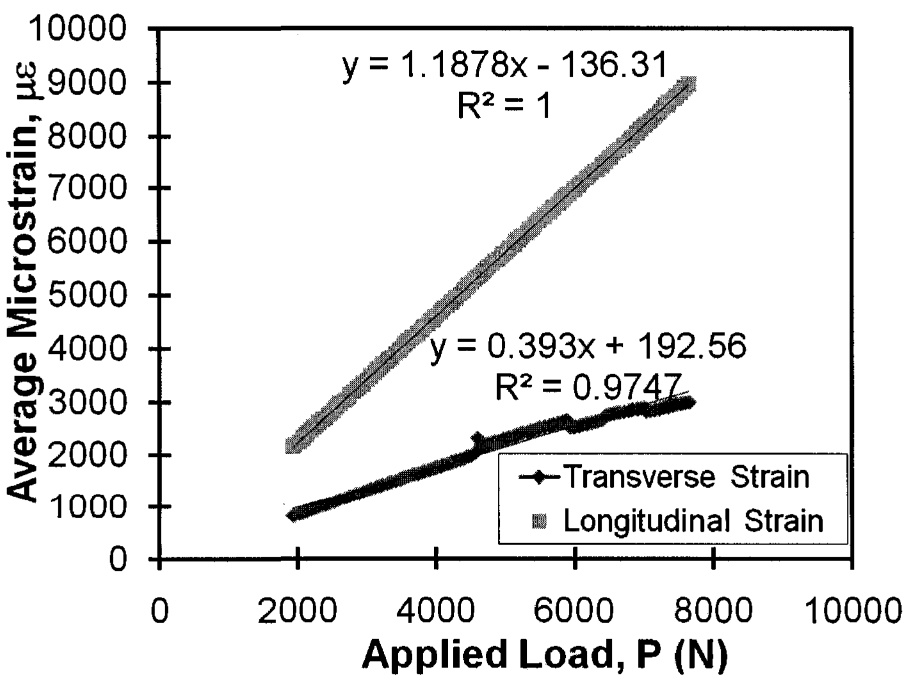

(a) - Coupon 2

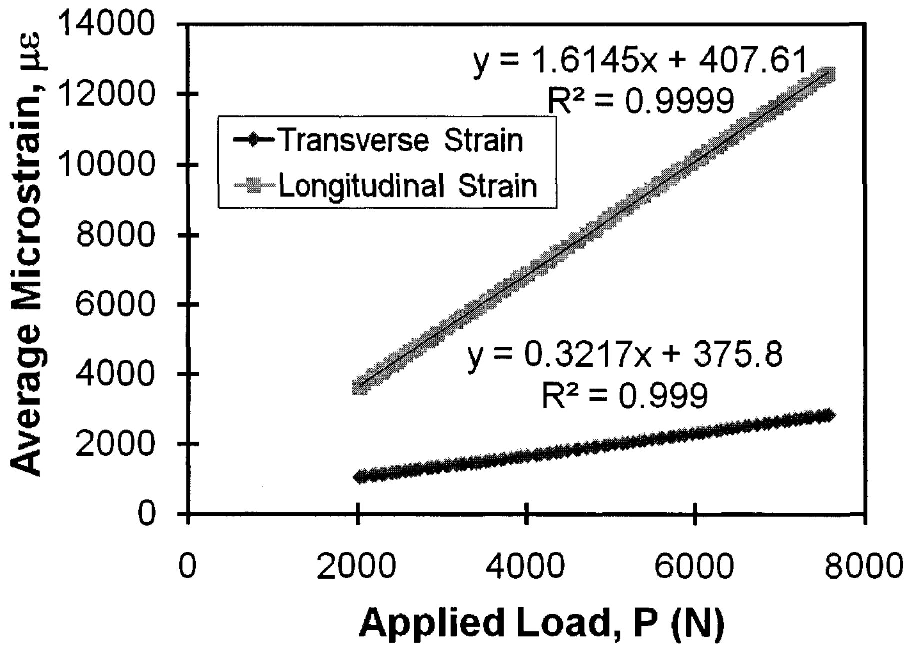

(b) - Coupon 3

Figure 3.5 - Load vs. Strain

3.3 Specimen Preparation

Specimens were designed and tested in accordance with CSA S806-02, Annex P (Canadian Standards Association, 2002).

3.3.1 Forms

All specimens were fabricated in aluminum forms that are 150 mm wide x 150 mm deep x 500 mm long (Figure 3.6). A 3 mm thin aluminum plate was located in the middle of each form before casting to initiate a crack, and to ensure that the specimen separates at that location under load. In addition, two 15M threaded steel bars (i.e. steel bars with a 15 mm diameter) were driven through a hole punched at the center of the form's depth. Several nuts were placed as shown in Figure 3.6 in order to prevent bar slippage.

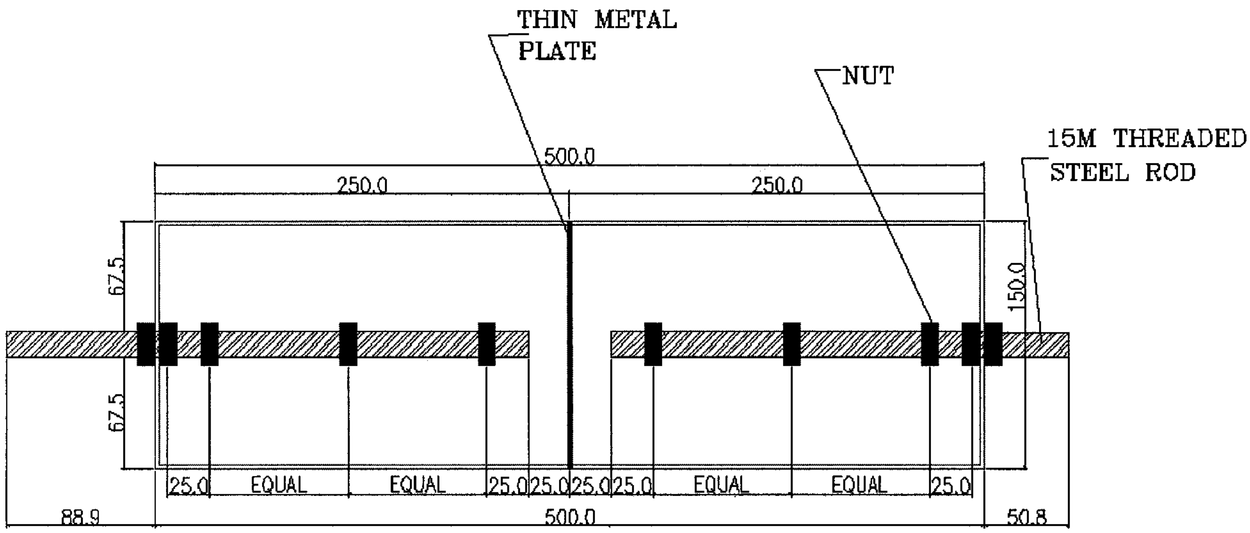

Figure 3.6 - Top View of Form
(All Dimensions in mm)

3.3.2 Casting

This preparation phase is very crucial, since test results rely to a great extent on the concrete properties.

The first step before casting was to grease the forms thoroughly to ensure that the concrete specimen disengage from the form easily. Next, a level check was performed on all steel bars in order to minimize eccentricity during the test. Concrete proportions as mentioned in section 3.2.1 were used. Quantities required to make six specimens were measured at a time. The concrete was mixed in two halves because of the mixer's capacity available at the University of Windsor's structural lab.

The slump test and the cylinders for the compression test were prepared as discussed in sections 3.3.2.1 and 3.3.2.2, respectively. While one individual was filling up the cylinders, another was pouring the concrete in the forms using a small shovel. No concrete was poured directly on the bars, since that would create eccentricity. All sides of the forms were tampered with a hammer in order to tamp the concrete and minimize air voids. A trowel was used to remove excess materials from the forms and to level the concrete. Burlap Jute cloth was used to cover all forms to minimize loss of moisture and permit removing the forms within 24 hours after casting. Subsequent to removing the forms, the Burlap sheets were kept moist with water twice a day for the first three days, and then once a day for four more days for curing of the specimens.

3.3.2.1 Slump Test

The slump test was performed in accordance to ASTM C143/C143M-03 (ASTM Committee 143, 2003) and ASTM 172-71 (ASTM Committee, 1977). Representative samples were taken from the middle of the mixer discharge, and the slump test was made within five minutes after taking the samples. On average, the specimens had a slump of 225 mm (Table 3.11), which fulfills the requirement of this study. As can be noted in Table 3.11, all slump values are comparatively similar except for the last casting, and that was because the temperature in the Laboratory was much lower that day.

Table 3.11 - Slump Values

Casting Date	Slump (mm)
October 03, 2007	240
October 04, 2007	240
October 15, 2007	230
October 17, 2007	240
November 29, 2007	175
AVERAGE	***225***

3.3.2.2 Cylinder Test

In order to determine the concrete's compressive strength, the cylinder test was carried out following the standard ASTM C39/C39M-05 (ASTM Committee C09, 2005). Cylinder dimensions are 100 mm in diameter and 200 mm in length. The cylinders were covered with Burlap sheets and cured under the same environment as the specimens (i.e. the Burlap sheets that were on top of the specimens and the cylinders were moistened with water simultaneously). Two cylinders for each concrete mix batch were tested at the age of seven days, while the other two were tested at the age of 28 days.

The cylinder specimens were capped with sulfur capping compound after removing them from their forms. Each cylinder was then placed in the Riehle compression testing machine. The compressive load was applied monotonically until the load indicator showed that the load is decreasing steadily, and the specimen displayed a well-defined fracture pattern as shown in Figure 3.7(a) (ASTM Committee C09, 2005). Fracture pattern type 3 was observed every time the cylinder test was performed, which indicated a typical failure (Figure 3.7(b)).

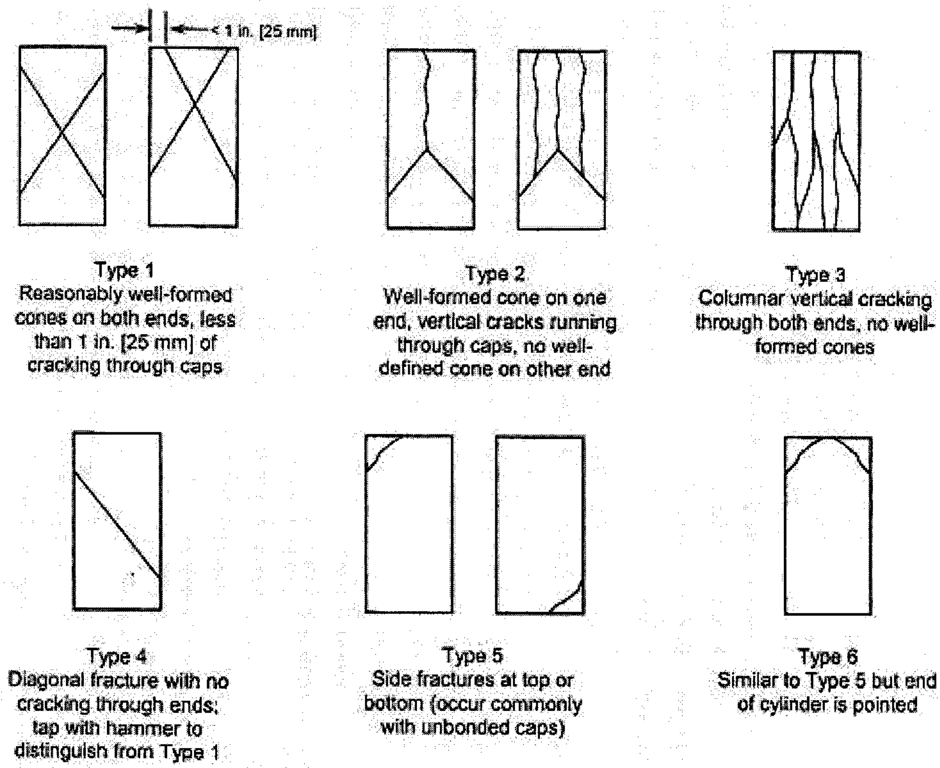

(a) - Schematic of Typical Fracture Patterns
(ASTM Committee C09, 2005)

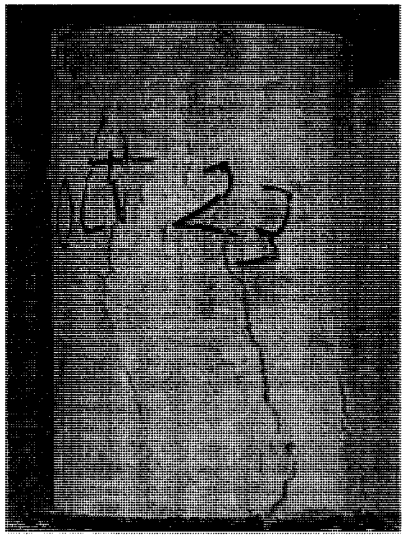

(b) – Tested Cylinder Fracture Pattern

Figure 3.7 - Compression Test Failure

The compressive strength of the specimen was calculated by dividing the maximum load carried by the specimen during the test by the average cross-sectional area as specified in section 8 of ASTM C39/C39M-05 (ASTM Committee C09, 2005). On average, the specimens had a seven-day compressive strength of 22 MPa (Table 3.12), and a 28-day compressive strength of 31 MPa (Table 3.13).

Table 3.12 - Seven-Day Compression Strength Values

Date of Compression Test	**7-day Compressive Strength (MPa)**
October 10, 2007	22.5
October 11, 2007	23.2
October 22, 2007	23.7
October 23, 2007	20.9
November 27, 2007	21.6
AVERAGE	***22***

Table 3.13 - 28-Day Compression Strength Values

Date of Compression Test	28-day Compressive Strength (MPa)
October 31, 2007	29.4
November 01, 2007	31.2
November 13, 2007	32.7
November 14, 2007	30.1
December 20, 2007	29.5
AVERAGE	***31***

3.3.3 Application of CFRP

The concrete was allowed to cure for seven days while covered with the moist Burlap sheets. It was then left in the air for curing for three more days.

3.3.3.1 Surface Preparation

A total of 32 specimens were tested (Table 3.1). Half of them were prepared to have a rough surface, whereas the other half were prepared to have a smooth surface. No surface preparation was done for the control specimens.

For specimens with rough surface, a grinder without any disk was used until aggregates were visible, and a good roughness was produced (Figure 3.8(a)). A resin bond aluminum oxide "grind and sand" disk number 24 was attached to the grinder and utilized for specimens with smooth surfaces until aggregates could be seen (Figure 3.8(b)).

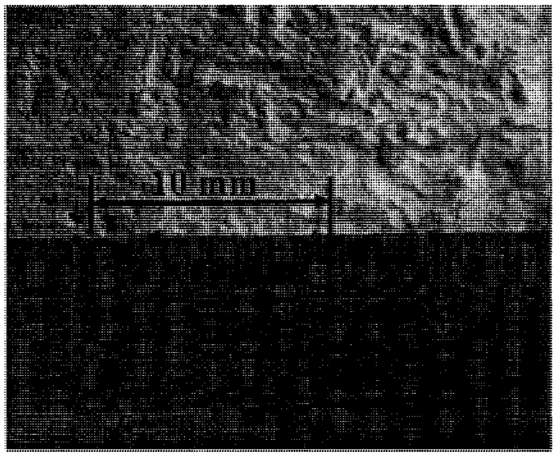

(a) - Rough Surface

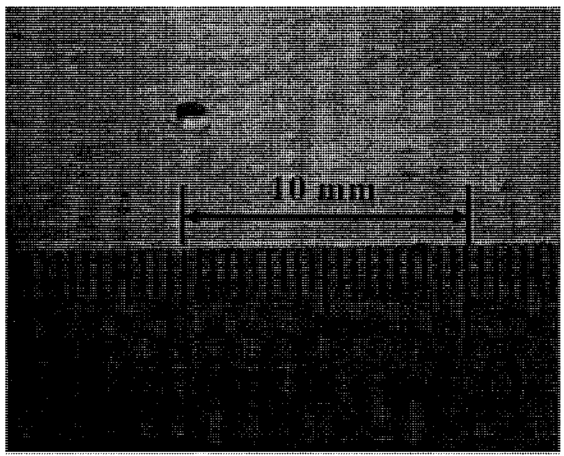

(b) - Smooth Surface

Figure 3.8 - Surface Preparation

In order to prevent potential failure of CFRP sheets caused by stress concentrations at the corners of the specimens, all concrete corners of the specimens were rounded to a minimum radius of 15 mm (ISIS, 2004) (Figure 3.9). A graduated steel angle was used on all corners to ensure the radius.

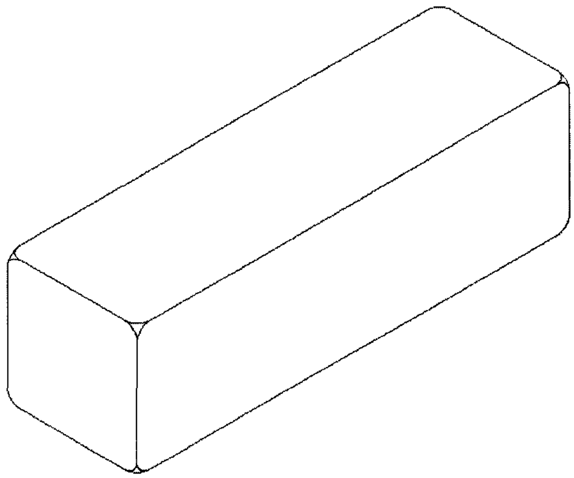

(a) - Sketch of Specimen

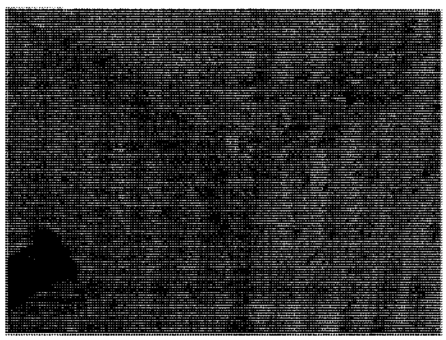

(b) – View of Corner

Figure 3.9 - Detail of Rounded Corner

3.3.3.2 CFRP Bonding

After grinding, the surface was cleaned with a broom to remove any dust or debris that can influence the bond strength of the concrete-CFRP interface.

Sikadur 330, which is a two-component primer, was mixed by adding required amount of component B to required amount of component A. It is important to apply the primer before exceeding its pot life (section 3.2.3) in order to maximize bonding. Hence, quantities for four specimens or less were mixed in a small measuring cup to denote the proportions. The two components were then mixed thoroughly using a wooden stick for two to three minutes until all coloured streaks disappeared. After marking the location of the CFRP with a marker, the primer was applied on the specimen by means of a small brush (Figure 3.10). All air voids that appeared on the concrete surface were also filled with the same primer.

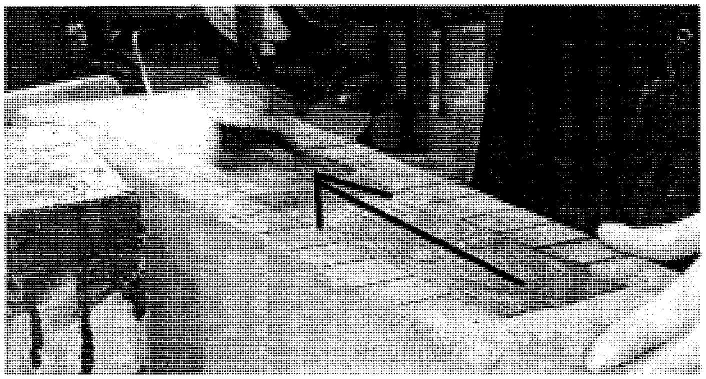

Figure 3.10 - Application of Primer

Sikadur 300 is a two-component saturant that is prepared by mixing required amount of component B with required amount of component A. Keeping in mind that the saturant would only be effective before reaching its pot life (60 minutes at 20°C), quantities for four specimens or less were mixed following the same technique as that for preparing the primer. Subsequently, the saturant was transferred onto a plastic tray. A small paint roller was soaked with the saturant. Then the CFRP that was cut to the desired dimension was impregnated on both sides (Figure 3.11).

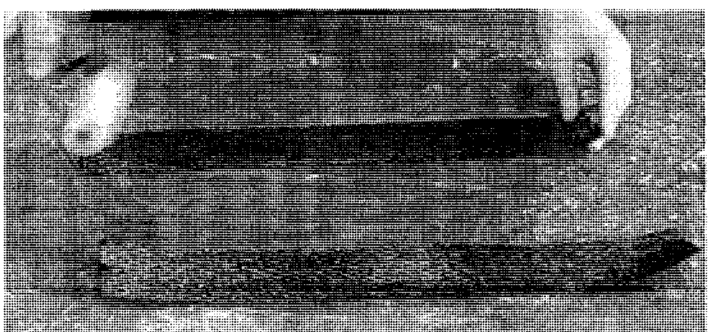

Figure 3.11 - Impregnating the CFRP

Next, the impregnated CFRP sheet was applied on the sealed concrete surface using the same roller. All irregularities and air voids that the concrete-CFRP interface could have experienced were removed by pressing the CFRP sheet on the specimen by the roller in one direction parallel to the fiber orientation (Figure 3.12).

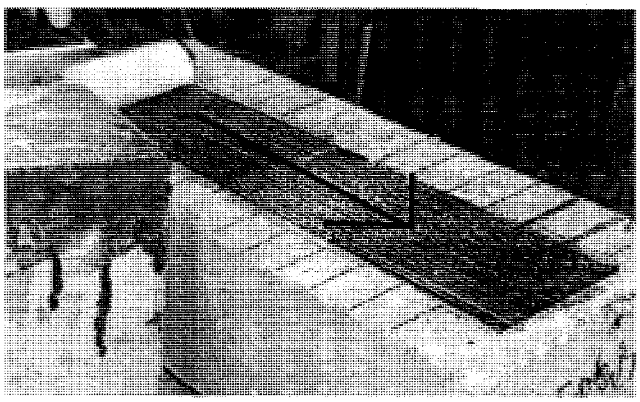

Figure 3.12 - Technique of Applying Roller

The same process was repeated if a second layer of CFRP composite was needed. It should be noted that the second layer was 5 mm in length shorter than the first layer on both sides to avoid any stress concentration at the termination edge of CFRP composite. In order to maximize bonding and fully saturate the carbon fiber fabric, a fair amount of epoxy was compressed out of the roller (Figure 3.13(a)) and tapped on top of the fiber by hand (Figure 3.13(b)).

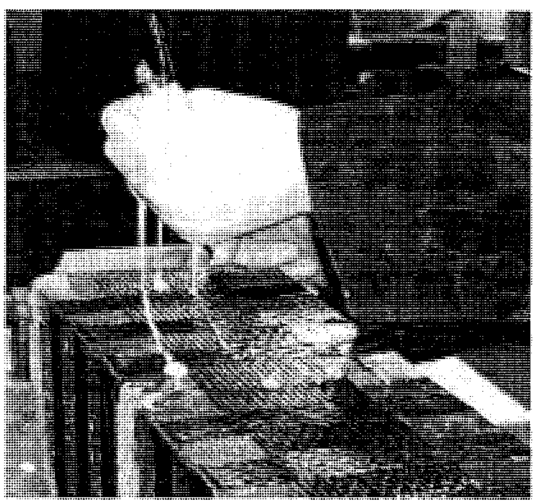

(a) - Compressing Epoxy out of Roller

(b) - Tapping Epoxy by Hand

Figure 3.13 - Saturation of CFRP Sheet on Specimen

Cross wraps (carbon fiber strips placed in the direction normal to the main carbon fiber) were cut to have a length equivalent to the specimen's envelop plus an overlap that equaled their width in order to minimize wrap failure (Figures 3.14 and 3.15). They were bonded to the specimen using the same method as mentioned above for the layers.

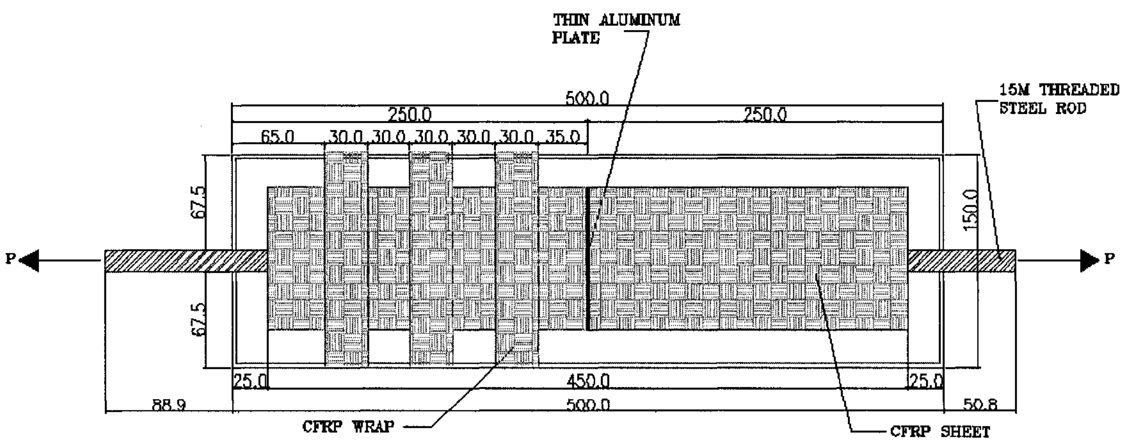

(a) - Cross Wrap Design for Specimens with 450 mm long CFRP Sheets (All Dimensions in mm)

(b) - Photo of the L450W100 Specimen

Figure 3.14 – Specimen L450W100 Layout

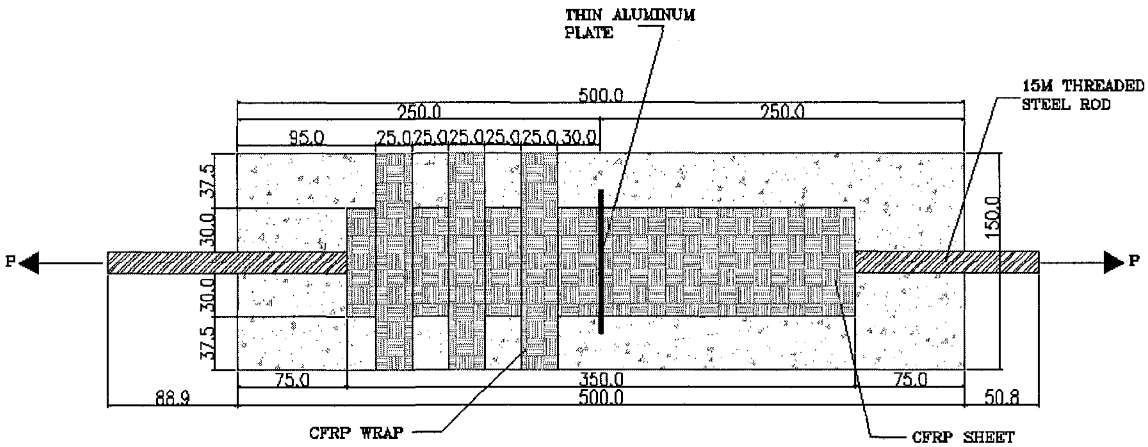

(a) - Cross Wrap Design for Specimens with 350 mm long CFRP Sheets (All Dimensions in mm)

(b) - Photo of the L350W75 Specimen

Figure 3.15 - Specimen L350W75 Layout

After the CFRP was applied to the concrete specimen, the specimens were wrapped with a thin plastic sheet to ensure a smooth and nice finished surface after curing, and to keep all the dust and debris off. This is very important since the strain gauges need a smooth and leveled surface for their proper installation and bonding. The specimens were kept wrapped at room temperature for seven days prior to testing.

3.4 Instrumentation

The instrumentations used in this study were: strain gauges 5 mm long with 350 ohm resistance (Omega brand) to measure the CFRP strain, an LVDT (Linear Voltage Differential Transformer) to measure the specimen's global deflection, a testing machine to perform the test, and a data acquisition system to collect the readings from the strain gauges and reproduce the strain at desired locations.

3.4.1 Strain Gauges

The strain gauges used in this study are from Omega Engineering Inc. They are designated as SGD-5/350-LY11, indicating that they are 5mm long strain gauges having a resistance of 350 Ohms. They are encapsulated with ribbon leads matched to steel. They have an tolerance of ±0.25%, and a gauge factor of 2.00. Figure 3.16(a) and Figure 3.16(b) show the strain gauge locations for specimens with 450 mm long CFRP sheets and specimens with 350 mm long CFRP sheets, respectively. Therefore, a total of seven and six strain gauges for the L450 specimens and the L350 specimens, respectively were used. These strain gauges were installed in the longitudinal (x-axis) direction.

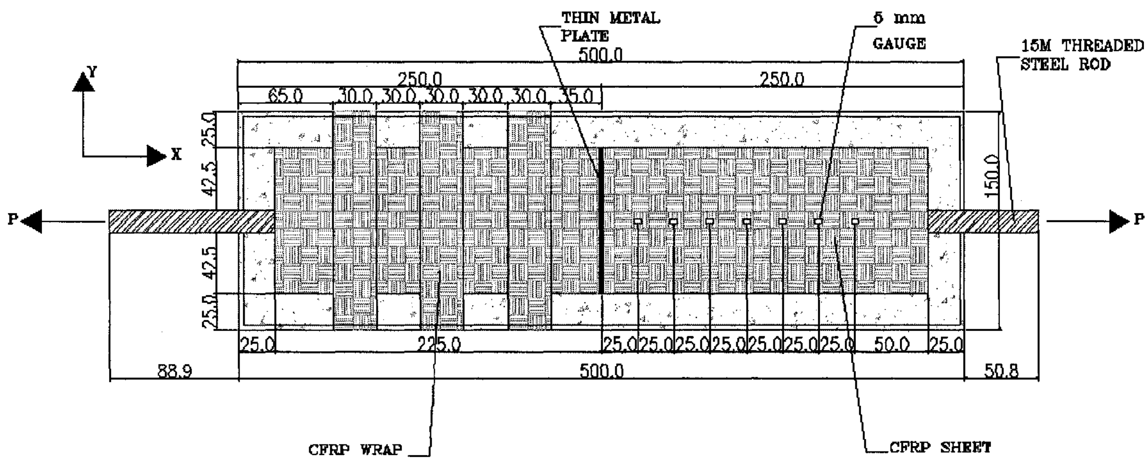

(a) – Specimens with 450 mm long CFRP Sheets

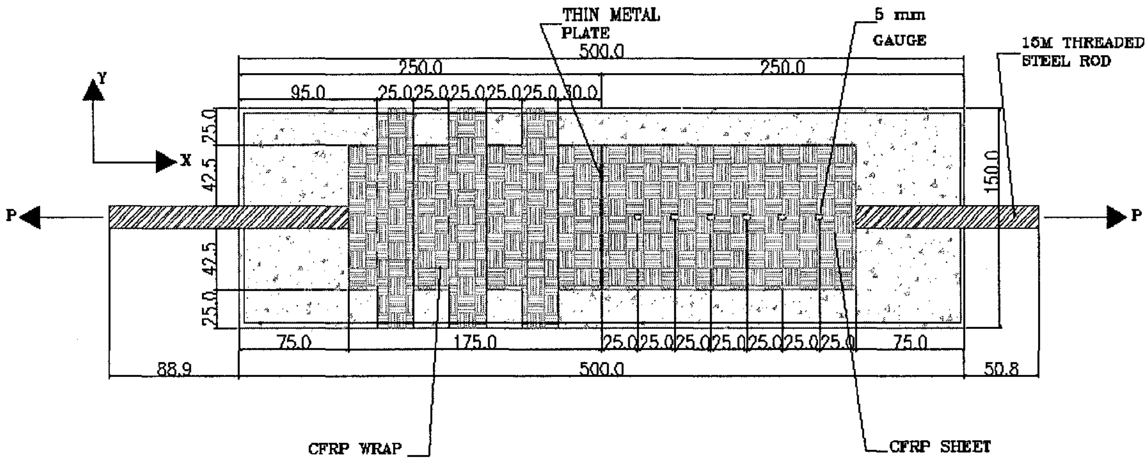

(b) - Specimens with 350 mm long CFRP Sheets

Figure 3.16 – Strain Gauge Locations (All Dimensions in mm)

Four specimens had two additional strain gauges in the transverse (y-axis) direction 30 mm away from the strain gauge nearest to the centre across the width of the specimen on either side. Therefore, a total of two transverse (y-axis) strain gauges were installed on each of these specimens. Their purpose was to verify whether the strain value changes in that direction (Figure 3.17). Those specimens were: L450W100L1SW2, L450W75L1SW2, L350W100L1SW2, and L350W75L1SW2 (Table 3.1).

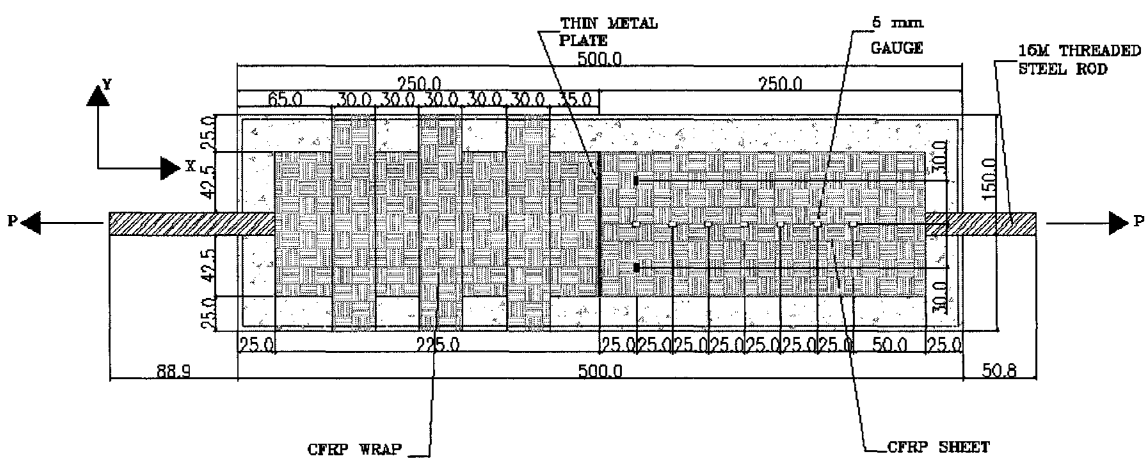

Figure 3.17 - Strain Gauges Installed in Transverse Direction (All Dimensions in mm)

Before installation of the strain gauges on the top surfaces of the CFRP composite, their desired locations were lightly sanded with sand paper. That process is important since it provides a very smooth and leveled finish for the strain gauges to work as accurately as possible. Next, the surface was rubbed with a water-based acidic surface cleaner, MCA-1 M-prep conditioner A, by a paper towel to remove any loose particles. Then, MN5A-1 M-prep neutralizer 5A, which is a water-based alkaline surface cleanser, was applied to neutralize the acid from the surface. Care was taken in rubbing the conditioner and neutralizer against the surface in a single stroke only for maximum effect.

It is worth noting that only tweezers were used to handle the strain gauges, since this would prevent contamination of the contact surface. First, the gauge and strain relief terminals were placed on a clean surface with their bonding side down. Next, a piece of Cellophane tape was aligned over the strain gauge. Then, the strain gauge was picked up by the tape and aligned in the appropriate location. After the gauge was repositioned as necessary, the tape was lifted from the end opposite the strain relief terminals until the gauge and terminals were clear of the surface. The tape was then folded and tacked behind the gauge.

A Catalyst-C, which is a catalyst for use with certified M-bond adhesive, was brushed on the bonding area sparingly in a thin and uniform coat. Subsequent to un-tacking the end of the tape farthest from the bonding area, a single drop of M-bond 200 was applied to the region of the tape and the surface nearest the bonding area. Immediately after, thumb pressure was applied to the tape directly over the gauge for one to two minutes. The thumb's heat helps in setting the adhesive. After approximately two additional minutes have passed, the tape was removed from the gauge assembly by peeling it back carefully. All chemicals cited in this section were obtained from Vishay Ltd.

Prior to securing the strain gauges in place, the gauge terminals were soldered with the conductors of the lead wire cable. The wire assembly was taped in place using a PVC electrical tape. All wires were labeled by attaching a piece of drafting tape at their ends and assigning them different channel numbers. Their effectiveness was confirmed prior to each step of installation using a digital multimeter.

3.4.2 Linear Voltage Differential Transformer (LVDT)

Global deformation in x-direction was continuously monitored and acquired by installing an LVDT on the side of each specimen as illustrated in Figure 3.17. A 152 mm LVDT #3 with a free core was used. The gauge length for measuring deformation was 432 mm (17 in) of the specimen's length. It was pre-calibrated shortly before the first test was conducted.

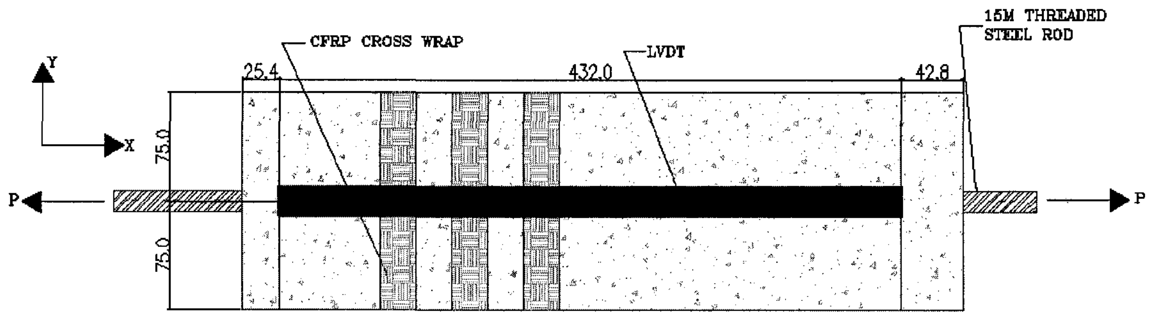

(a) - LVDT Location
(All Dimensions in mm)

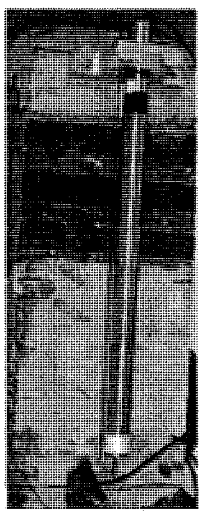

(b) – LVDT Photo

Figure 3.18 - LVDT Location on the Specimen

3.4.3 Test Machine

The Tinius Olsen Universal Testing Machine was used to perform the tensile tests. It is a hydraulic testing machine with a capacity of 300 kN (60,000 lbs). The maximum load capacity expected is set on the machine, and the load readings were acquired through a data acquisition system (Figure 3.19).

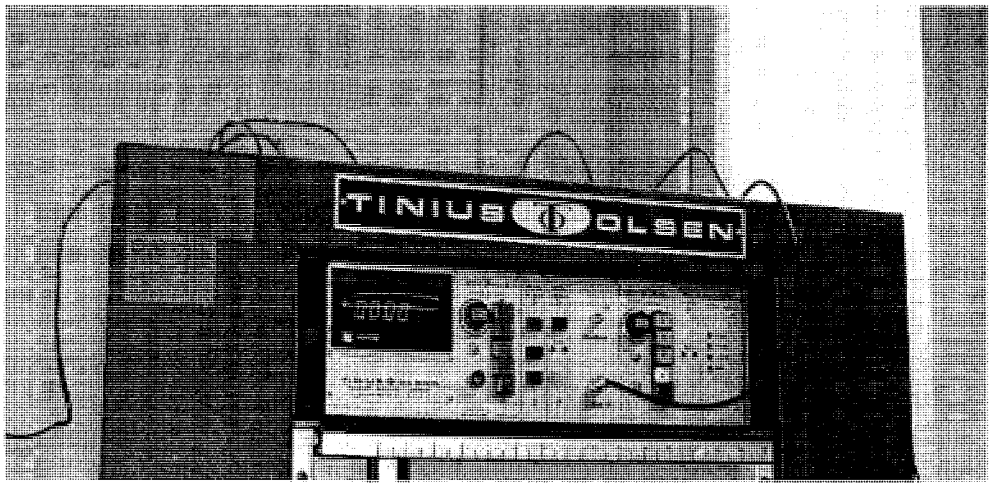

Figure 3.19 - Tinius Olsen Machine Controller

3.4.4 Data Acquisition System

The data acquisition system "Data Scan 7021" was used in this study. It is manufactured by Adept Scientific situated in England. Each module has eight channels.

Two modules were installed in the data acquisition system, since some specimens required up to nine quarter bridge strain channels. In addition to that, one channel was needed for the load obtained from the Tinius Olsen machine, and another for the LVDT displacement. The data scanning speed was adjusted to collect one reading every second. All data was transferred to the computer via the Dalite software, which stored all findings in computer files.

3.5 Test Set-up

The test set up followed the recommended guideline of CSA S806-02 (Canadian Standards Association, 2002), test method A of Annex P. Each specimen was mounted carefully on the Tinius Olsen machine as illustrated in Figure 3.20. To fulfill the machine's clearance requirements, the side with the longer steel bar (88.9 mm) was connected to the upper (fixed) cross-head of the machine, whereas the side with the shorter steel bar (50.8 mm) was mounted on the lower (moving) cross-head of the machine. For specimens with cross wraps on one side only, the cross wraps were bonded to the side with the longer steel bar. The load was controlled manually via a wheel attached to the machine at a rate of 11 kN/min. Since the test machine used does not allow controlling the rate automatically, a stop watch was used while the technician was controlling the wheel in order to ensure accuracy. After cracking of concrete, the test was continued until the CFRP debonded, and then the specimen was considered as failed (Figure 3.21).

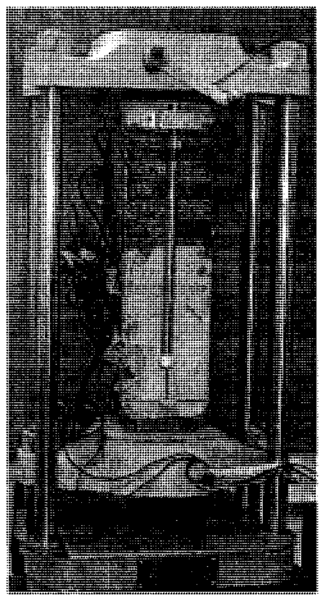

Figure 3.20 - Test Set-up

Figure 3.21 - CFRP Debonding

The load from the machine, the LVDT, and all strain gauges were checked and connected to the data acquisition system that was hooked up to the computer to collect and store all test data.

CHAPTER 4
EXPERIMENTAL RESULTS AND ANALYSIS

4.1 General

The objective of this study is to investigate the mechanical behaviour at the interface between the Carbon Fiber Reinforced Polymer (CFRP) sheet and the concrete. The effectiveness of the bond, which is the means to develop composite action by the stress transfer between concrete and CFRP, is thought to be affected by various variables. Only those that are believed to be of crucial importance were investigated in this research. The composite's length and width are critical parameters because they are part of the equation used to calculate the average bond strength (equation 4.3, section 4.7). The composite's stiffness (stiffness = thickness x elastic modulus) is a factor of the effective length equation (equation 4.10, section 4.8), and hence should be examined. It is important to observe the influence of the concrete surface preparation since that affects the load required for debonding. Finally, it is known that the main task of cross wraps is to prevent debonding to occur in a desired area. Therefore, the amount of cross wraps definitely plays an important role in the behaviour of the concrete-CFRP interface.

The test results and failure mechanisms for all specimens are discussed in this chapter. After performing the test for each specimen, strain versus position from center (midspan) of the specimen, and load versus displacement charts were prepared based on data collected from the strain gauges and the LVDT, respectively. Then, the following charts were reproduced: average stress versus average slip, average stress versus gauge distance, average stress versus normalized load (F/F_{max}), effective bond length versus CFRP stiffness, average bond strength versus bond width and average bond strength versus bond length. It should be noted that because of the massive number of charts, those that were thought to best represent each group both qualitatively and quantitatively are included in this chapter. All others can be found in the appendices.

Table 4.1 is a summary of all test results and failure modes. It was found that the maximum load increased whereas displacement decreased when (a) increasing the CFRP stiffness, (b) the effective bond length, (c) the effective bond width, (d) when having a rough surface, or having cross wraps on both halves of the specimen.

Table 4.1(a) - Test Matrix and Test Results for Group 1

GROUP #	SPECIMEN DESIGNATION	MAX. LOAD (KN)	AVERAGE BOND STRENGTH (Mpa)	MAX. STRAIN (με)	EFFECTIVE LENGTH (mm)	STIFF. (KN/mm)	Δ_{20} (mm)	FAILURE TYPE
CNTRL	**Control 1**	**22**					**0.442**	
	Control 2	**21**					**0.475**	
1	L450W100L1SW1	26	0.29	6,892.93	52	28	0.084	Type: debonding at S.G. side Location: lower portion of specimen
	L450W100L1SW2	39	0.43	4,684.88	150	28	0.013	Type: debonding at S.G. side Location: centre of specimen
	L450W100L1RW1	40	0.44	6,597.34	68	28	0.008	Type: debonding at S.G. side Location: lower portion of specimen
	L450W100L1RW2	42	0.47	8,356.00	118	28	0.094	Type: debonding at S.G. side Location: lower portion of specimen
	L450W100L2SW1	42	0.47	4,749.92	56	56	0.013	Type: debonding at no S.G. side Location: lower portion of specimen
	L450W100L2SW2	50	0.56	5,228.89	110	56	0.038	Type: wrap failure & debonding at S.G. side Location: lower portion of specimen
	L450W100L2RW1	43	0.48	3,792.00	163	56	0.010	Type: debonding at S.G. side Location: lower portion of specimen
	L450W100L2RW2	45	0.50	4,952.66	37	56	0.180	Type: debonding at S.G. side Location: lower portion of specimen

Table 4.1(b) - Test Matrix and Test Results for Group 2

GROUP #	SPECIMEN DESIGNATION	MAX. LOAD (KN)	AVERAGE BOND STRENGTH (Mpa)	MAX. STRAIN (με)	EFFECTIVE LENGTH (mm)	STIFF. (KN/mm)	Δ_{20} (mm)	FAILURE TYPE
2	L450W75L1SW1	23	0.34	3,241.22	56	28	0.010	Type: debonding at no S.G. side Location: lower portion of specimen
	L450W75L1SW2	26	0.38	4,243.08	109	28	0.030	Type: debonding at S.G. side Location: upper portion of specimen
	L450W75L1RW1	21	0.31	2,763.12	97	28	0.167	Type: debonding at no S.G. side Location: lower portion of specimen
	L450W75L1RW2	27	0.40	4,894.37	78	28	0.018	Type: debonding at no S.G. side Location: upper portion of specimen
	L450W75L2SW1	40	0.59	4,157.77	118	56	0.010	Type: debonding at S.G. side Location: lower portion of specimen
	L450W75L2SW2	38	0.56	3,917.86	51	56	0.038	Type: debonding at no S.G. side Location: lower portion of specimen
	L450W75L2RW1	28	0.41	4,155.22	58	56	0.036	Type: debonding at S.G. side Location: lower portion of specimen
	L450W75L2RW2	40	0.59	4,525.22	105	56	0.094	Type: debonding at S.G. side Location: upper portion of specimen

Table 4.1(c) - Test Matrix and Test Results for Group 3

GROUP #	SPECIMEN DESIGNATION	MAX. LOAD (KN)	AVERAGE BOND STRENGTH (Mpa)	MAX. STRAIN ($\mu\varepsilon$)	EFFECTIVE LENGTH (mm)	STIFF. (KN/mm)	Δ_{20} (mm)	FAILURE TYPE
3	L350W100L1SW1	33	0.47	5,528.76	77	28	0.208	Type: debonding at no S.G. side Location: lower portion of specimen
	L350W100L1SW2	27	0.39	3,402.57	150	28	0.074	Type: debonding at no S.G. side Location: lower portion of specimen
	L350W100L1RW1	36	0.51	6,082.90	59	28	0.023	Type: debonding at S.G. side Location: lower portion of specimen
	L350W100L1RW2	38	0.54	4,488.05	110	28	0.020	Type: wrap failure & debonding at no S.G. side Location: upper portion of specimen
	L350W100L2SW1	44	0.63	4,287.86	80	56	0.018	Type: debonding at S.G. side Location: lower portion of specimen
	L350W100L2SW2	43	0.61	2,917.70	54	56	0.013	Type: wrap failure & debonding at no S.G. side Location: upper portion of specimen
	L350W100L2RW1	42	0.60	3,400.89	78	56	0.064	Type: wrap failure & debonding at S.G. side Location: lower portion of specimen
	L350W100L2RW2	46	0.66	3,716.81	46	56	0.142	Type: debonding at no S.G. side Location: upper portion of specimen

Table 4.1(d) - Test Matrix and Test Results for Group 4

GROUP #	SPECIMEN DESIGNATION	MAX. LOAD (KN)	AVERAGE BOND STRENGTH (Mpa)	MAX. STRAIN ($\mu\varepsilon$)	EFFECTIVE LENGTH (mm)	STIFF. (KN/mm)	Δ_{20} (mm)	FAILURE TYPE
4	L350W75L1SW1	25	0.47	5,867.51	78	28	0.008	Type: debonding at S.G. side Location: lower portion of specimen
	L350W75L1SW2	21	0.40	6,234.34	58	28	0.790	Type: debonding at no S.G. side Location: upper portion of specimen
	L350W75L1RW1	20	0.38	2,942.20	58	28	0.140	Type: debonding at no S.G. side Location: lower portion of specimen
	L350W75L1RW2	36	0.69	8,171.92	73	28	0.046	Type: debonding at S.G. side Location: centre of specimen
	L350W75L2SW1	34	0.65	2,399.04	53	56	0.013	Type: debonding at no S.G. side Location: lower portion of specimen
	L350W75L2SW2	32	0.61	4,075.82	36	56	0.074	Type: debonding at S.G. side Location: lower portion of specimen
	L350W75L2RW1	34	0.65	3,122.97	125	56	0.076	Type: debonding at S.G. side Location: lower portion of specimen
	L350W75L2RW2	42	0.80	4,531.98	50	56	0.020	Type: debonding at no S.G. side Location: lower portion of specimen

4.2 Load versus Displacement Response

The load versus displacement charts are presented in this section. The load data was acquired from the Tinius Olsen machine, and the displacement data was obtained from a Linear Voltage Differential Transformer (LVDT) over a gauge length of 432 mm. The LVDT was installed on the specimen (Figure 4.1), and was removed when the load reached 20 kN to avoid any damage in the LVDT. Table 4.2 and Figure 4.2 illustrate the load-displacement behaviour for the two control specimens that were tested. In Figure 4.2, a little discontinuity (point A for control 1 and point C for control 2) takes place at a load of 5 kN suggesting that some slippage was present between the steel bar and the machine's cross-head grips at the beginning of the test. Once the grips were tightened, a change in slope is noticed. The slope of the load-displacement curve changes again at point B for control 1 and point D for control 2, which indicates that cracks in concrete initiated and grew making the load-displacement curve softer.

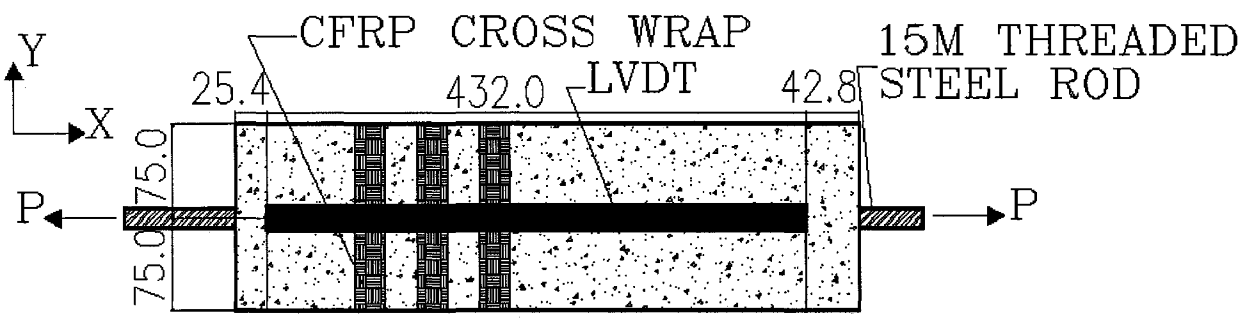

Figure 4.1 - LVDT Location (All Dimensions in mm)

Table 4.2 - Load versus Displacement Data for the Control Specimens

LOAD (kN)	DISPLACEMENT (mm)		REMARKS
	Control 1	Control 2	
0	0.00	0.00	
5	0.15	0.14	
10	0.22	0.21	
15	0.30	0.32	
20	0.44	0.48	LVDT removed

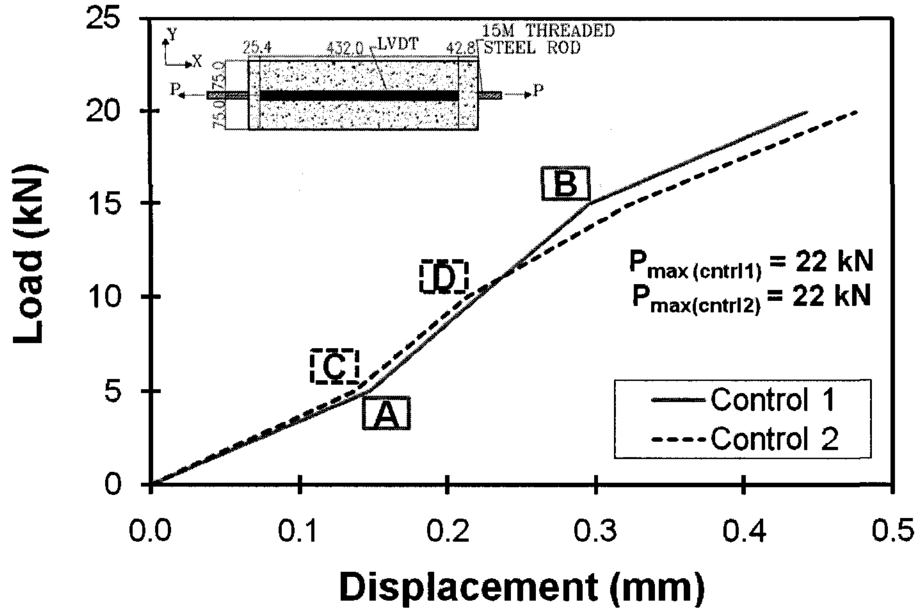

Figure 4.2 - Load vs. Displacement for the Control Specimens

CFRP's Stiffness Effect:

Figure 4.3 shows the load versus displacement behaviour for specimens with one and two CFRP layers. By comparing the two specimens, it can be seen that up to a load of 30 kN (F/F_{max} = 0.71), the load versus displacement curve data points for the specimen with two CFRP layers are present at a displacement that is less than 0.05 mm. That value is surpassed when the load exceeds 10 kN (F/F_{max} = 0.38) for the specimen with one CFRP layer. Moreover, the latter has a displacement value that is almost 6.5 times that of the former ($\Delta_{20\ (\text{one CFRP layer})}$ = 0.084 mm, $\Delta_{20\ (\text{two CFRP layers})}$ = 0.013 mm). It is because of that difference that the load versus displacement curve appears to be more concave for the specimen with two CFRP layers. This all suggests that displacement decreases significantly when the stiffness of CFRP increases.

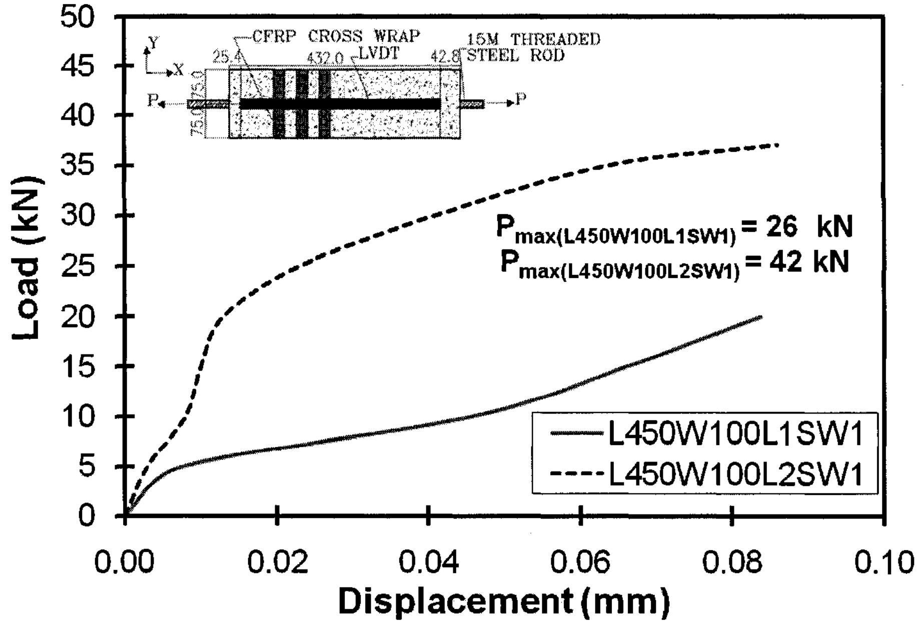

Figure 4.3 - Load versus Displacement for L450W100L1SW1 and L450W100L2SW1

Bond Length Effect:

Figure 4.4 show the load-displacement behaviour for specimens with a bond length of 450 mm (L450) and 350 mm (L350). It is found that the displacement for the L450 specimen at a 20 kN load is larger than the displacement for the L350 specimen ($\Delta_{L450(20\ kN)} = 1.3\ \Delta_{L350(20\ kN)}$). This indicates that increasing the bond length would give more displacement. The maximum loads for specimens L450 and L350 are 40 kN and 34 kN, respectively. Therefore, the maximum load carrying capacity for the L450 specimen was 16% higher than the L350 specimen. The load-displacement behaviour for other L450 and L350 specimens is comparatively similar.

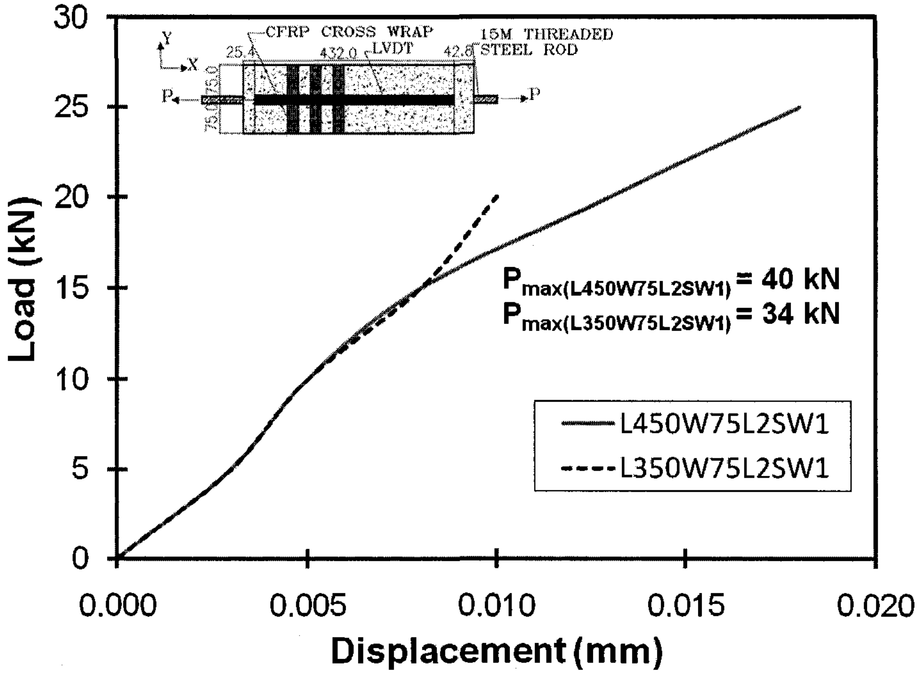

Figure 4.4 - Load versus Displacement for L450W75L2SW1 and L350W75L2SW1

Bond Width Effect:

Figure 4.5 demonstrates the difference in load versus displacement behaviour for specimens with different bond widths (100 mm and 75 mm). It can be seen that the specimen with a bond width of 100 mm (W100) has a larger displacement value than the specimen with a bond width of 75 mm (W75). At a load of 20 kN, $\Delta_{W100} = 5.2\ \Delta_{W75}$ ($\Delta_{W100} = 0.094$ mm, whereas $\Delta_{W75} = 0.018$ mm). This significant difference in displacement values along with the variation in the maximum load values ($P_{max(W100)} = 42$ kN and $P_{max(W75)} = 27$ kN) gives the W100 load versus displacement curve more concavity than that of W75. This all concludes that increasing the bond width increases displacement. Since the displacement values are affected by changing both the bond width and the bond length, it can be stated that a smaller bond area gives less displacement, and vice versa.

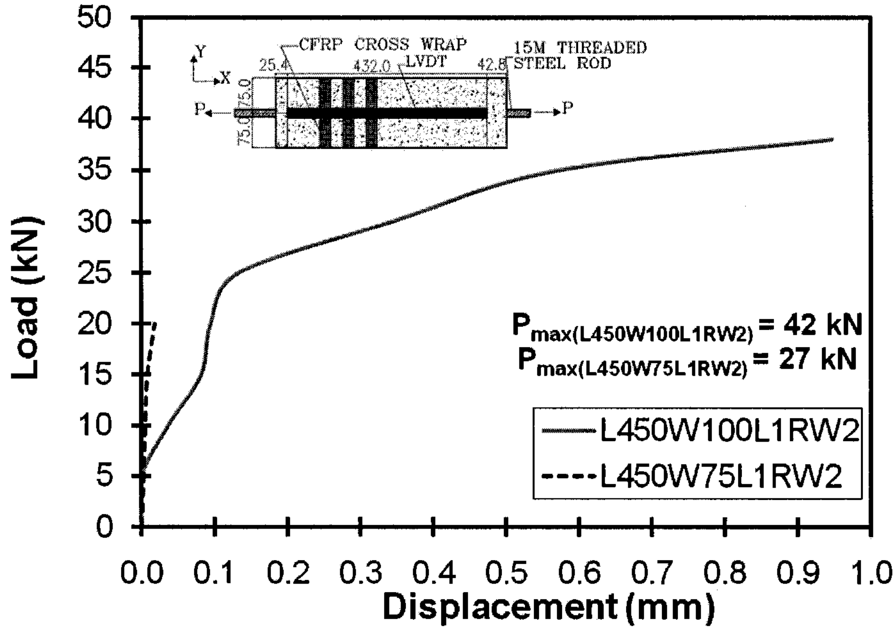

Figure 4.5 - Load versus Displacement for L450W100L1RW2 and L450W75L1RW2

Surface Preparation Effect:

Figure 4.6 shows the load-displacement curves for two specimens that have different surface preparations (rough and smooth). The displacement value at a load of 20 kN for the specimen with smooth surface at maximum load is 3.4 times that for the specimen with rough surface ($\Delta_{S(20\ kN)} = 0.092$ mm, $\Delta_{R(20\ kN)} = 0.027$ mm). The load versus displacement curve for the specimen with smooth surface is almost linear, whereas the load-displacement for rough surface specimen is tri-linear. The latter (specimen with rough surface) does not allow much elongation before debonding. The maximum load value obtained for the smooth surface specimen is 27 kN, whereas that for rough surface specimen is 38 kN (34% higher than the smooth surface specimen). It is concluded that preparing the specimen to have a rough surface would decrease displacement but increase the load carrying capacity.

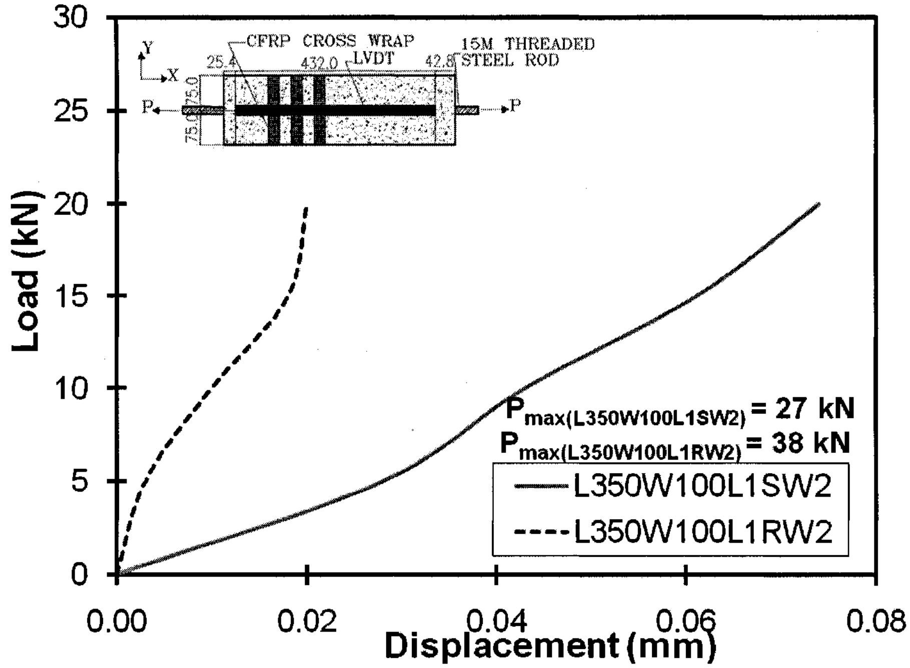

Figure 4.6 - Load versus Displacement for L350W100L1SW2 and L350W100L1RW2

Cross Wraps Effect:

Many researchers (De Lorenzis *et al. (2001)*, Nakaba *et al. (2001)*, Sato *et al. (2001)*, and Ueda *et al. (1998)*) placed cross wraps on one half of their specimens to avoid bond failure in that area. Their studies indicate that use of cross-wraps on both halves minimizes bond failure. Figure 4.7 illustrates the effect of cross wraps placed on one half (W1 specimen) or both halves (W2 specimen) of the specimen on the load versus displacement curve. The displacement value at 20 kN load is 0.14 mm for the specimen having cross wraps on one half of the specimen. For the specimen having cross wraps on both halves, however, this value dropped to 0.05 mm. This verifies that having cross wraps on both halves of the specimen reduces displacement, and thus reduces the bond failure.

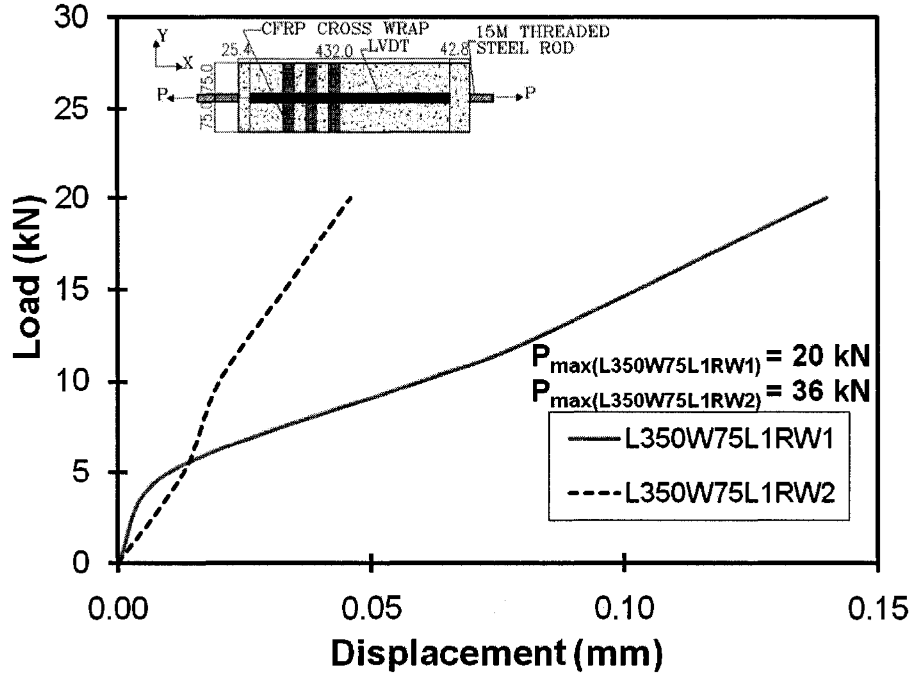

Figure 4.7 - Load versus Displacement for L350W75L1RW1 and L350W75L1RW2

4.3 Strain Distribution

As stated in chapter 3, seven strain gauges were installed along the length of all L450 specimens at an interval of 25 mm starting at 25 mm away from the specimen's centre (mid-span, x = 0 mm) (Figure 3.16(a)). Six strain gauges were installed along the length of all L350 specimens at the same interval (Figure 3.16(b)). In order to verify the strain distribution across the width of the specimen, two additional strain gauges were installed at 30 mm away from the strain gauge nearest to the centre across the width of four specimens on either side (Figure 3.17) (namely, L450W100L1SW2, L450W75L1SW2, L350W100L1SW2, and L350W75L1SW2).

4.3.1 Longitudinal Strain Distribution

The test data obtained from the strain gauges was used to generate the strain versus distance from midspan (x = 0 mm) of the specimen. Figures 4.8 – 4.11 illustrate the strain behaviour at the various strain locations for the specimens (Table 4.3). Similar plots for other specimens are shown in Appendix A. Each curve is plotted for a specific load level. As the load increases, the strain values increase and more strain gauges become active. This behaviour demonstrates that more bond area is activated as the load level is increases. Some strain can be noted further than the location of the farthest strain gauge (i.e. when x > 175 mm) in some specimens. For example, some strain is still present beyond point Y in Figure 4.8. This indicates the possibility of slip occurring at that location.

Table 4.3 - Specimen Groups Details

Group	Specimen Designation	Length (mm)	Width (mm)
1	L450W100	450	100
2	L450W75	450	75
3	L350W100	350	100
4	L350W75	350	75

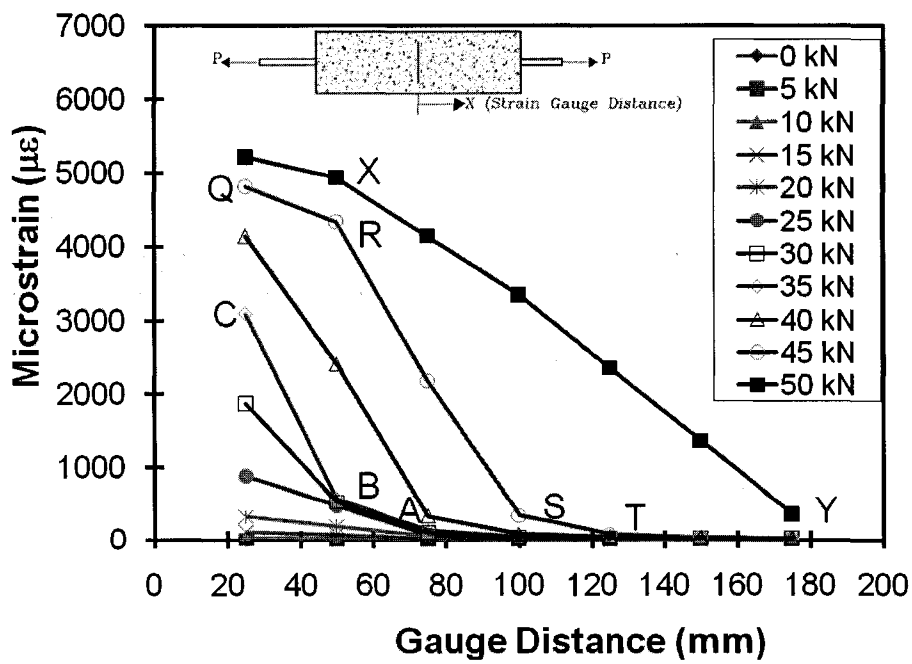

Figure 4.8 – Strain versus Gauge Distance for Group 1

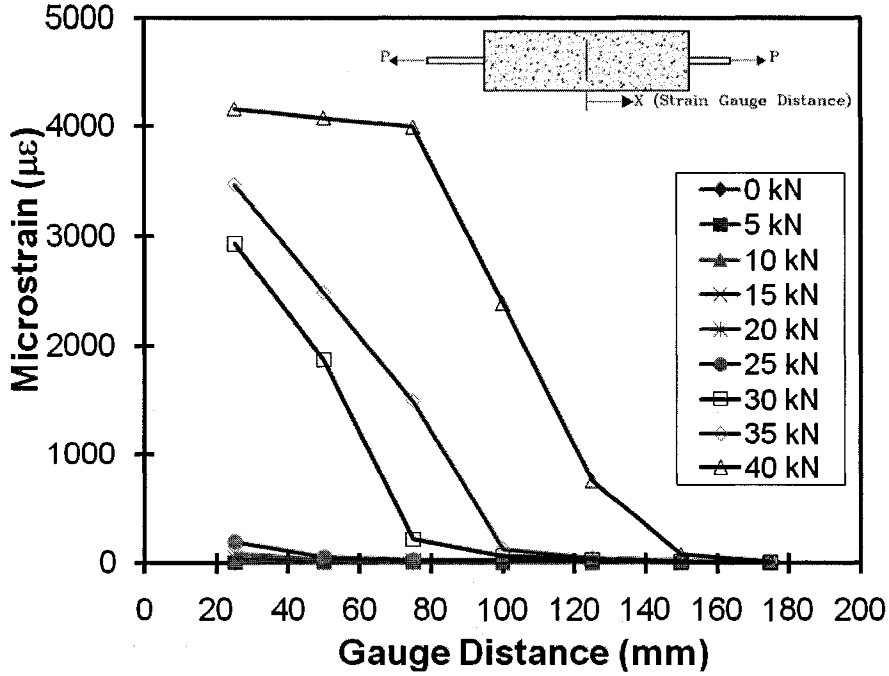

Figure 4.9 – Strain versus Gauge Distance for Group 2

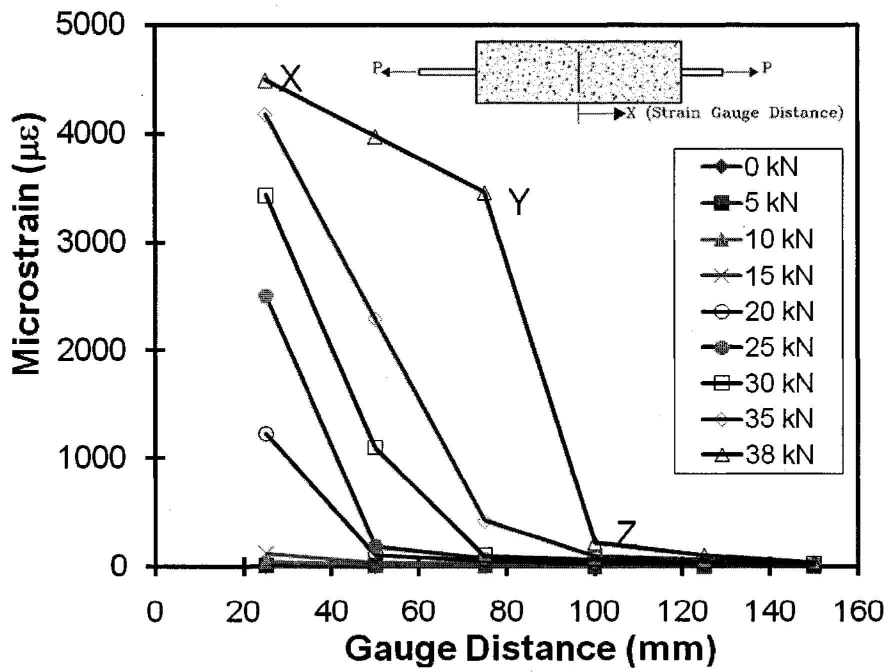

Figure 4.10 - Strain versus Gauge Distance for Group 3

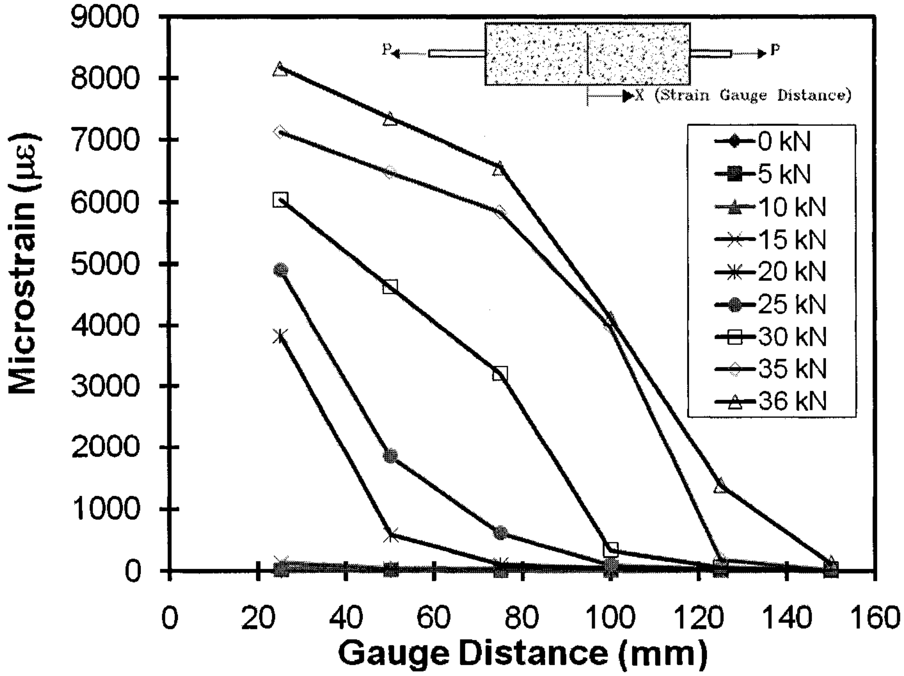

Figure 4.11 – Strain versus Gauge Distance for Group 4

By comparing Figures 4.8 – 4.11 for two different bond lengths (450 mm and 350 mm), and two different bond widths (100 mm and 75 mm), it can be seen that at the earlier stages of loading, there is a resemblance in the strain versus distance. They all depict a non linear shape and strain gauges that are far away from the specimen's midspan show negligible strain readings. However, as the load increases, the curves become more linear in shape. It can be assumed that bond failure commences shortly after the point when the curve becomes linear. For example, a large segment of the curve reflecting the strain versus distance behaviour at a load of 50 kN in Figure 4.8 has a linear slope (segment XY). This agrees with findings of De Lorenzis et *al.* (2001) and indicates that a uniform bond stress is achieved as the maximum load is reached.

The strain distribution is concave at lower loads (for example, segment ABC at 35 kN in Figure 4.8), and then changes into a convex shape as the load reaches 70% or more of the maximum load (for example, segment QRST in Figure 4.8 at 45 kN). This agrees with what Kamel et *al.* (2006) observed. The change in the strain distribution gradient (slope) between consecutive ascending load ranges followed by a significant increase in the strain values (for example, in Figure 4.10, there is a considerable increase in the strain value at a strain gauge distance of 25 mm when the load increases from 15 kN to 20 kN) is due to the inability of the stress to be transferred as fast as the strain values change. Hence, the debonding of the CFRP sheet is signaled by a rapid increase in the strain values that takes place at gauge distances closest to midspan.

Bond Width Effect:

From Figures 4.12 and 4.13, it can be observed that the sudden increase in the strain values (i.e. maximum difference between two consecutive strain values) is more pronounced in specimens with smaller bond width. For instance, by examining the data in Tables 4.4 and 4.5 at a gauge distance of 25 mm and a load range of 15 kN – 20 kN, it can be seen that the increase percentage in strain value is 275% for the specimen with a 75 mm bond width (strains of 784.8 $\mu\varepsilon$ versus 2942.2 $\mu\varepsilon$). That percentage is only 99% for the specimen with a 100 mm bond width (strains of 867.5 $\mu\varepsilon$ versus 1723.3 $\mu\varepsilon$). This indicates that debonding of CFRP is faster in specimens with narrower bond width. Thus, the maximum load value increases but debonding becomes slower as the bond width increases.

Table 4.4 - Strain Distribution Data for L350W100L1RW1

LOAD (kN)	**Gauge Distance (mm)**					
	25	**50**	**75**	**100**	**125**	**150**
0	0.00	0.00	0.00	0.00	0.00	0.00
5	7.60	7.18	6.76	5.07	3.37	1.67
10	11.82	11.26	10.70	10.14	7.60	5.06
15	**867.54**	89.26	55.61	28.30	19.01	16.04
20	**1723.25**	167.25	100.52	46.46	30.41	27.02
25	**4263.35**	1179.24	153.74	70.96	42.23	33.78
30	4981.37	4711.91	429.97	105.59	59.98	42.23
35	5905.50	5106.95	4308.41	3509.86	292.28	72.64
36	6082.90	5725.30	5367.70	5010.10	4878.31	78.72

Table 4.5 - Strain Distribution Data for L350W75L1RW1

LOAD (kN)	Gauge Distance (mm)					
	25	50	75	100	125	150
0	0.00	0.00	0.00	0.00	0.00	0.00
5	6.76	5.92	5.07	4.22	3.37	2.52
10	10.98	10.14	9.29	8.44	7.59	6.74
15	**784.76**	129.24	56.59	38.01	24.50	10.99
20	**2942.20**	1565.87	1269.25	64.20	48.15	19.42

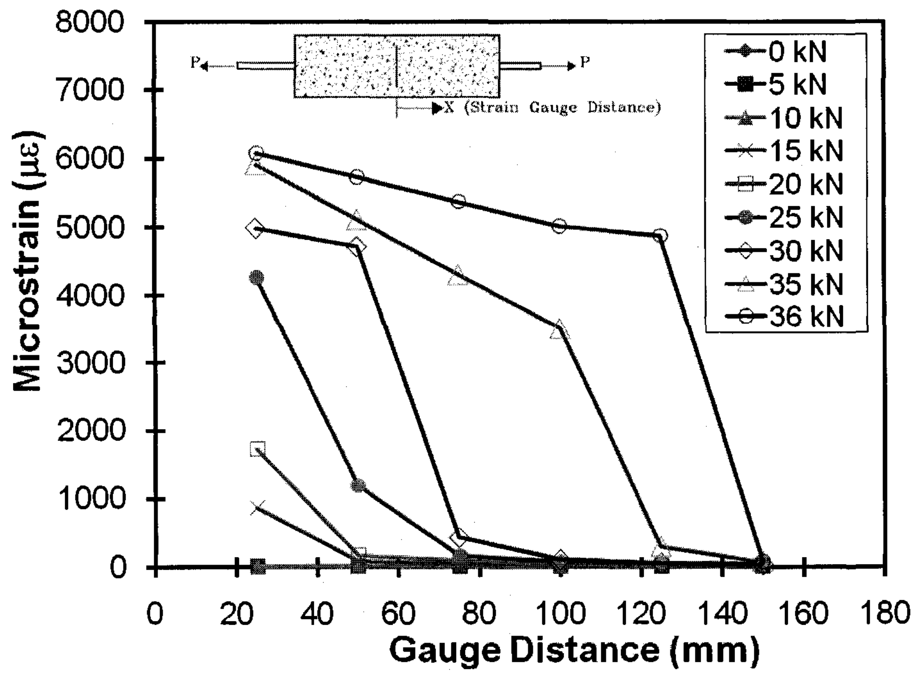

Figure 4.12 - Strain versus Gauge Distance for L350W100L1RW1

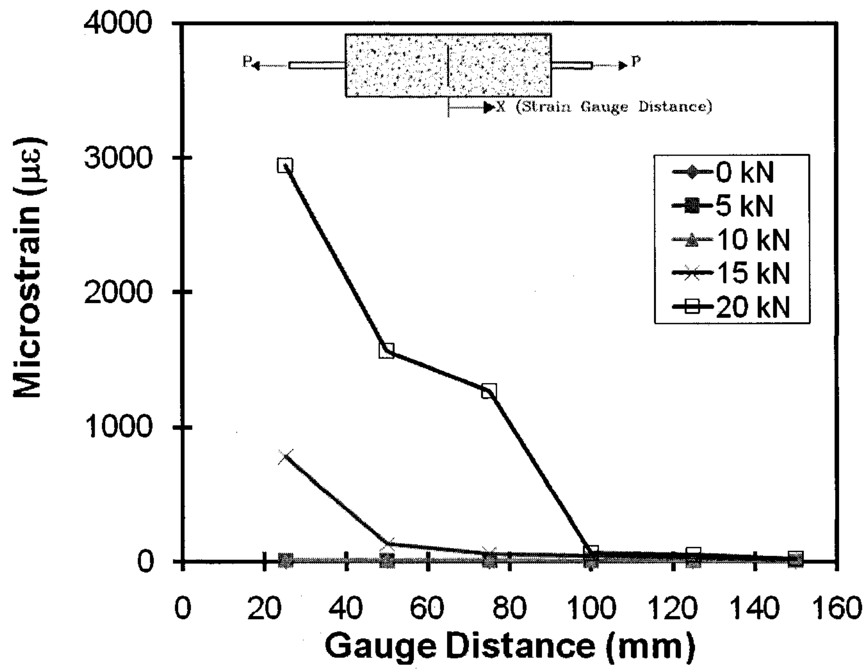

Figure 4.13 - Strain versus Gauge Distance for L350W75L1RW1

Bond Length Effect:

Debonding takes place at the maximum load and as a result, the failure of the specimen occurs. By referring to Figures 4.10 (350 mm bond length) and 4.14 (450 mm bond length), it is observed that changing the bond length affects the behaviour of the strain versus distance curve at maximum load. Line XYZ in Figure 4.10 (specimen L350W100L1RW2) has a steeper slope and more non-linearity than line ABC in Figure 4.14 (specimen L450W100L1RW2). This indicates that the specimen with shorter bond length (350 mm) failed rapidly, whereas failure of the specimen with longer bond length (450 mm) happened gradually because of the longer bonded length.

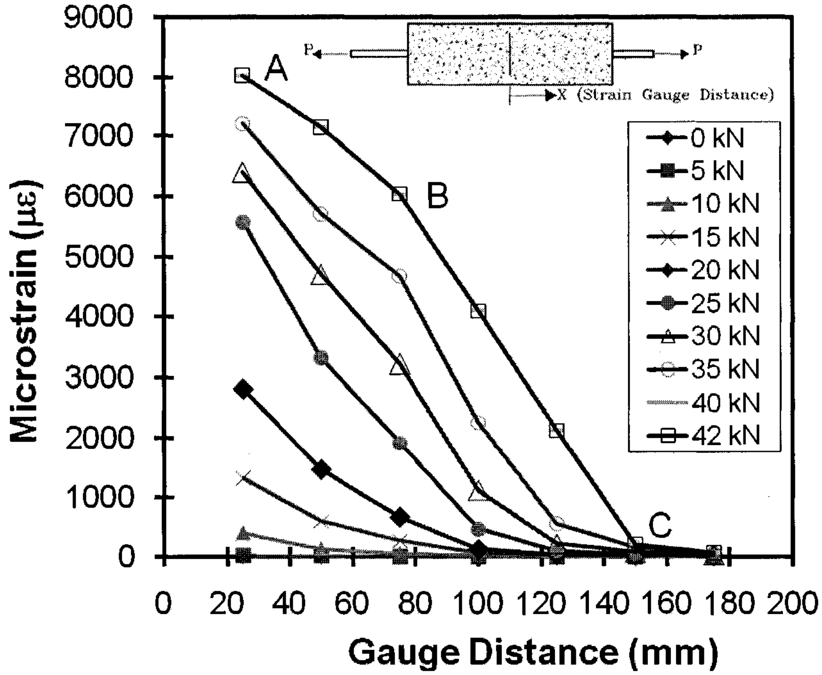

Figure 4.14 - Strain versus Gauge Distance for L450W100L1RW2

CFRP's Stiffness Effect:

It is noted that as the stiffness of CFRP increases, the length of the segment with the steeper slope at maximum load becomes comparatively longer. For example, segment RS in Figure 4.16 for specimen with two CFRP layers is 1.4 times longer than segment TU in Figure 4.15 for specimen with one CFRP layer. This observation indicates that the active bond stress section increases with the stiffness. This finding agrees with the results that Nakaba et *al.* (2001) obtained from their studies.

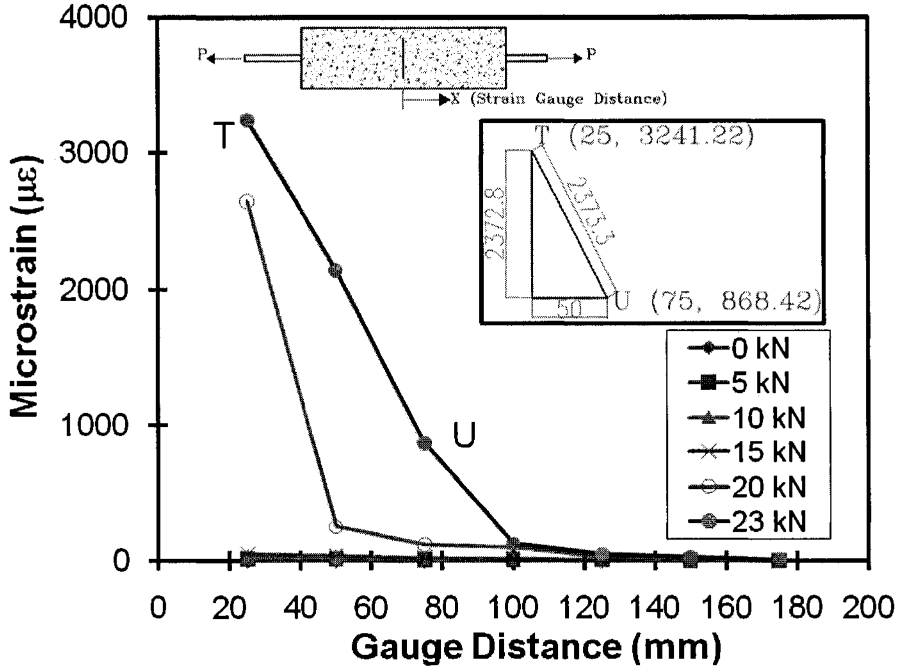

Figure 4.15 - Strain versus Gauge Distance for L450W75L1SW1

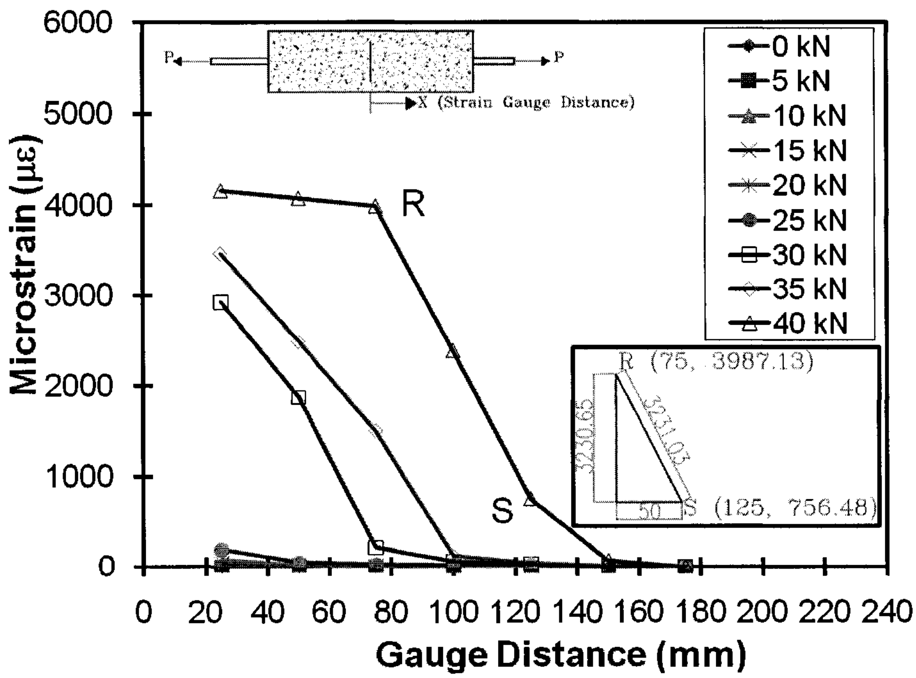

Figure 4.16 - Strain vs. Gauge Distance for L450W75L2SW1

Surface Preparation Effect:

The effect of surface preparation is examined in Figures 4.12 and 4.17. As the load increases, the increase of the strain values for specimens with rough surface (Figure 4.12) was more gradual than those with smooth surface (Figure 4.17). For example, by referring to Tables 4.4 and 4.6, for specimens with rough and smooth surfaces, respectively, it can be observed that the percentage increase of the strain values at a gauge distance of 25 mm and a load range of 20 kN – 25 kN is 335% for the specimen with smooth surface (342.12 $\mu\varepsilon$ versus 1488.41 $\mu\varepsilon$). This percentage is only 147% for the specimen with rough surface (1723.25 $\mu\varepsilon$ versus 4263.35 $\mu\varepsilon$). This indicates that the rough surface enhances the ability of the stress transfer to keep up with the change in strain, and hence debonding occurs at a higher load level. The percent difference in the maximum load (36 kN for the specimen with rough surface, and 33 kN for the specimen with smooth surface), and maximum strain (6,082.9 $\mu\varepsilon$ for the specimen with rough surface, and 5,528.76 $\mu\varepsilon$ for the specimen with smooth surface) is insignificant (less than 10%).

Table 4.6 - Strain Distribution Data for L350W100L1SW1

LOAD (kN)	Distance from Centre (mm) 25	50	75	100	125	150
0	0.00	0.00	0.00	0.00	0.00	0.00
5	6.76	5.07	4.65	4.23	3.39	2.54
10	21.96	15.20	13.09	10.98	9.29	7.60
15	38.85	24.50	19.86	15.21	12.26	9.30
20	**342.12**	119.11	52.37	37.17	26.19	15.21
25	**1488.41**	158.80	66.73	50.69	20.27	17.74
30	4431.46	1502.77	105.59	69.27	29.57	24.50
33	5528.76	2763.12	424.04	129.25	57.45	42.24

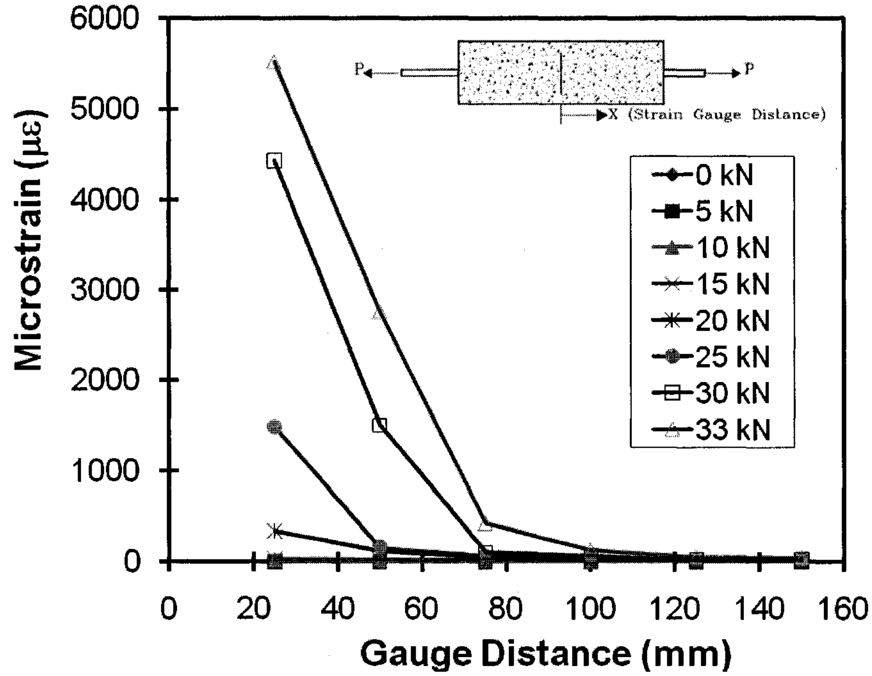

Figure 4.17 - Strain versus Gauge Distance for L350W100L1SW1

Cross Wraps Effect:

The last variable that was studied is the influence of cross wraps on one half or on both halves of the specimen. Figures 4.18 and 4.19 illustrate that the effect of using cross wraps on both halves (Figure 4.19) shows a smaller strain value than the specimen with cross wraps on one half (Figure 4.18) at the same load level and the same distance away from the specimen's centre. For instance, at a gauge distance of 50 mm and a load of 20 kN, the strain value of the latter is 11.8 times that of the former (1668.5 με versus 141.9 με). This indicates that less slip between the CFRP composite and concrete occurs when the number of cross wraps is increased. Comparisons for other specimens are shown in Appendix A, and a similar trend is observed.

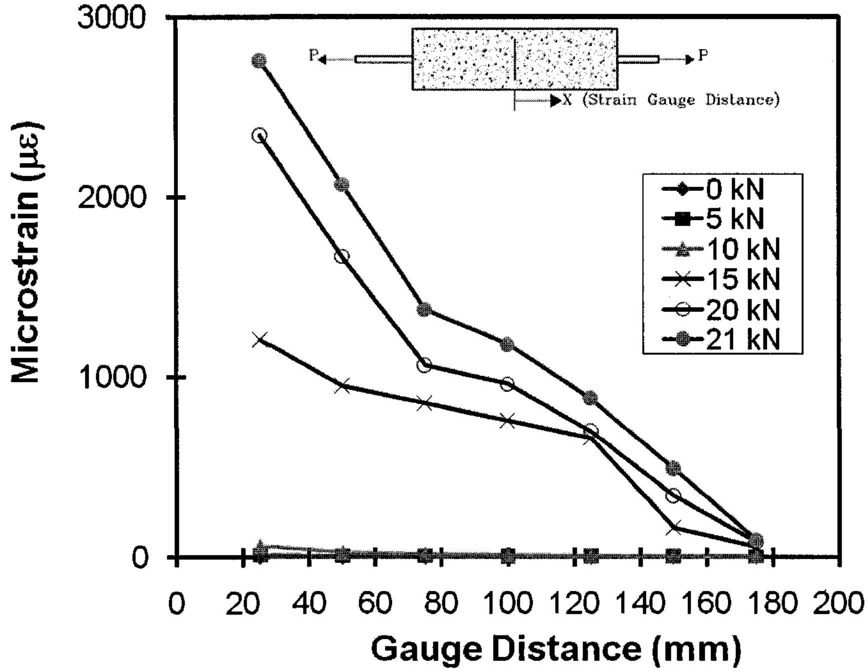

Figure 4.18 - Strain versus Gauge Distance for L450W75L1RW1

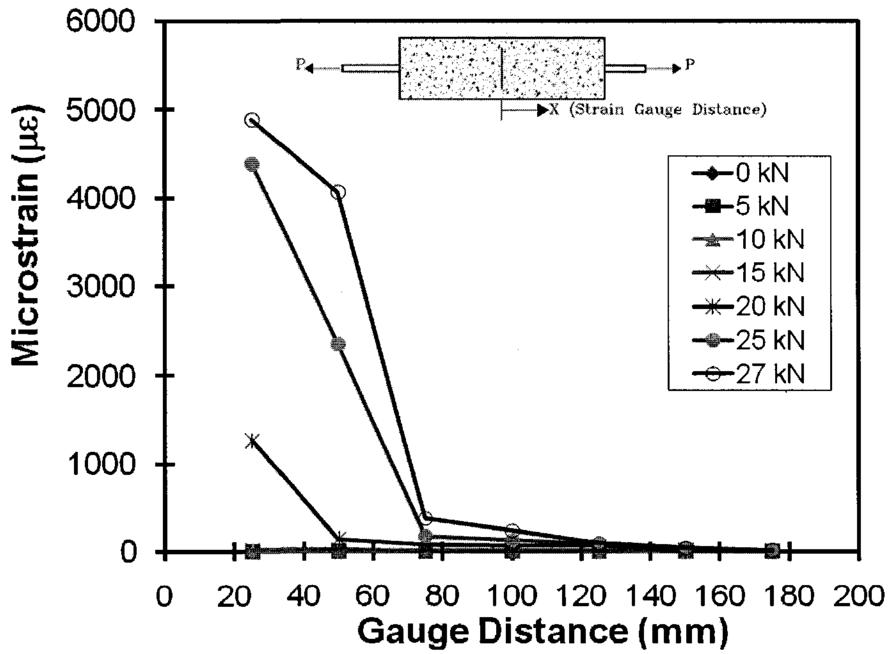

Figure 4.19 - Strain versus Gauge Distance for L450W75L1RW2

4.3.2 Transverse Strain Distribution

The locations of transverse strain gauges are shown in Figure 3.17. Table 4.7 shows strain values across the width of the CFRP composite for specimen L450W75L1SW2. Figures 4.20 – 4.23 show the graphical distribution of strains across the width of the specimen for the four specimens that had transverse strain gauges. It was observed that, at higher load levels, strain values 30 mm away from the centerline of the CFRP composite across the width of the specimen were higher as compared to those at the centreline of the CFRP composite. This implies that debonding does not occur evenly across the sheet width, and starts at the edge of the CFRP sheet. This observation agrees with the results obtained by Kamel *et al.* (2006), who had transverse strain gauges along the entire bonded length at an interval of 25 mm. In this current study, the average strain values closer to the edge of the CFRP composite compared to that at the centreline of the CFRP composite at maximum load ranged from 0.6% to 22% for specimens with a 100 mm bond width, whereas the range varied between 2% to 37% for specimens with a 75 mm bond width. The strain values for the gauges located to the left were slightly different from those located to the right indicating the presence of uncontrollable eccentricity in the load.

Table 4.7 - Transverse Strain Distribution Data for L450W75L1SW2

LOAD (kN)	Distance Across from Centreline (mm)		
	30 (left)	**Centreline**	**30 (right)**
0	0.00	0.00	0.00
5	5.91	12.91	8.45
10	13.52	13.52	15.20
15	21.12	20.27	27.03
20	2013.00	3218.42	5092.88
25	5834.56	3888.30	6397.99
26	6076.99	4243.08	6765.45

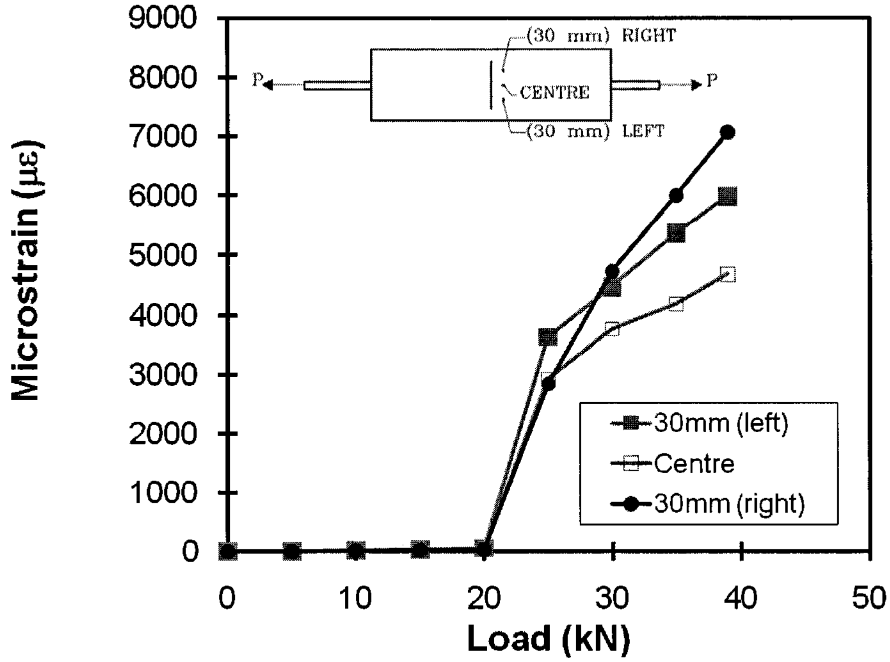

Figure 4.20 - Transverse Strain Distribution for L450W100L1SW2

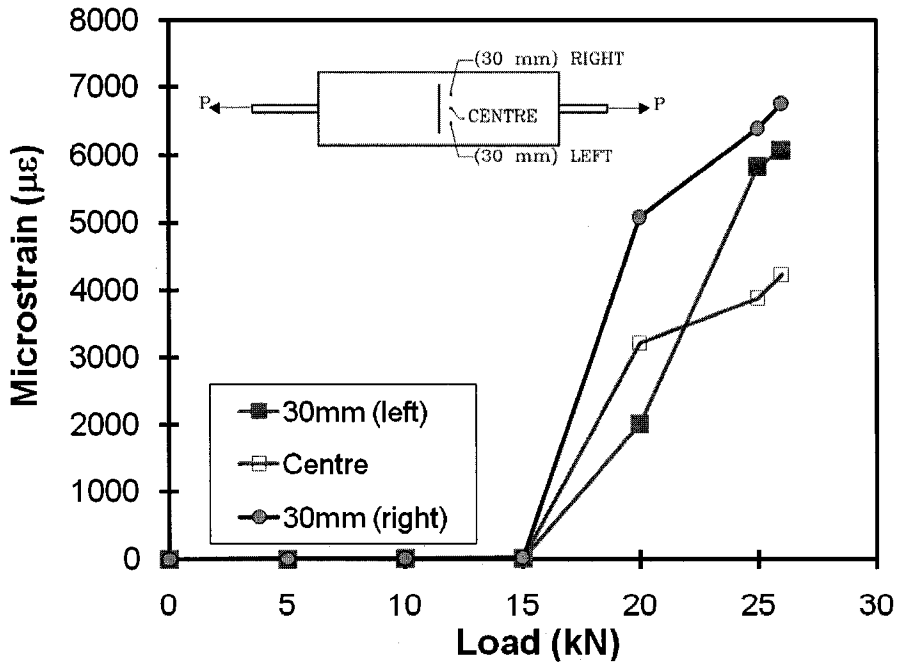

Figure 4.21 - Transverse Strain Distribution for L450W75L1SW2

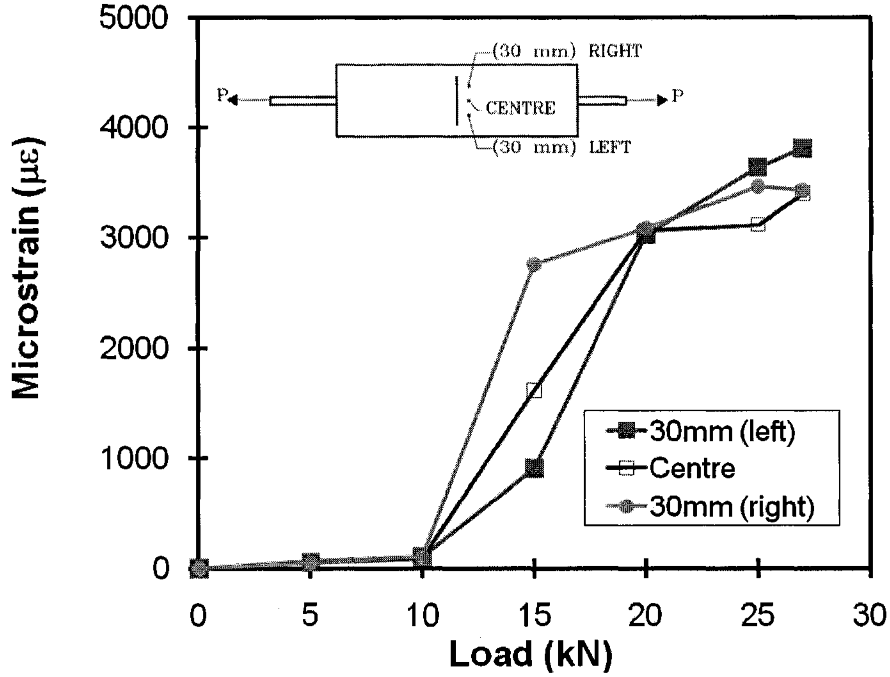

Figure 4.22 - Transverse Strain Distribution for L350W100L1SW2

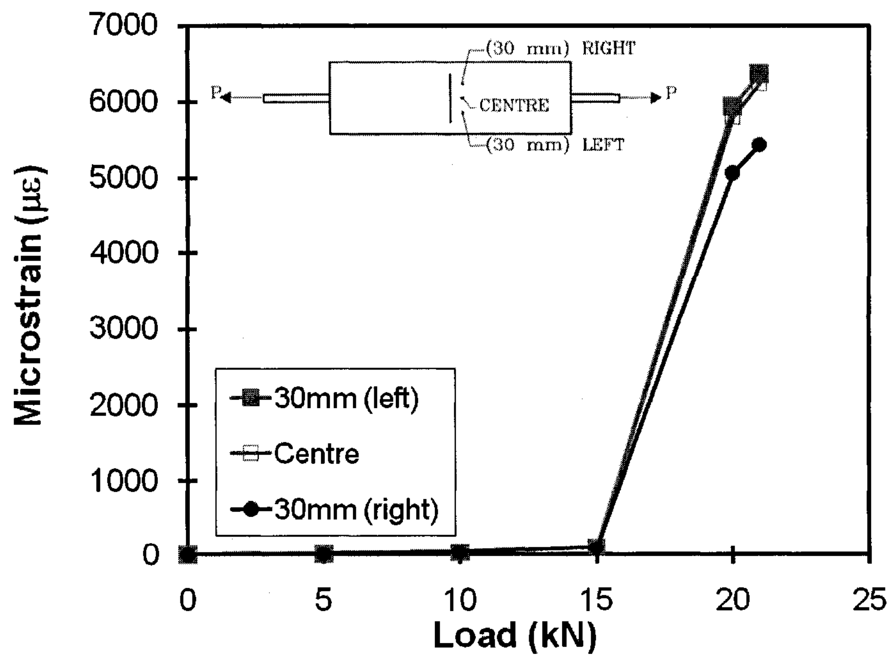

Figure 4.23 - Transverse Strain Distribution for L350W75L1SW2

Bond Length Effect:

By comparing Figures 4.21 and 4.23, it is noted that the difference in strain values between the centreline and the edges of the specimen increases significantly as the bond length increases. For example, at a load of 20 kN, the strain value at the left edge of the specimen with a bond length of 450 mm (Figure 4.21) is 1.6 times of the strain at the centreline. For the specimen with a bond length of 350 mm (Figure 4.23), on the other hand, the strain value at the left edge is only 1.02 times that at the centreline.

Bond Width Effect:

Figures 4.20 and 4.21 show the difference in strain values between the edges and the centre of the specimen increases as the bond width increases. For instance, at a load of 25 kN, the strain value at the left edge of the specimen with a bond width of 100 mm (Figure 4.20) is 1.24 times that at the centreline. For the specimen with a bond width of 75 mm (Figure 4.21), however, the strain value at the left edge is 1.16 times that at the centreline. That concludes that as the bond area increases, debonding at the edges become more severe.

Since only four specimens were prepared to have transverse strain gauges, it was not possible to investigate the behavioural changes in transverse strains for changing the CFRP stiffness, the surface preparation, or the number of cross wraps.

4.4 Average Bond Stress versus Average Bond Slip

Figure 4.24 is an example of the average bond stress versus average bond slip relationship. In order to create these charts, the average bond stress between two subsequent strain gauges, $\tau_{i+\frac{1}{2}}$, and the average bond slip, s_x, were calculated by using equations 4.1 and 4.2. Many other researchers (De Lorenzis *et al.* (2001), Nakaba *et al.* (2001), and Ueda *et al.*) used similar equations in order to create the bond stress versus slip charts.

$$\tau_{i+\frac{1}{2}} = \frac{E_f A_f (\varepsilon_{i+1} - \varepsilon_i)}{2b_f (x_{i+1} - x_i)} \tag{4.1}$$

$$s_x = s(x_i) + \frac{(\varepsilon_{i+1} - \varepsilon_i)x^2}{(x_{i+1} - x_i)} + \varepsilon_i x \tag{4.2}$$

where E_f is the elastic modulus of the CFRP composite (E_f = 230 GPa)

A_f is the cross sectional area of the CFRP composite ($A_f = b_f \times t_f$)

b_f is the width of the CFRP composite

t_f is the thickness of the CFRP composite

ε is the measured strain, and

x is the strain gauge location from centre of specimen, $x_i \le x \le x_{i+1}$.

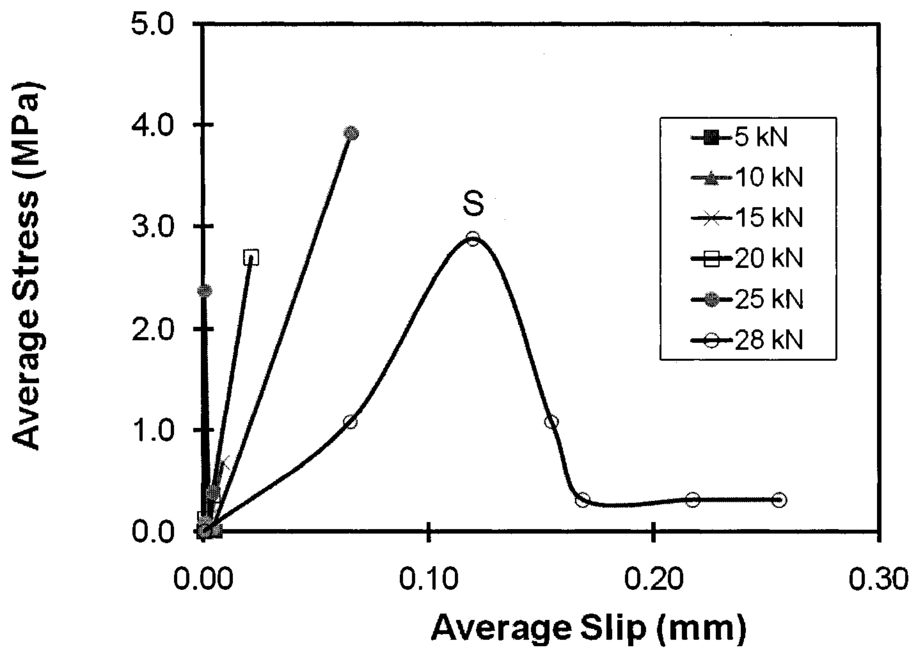

Figure 4.24 – Example of Average Bond Stress versus Average Bond Slip

Sato *et al.* (2001) discussed the softening behaviour of the average bond stress versus average bond slip at the maximum load. This is also observed in this study (point S in Figure 4.24). Sato *et al.* (2001) suggested that since the bonding layer at the concrete surface consists of aggregate and mortar in a random distribution or orientation relative to the fibers, the CFRP composite's strength varies depending on which material it bonds to. It is likely that bond strength is greater when the CFRP composite bonds to the aggregate. Hence, when the maximum stress is reached, the fall in bond stress does not follow a vertical line because debonding from the mortar and from the aggregate do not happen simultaneously.

CFRP's Stiffness Effect:

Figure 4.25 compares the average bond stress versus average bond slip relationship at the maximum load for a specimen with one layer of CFRP (specimen L350W75L1RW2) versus a specimen with two layers of CFRP (specimen L350W75L2RW2). It can be observed that the gradient of the curve becomes steeper as the stiffness of the fiber increases (specimen L350W75L2RW2). For the specimen with two layers, the maximum bond stress was 1.4 times of that with one layer (4.5 MPa versus 3.1 MPa). This finding agrees with Sato *et al.* (2001) who stated that with two layers, the maximum bond stress is 1.7 times that with one layer, and the same as that with three layers. As can be seen, the average bond slip at maximum stress occurs earlier for the specimen with two layers of CFRP (average bond slip for the specimen with one layer is 0.11 mm, whereas that value is 0.23 mm for the specimen with two layers). Moreover, the area under the curve for the specimen with lower stiffness (one CFRP composite layer) is greater than that with higher stiffness ($G_{f(one\ layer)}$ = 0.90 N.mm/mm^2; $G_{f(two\ layers)}$ = 0.45 N.mm/mm^2) indicating that the value for fracture energy is higher for the former. This indicates that adding a second CFRP layer reduces bond strength.

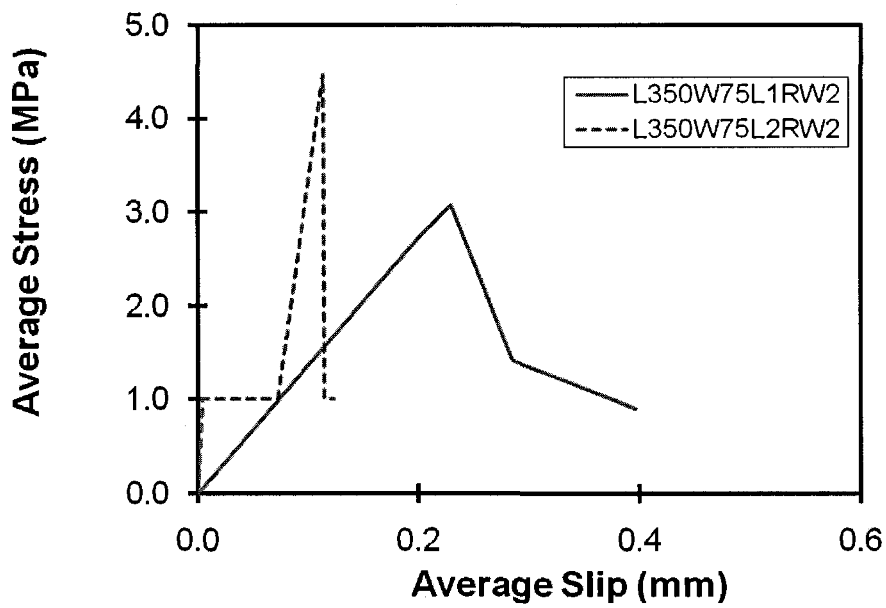

Figure 4.25 – Average Bond Stress versus Average Bond Slip Curves for Specimens with Different Stiffness

Bond Length Effect:

Figure 4.26 compares the behaviour of the average bond stress-slip relationship at maximum load for specimens with different bond length (450 mm and 350 mm). The maximum stress for the specimen with longer bond length is 1.3 times larger than that with shorter bond length (4.1 MPa versus 3.1 MPa). The slip at maximum stress occurs earlier for the specimen with a 450 mm bond length (average bond slip for the L450 specimen is 0.03 mm, whereas it is 0.23 mm for the L350 specimen). In addition, the area under the curve is larger for the L450 specimen ($G_{f(L450)}$ = 1.86 N.mm/mm^2; $G_{f(L350)}$ = 0.90 N.mm/mm^2) indicating that the bond strength improves with increasing the bond length.

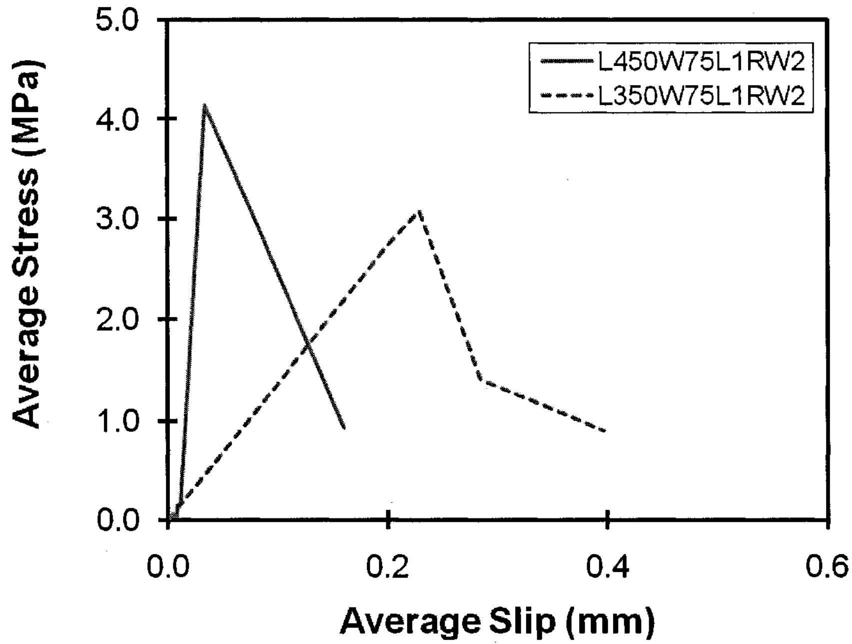

Figure 4.26 – Average Bond Stress versus Average Bond Slip Curves for Specimens with Different Bond Lengths

Bond Width Effect:

Sato *et al.* (2001) concluded that the maximum bond stress for specimens with fiber width of 20 mm are approximately 1.5 times those with fiber width of 50 mm and 100 mm. According to Figure 4.27, the maximum stress for specimens with a CFRP width of 75 mm is approximately 1.7 times that of specimens with a CFRP width of 100 mm (4.1 MPa versus 2.4 MPa). The average bond slip at maximum stress occurs earlier for the specimen with less bond width (the average bond slip is 0.23 mm for the specimen with a bond width of 100 mm, whereas it is 0.03 mm for the specimen with a bond width of 75 mm). The area under the curve is larger for the specimen with a bond width of 75 mm ($G_{f(W100)} = 1.44$ N.mm/mm^2; $G_{f(W75)} = 1.86$ N.mm/mm^2) indicating that decreasing the bond width improves the bond strength.

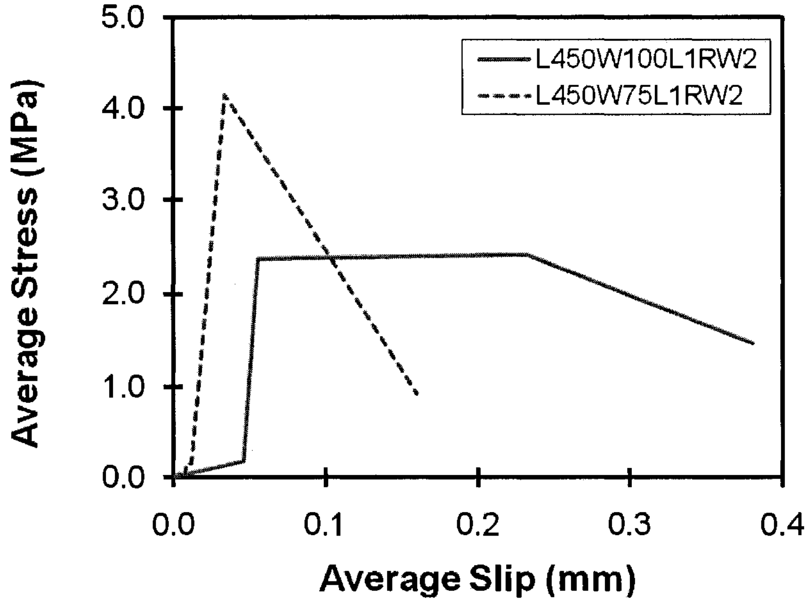

Figure 4.27 - Average Bond Stress versus Average Bond Slip Curves for Specimens with Different Bond Width

Surface Preparation Effect:

Figure 4.28 illustrates that the maximum average bond stress for specimens with a rough surface is larger than that for specimens with a smooth surface. For instance, the specimen with a smooth surface in Figure 4.28 has a maximum average bond stress of 1.7 MPa. The specimen with a rough surface, on the other hand, has a maxiumum average bond stress of 2.3 MPa. The average bond slip at maximum average bond stress, however, occurs earlier in specimens with a smooth surface (it occurs at 0.01 mm for the specimen having a smooth surface, and at 0.05 mm for the specimen having a rough surface). The area under the curve is larger for specimens with a smooth surface ($G_{f(smooth)}$ = 0.43 N.mm/mm^2; $G_{f(rough)}$ = 0.14 N.mm/mm^2) indicating that having a smooth surface improves bond strength.

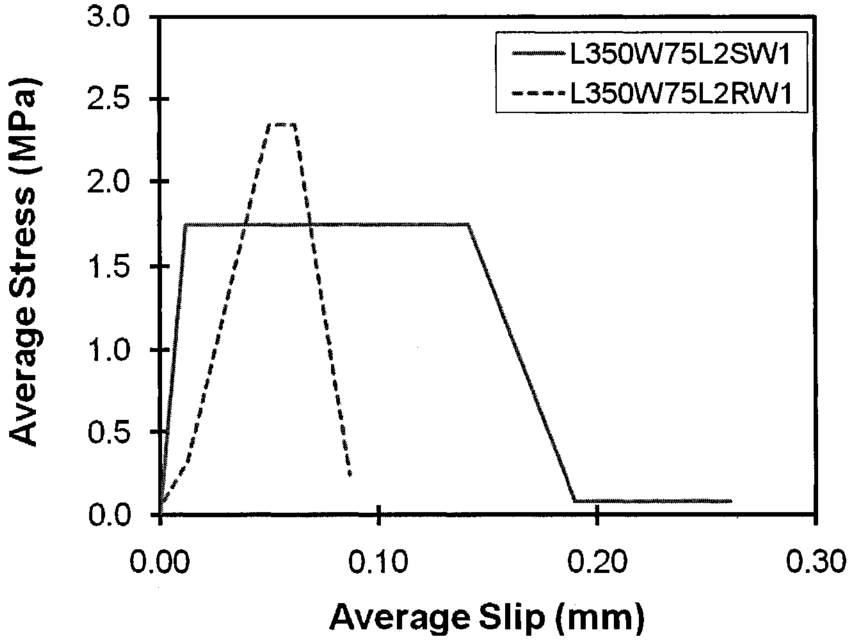

Figure 4.28 – Average Bond Stress versus Average Bond Slip Curves for Specimens with Different Surface Preparations

Cross Wraps Effect:

Lastly, when comparing the influence of cross wraps on either one half or both halves of the specimen, it is concluded that the average bond stress for specimens with cross wraps on one half "W1" is greater than the average bond stress for specimens with cross wraps on both halves "W2". For example, in Figure 4.29, the average bond stress for specimen "W1" is 1.4 MPa, and that for specimen "W2" is 1.3 MPa. The gradient of the average bond stress-slip curve at maximum load is steeper for specimen "W1", and the average bond slip at maximum average bond stress occurs earlier for specimen "W1" (0.03 mm versus 0.12 mm) indicating that adding cross wraps on both halves increases bond strength. The area under the curve is slightly larger for the "W2" specimens ($G_{f(W1)}$ = 0.26 N.mm/mm^2; $G_{f(W2)}$ = 0.27 N.mm/mm^2) demonstrating having cross wraps on both halves of the specimen does not influence the bond strength capacity significantly.

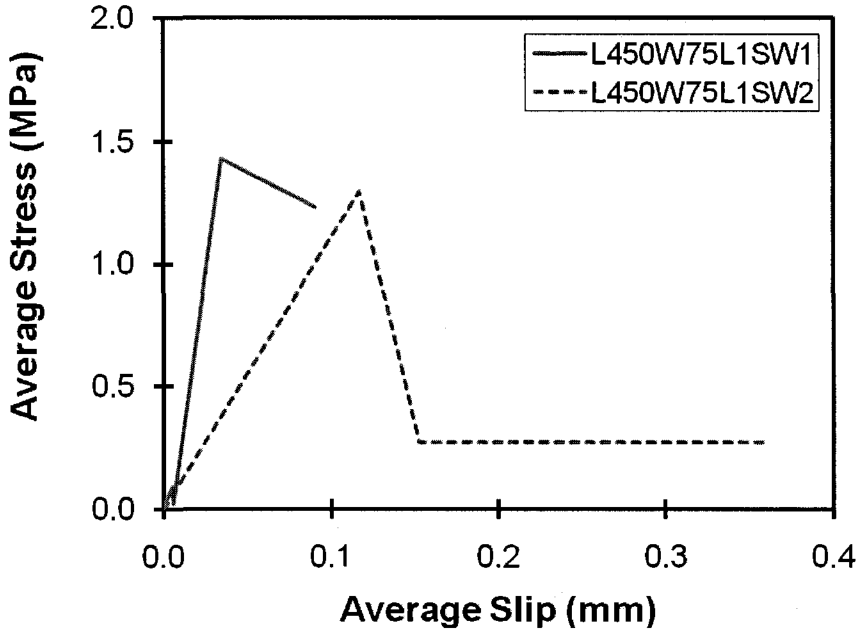

Figure 4.29 - Average Bond Stress versus Average Bond Slip Curves for Specimens with Different Cross Wrap Locations

4.5 Average Bond Stress versus Normalized Load

A normalized load relates the level of an applied load to that of the maximum load reached at debonding.

$$\xi = F / F_{\max} \tag{4.3}$$

where, ξ is the normalized load ($0 \le \xi \le 1$)

F is the applied load level, and

$F_{\max}$ is the maximum load reached at debonding

Table 4.8 and Figure 4.30 are examples of the relationship of average bond stress versus normalized load. These bond stress curves were generated for the regions between two consecutive strain gauges by relating the calculated average bond stress values to the corresponding normalized load. Bizindavyi and Neale (1999) explained that these curves show that there exists a load level at which the stress near the centre of the specimen reaches a peak and then begins to decrease rapidly, while at the same time the stress in the neighboring region begins to increase. They indicated that the decrease of the bond stress is a sign of cracking in that region, whereas the build-up of stress in the adjacent region shows that the load is being transferred there. This behaviour continues until complete debonding takes place and the specimen fails.

Table 4.8 - Average Bond Stress versus Normalized Load Data for L450W100L2SW2

F/F_{max} (kN)	Gauge Distance (mm)					
	37.5	62.5	87.5	112.5	137.5	162.5
	Average Bond Stress (MPa)					
0.0	0.00	0.00	0.00	0.00	0.00	0.00
0.1	0.00	0.00	0.00	0.00	0.00	0.00
0.2	0.02	0.02	0.01	0.01	0.01	0.00
0.3	0.09	0.09	0.02	0.02	0.02	0.02
0.4	0.31	0.31	0.03	0.03	0.03	0.02
0.5	0.90	0.90	0.11	0.02	0.00	0.02
0.6	3.03	0.96	0.14	0.02	0.01	0.01
0.7	5.65	0.96	0.20	0.04	0.02	0.02
0.8	3.90	4.65	0.58	0.07	0.03	0.03
0.9	1.08	4.84	4.11	0.59	0.10	0.07
1.0	0.63	1.78	1.78	2.24	2.24	2.24

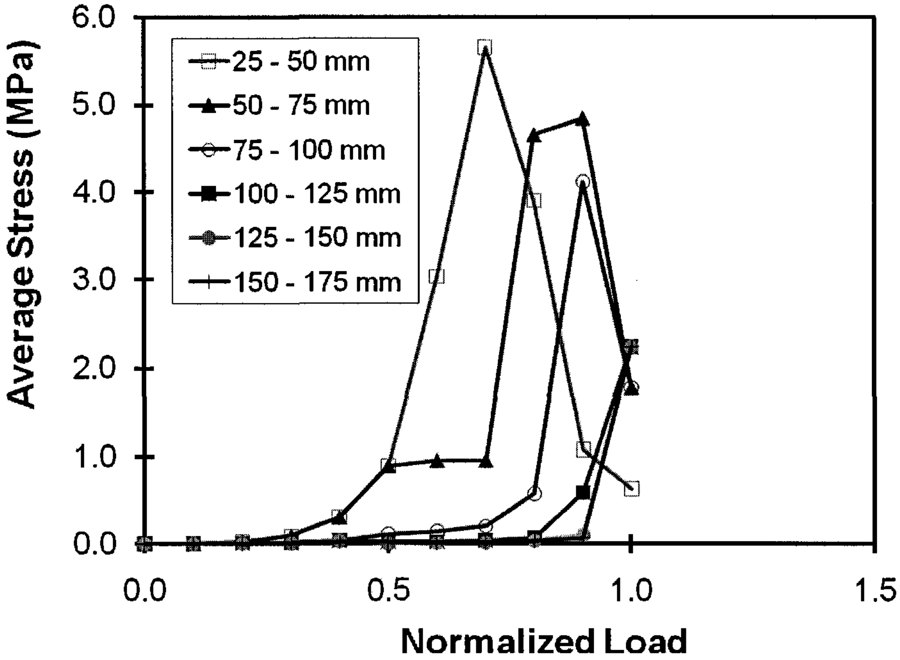

Figure 4.30 – Average Bond Stress as a Function of Normalized Load

CFRP's Stiffness Effect:

Figures 4.31 and 4.32 compare the stiffness for the average bond stress versus normalized load for the same specimen properties (bond length of 350 mm, bond width of 100 mm, and prepared with rough surface), but with one and two layers of CFRP composites. As illustrated, the average bond stress for specimens with two CFRP layers is approximately 1.2 times that for specimens with one CFRP layer for this example. It is also noted that the maximum average bond stress occurs in both cases at a distance range of 25 – 50 mm at a load that is 90% and 80% of the maximum load for specimens having one and two CFRP layers, respectively. In addition, it is observed that for specimens with one CFRP layer, the rapid decrease of the bond stress as was observed by Bizindavyi and Neale (1999) happened only at a distance range of 25 – 50 mm after reaching a peak value. That means that debonding was reached shortly after cracking took place in that distance range (25 – 50 mm). The segment length after the peak is reached is longer for the specimen having two CFRP layers (segment AB in Figure 4.31 is shorter than segment CDE in Figure 4.32). This denotes that more load was being transferred from one distance range to the neighbouring one in specimens with two CFRP layers.

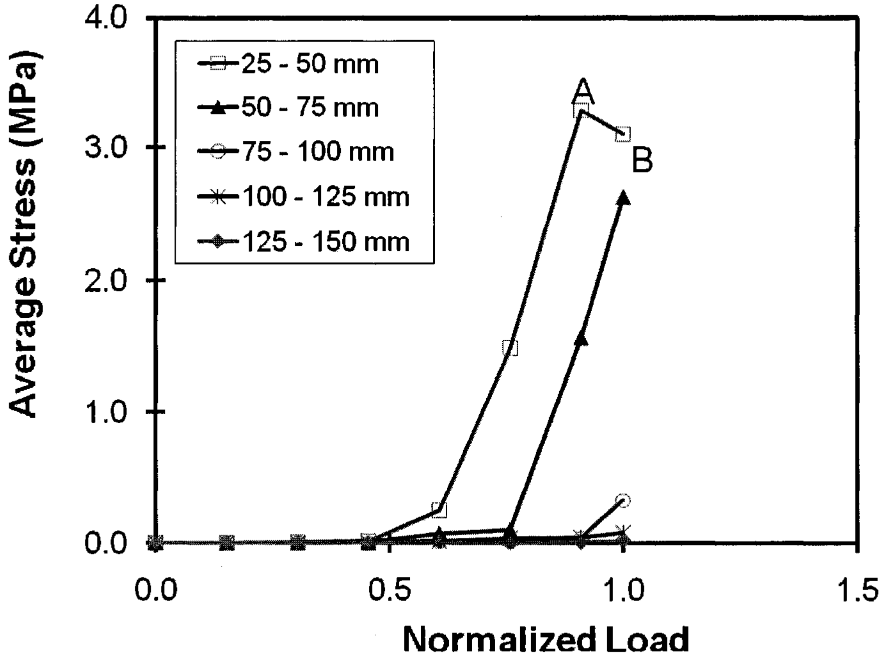

Figure 4.31 – Average Bond Stress versus Normalized Load for L350W100<u>L1</u>SW1

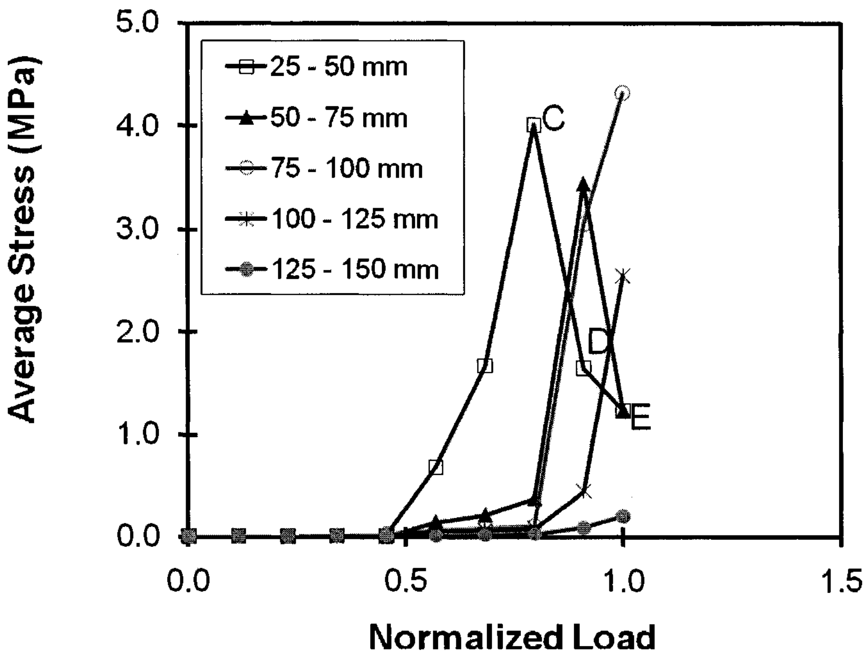

Figure 4.32 – Average Bond Stress versus Normalized for L350W100<u>L2</u>SW1

Bond Length Effect:

Figures 4.33 and 4.34 compare the average bond stress versus normalized load behaviour for the two CFRP composite lengths used in this study. As shown, the average bond stress increases with the increase in the CFRP composite length. For the specimen with a CFRP length of 450 mm (L450W100L2RW2), the maximum average bond stress of 4.5 MPa occurs at a distance range of 25 – 50 mm at about 70% of the maximum load, whereas the maximum bond stress is 3.8 MPa and occurs at approximately 87% of the maximum load at a distance range of 50 – 75 mm for specimens with a CFRP length of 350 mm (L350W100L2RW2). It is also seen that the decrease in average bond stress after reaching its maximum value is more rapid when the CFRP length is smaller (350 mm). For example, line CD in Figure 4.34 is significantly longer than line AB in Figure 4.33. This indicates that cracking is more severe for the specimen with a shorter bond length (350 mm).

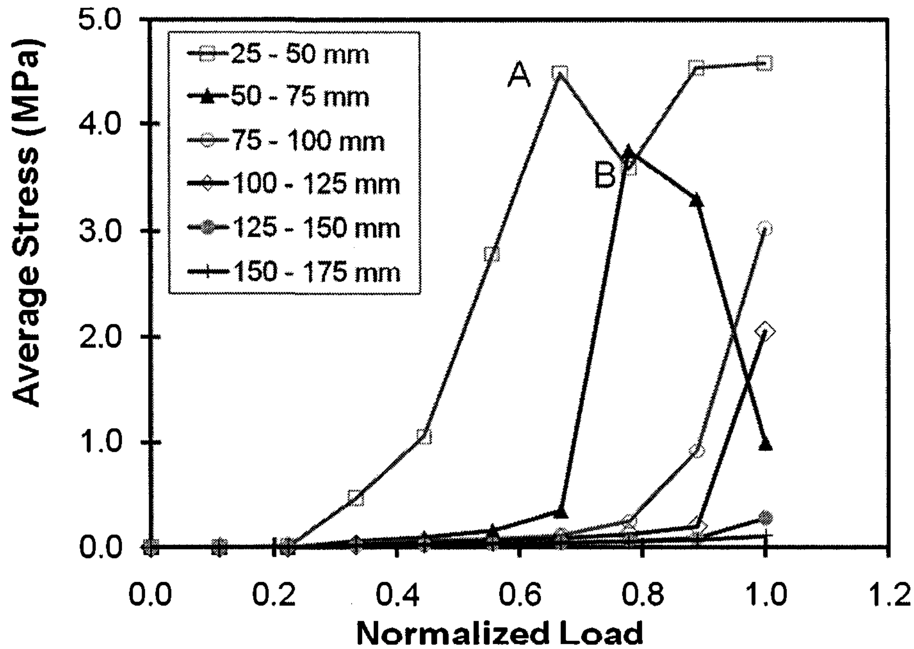

Figure 4.33 – Average Bond Stress versus Normalized Load for L450W100L2RW2

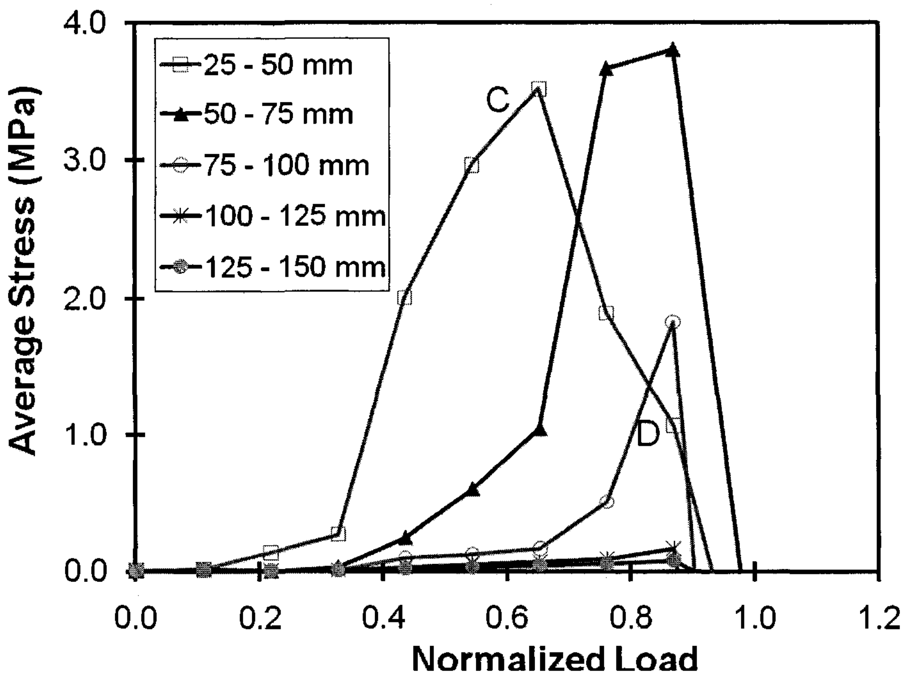

Figure 4.34 – Average Bond Stress versus Normalized Load for L350W100L2RW2

Bond Width Effect:

When comparing specimens with different CFRP composite width, it is noted that the maximum average bond stress increases when the bond width decreases. For example, the maximum average bond stress for a 100 mm wide CFRP composite in Figure 4.35 is 3.6 MPa, whereas it is 4.3 MPa for a 75 mm wide CFRP composite as in Figure 4.36. The increase of average bond stress at regions further away from midspan in Figure 4.36 (for example, at a distance range of 75 – 100 mm, point Y in Figure 4.36 that marks the initial noticeable increase of average bond stress for that curve occurs earlier than point X in Figure 4.35) indicates that for a narrower width, more load is transferred to the neighbouring region. The maximum average bond stress takes place at a normalized load that is approximately 0.8 of the maximum load for specimens with a CFRP width of 100 mm. On the other hand, it occurs at a normalized load of 0.95 of the maximum load for specimens with a CFRP width of 75 mm. That fact verifies once more that decreasing the bond width improves the bond strength.

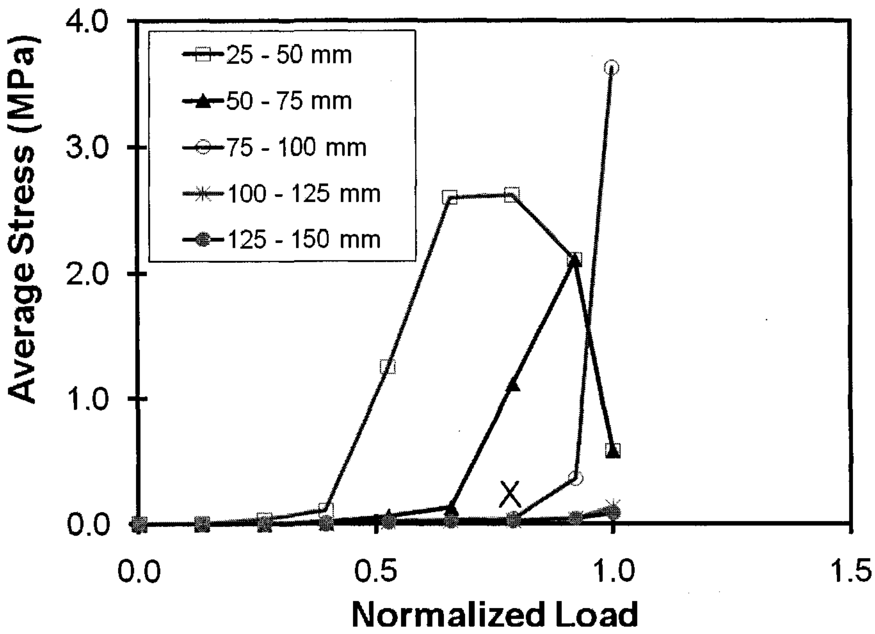

Figure 4.35 – Average Bond Stress versus Normalized Load for L350<u>W100</u>L1RW2

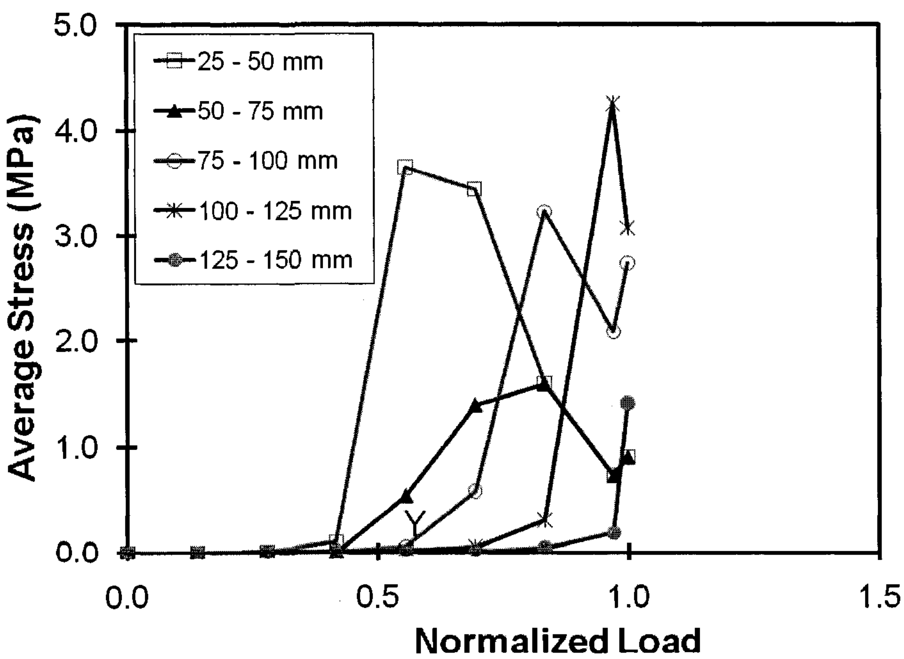

Figure 4.36 – Average Bond Stress versus Normalized Load for L350<u>W75</u>L1RW2

Surface Preparation Effect:

Figures 4.37 and 4.38 show that surface preparation influences the behaviour of the average bond stress versus normalized load curves. For the specimen having a rough surface (Figure 4.37), the maximum average bond stress was approximately 1.7 times that of specimens with a smooth surface (Figure 4.38). It should be noted, however, that the maximum average bond stress was reached in both cases at around the same normalized load, which was 73% of the maximum load in this case. The figures also illustrate that more load is transferred from one distance range to the adjoining one in specimens having a rough surface (this is illustrated in Figure 4.38 by the presence of more maximum average bond stress "peaks" further away from midspan) denoting that roughening the surface enhances the ability of stress transfer.

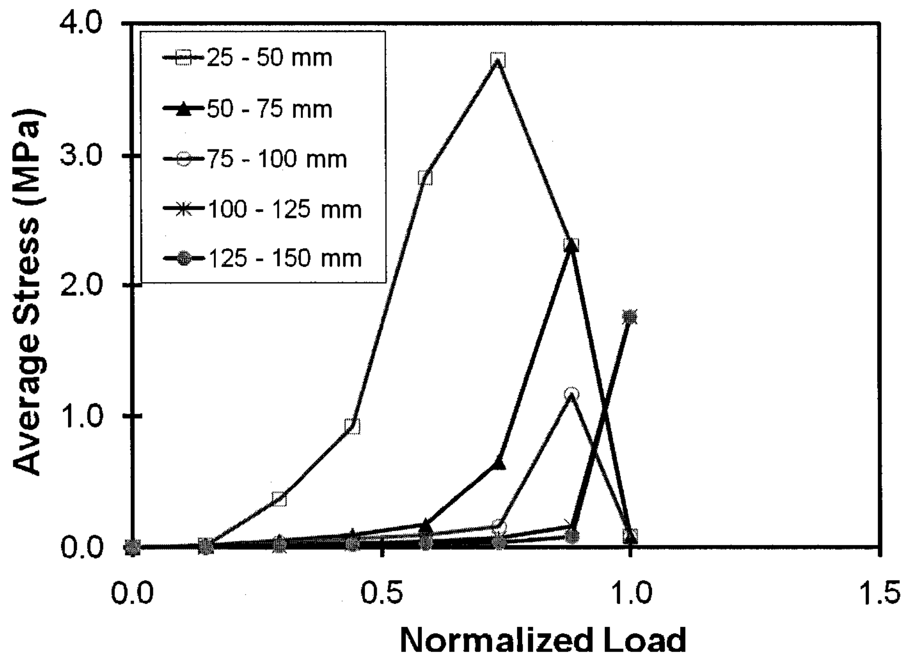

Figure 4.37 – Average Bond Stress versus Normalized Load for L350W75L2RW1

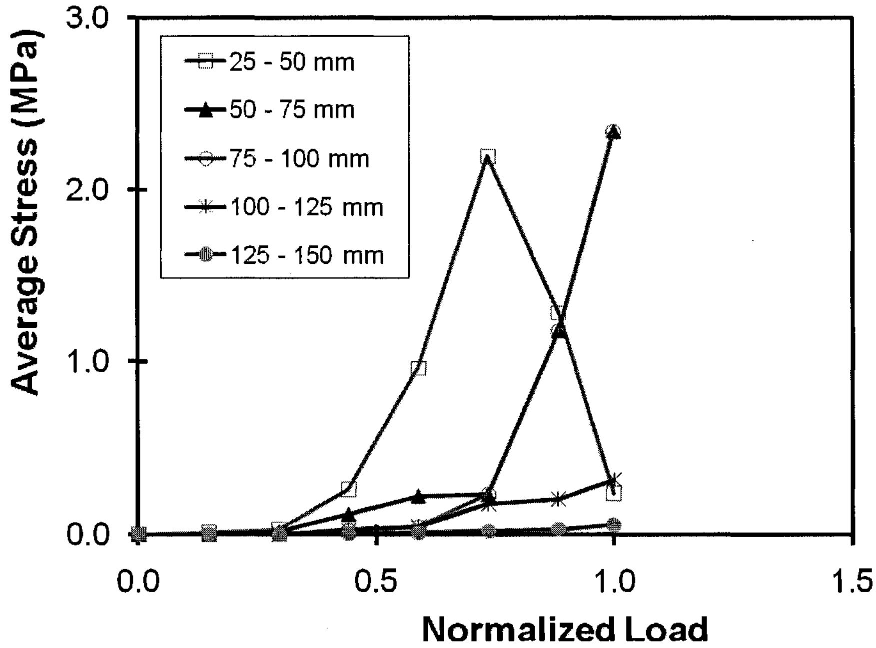

Figure 4.38 – Average Bond Stress versus Normalized Load for L350W75L2SW1

Cross Wraps Effect:

Adding cross wraps on both halves of the specimen (W2) instead of one half (W1) reduces the average bond stress. For instance, the largest average bond stress at a distance range of 25 – 50 mm for specimen "W1" in Figure 4.39 is 3.9 MPa, whereas it is 3.1 MPa for specimen "W2" (Figure 4.40). In addition, it is shown that the rapid decrease in bond stress that takes place after the maximum average stress peak is reached only happened for the two distance ranges closest to the centre of the "W1" specimen (i.e. 25 – 50 mm and 50 – 75 mm). This implies that, when compared to the "W2" specimen, not so much load transfer was achieved for the "W1" specimen. Hence debonding occurs earlier in specimen "W1", and adding cross wraps on both halves improves bond strength.

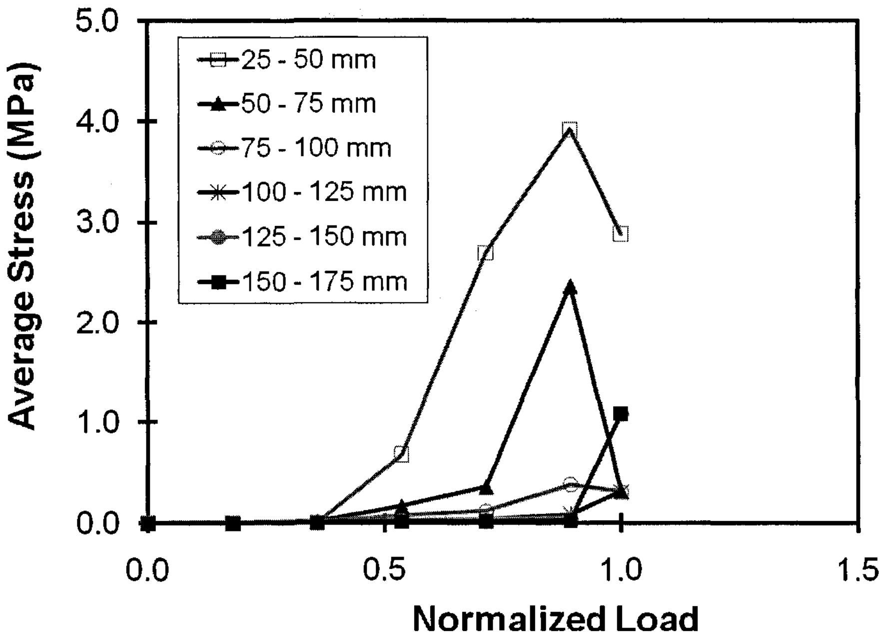

Figure 4.39 – Average Bond Stress versus Normalized Load for L450W75L2RW1

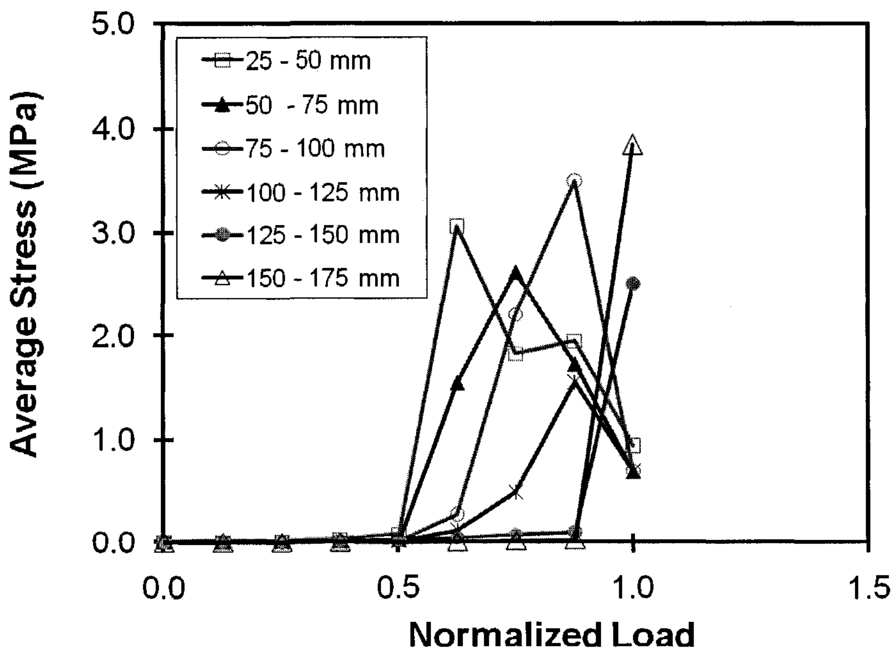

Figure 4.40 – Average Bond Stress versus Normalized Load for L450W75L2RW2

4.6 Average Bond Stress Distribution

The average bond stress versus gauge distance plots are obtained from the first derivative of the strain versus gauge distance diagram multiplied by the CFRP's elastic modulus (*E*) and the CFRP's thickness (*t*) (equation 4.1, section 4.4). Table 4.9 and Figure 4.41 are good examples of this relationship. As illustrated by the arrows in that figure, as the load increases, the average bond stress decreases in the area within 87.5 mm from midspan (x = 87.5 in Figure 4.41). At any point farther from that point (x > 87.5), an increase in the average bond stress is observed as the load increases.

This agrees with the findings of Sato *et al.* (2001) who assumed that the decrease in bond stress is caused by the start of delamination. They believe that the maximum bond stress varies with gauge distance because once delamination of the concrete-CFRP is initiated, it induces some mechanical damage in the bonding layer surrounding it. As delamination propagates towards centreline of the specimen, less bond stress is required and the rate of damage is reduced until it finally reaches an insignificant level at a certain distance.

Table 4.9 - Average Bond Stress Distribution for L450W100L1SW2

LOAD (kN)	Gauge Distance (mm)					
	37.5	62.5	87.5	112.5	137.5	162.5
	Average Bond Stress (MPa)					
0	0.000	0.000	0.000	0.000	0.000	0.000
5	0.001	0.000	0.000	0.002	0.002	0.002
10	0.001	0.001	0.005	0.002	0.002	0.006
15	0.006	0.006	0.004	0.001	0.008	0.008
20	0.013	0.013	0.005	0.001	0.009	0.009
25	0.656	0.656	1.838	0.077	0.032	0.022
30	0.850	0.639	2.211	0.417	0.071	0.027
35	0.571	0.571	0.571	1.640	1.084	0.235
39	0.063	0.063	0.063	0.815	0.812	0.812

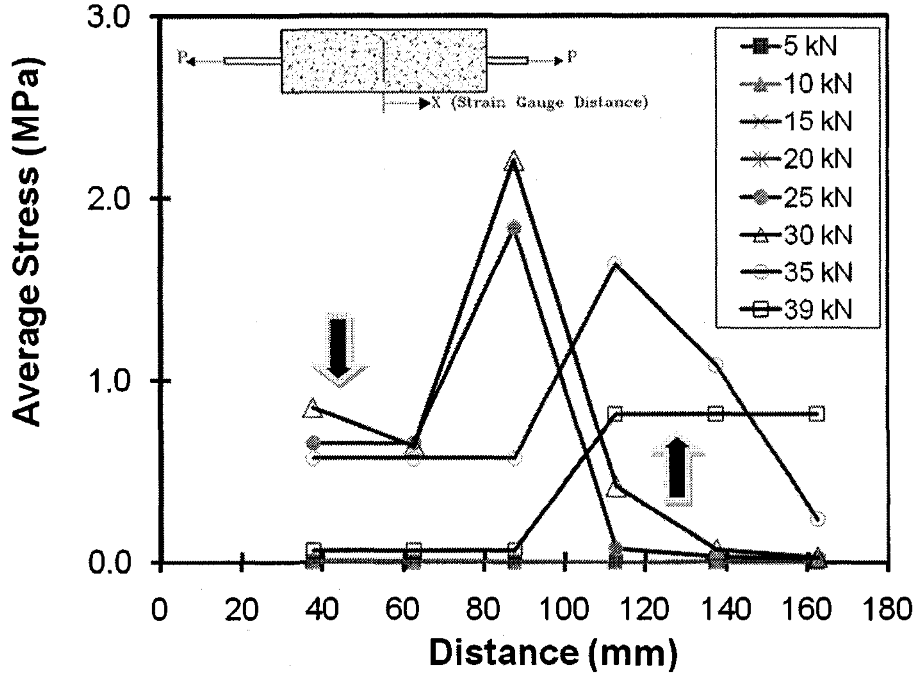

Figure 4.41 - Example of Average Bond Stress Distribution

CFRP's Stiffness Effect:

By comparing the effect of stiffness of CFRP composite on the average bond stress distribution, it is observed that increasing the stiffness (one layer to two layers of CFRP composites) allows the specimen to experience less damage at the point closest to the midspan of the specimen (x = 0) as the load reaches a maximum (25 kN in Figure 4.42). For example, the average bond stress in Figure 4.42 at a distance 37.5 mm away from midspan at maximum load is 0.93 MPa. Figure 4.43 illustrates that the average bond stress value at maximum load (34 kN) drops to 0.24 MPa when a second CFRP layer is added.

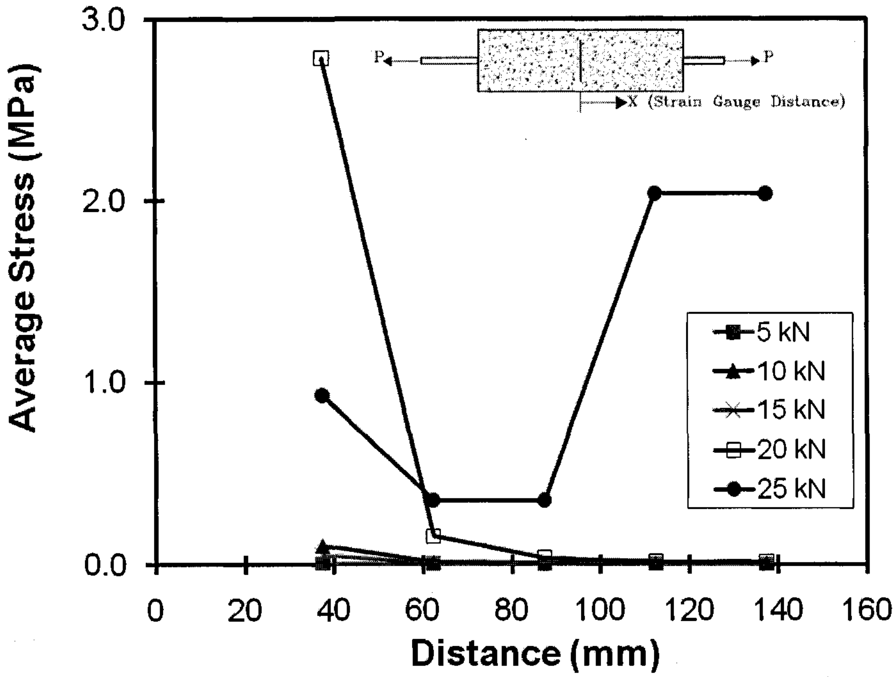

Figure 4.42 – Average Bond Stress Distribution for L350W75L1SW1

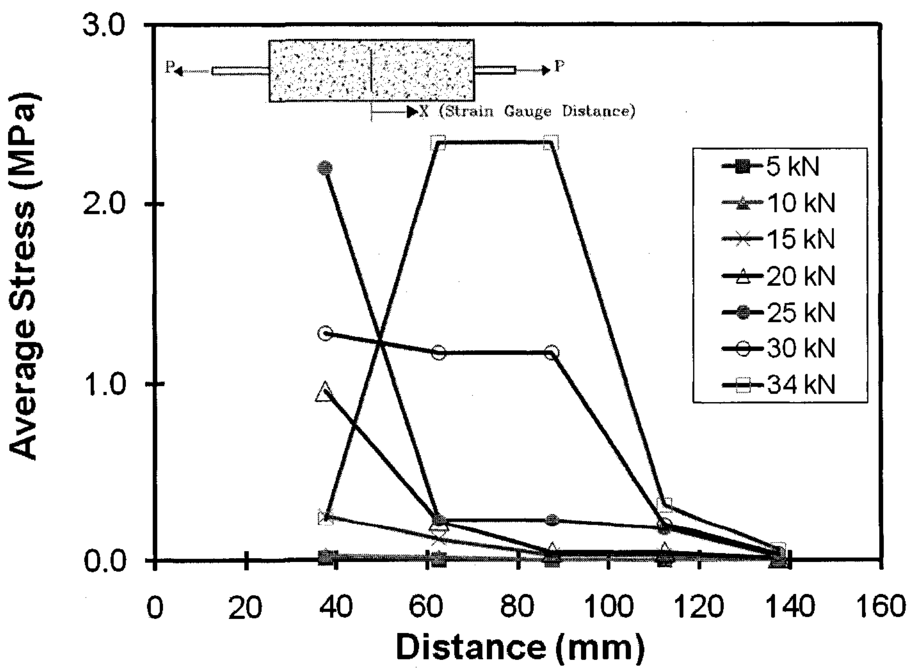

Figure 4.43 – Average Bond Stress Distribution for L350W75L2SW1

Bond Length Effect:

Figures 4.44 and 4.45 compare the behaviour of the average bond stress distributions for different bond lengths (450 mm and 350 mm long). It is shown that as the bond length increases, the length of the segment showing a decrease in the average bond stress-distance plot immediately after the peak stress value increases (for example, segment RS for L450W100L2RW1 (Figure 4.44) is longer than segment TU (Figure 4.45)). Hence, delamination becomes more evident as the bond length increases. Increasing the bond length, however, enables the specimens to experience less damage at the point closest to the centre (midspan, x = 0 mm) as the load reaches a maximum. For the specimen with a bond length of 450 mm (Figure 4.44), the average bond stress at a distance 37.5 mm away from the centre when the maximum load (34 kN) is reached is 0.12 MPa, whearas that value increases to 0.72 MPa if the bond length changes to 350 mm when the maximum load (42 kN) is reached (Figure 4.45).

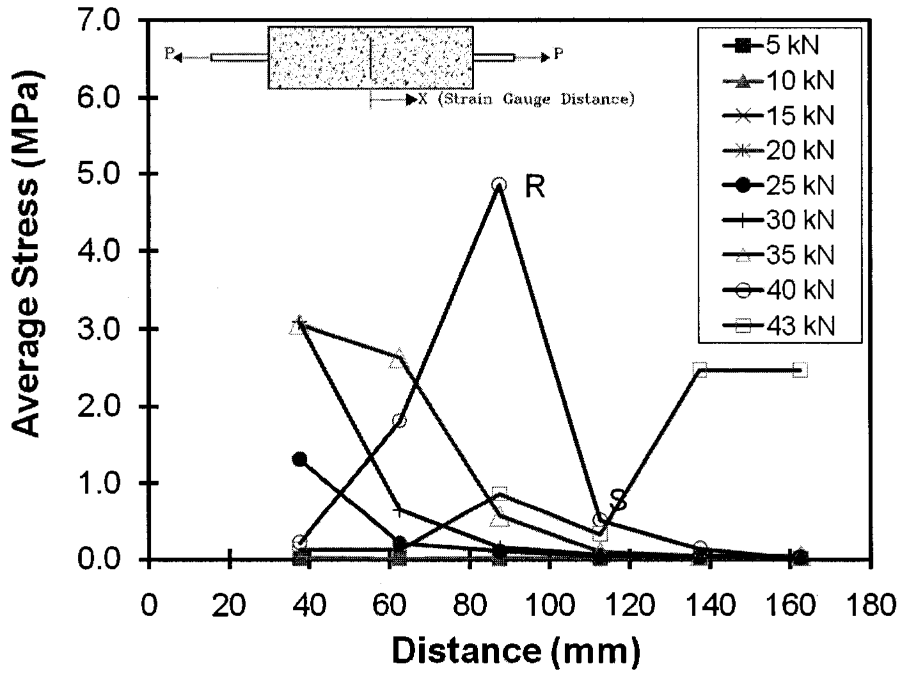

Figure 4.44 – Average Bond Stress Distribution for <u>L450</u>W100L2RW1

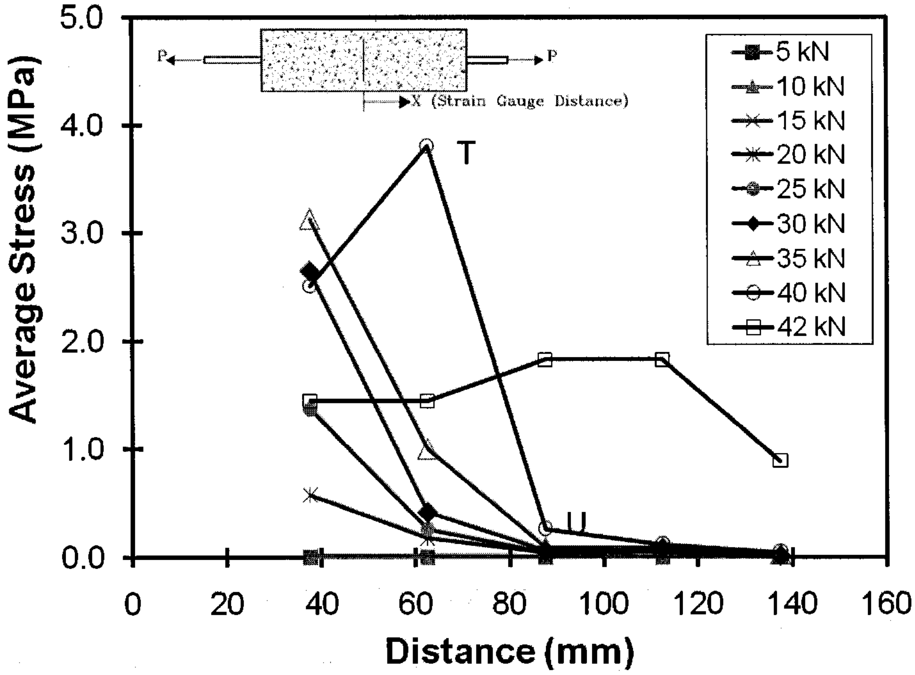

Figure 4.45 – Average Bond Stress Distribution for L350W75L2SW1

Bond Width Effect:

As for the bond width, Figures 4.46 and 4.47 indicate that when the bond width decreases, less damage occurs at the point closest to midspan (x = 0 mm) as the load reaches a maximum. This could be explained by observing the difference in the maximum load values (42 kN versus 27 kN). It is concluded that the bond width does not influence the average bond stress distribution behaviour much, since the difference in the average bond stress values at the point closest to midspan (x = 0 mm) as the maximum load is reached is not as significant as changing the bond length. For the specimen with a bond width of 100 mm (Figure 4.46), the average bond stress at a distance 37.5 mm away from midspan (x = 37.5 mm) when the maximum load (42 kN) is reached is 0.71 MPa, whearas that value changes to 0.92 MPa when the bond width changes to 75 mm (Figure 4.47).

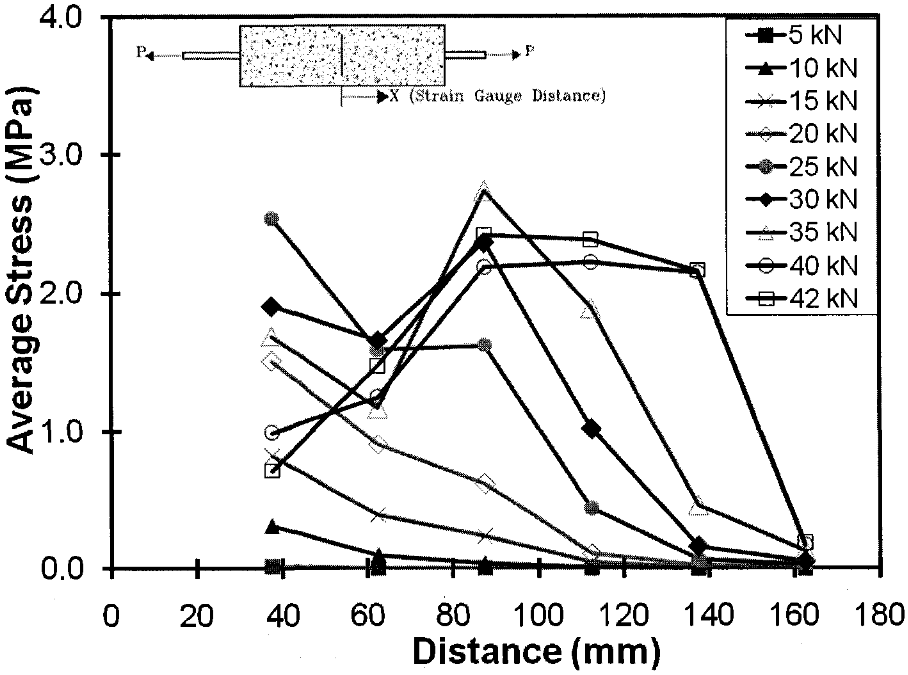

Figure 4.46 – Average Bond Stress Distribution for L450W100L1RW2

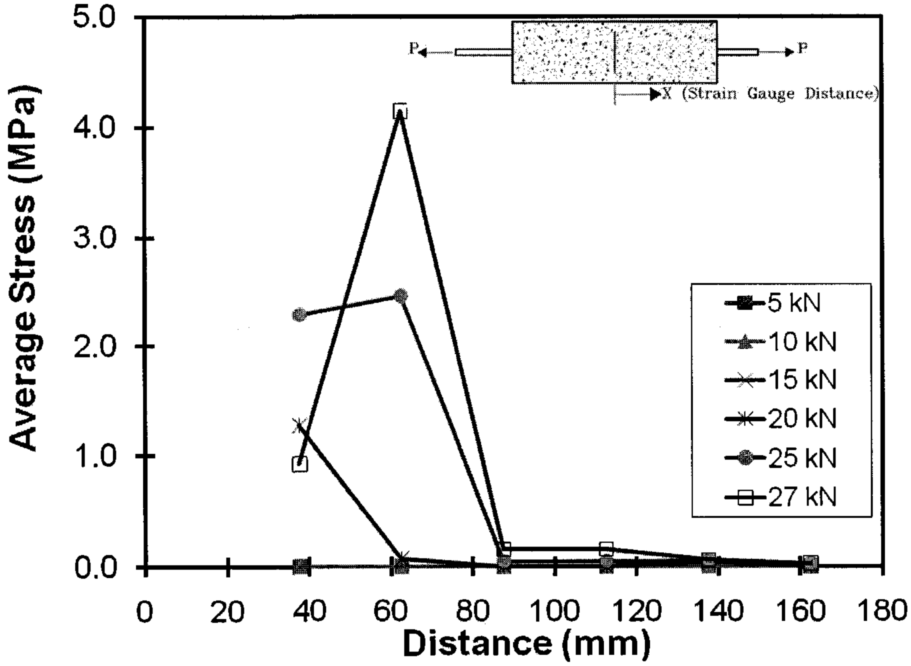

Figure 4.47 – Average Bond Stress Distribution for L450W75L1RW2

Surface Preparation Effect:

Figures 4.45 and 4.48 compare the behaviour of the average bond stress distribution curves for specimens having different surface preparations (smooth and rough, respectively). It is shown that for the specimen having a smooth surface, the length of the segment showing a decrease in the bond stress distribution after the peak value is reached (for example, segment TU in Figure 4.45) is the largest at the maximum load, and hence delamination becomes more evident for specimens having a smooth surface. For specimen with rough surface (Figure 4.48), on the other hand, the average bond stress becomes constant after the maximum load is reached (segment VW in Figure 4.48), indicating that barely any delamination took place. Moreover, having a rough surface causes the bond of the concrete-CFRP interface to be stronger, and hence less damage takes place at the point closest to midspan (x = 0 mm) as the load reaches a maximum. For instance, for the specimen having a rough surface (Figure 4.48), the average bond stress at a distance 37.5 mm away from midspan (x = 37.5 mm) when the maximum load is reached is only 0.08 MPa, whearas that value is 0.24 MPa for the specimen with smooth surface (Figure 4.45).

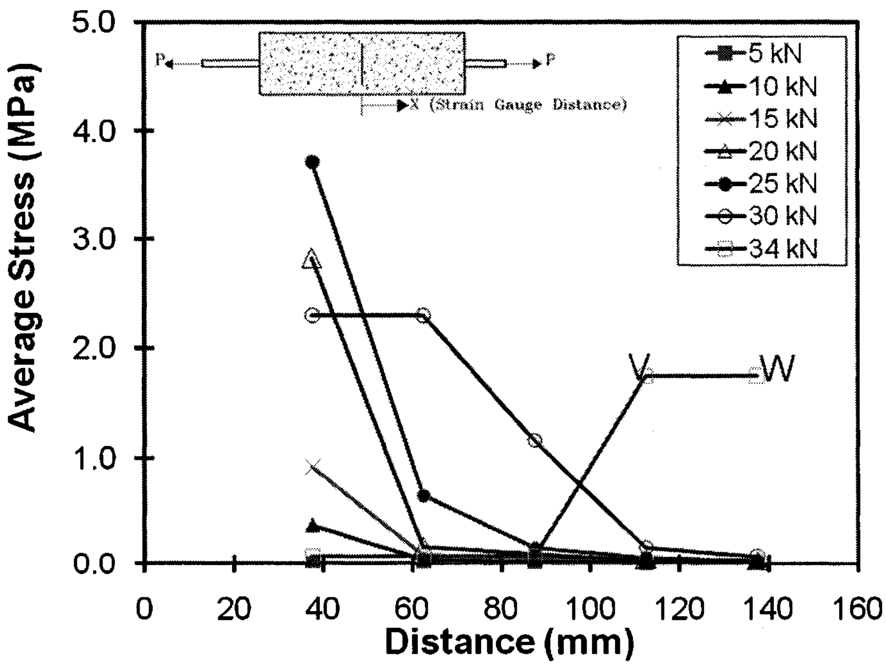

Figure 4.48 – Average Bond Stress Distribution for L350W75L2RW1

Cross Wraps Effect:

It is apparent that adding cross wraps on both halves of the specimen, "W2", decreases the possibility of debonding and increases the maximum average stress. For example, the maximum average stress for the "W1" specimen in Figure 4.49 is 4.44 MPa, whereas it 5.65 MPa for the "W2" specimen (Figure 4.50). It is noted that the "W2" specimen has less damage at the point closest to midspan (x = 0 mm) as the load reaches a maximum (50 kN). For instance, for L450W100L2SW1 in Figure 4.49, the average bond stress at a distance 37.5 mm away from midspan (x = 37.5 mm) when the maximum load is reached (42 kN) is only 3.3 MPa, whearas that value is 0.6 MPa for L450W100L2SW2 at maximum load (50 kN) (Figure 4.50).

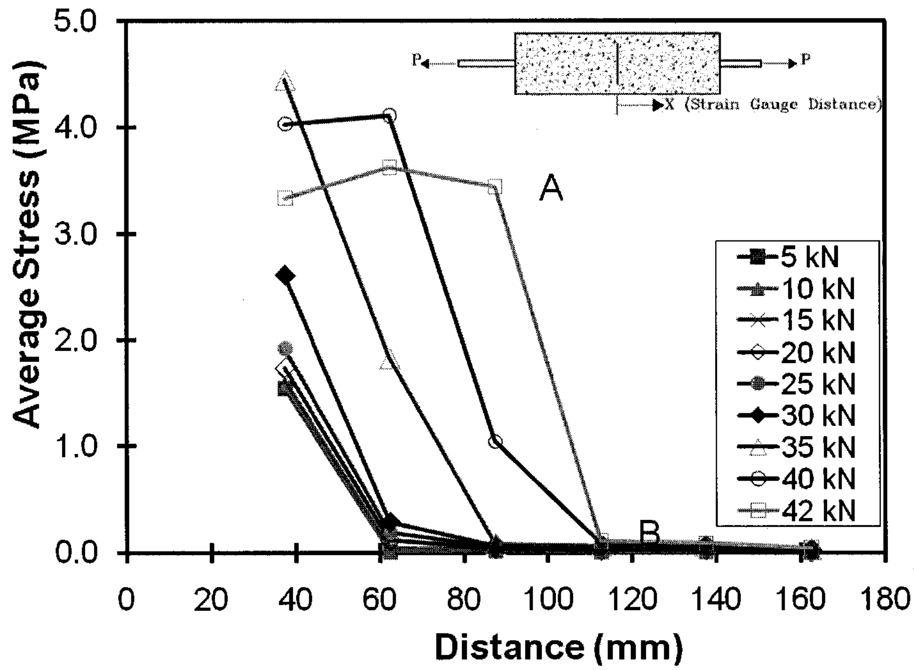

Figure 4.49 – Average Bond Stress Distribution for L450W100L2S<u>W1</u>

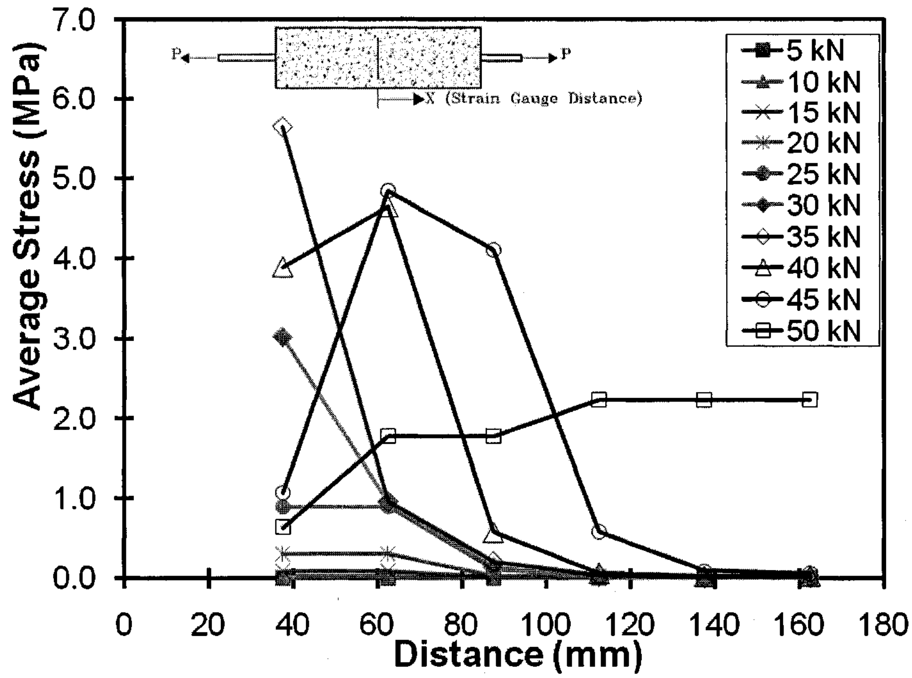

Figure 4.50 – Average Bond Stress Distribution for L450W100L2SW2

4.7 Average Bond Strength

The average bond strength can be defined as being the maximum force obtained during the tensile test divided by the bond area of the concrete-CFRP interface as shown in Equation 4.4 (ASTM Committee D30, 2006):

$$\tau_b = \frac{P_u}{2Lw} \tag{4.4}$$

where τ_b is the average bond strength in MPa

P_u is the maximum load acquired from the tensile test in N

L is the CFRP composite length in mm, and

w is the CFRP composite width in mm.

4.7.1 Average Bond Strength versus Bonded Length

Specimens with Larger Bond Width:

Table 4.10 shows the relationship of the average bond strength versus bonded length for specimens with a bond width of 100 mm. For specimens having cross wraps located on one half of the specimen, the average bond strength increased when decreasing the bond length (L). For example, the average bond strength (τ_b) for L450W100L1SW1 with a 450 mm bond length is 0.29 MPa, whereas that for L350W100L1SW1 with a 350 mm bond length is 0.47 MPa (Table 4.10(a)). That behaviour was reversed when cross wraps were placed on both halves of the specimen. For example, the average bond strength for L450W100L1SW2 for a 450 mm bond length with one layer of CFRP composite is 0.43 MPa, while that for L350W100L1SW2 is 0.39 MPa (Table 4.10(a)). This reversed behaviour for different cross wraps locations (one or both halves of the specimen) indicates that, in order to improve bond strength in a specimen, cross wraps should only be located on both halves when the bond length relative to specimen length is small (i.e. $L_{CFRP} : L_{specimen} \leq 0.9$).

As illustrated, increasing the stiffness from one CFRP layer (Table 4.10(a)) to two CFRP layers (Table 4.10(b)) increased the average bond strength. This difference was more significant for specimens that had a smooth surface as it reached up to 47% when L450W100L1SW1 (0.29 MPa) is compared to L450W100L2SW1 (0.47 MPa). For specimens that had a rough surface, however, the maximum difference was 20% when L350W100L1RW2 (0.54 MPa) is compared to L350W100L2RW2 (0.66 MPa). As noted in Table 4.10, specimens that had one layer of CFRP and a smooth surface had a lower average bond strength than those with a rough surface. For example, the average bond strength is 0.43 MPa for L450W100L1SW2, whereas it is 0.47 MPa for L450W100L1RW2. Specimens having two CFRP layers did not have exactly the same behaviour as those having one CFRP layer composite. The average bond strength varied depending on the surface preparation (smooth or rough), especially for specimens with two layers of CFRP composite.

Table 4.10 - Data for the Average Bond Strength versus Bonded Length Relationship for (a) W100 (One Layer), and (b) W100 (Two Layers)

(a)

SPECIMEN DESIGNATION	WIDTH (mm)	LENGTH (mm)	AVERAGE BOND STRENGTH (MPa)
L450W100L1SW1	100	450	**0.29**
L450W100L1SW2	100	450	***0.43***
L450W100L1RW1	100	450	0.44
L450W100L1RW2	100	450	**0.47**
L350W100L1SW2	100	350	***0.39***
L350W100L1SW1	100	350	**0.47**
L350W100L1RW1	100	350	0.51
L350W100L1RW2	100	350	**0.54**

(b)

SPECIMEN DESIGNATION	WIDTH (mm)	LENGTH (mm)	AVERAGE BOND STRENGTH (MPa)
L450W100L2SW1	100	450	**0.47**
L450W100L2RW1	100	450	0.48
L450W100L2RW2	100	450	0.50
L450W100L2SW2	100	450	0.56
L350W100L2RW1	100	350	0.60
L350W100L2SW2	100	350	0.61
L350W100L2SW1	100	350	0.63
L350W100L2RW2	100	350	**0.66**

Specimens with Smaller Bond Width:

Table 4.11 shows the relationship of the average bond strength (τ_b) versus bonded length (L) for specimens with a bond width of 75 mm. In all cases, the average bond strength increased when decreasing the bond length. As shown, increasing the stiffness (one CFRP layer to two CFRP layers) increased the average bond strength. As noted in Table 4.11, the difference in the bond strength values when varying the stiffness for specimens having a bonded length of 450 mm and a smooth surface was higher than the values for specimens having a bonded length of 350 mm. For example, the percent difference in the average bond strength values between L450W75L1SW1 and L450W75L2SW1 is 42%, whereas that difference between L350W75L1SW1 and L350W75L2SW1 is 28%. When the surface preparation changes from smooth to rough, this behaviour is reversed. The percent difference in the average bond strength values between L450W75L1RW1 and L450W75L2RW1 is 24%, and that difference between L350W75L1RW1 and L350W75L2RW1 is 42%. Further, placing cross wraps on both halves of the specimen increased the average bond strength values for specimens having a rough surface only. Specimens having a smooth surface, on the other hand, were not always influenced by that variation. In fact, in most cases shown in Table 4.11, specimens having a smooth surface and cross wraps on both halves had lower average bond strength than those having cross wraps on one half of the specimen only.

Table 4.11 - Data for the Average Bond Strength versus Bonded Length Relationship for (a) W75 (One Layer), and (b) W75 (Two Layers)

(a)

SPECIMEN DESIGNATION	WIDTH (mm)	LENGTH (mm)	AVERAGE BOND STRENGTH (MPa)
L450W75L1RW1	75	450	0.31
L450W75L1SW1	75	450	0.34
L450W75L1SW2	75	450	0.38
L450W75L1RW2	75	450	0.40
L350W75L1RW1	75	350	0.38
L350W75L1SW2	75	350	0.40
L350W75L1SW1	75	350	0.47
L350W75L1RW2	75	350	0.69

(b)

SPECIMEN DESIGNATION	WIDTH (mm)	LENGTH (mm)	AVERAGE BOND STRENGTH (MPa)
L450W75L2RW1	75	450	0.41
L450W75L2SW2	75	450	0.56
L450W75L2SW1	75	450	0.59
L450W75L2RW2	75	450	0.59
L350W75L2SW2	75	350	0.61
L350W75L2SW1	75	350	0.65
L350W75L2RW1	75	350	0.65
L350W75L2RW2	75	350	0.80

4.7.2 Average Bond Strength versus Bonded Width

Specimens with Longer Bond Length:

Table 4.12 illustrates the relationship of the average bond strength (τ_b) versus bonded width (W) for specimens with a bond length of 450 mm. The average bond strength increases when increasing the bond width for specimens having one layer of CFRP. For example, the average bond strength for L450W100L1RW1 (100 mm bond width) is 0.44 MPa, while it is 0.31 MPa for L450W75L1RW1 (75 mm bond width). This behaviour became the exact opposite for specimens having two layers of CFRP. For instance, the average bond strength for L450W100L2SW1 is 0.47 MPa, whereas that for L450W75L2SW1 is 0.59 MPa. As indicated, increasing the stiffness from one CFRP layer to two CFRP layers increases the average bond strength. The percent difference in average bond strength values for specimens with different stiffness (one layer of CFRP composite or two layers of CFRP composite) was more significant for specimens that had a smooth surface rather than a rough surface. For example, the percent difference in the average bond strength between L450W100L1RW1 and L450W100L2RW1 is 8%, whereas that difference between L450W100L1SW1 and L450W100L2SW1 is 38%. The results suggest that adding cross wraps on both halves of the specimen instead of just one half increases the average bond strength. The average bond strength for L450W100L1SW1 is 0.29 MPa, whereas that for L450W100L1SW2 is 0.43 MPa.

Table 4.12 - Data for the Average Bond Strength versus Bonded Width Relationship for (a) L450 (One Layer), and (b) L450 (Two Layers)

(a)

SPECIMEN DESIGNATION	WIDTH (mm)	LENGTH (mm)	AVERAGE BOND STRENGTH (MPa)
L450W100L1SW1	100	450	0.29
L450W100L1SW2	100	450	0.43
L450W100L1RW1	100	450	**0.44**
L450W100L1RW2	100	450	0.47
L450W75L1RW1	75	450	**0.31**
L450W75L1SW1	75	450	0.34
L450W75L1SW2	75	450	0.38
L450W75L1RW2	75	450	0.40

(b)

SPECIMEN DESIGNATION	WIDTH (mm)	LENGTH (mm)	AVERAGE BOND* STRENGTH (MPa)
L450W100L2SW1	100	450	***0.47***
L450W100L2RW1	100	450	0.48
L450W100L2RW2	100	450	0.50
L450W100L2SW2	100	450	0.56
L450W75L2RW1	75	450	0.41
L450W75L2SW2	75	450	0.56
L450W75L2SW1	75	450	***0.59***
L450W75L2RW2	75	450	0.59

Specimens with Shorter Bond Length:

Table 4.13 shows the relationship of the average bond strength (τ_b) versus bonded width (W) for specimens with a bond length of 350 mm. The average bond strength increases when increasing the bond width for specimens having one layer of CFRP. For example, the average bond strength of L350W100L1RW1 is 0.51 MPa, while for L350W75L1RW1, that value is 0.38 MPa. This behaviour is converted to the exact opposite for specimens having two layers of CFRP. For instance, the average bond strength of L350W100L2RW1 is 0.60 MPa, and it is 0.65 MPa for L350W75L2RW1. As shown, increasing the stiffness from one CFRP layer to two CFRP layers increases the average bond strength. For example, the average bond strength for L350W100L1SW1 is 0.47 MPa, while that for L350W100L2SW1 is 0.63 MPa. As noted in Table 4.13, specimens having a smooth surface generally had lower average bond strengths than those with a rough surface. Further, placing cross wraps on both halves of the specimen improved the average bond strength for specimens having a rough surface only. Specimens having a smooth surface, on the other hand, were not influenced with that. In fact, in all cases shown in Table 4.13, specimens having a smooth surface and cross wraps on both halves had lower average bond strength than those having cross wraps on one half of the specimen only.

Table 4.13 - Data for the Average Bond Strength versus Bonded Width Relationship for (a) L350 (One Layer), and (b) L350 (Two Layers)

(a)

SPECIMEN DESIGNATION	WIDTH (mm)	LENGTH (mm)	AVERAGE BOND STRENGTH (MPa)
L350W100L1SW2	100	350	0.39
L350W100L1SW1	100	350	***0.47***
L350W100L1RW1	100	350	**0.51**
L350W100L1RW2	100	350	0.54
L350W75L1RW1	75	350	**0.38**
L350W75L1SW2	75	350	0.40
L350W75L1SW1	75	350	0.47
L350W75L1RW2	75	350	0.69

(b)

SPECIMEN DESIGNATION	WIDTH (mm)	LENGTH (mm)	AVERAGE BOND STRENGTH (MPa)
L350W100L2RW1	100	350	**0.60**
L350W100L2SW2	100	350	0.61
L350W100L2SW1	100	350	***0.63***
L350W100L2RW2	100	350	0.66
L350W75L2SW2	75	350	0.61
L350W75L2SW1	75	350	0.65
L350W75L2RW1	75	350	**0.65**
L350W75L2RW2	75	350	0.80

4.8 Effective Bond Length

All figures shown in section 4.4 were obtained at maximum load, which can be defined as the load capacity reached prior to delamination. As mentioned before (subsection 4.3.1), this load can be identified as the load level at which the strain distribution becomes linear (De Lorenzis *et al.*, 2001). The area underneath the stress-slip curve (G_f) is the fracture energy per unit area of the concrete-CFRP interface (Figure 4.51).

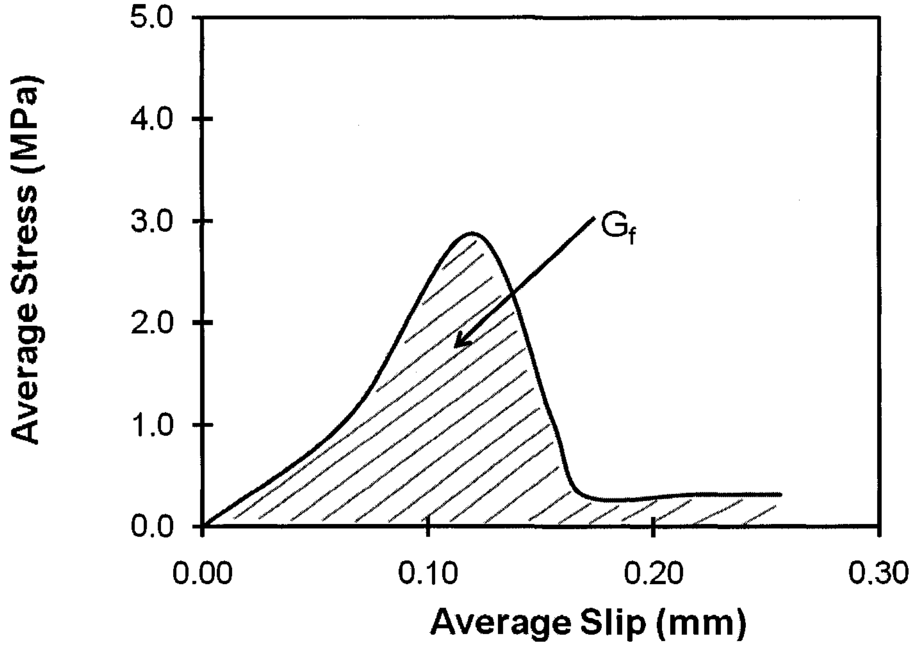

Figure 4.51 - Fracture Energy, G_f

If failure is bond-controlled, the maximum stress in the composite to be utilized for design cannot equal the tensile strength of the composite material (De Lorenzis *et al.*, 2001). Hence, ACI Committee 440 (ACI Committee 440, 2004) proposed the following relationship to determine the reduction factor required:

$$\varepsilon_{ub} = k_r \cdot \varepsilon_u \qquad (4.5)$$

Where ε_{ub} is the reduced ultimate strain level of the composite

ε_u is the composite's ultimate strain, and

k_r is a reduction factor that needs to be determined.

In order to determine the bond failure load, a linear constitutive law can be used. Figure 4.52 illustrates a stress-strain plot where the relationship is linear.

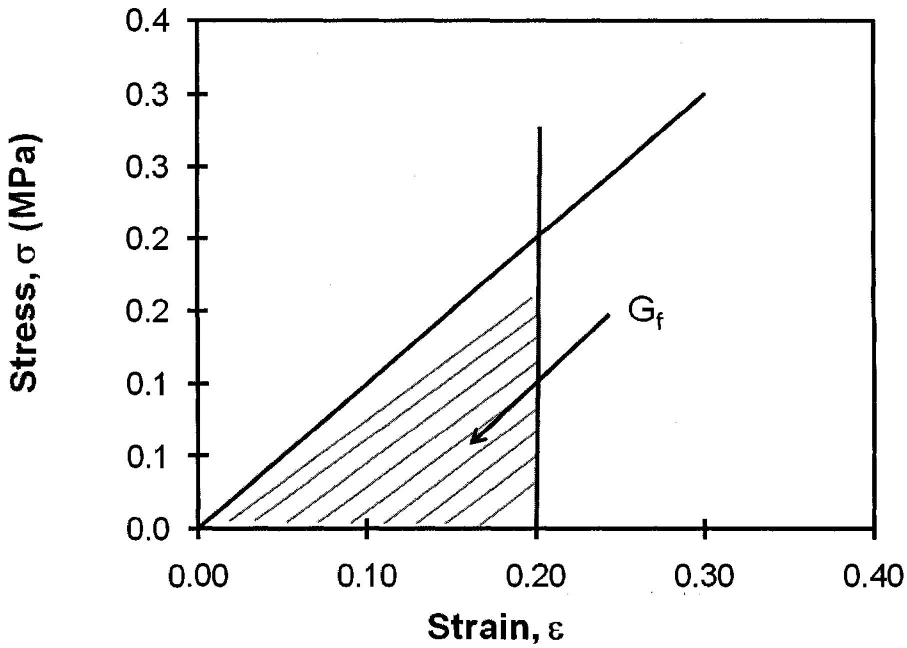

Figure 4.52 – Gf for a Stress-Strain Linear Relationship

Since G_f is the area under the curve, then

$$G_f = \tfrac{1}{2} t \sigma \varepsilon \quad (4.6)$$

For materials stressed in tension, stress and strain are defined by Hooke's Law:

$$\sigma = E\varepsilon \quad (4.7)$$

By substituting Equation 4.7 into Equation 4.6, the tensile strain at bond failure is obtained:

$$\varepsilon_{ub} = \sqrt{\frac{2 \cdot G_f}{E \cdot t}} \quad (4.8)$$

where E, and t are elastic modulus, and thickness of CFRP, respectively

G_f is the fracture energy per unit area of the interface.

and hence comparing Equation 4.8 with Equation 4.5, k_r is determined as in Equation 4.9,

$$k_r = \frac{\sqrt{2 \cdot G_f}}{\varepsilon_u \sqrt{E \cdot t}} \tag{4.9}$$

De Lorenzis *et al.* (2001) expressed the effective bond length (l_{eff}) as per Equation 4.10. They also mentioned that in order to calculate the effective bond length, an assumption is required on the shape of the local stress versus slip relationship. They assumed that the stress-slip relationship have an initial ascending branch followed by perfectly plastic behaviour at a value τ_m of bond stress as shown in Figure 4.51 and expressed by Equation 4.11.

$$l_{eff} = \frac{\varepsilon_{ub}}{\left.\frac{d\varepsilon}{dx}\right|_{peel}} \tag{4.10}$$

$$\left.\frac{d\varepsilon}{dx}\right|_{peel} = \frac{\tau_m}{tE} \tag{4.11}$$

Therefore, using Equations 4.8 and 4.11, Equation 4.10 becomes:

$$l_{eff} = \frac{\sqrt{2EtG_f}}{\tau_m} \tag{4.12}$$

Nakaba *et al.* (2001) suggested that the effective bond length is less than 100 mm, while Horiguchi and Saeki (1997) reported that it is between 76 mm and 102 mm. According to this study, the effective bond length was less than 100 mm in most cases, but it reached up to 150 mm for few specimens (Tables 4.14 and 4.15).

4.8.1 Effective Bond Length versus Stiffness

The simplest way to obtain the composite's stiffness would be to multiply its thickness by its elastic modulus (Nakaba et *al.*, 2001). Table 4.14 and Figure 4.53 illustrate the relationship of the effective bond length versus composite stiffness (kN/mm) for specimens with a bond length of 450 mm and a bond width of 100 mm. The behaviour pattern shown for a specimen with rough surface and that for a specimen with smooth surface is similar. The effective bond length for a specimen with smooth surface, however, is larger than that for rough surface. For example, the effective bond length for L450W100L1RW2 is 118 mm, whereas that value is 150 mm for L450W100L1SW2. By reviewing Table 4.14, it is observed that the difference between the effective bond length values for specimens with two CFRP layers is larger than the values for specimens with one CFRP layer. For instance, the percent difference between the effective bond length values of L450W100L1SW2 and L450W100L1RW2 is 21%, whereas that difference is 50% when comparing L450W100L2SW2 and L450W100L2RW2. In most cases, placing cross wraps on both halves of the specimen instead of one increased the effective bond length. The behaviour of the effective bond length versus stiffness relationship for specimens having a bond length of 350 mm and a bond width of 100 mm is identical.

Table 4.14 - Data for the Effective Bond Length vs. Stiffness Relationship for L450W100 Specimens with (a) Rough Surface, and (b) Smooth Surface

(a)

SPECIMEN DESIGNATION	EFFECTIVE LENGTH (mm)	STIFFNESS (KN/mm)
L450W100L1RW1	68	28
L450W100L1RW2	118	28
L450W100L2RW2	55	56
L450W100L2RW1	124	56

(b)

SPECIMEN DESIGNATION	EFFECTIVE LENGTH (mm)	STIFFNESS (KN/mm)
L450W100L1SW1	52	28
L450W100L1SW2	150	28
L450W100L2SW1	110	56
L450W100L2SW2	156	56

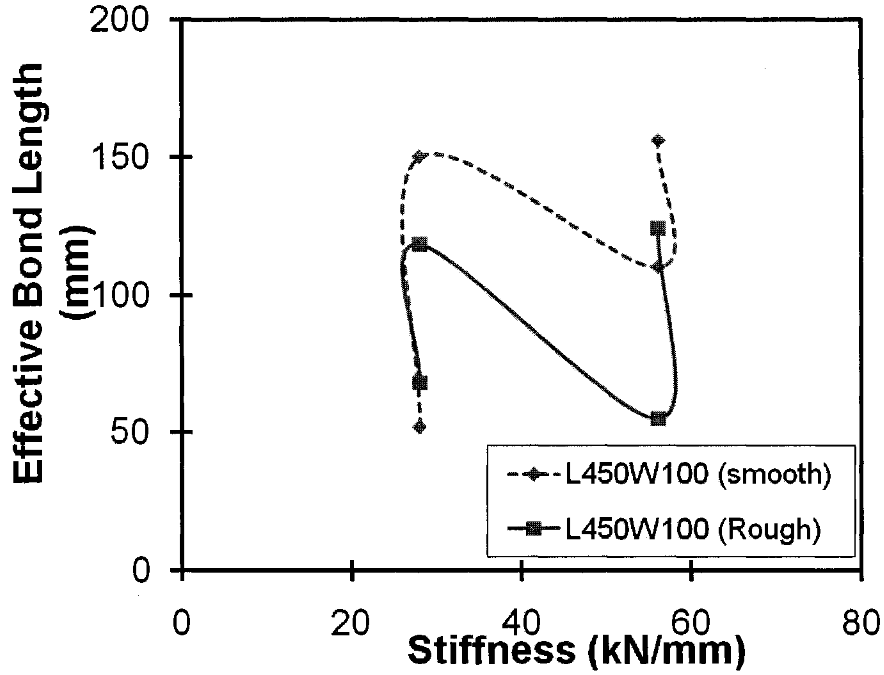

Figure 4.53 - Effective Bond Length versus Stiffness for Specimens with a Bond Length of 450 mm and a Bond Width of 100 mm

Table 4.15 and Figure 4.54 illustrate the relationship of the effective bond length versus stiffness for specimens having a bond length of 450 mm and a bond width of 75 mm. As shown, the behaviour pattern for a specimen having rough surface and that for a specimen having smooth surface is similar. The effective bond length values for specimens with smooth surface, however, are larger than those with rough surface. For example, the effective bond length for L450W75L1SW2 is 109 mm, whereas that for L450W75L1RW2 is 78 mm. In most cases, placing cross wraps on both halves of the specimen instead of one increased the effective length. The behaviour of the effective bond length versus stiffness relationship for specimens having a bond length of 350 mm and a bond width of 75 mm was identical.

Table 4.15 - Data for the Effective Bond Length versus Stiffness Relationship for L450W75 Specimens with (a) Rough Surface, and (b) Smooth Surface

(a)

SPECIMEN DESIGNATION	EFFECTIVE LENGTH (mm)	STIFFNESS (KN/mm)
L450W75L1RW2	78	28
L450W75L1RW1	97	28
L450W75L2RW1	82	56
L450W75L2RW2	188	56

(b)

SPECIMEN DESIGNATION	EFFECTIVE LENGTH (mm)	STIFFNESS (KN/mm)
L450W75L1SW1	98	28
L450W75L1SW2	109	28
L450W75L2SW1	118	56
L450W75L2SW2	199	56

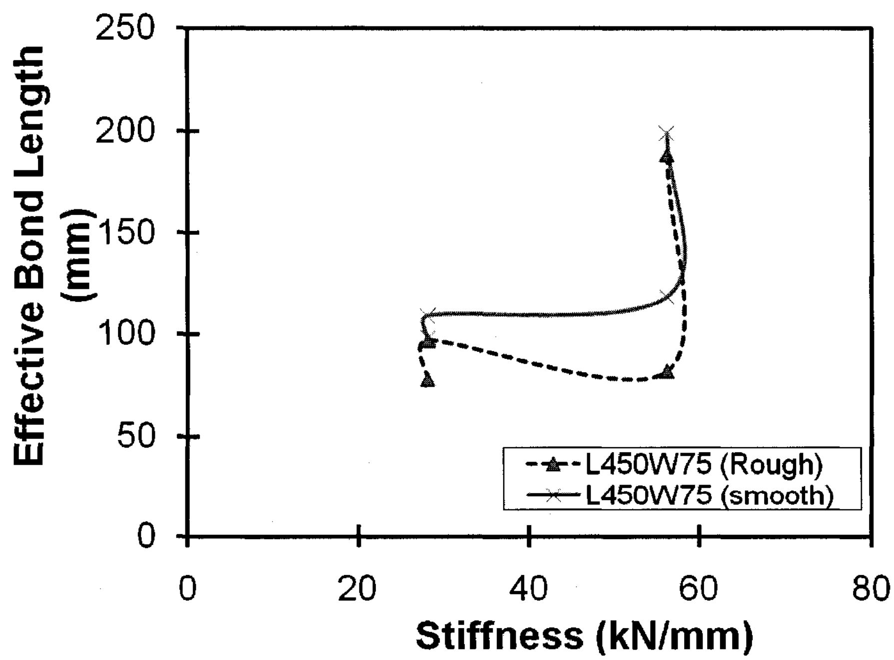

Figure 4.54 - Effective Bond Length versus Stiffness for Specimens with a Bond Length of 450 mm and a Bond Width of 75 mm

4.9 Failure Modes

As shown in Table 4.1, four modes of failure were observed in this study,

1- debonding at the lower part of the specimen (x > 0 mm),
2- debonding at the upper part of the specimen (x < 0 mm),
3- debonding with cross wrap failure at the lower part of the specimen, and
4- debonding with cross wrap failure at the upper part of the specimen.

Some of these failures took place at the strain gauge side of the specimen, whereas others took place at the no strain gauge side of the specimen, but it is believed that this variation was only due to the presence of small eccentricity that could not be controlled during the test. Most of the specimens (66%) experienced the first failure mode (debonding at the lower part of the specimen). The second failure mode (debonding at the upper part of the specimen) was not very severe because the cross wraps whose main role was to prevent debonding to occur were always located at the upper portion of the specimen. That mode of failure occurred in 22% of the specimens and was mostly experienced by specimens having a rough surface, a bond width of 350 mm, and cross wraps placed on both halves of the specimen. The third failure mode (debonding with cross wrap failure at the lower part of the specimen) only occurred in L450W100L2SW2 and L350W100L2RW1. Finally, only two specimens experienced the fourth failure mode, namely, L350W100L1RW2 and L350W100L2SW2. In all modes of failure, only a very thin layer of concrete was attached to the CFRP sheet after debonding took place (Nakaba et *al.*, 2001). Figures 4.55 to 4.58 illustrate the four failure modes.

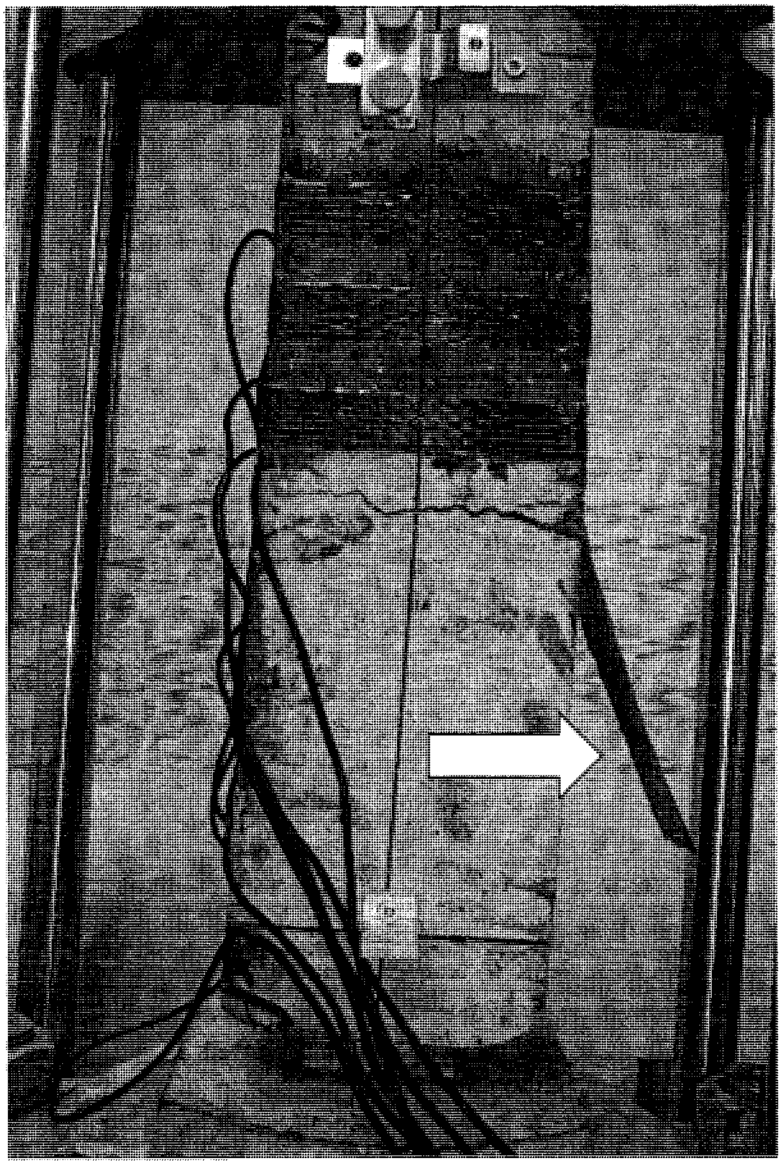

Figure 4.55 - Debonding at the Lower Part of the Specimen

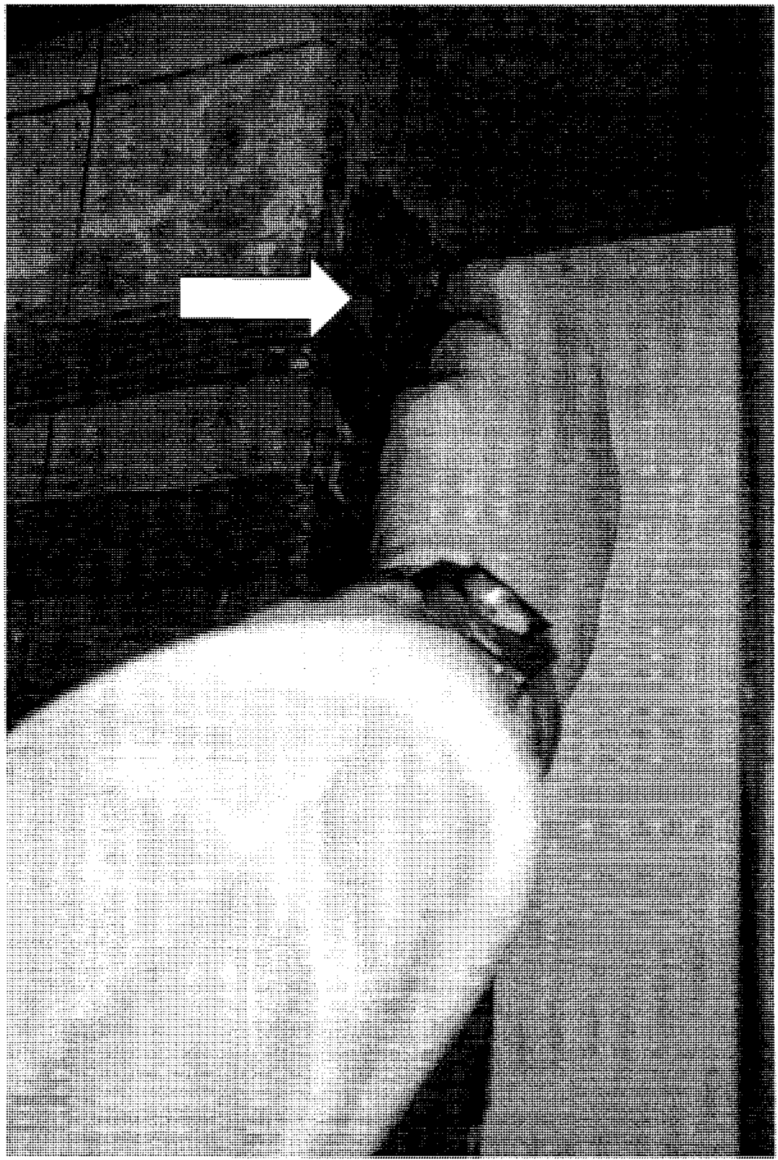

Figure 4.56 - Debonding at the Upper Part of the Specimen

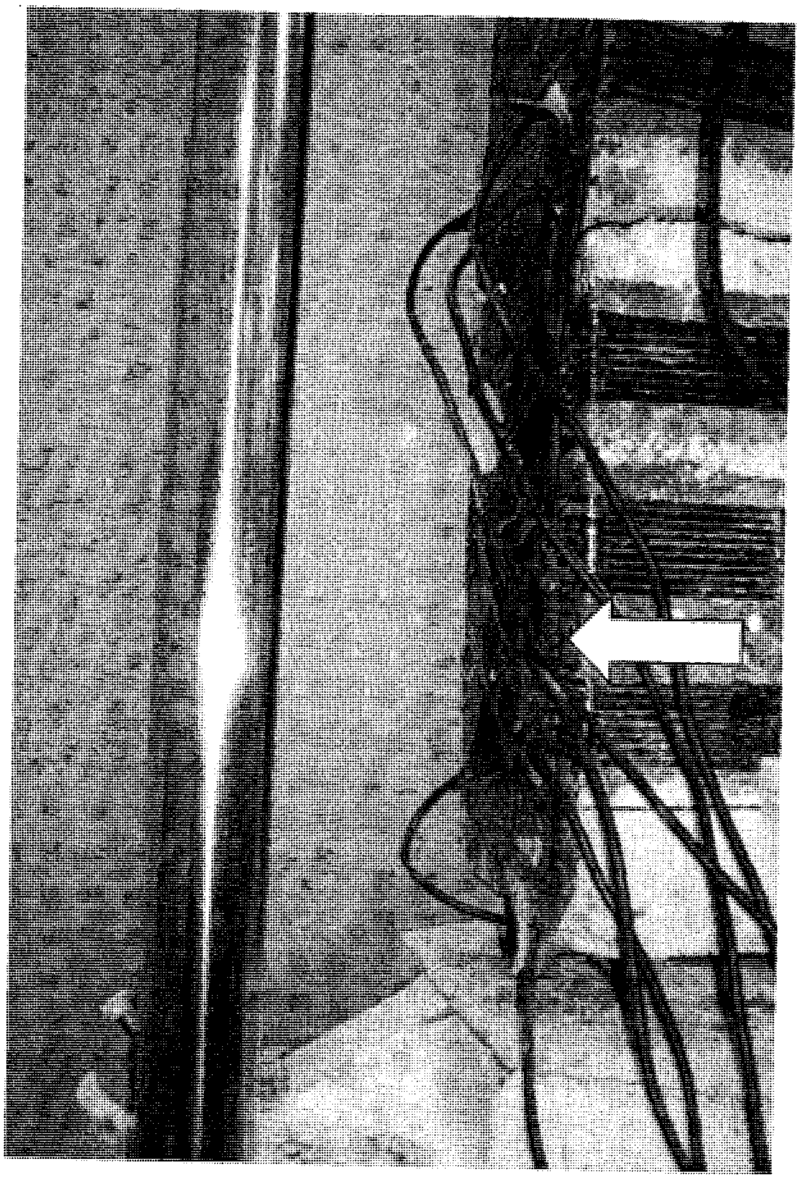

Figure 4.57 - Debonding and Wrap Failure at the Lower Part of the Specimen

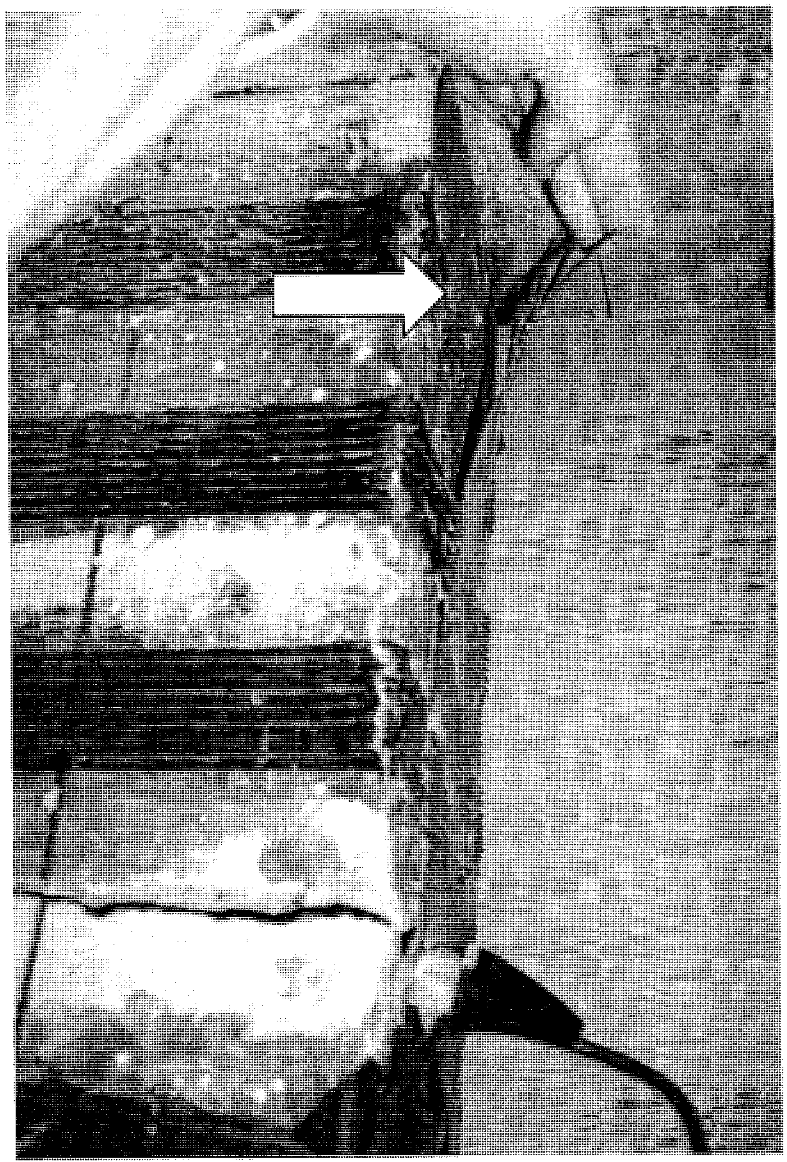

Figure 4.58 - Debonding and Wrap Failure at the Upper Part of the Specimen

CHAPTER 5
SUMMARY, CONCLUSIONS AND RECOMMENDATIONS

5.1 General

The present research was to study the effect of the parameters that are believed to influence the behaviour of the concrete-CFRP interface the most. The effective length required to achieve the bond strength capacity was also determined. The behaviour of thirty two specimens and two control specimens has been reported in details. This chapter summarizes the findings, provides conclusions, and recommends further work necessary for future studies in the area of this thesis.

5.2 Summary

Findings obtained in this study can be summarized as follows:

(a) Load versus displacement:

- Due to lack of displacement data at maximum load, all comparisons were performed at a load value of 20 kN.
- In average, the displacement measured on specimens with only one CFRP layer is 6.5 times the displacement measured from specimens with two CFRP layers.
- The displacement measured on specimens having a bond length of 450 mm is 1.3 times the displacement measured from specimens having a bond length of 350 mm.
- Specimens having a bond width of 100 mm have a displacement that is 5.2 times that of specimens having a bond width of 75 mm.
- Displacement for specimens having a smooth surface is 3.4 times the displacement measured from specimens having a rough surface.
- Specimens with cross wraps on one half have a displacement that is 2.8 times the displacement of specimens having cross wraps on both halves.

(b) Longitudinal strain versus gauge distance:

- At the earlier stages of loading, there is a resemblance in the strain versus distance curves' behaviour. They all depict a non linear shape, but as the load increases, the curves become more linear in shape.
- The specimen with shorter bond length fails rapidly, whereas failure of the specimen with longer bond length happens gradually.
- As the stiffness of the composite increases, the length of the segment with the steeper slope at maximum load becomes comparatively longer.
- At higher load levels, the percent difference between two consecutive strain readings for specimens having rough surface is lower than that for specimens having smooth surface.
- The use of cross wraps on both halves of the specimen shows a smaller strain value than the specimen with cross wraps on one half at the same load level and the same distance away from the specimen's midspan.

(c) Transverse strain versus gauge distance:

- The strain values 30 mm away from centerline across the width of the specimen were always higher compared with those at the centre. This implies that debonding does not occur evenly across the sheet's width and starts at the edge of the composite.
- The difference in strain values between the centreline and the edges of the specimen increases as the bond length or the bond width increase.

(d) Average bond stress versus average bond slip:

- The area under the average stress-average slip curve (fracture energy, G_f) decreases as the stiffness increases.
- The maximum average bond stress increases as the bond length increases, whereas it decreases as the bond width increases.
- The maximum average bond stress for specimens having a rough surface is larger than that for specimens with a smooth surface.
- The average bond stress for specimens with cross wraps on one half is greater than that for specimens with cross wraps on both halves.

(e) Average bond stress distribution:

- The average bond stress decreases in the area within 75 mm from midspan. At any point farther, an increase in the average bond stress is noticed.
- As stiffness increases, the length of the segment showing a decrease in the average bond stress distribution curve decreases. This denotes that increasing the stiffness allows the specimen to experience less damage at the point closest to midspan as the load reaches a maximum.
- As the bond length increases, the length of the segment showing a decrease in the average bond stress distribution curve immediately after the peak increases and hence delamination becomes more evident.
- When the bond width decreases, less damage occurs at the point closest to midspan as the load reaches a maximum.
- Less damage takes place at the point closest to midspan as the load reaches a maximum for specimens having a rough surface.
- Specimens with cross wraps on both halves have less damage at the point closest to the centre as the load reaches a maximum.

(f) Effective bond length:

- The effective bond length was less than 100 mm in most cases, but it reaches up to 150 mm for few specimens.
- The behaviour of the effective bond length versus stiffness curves for specimens having a rough surface and that for specimens having a smooth surface is similar. The effective bond length values for specimens with smooth surface, however, are larger than those with rough surface.
- In most cases, placing cross wraps on both halves of the specimen instead of one increased the effective bond length.

(g) Modes of failure:

- Four modes of failure were observed: 66% of the specimens experienced debonding at the lower part of the specimen ($x > 0$ mm), 22% of the specimens experienced debonding at the upper part of the specimen ($x < 0$ mm), 6% of the specimens had debonding with cross wrap failure at the lower part of the specimen, and 6% of the specimens had debonding with cross wrap failure at the upper part of the specimen. Most of the specimens experienced debonding at the lower part of the specimen.

5.3 Conclusions

In order to improve the design of concrete structures externally strengthened with FRP composites, it is necessary to understand the conditions at the concrete-CFRP interface.

This study concludes that the maximum load carrying capacity for specimens having a bond width of 100 mm is 43% higher than specimens having a bond width of 75 mm. It was also noted that the rate of debonding increases and the bond strength increases as the width decreases.

The maximum load carrying capacity for specimens having a bond length of 450 mm is 16% higher than specimens having a bond length of 350 mm. In addition, the rate of debonding increases but the bond strength decreases as the bond length decreases.

The maximum load carrying capacity for specimens having a rough surface is 30% higher than specimens having a smooth surface. Moreover, a rough surface preparation enhances the ability of the stress transfer to keep up with the change in strain and hence debonding occurs at higher load levels.

The maximum load carrying capacity for specimens having cross wraps on both halves is 17% higher than specimens having cross wraps on one half only. It was also noted that having cross wraps on both halves of the specimen does not influence the bond strength capacity significantly.

The maximum load carrying capacity increases by 25% as the CFRP's stiffness increases from one layer to two layers. Further, the active bond stress section increases but bond strength decreases as stiffness increases.

5.4 Recommendations

This study provided important conclusions with regards to five variables that influence the bond behaviour of the concrete-CFRP interface. However, in order to understand this bond behaviour further, it is recommended that:

(a) Instead of having one specimen of each combination, additional samples should be prepared to verify the results acquired.

(b) Additional specimens should have transverse strain gauges to investigate the behavioural changes for different CFRP stiffness, surface preparation, and number of cross wraps.

(c) Additional transverse strain gauges should be applied along the length of the specimen (i.e. not only at 25 mm away from midspan like the case was in this study) to observe any behavioural changes.

(d) From fracture mechanics theory, it is known that the size of a test sample has an impact on its resistance (Brosens and Van Gemert, 1997). That is, the smaller the test sample, the higher its resistance. Hence, different specimen sizes should be tested to verify the size effect on the bond behaviour of the concrete-CFRP interface.

REFERENCES

1. ACI Committee 440, 1996, "ACI 440R-96: State-of-The-Art Report on Fiber Reinforced Plastic Reinforcement for Concrete Structures." American Concrete Institute, Detroit, Michigan, USA.

2. ACI Committee 440, 2004, "ACI 440.3R-04: Guide Test Methods for Fiber-Reinforced Polymers (FRPs) for Reinforcing or Strengthening Concrete Structures." American Concrete Institute, Farmington Hills, Michigan, USA.

3. Alagusundaramoorthy, P., Harik, I.E., and Choo, C.C., 2003, "Flexural Behavior of R/C Beams Strengthened with Carbon Fiber Reinforced Polymer Sheets or Fabric." Journal of Composites for Construction, vol. 7, no. 4, pp. 292-301.

4. Alma Memo Series, 1995, "Visit to Thermoplastic Pultrusion, Inc.," http://www.alma.nrao.edu/memos/html-memos/alma133/memo133.html, updated on June 11, 2003, viewed on 10 July, 2006.

5. Almakt, M., Balazs, G., and Pilakoutas, K., 1998, "Strengthening of RC Elements by CFRP Plates Local Failure." 2nd International Symposium in Civil Engineering, Budapest.

6. ASTM Committee, "ASTM 172-71: Standard Method of Sampling Fresh Concrete." ASTM International, West Conshohocken, PA, USA. 1977.

7. ASTM Committee C09, "C 39/C 39M-05: Standard Test Method for Compressive Strength of Cylindrical Concrete Specimens." ASTM International, West Conshohocken, PA, USA. 2005.

8. ASTM Committee C143, "ASTM C143/C143M-03: Standard Test Method for Slump of Hydraulic Cement Concrete." ASTM International, West Conshohocken, PA, USA. 2003.

9. ASTM Committee D01, "D 4541-02: Standard Test Method for Pull-off Strength of Coatings Using Portable Adhesion Testers." ASTM International, West Conshohocken, PA, USA. 2002.

10. ASTM Committee D30, "D 3039/D 3039M-00: Standard Test Method for Tensile Properties of Polymer Matrix Composite Materials." ASTM International, West Conshohocken, PA, USA. 2006.

11. ASTM Committee E28, "E 132-04: Standard Test Method for Poisson's Ratio at Room Temperature." ASTM International, West Conshohocken, PA, USA. 2004.

12. Bizindavyi, L., and Neale, K.W., 1999, "Transfer Lengths and Bond Strengths for Composites Bonded to Concrete." Journal of Composites for Construction, vol. 3, no. 4, pp. 153-160.

13. Brosens, K., and Van Gemert, D., 1997, "Anchoring Stresses between Concrete and Carbon Fibre Reinforced Laminates." Proceedings of the Third International Symposium on Non-Metallic (FRP) Reinforcement for Concrete Structures, vol. 1, pp. 271-278.

14. Brozens, K., and Van Gemert, D., 1999, "Anchorage Design for Externally Bonded Carbon Fiber-Reinforced Polymer Laminates." Proceedings of the FRPRCS-4, SP-188-56, American Concrete Institute, Farmington Hills, Michigan, USA, pp. 635-645.

15. Canadian Highway Bridge Design Code, 2000, "CSA-S6-00 (R2005)." Canadian Standard Association, Mississauga, Ontario, Canada.

16. Canadian Standards Association (CSA), 1990, "A23.1-M90: Concrete Materials and Methods of Concrete Construction." Canadian Standards Association, Toronto, Ontario, Canada.

17. Canadian Standards Association (CSA), 1990, "A23.2-2A: Methods of Test for concrete." Canadian Standards Association, Toronto, Ontario, Canada.

18. Canadian Standards Association (CSA), 2002, "S806-02: Design and Construction of Building Components with Fibre-Reinforced Polymers." Canadian Standards Association, Toronto, Ontario, Canada.

19. Chen, JF, and Teng, JG, 2002, "Anchorage Strength Models for FRP and Steel Plates Bonded to Concrete." Journal of Structural Engineering, ASCE, vol. 127, no. 7, pp. 784-791.

20. Chung, D.L., 1994, "Carbon Fiber Composites." Butterworth-Heinemann, Newton, MA, USA.

21. Dai, J.G., 2003, "Interfacial Models for Fiber Reinforced Polymer (FRP) Sheets Externally Bonded to Concrete." Ph.D Dissertation, Hokkaido University, Japan.

22. De Lorenzis, L., Miller, B., and Nanni, A., 2001, "Bond of Fiber-Reinforced Polymer Laminates to Concrete." ACI Materials Journal, vol. 98, no. 3, pp.256-264.

23. Horiguchi, T., and Saeki, N., 1997, "Effect of Test Methods and Quality of Concrete on Bond Strength of CFRP Sheet." Proceedings of the Third International Symposium, Japan Concrete Institute, Japan, vol. 1, pp. 265-270.

24. Intelligent Sensing for Innovative Structures (ISIS) Canada, 2004, "An Introduction to FRP Strengthening of Concrete Structures." ISIS Canada Educational Module No. 4, Department of Civil Engineering, Queen's University, Ontario, Canada.

25. Jaeger, L.G., Mufti, A.A., and Tadros, G., 1997, "The Concept of the Overall Performance Factor in Rectangular Section Reinforced Concrete Members." Proceedings of the 3rd international Symposium on Non-Metallic (FRP) Reinforcement for Concrete Structures." Sapporo, Japan, vol. 2, pp. 551-559.

26. Kamel, A., Elwi, A., and Cheng, R., 2006, "Experimental Study on the Behavior of Carbon Fiber Reinforced Polymer Sheets Bonded to Concrete." Canadian Journal of Civil Engineering, vol. 33, no. 11, pp. 1438-1449.

27. Karbhari, V.M., and Engineer, M., 1996, "Investigation of Bond between concrete and Composites: Use of a Peeling Test." Journal of Reinforced Plastics and Composites, vol. 15, no. 2, pp.208-227.

28. Kim, I., 2006, "Rehabilitation of Poorly Detailed RC Structures Using CFRP Materials." Thesis, College of Civil Engineering, University of Texas at Austin, Texas, USA.

29. Maeda, T., Asano, Y., Sato, Y., Ueda, T., and Kakuta, Y., 1997, "A Study on Bond Mechanism of Carbon Fiber Sheet." Proceedings of the Third International Symposium on Non-Metallic (FRP) Reinforcement for Concrete Structures, vol. 1, pp. 279-286.

30. Meier, U., 1987, "Bridge Repair with High Performance Composite Materials." Material und Technik, vol. 4, pp. 125-128 (in German)

31. Meier, U., 1995, "Strengthening of Structures Using Carbon Fibre / Epoxy Composites." Construction and Building Materials, vol. 9, no. 6, pp. 341-351.

32. Mufti, A, 2002, "Structural Health Monitoring of Innovative Canadian Civil Engineering Structures." Structural Health Monitoring, vol. 1, no. 89, pp. 89-103.

33. Nakaba, K., Kanakubo, T., Furuta, T., and Yoshizawa, H., 2001, "Bond Behavior between Fiber-Reinforced Polymer Laminates and Concrete." ACI Structural Journal, vol. 98, no. 3, pp. 359-367.

34. Niu, H., and Wu, Z., 2006, "Effects of FRP-Concrete Interface Bond Properties on the Performance of RC Beams Strengthened in Flexure with Externally Bonded FRP Sheets." Journal of Materials in Civil Engineering, vol. 18, no. 5, pp. 723-731.

35. Plevris, N., Triantafillou, T.C., and Veneziano, D., 1995, "Reliability of RC Members Strengthened with CFRP Laminates." Journal of Structural Engineering, ASCE, vol. 121, no. 7, pp. 1037-1044.

36. Sato, Y., Asano, Y., Ueda, T., 2001, "Fundamental Study on Bond Mechanism of Carbon Fiber Sheet." Translation from Proceedings of JSCE, vol. 47, no. 648, pp. 97-115.

37. Sebastian, W.M., 2001, "Significance of Midspan Debonding Failure in FRP Plated Concrete Beams." Journal of Structural Engineering, ASCE, vol. 127, no. 7, pp. 792-798.

38. Shalaby, A. and Murison, S., 2001, "Using Fiber-Reinforced Polymer Load Transfer Devices in Jointed Concrete Pavements." Proceedings of 7th International Conference on Concrete Pavements, Orlando, Florida, USA.

39. Sika Canada Inc., 2004, "Product Data Sheet – CSC Master Format 03 01 30 – Sikadur 300." http://www.sikacanda.ca, viewed on 12 May, 2007.

40. Sika Canada Inc., 2004, "Product Data Sheet – CSC Master Format 03 01 30 – Sikadur 330." http://www.sikacanada.ca, viewed on 12 May, 2007.

41. Sika Canada Inc., 2004, "Product Data Sheet – CSC Master Format 03 01 30 – SikaWrap Hex 230C." http://www.sikacanada.ca, viewed on 12 May, 2007.

42. Svecova, D., Rizkalla, S., Tadros, G., and Mufti, A., 2001, "Reinforcing Concrete Structures with Fiber Reinforced Polymers." Design Manual No. 3, ISIS Canada Corporation, Manitoba, Canada.

43. Taljsten, B., 1994, "Plate Bonding. Strengthening of Existing Concrete Structures with Epoxy Bonded Plates of Steel or Fiber Reinforced Plastics." Doctoral Thesis, Lulea University of Technology, Sweden.

44. Technology Information, Forecasting and Assessment Council (TIFAC), 2004, "News and Views – Staff Publications – Composite Fabrication by Filament Winding," http://www.tifac.org.in/news/acfil.htm, viewed on 10 July, 2006.

45. Tennyson, R.C., Mufti, A., Rizkalla, S., Tadros, G., and Benmokrane, B., 2001, "Structural Health Monitoring of Innovative Bridges in Canada with Fiber Optic Sensors." Smart Materials and Structures, vol. 10, pp. 560-573.

46. Triantafillou, T., Matthys, S., and Taerwe, L., 2001, "Design of Concrete Members Strengthened with Externally Bonded FRP Reinforcement." FRPRCS-5, University of Cambridge, UK, pp. 157-166.

47. U.S. Department of Labor, 2002, "OSHA Technical Manual, Section III: Chapter 1," http://www.osha.gov/dts/osta/otm/otm_iii/otm_iii_1.html, viewed on 10 July 2006.

48. Ueda, T., Dai, J., 2005, "Interface Bond between FRP Sheets and Concrete Substrates: Properties, Numerical Modeling and Roles in Member Behaviour." Progress in Structural Engineering and Materials, vol. 7, no. 1, pp. 27-43.

49. Ueda, T., Sato, Y., and Asano, Y., 1998, "Experimental Study on Bond Strength of Continuous Carbon Fiber Sheets." Proceedings of the FRPRCS-4, SP-188-37, American Concrete Institute, Farmington Hills, Michigan, USA, pp. 407-416.

50. Union College, 2007, "Concrete Mix Design: Design Procedure," http://concrete.union.edu/general.htm, viewed on 31 May 2007.

51. Uomoto, T., Mutsuyoshi, H., Katsuki, F., and Misra, S., 2002, "Use of Fiber Reinforced Polymer Composites as Reinforcing Material for Concrete." Journal of Materials in Civil Engineering, vol. 14, no. 3, pp. 191-209.

52. Yao, J., Teng, J.G., and Chen, J.F., 2005, "Experimental Study on FRP-to-Concrete Bonded Joints." Composites, Part B: Engineering, vol. 36, no. 2, pp. 99-113.

53. Yoshizawa, H., Myojo, T., Okoshi, M., Mizukoshi, M., and Kliger, H., 1996, "Effect of Sheet Bonding Condition on Concrete Members Having Externally Bonded Carbon Fiber Sheet." Proceedings of the Fourth Materials Engineering Conference, ASCE, Annual Convention, Washington D.C., USA, pp. 1608-1616.

APPENDIX A

LONGITUDINAL STRAIN VERSUS GAUGE DISTANCE

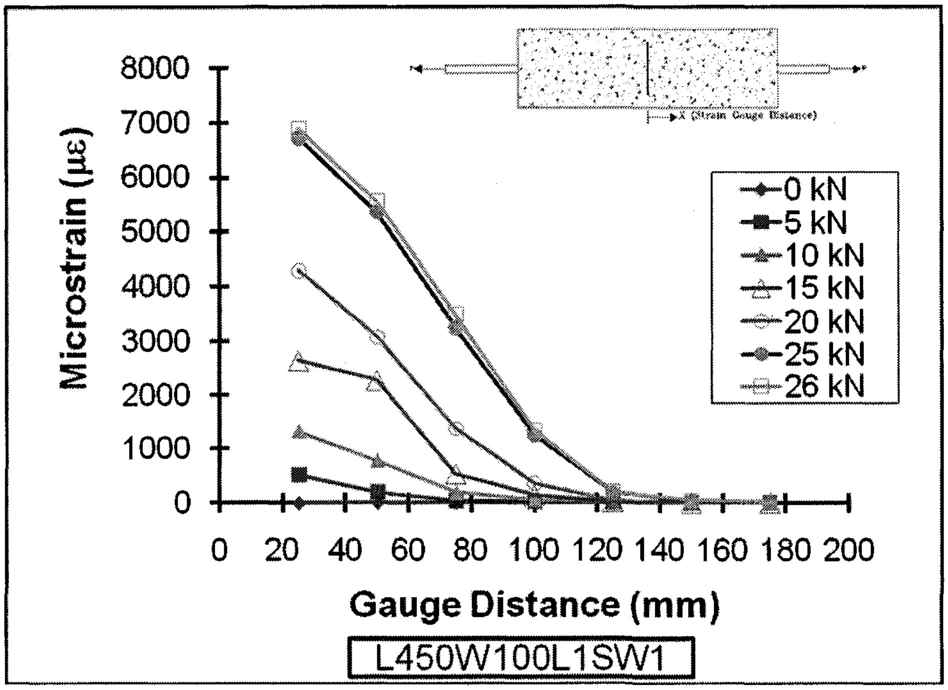

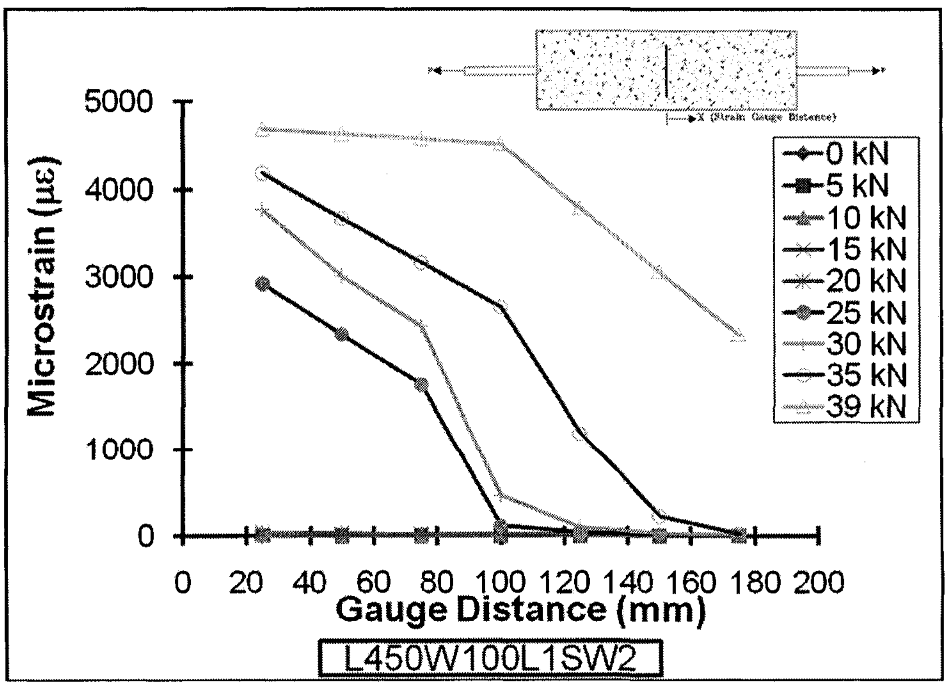

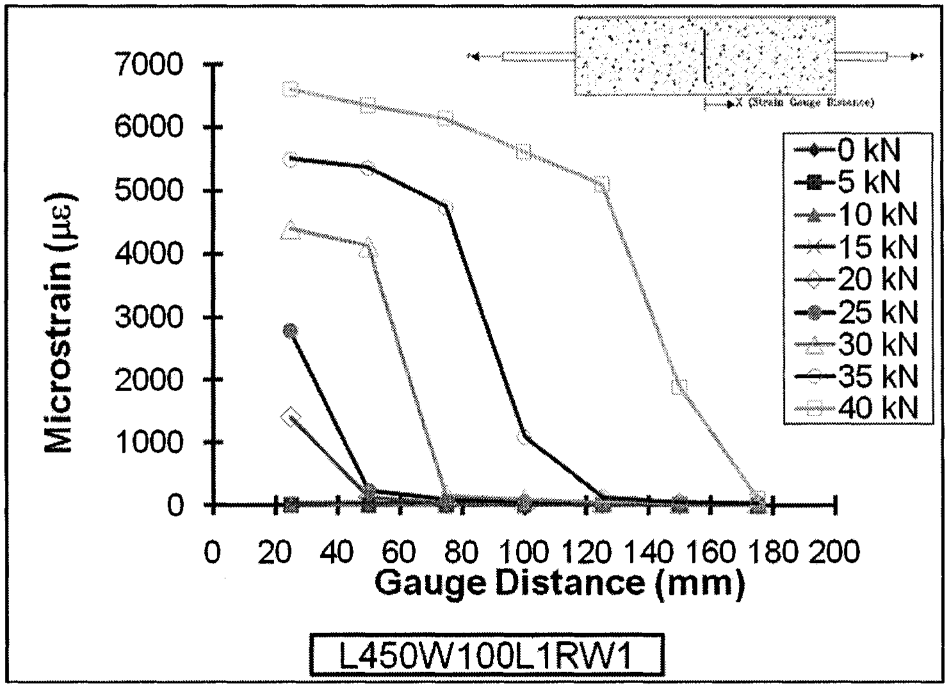

X (Strain Gauge Distance)
7000
6000
5000
4000
3000
2000
1000
0
Microstrain (με)
0 20 40 60 80 100 120 140 160 180 200
Gauge Distance (mm)
0 kN
5 kN
10 kN
15 kN
20 kN
25 kN
30 kN
35 kN
40 kN
L450W100L1RW1

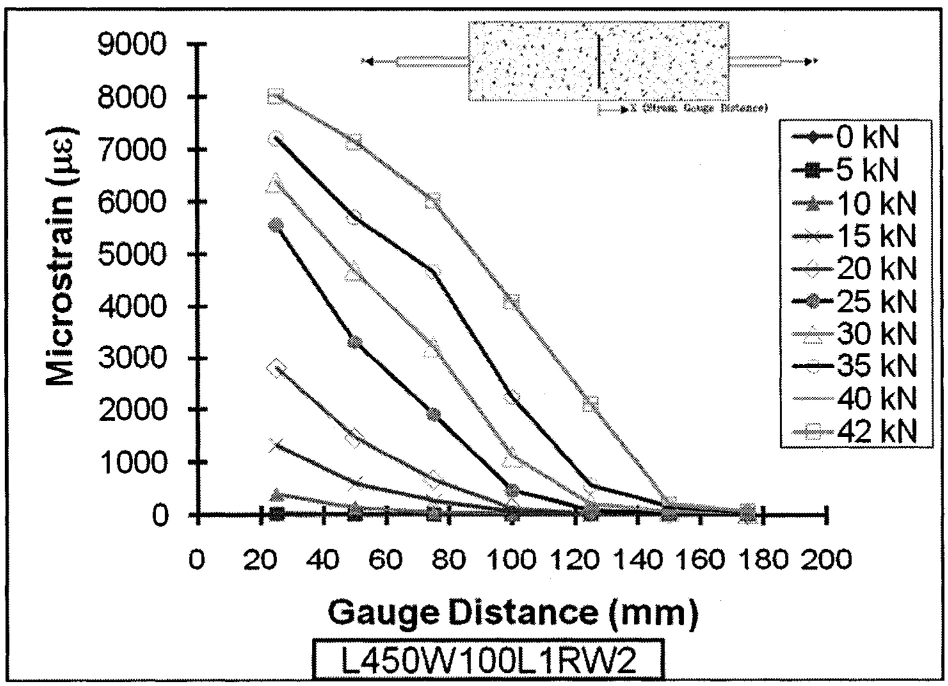

X (Strain Gauge Distance)
9000
8000
7000
6000
5000
4000
3000
2000
1000
0
Microstrain (με)
0 20 40 60 80 100 120 140 160 180 200
Gauge Distance (mm)
0 kN
5 kN
10 kN
15 kN
20 kN
25 kN
30 kN
35 kN
40 kN
42 kN
L450W100L1RW2

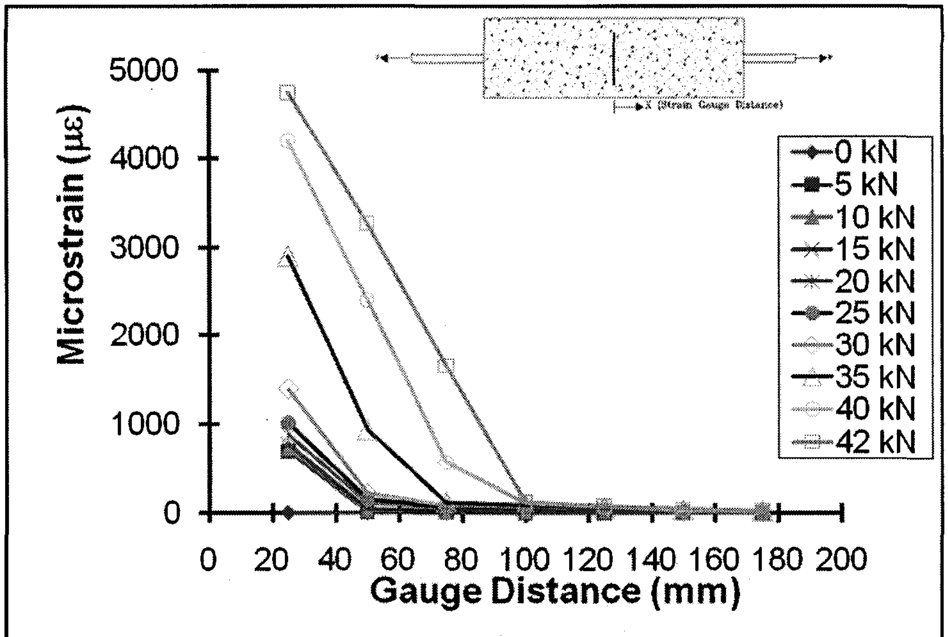

L450W100L2SW1

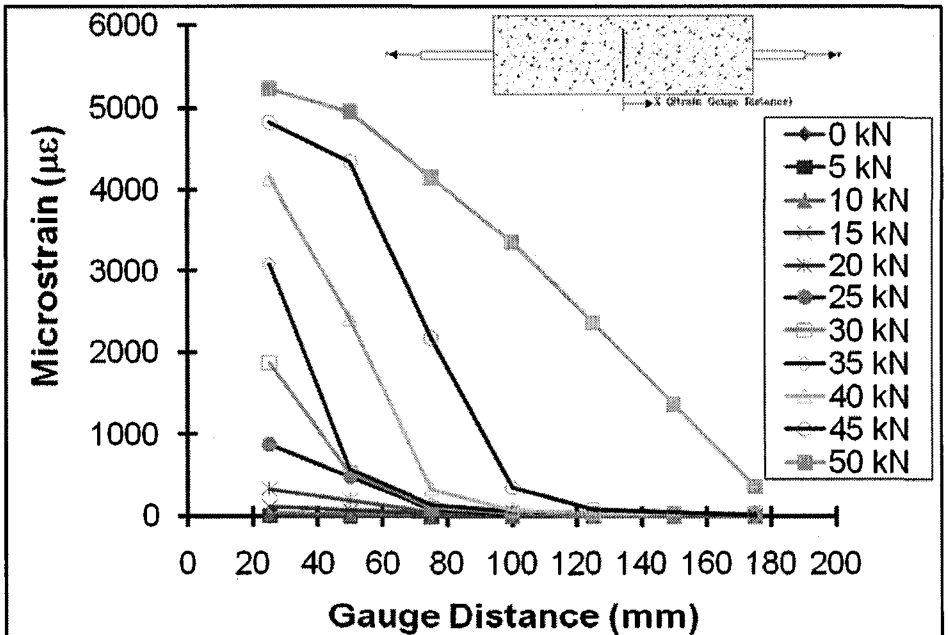

L450W100L2SW2

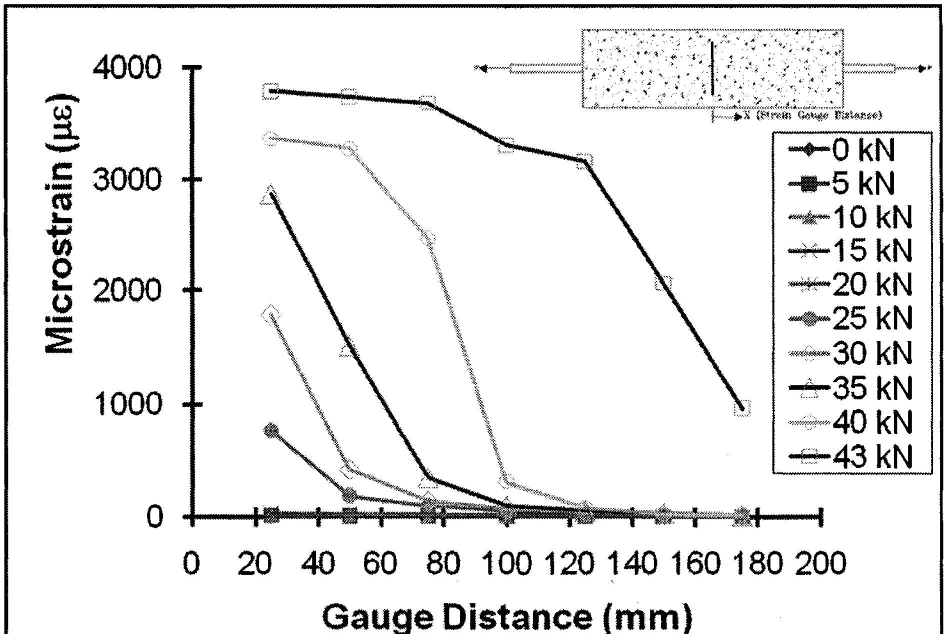

L450W100L2RW1

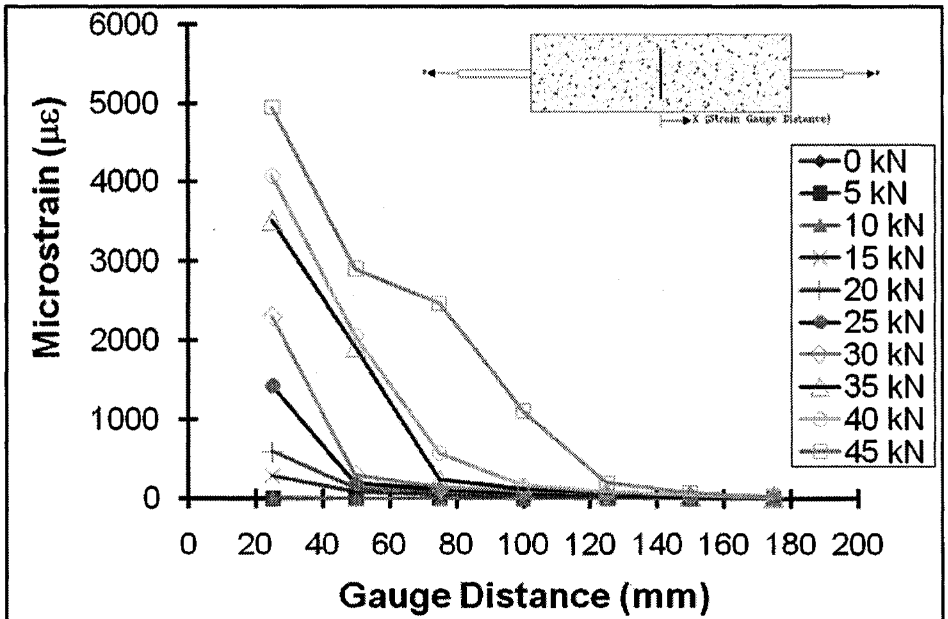

L450W100L2RW2

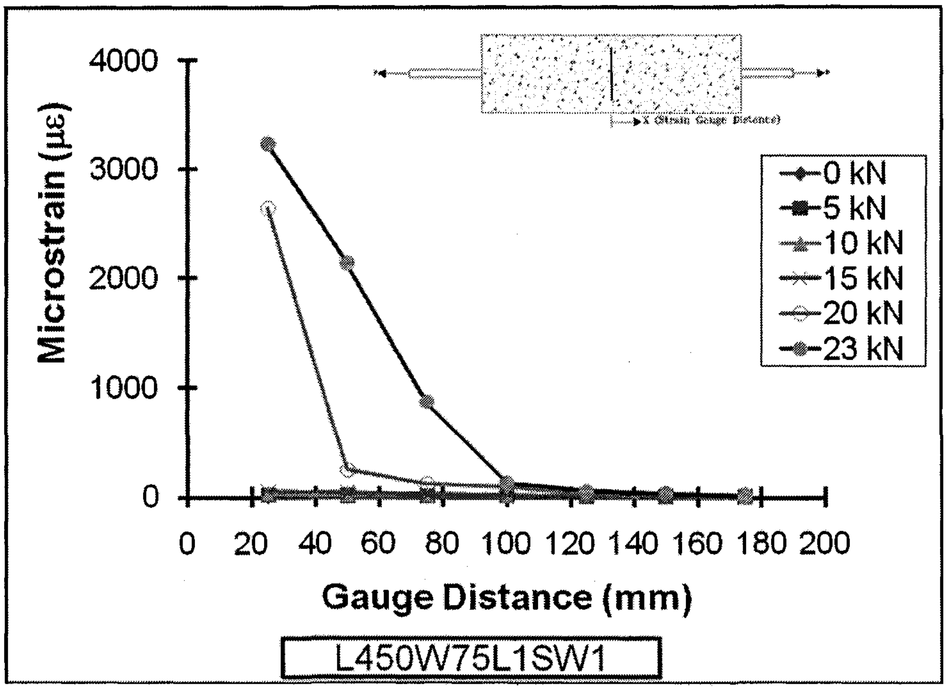
X (Strain Gauge Distance)
0 kN
5 kN
10 kN
15 kN
20 kN
23 kN
Microstrain (με)
Gauge Distance (mm)
L450W75L1SW1

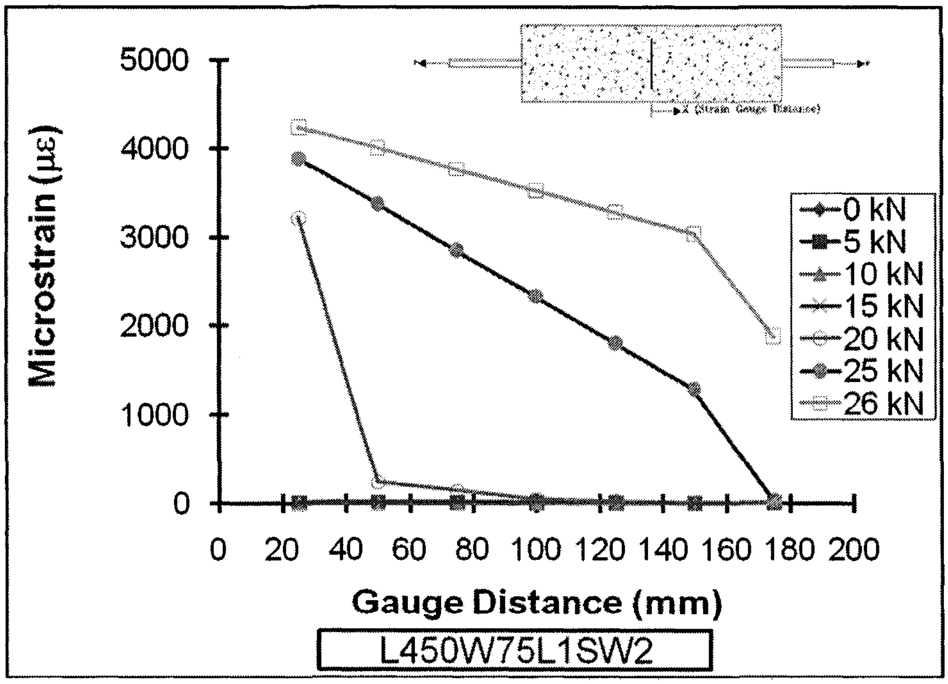
X (Strain Gauge Distance)
0 kN
5 kN
10 kN
15 kN
20 kN
25 kN
26 kN
Microstrain (με)
Gauge Distance (mm)
L450W75L1SW2

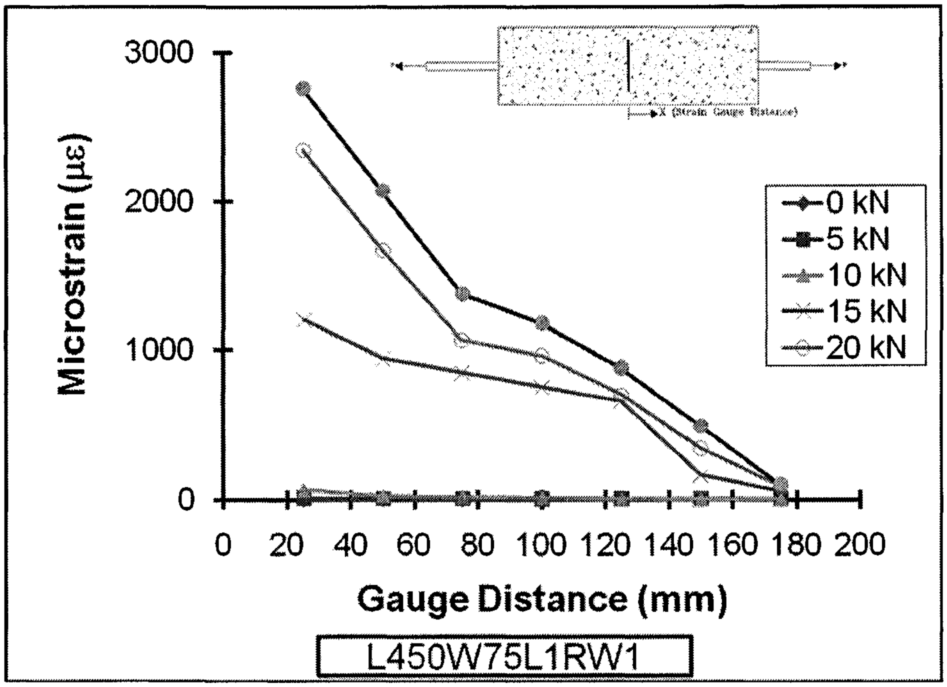
3000
2000
1000
0
Microstrain (με)
X (Strain Gauge Distance)
0 kN
5 kN
10 kN
15 kN
20 kN
0 20 40 60 80 100 120 140 160 180 200
Gauge Distance (mm)
L450W75L1RW1

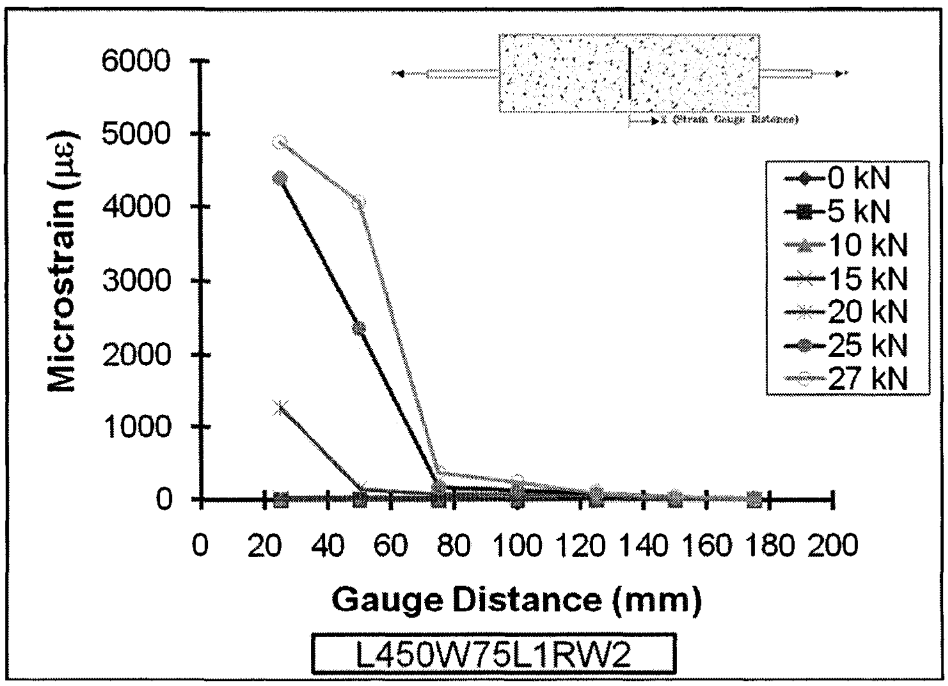
6000
5000
4000
3000
2000
1000
0
Microstrain (με)
X (Strain Gauge Distance)
0 kN
5 kN
10 kN
15 kN
20 kN
25 kN
27 kN
0 20 40 60 80 100 120 140 160 180 200
Gauge Distance (mm)
L450W75L1RW2

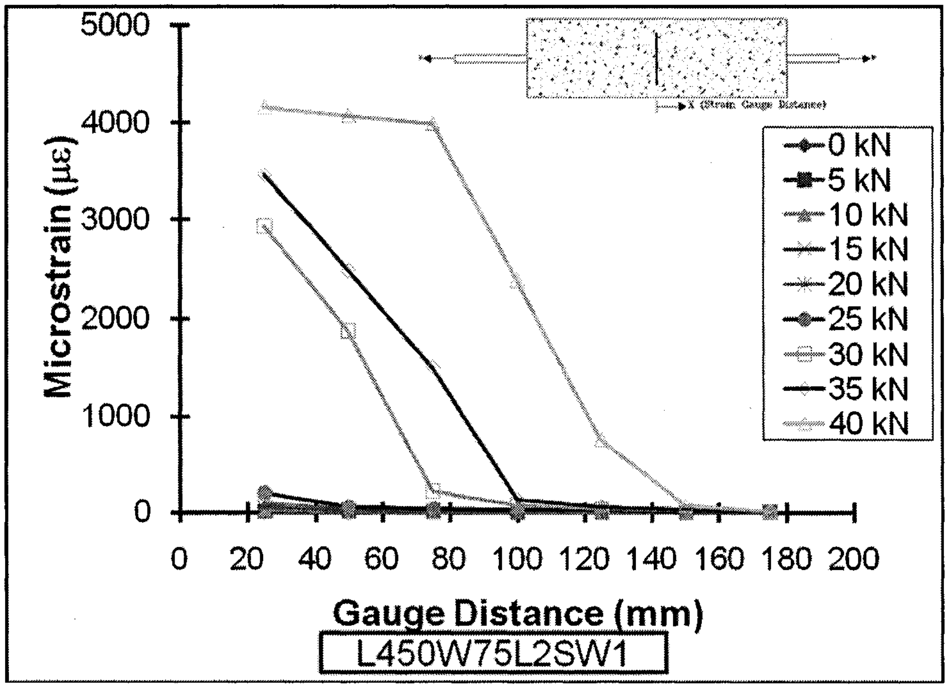
5000
4000
3000
2000
1000
0
Microstrain (με)
0 20 40 60 80 100 120 140 160 180 200
Gauge Distance (mm)
0 kN
5 kN
10 kN
15 kN
20 kN
25 kN
30 kN
35 kN
40 kN
L450W75L2SW1

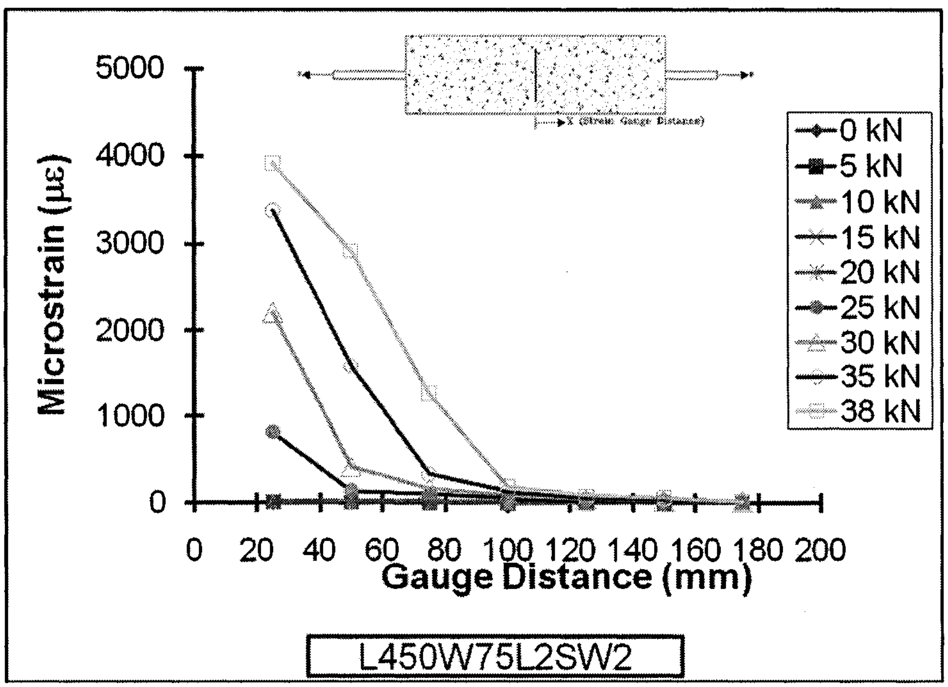
5000
4000
3000
2000
1000
0
Microstrain (με)
0 20 40 60 80 100 120 140 160 180 200
Gauge Distance (mm)
0 kN
5 kN
10 kN
15 kN
20 kN
25 kN
30 kN
35 kN
38 kN
L450W75L2SW2

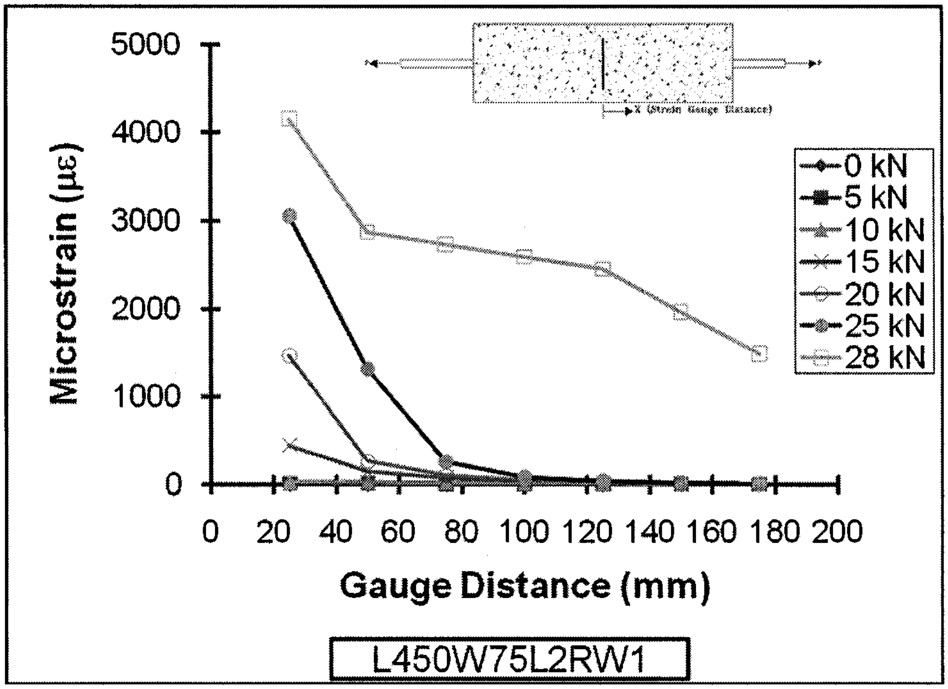
X (Strain Gauge Distance)
0 kN
5 kN
10 kN
15 kN
20 kN
25 kN
28 kN
Microstrain (με)
Gauge Distance (mm)
L450W75L2RW1

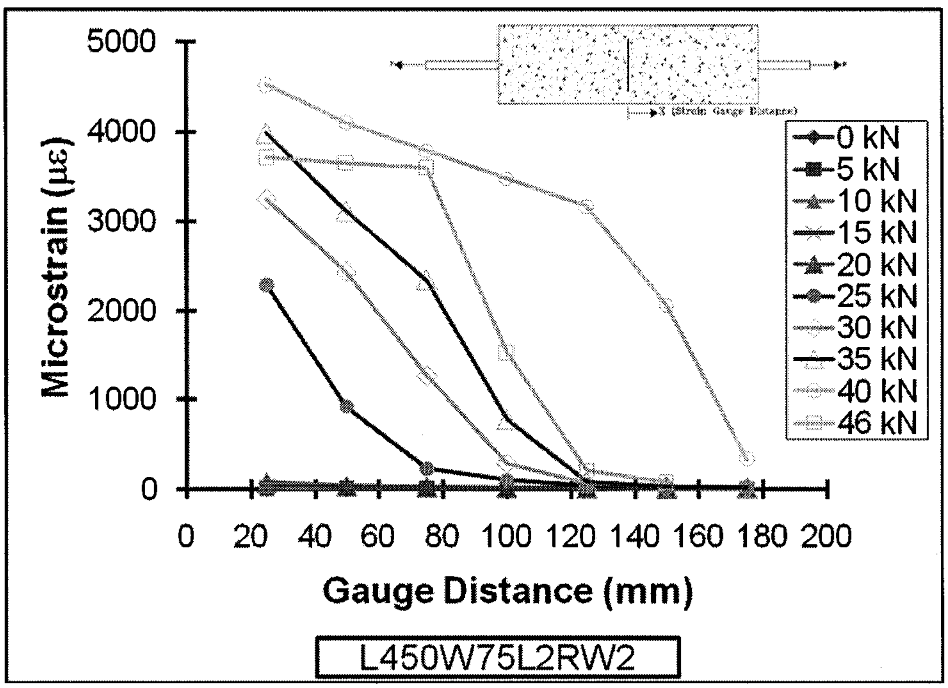
X (Strain Gauge Distance)
0 kN
5 kN
10 kN
15 kN
20 kN
25 kN
30 kN
35 kN
40 kN
46 kN
Microstrain (με)
Gauge Distance (mm)
L450W75L2RW2

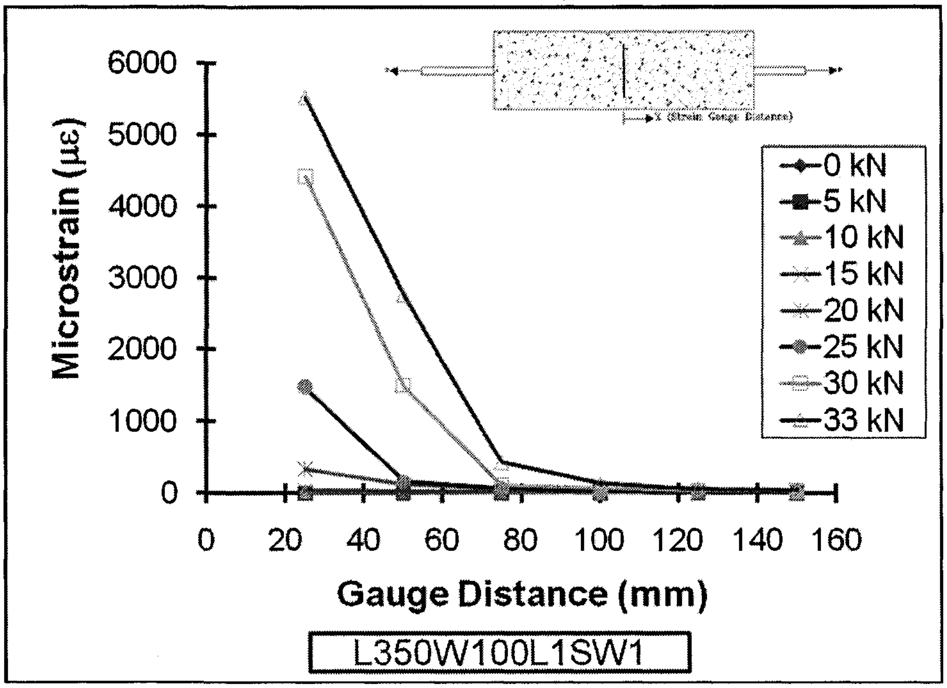

6000
5000
4000
3000
2000
1000
0
Microstrain (με)
0
20
40
60
80
100
120
140
160
Gauge Distance (mm)
0 kN
5 kN
10 kN
15 kN
20 kN
25 kN
30 kN
33 kN
L350W100L1SW1

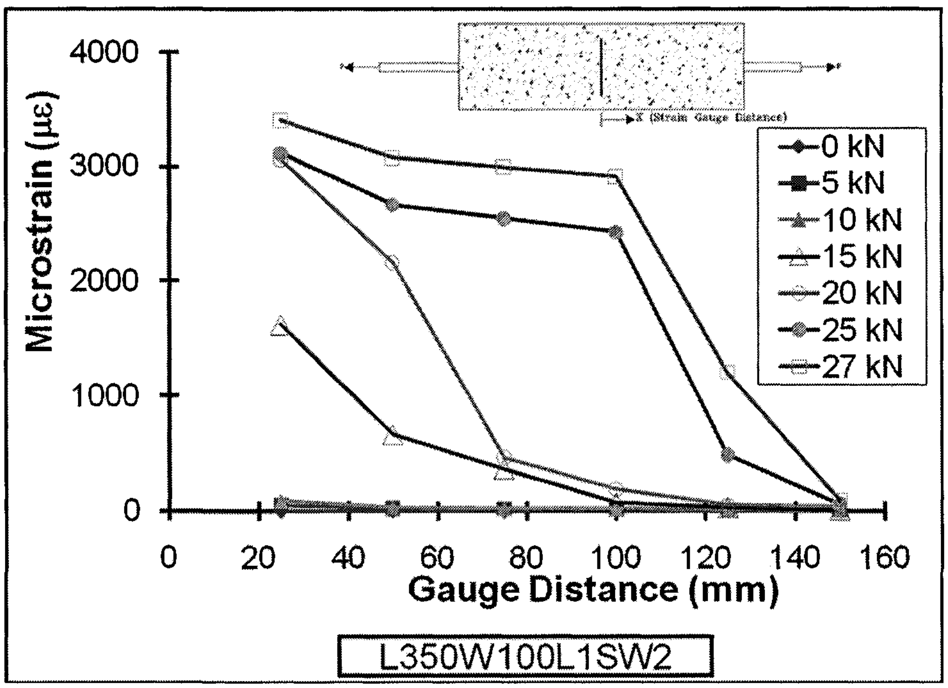

4000
3000
2000
1000
0
Microstrain (με)
0
20
40
60
80
100
120
140
160
Gauge Distance (mm)
0 kN
5 kN
10 kN
15 kN
20 kN
25 kN
27 kN
L350W100L1SW2

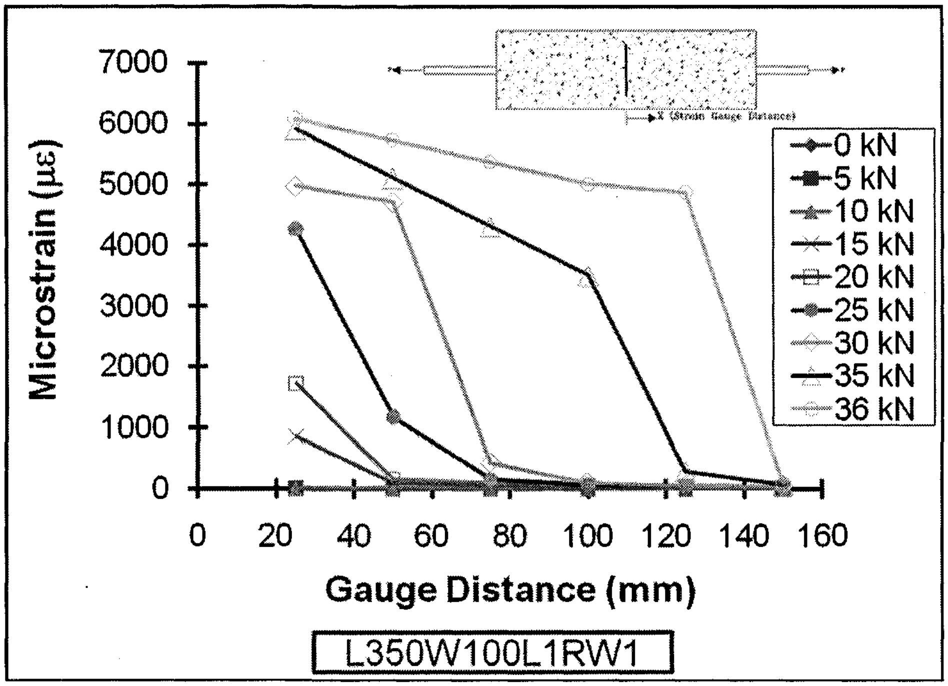

7000
6000
5000
4000
3000
2000
1000
0
Microstrain (με)
0
20
40
60
80
100
120
140
160
Gauge Distance (mm)
0 kN
5 kN
10 kN
15 kN
20 kN
25 kN
30 kN
35 kN
36 kN
L350W100L1RW1

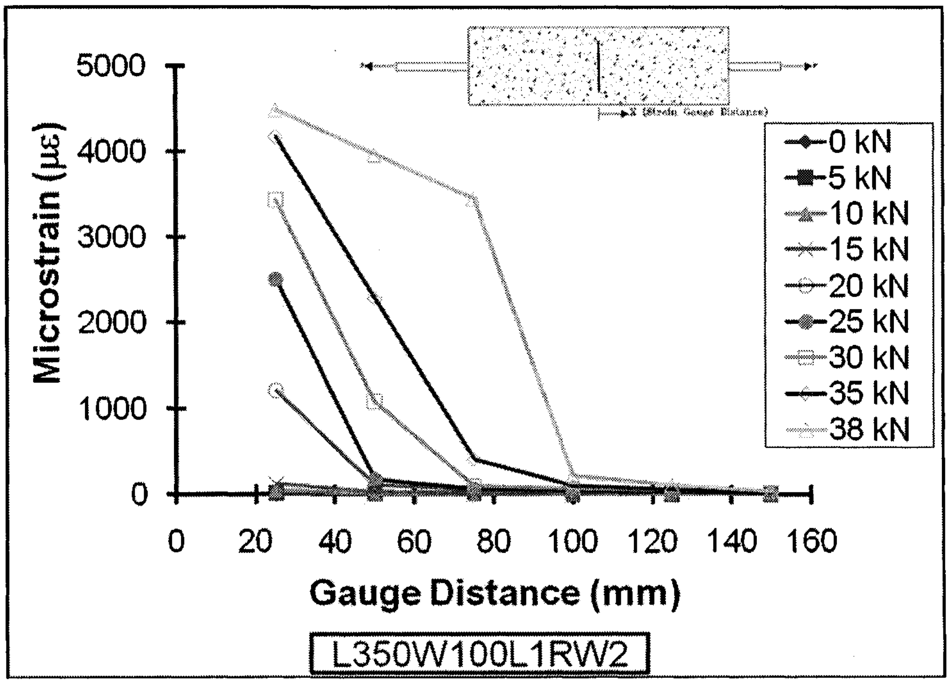

5000
4000
3000
2000
1000
0
Microstrain (με)
0
20
40
60
80
100
120
140
160
Gauge Distance (mm)
0 kN
5 kN
10 kN
15 kN
20 kN
25 kN
30 kN
35 kN
38 kN
L350W100L1RW2

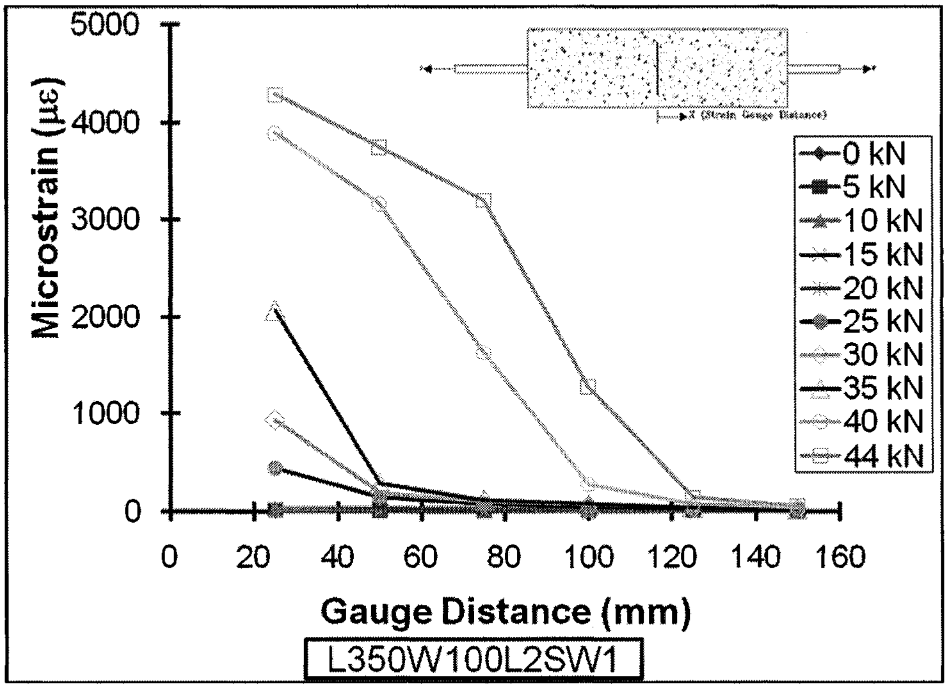
5000
4000
3000
2000
1000
0
Microstrain (με)
X (Strain Gauge Distance)
0 kN
5 kN
10 kN
15 kN
20 kN
25 kN
30 kN
35 kN
40 kN
44 kN
0
20
40
60
80
100
120
140
160
Gauge Distance (mm)
L350W100L2SW1

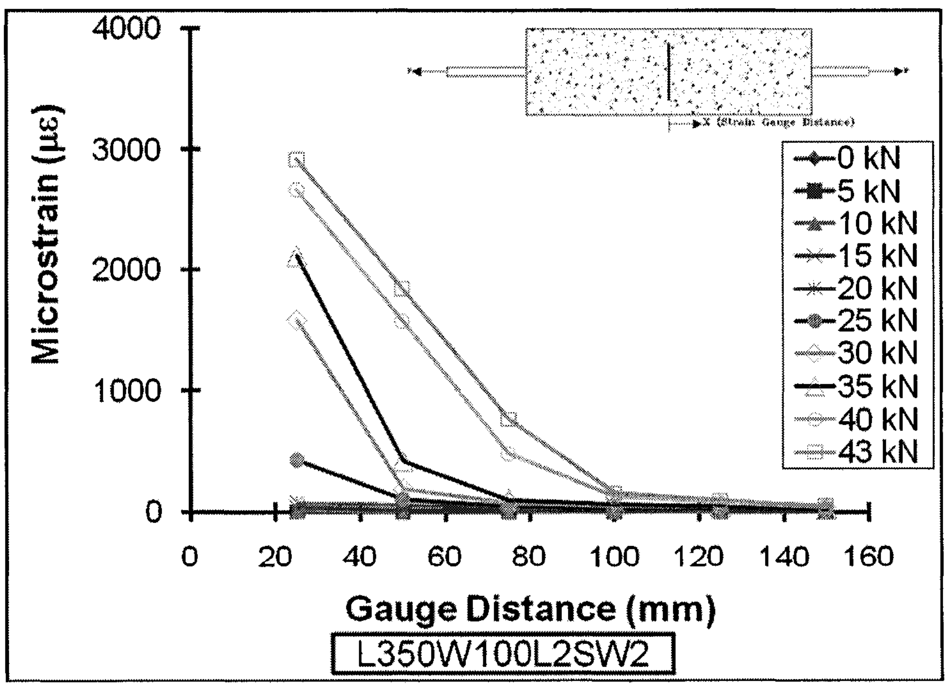
4000
3000
2000
1000
0
Microstrain (με)
X (Strain Gauge Distance)
0 kN
5 kN
10 kN
15 kN
20 kN
25 kN
30 kN
35 kN
40 kN
43 kN
0
20
40
60
80
100
120
140
160
Gauge Distance (mm)
L350W100L2SW2

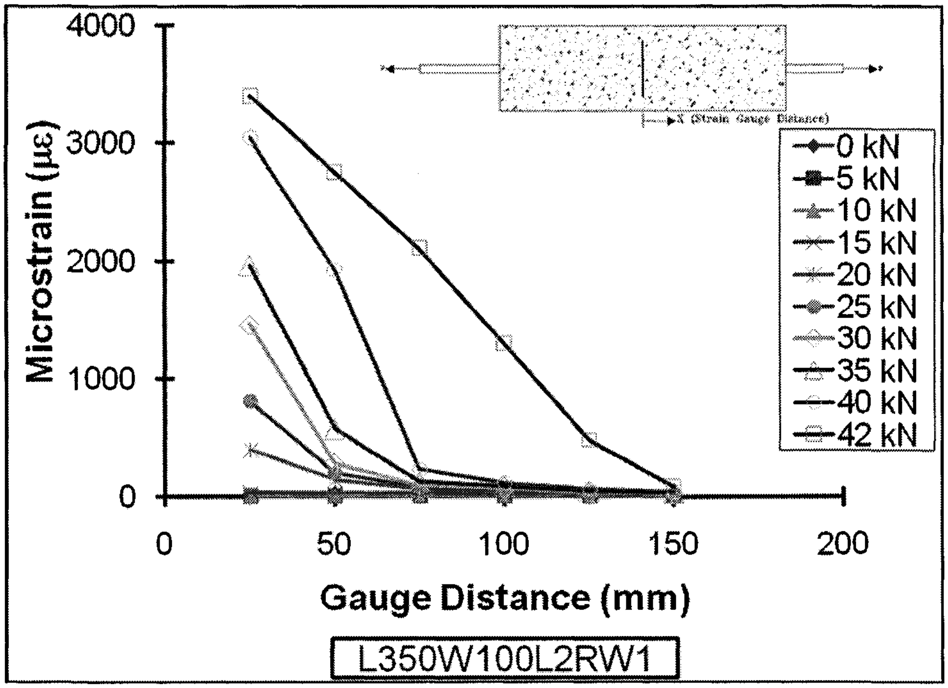

4000
3000
2000
1000
0
Microstrain (με)
0
50
100
150
200
Gauge Distance (mm)
X (Strain Gauge Distance)
0 kN
5 kN
10 kN
15 kN
20 kN
25 kN
30 kN
35 kN
40 kN
42 kN
L350W100L2RW1

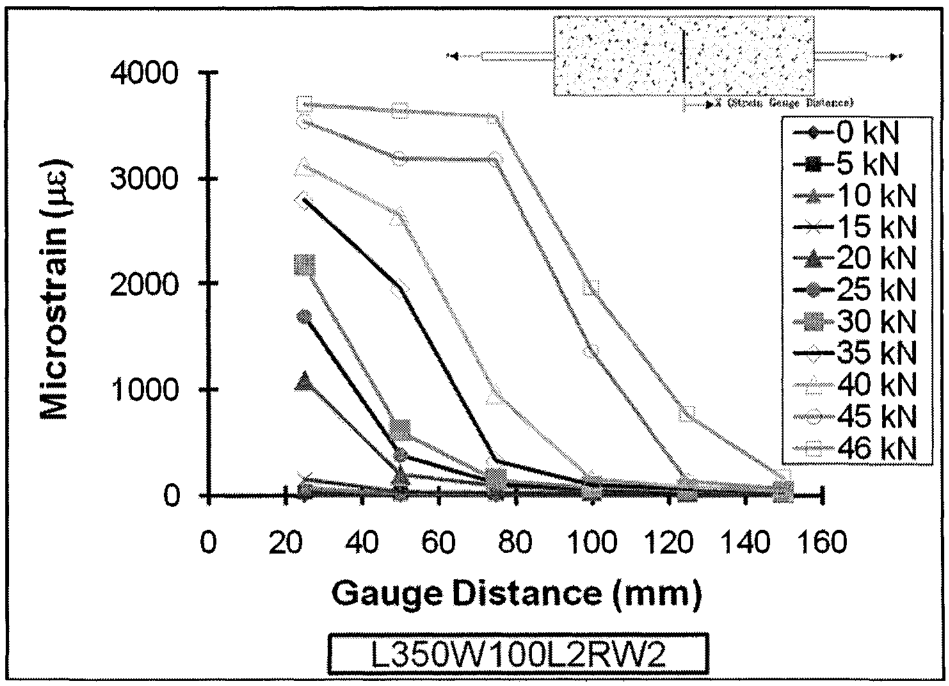

4000
3000
2000
1000
0
Microstrain (με)
0
20
40
60
80
100
120
140
160
Gauge Distance (mm)
X (Strain Gauge Distance)
0 kN
5 kN
10 kN
15 kN
20 kN
25 kN
30 kN
35 kN
40 kN
45 kN
46 kN
L350W100L2RW2

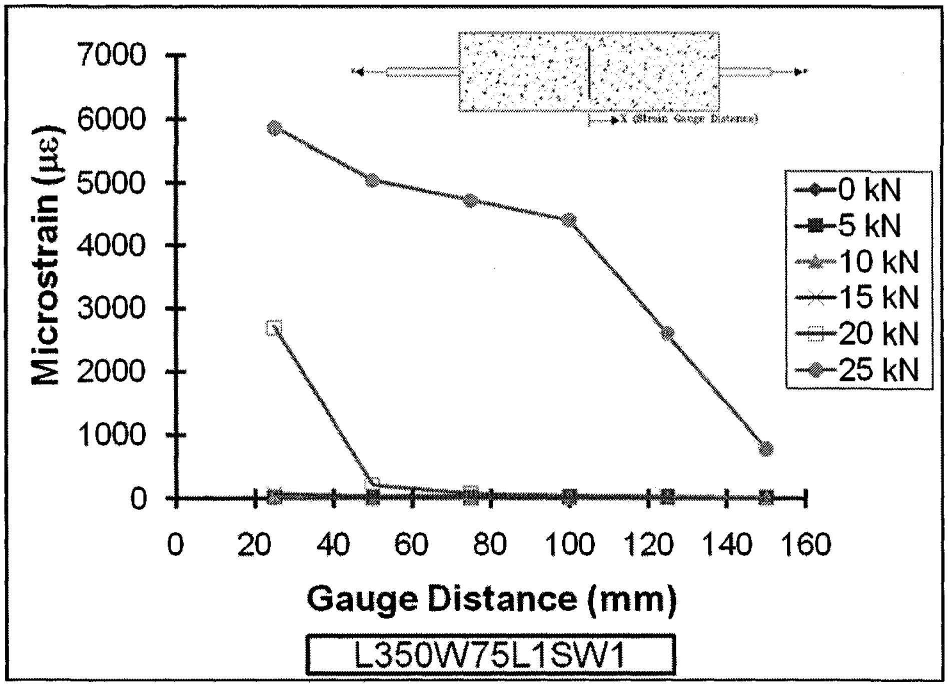
7000
6000
5000
4000
3000
2000
1000
0
Microstrain (με)
X (Strain Gauge Distance)
0 kN
5 kN
10 kN
15 kN
20 kN
25 kN
0 20 40 60 80 100 120 140 160
Gauge Distance (mm)
L350W75L1SW1

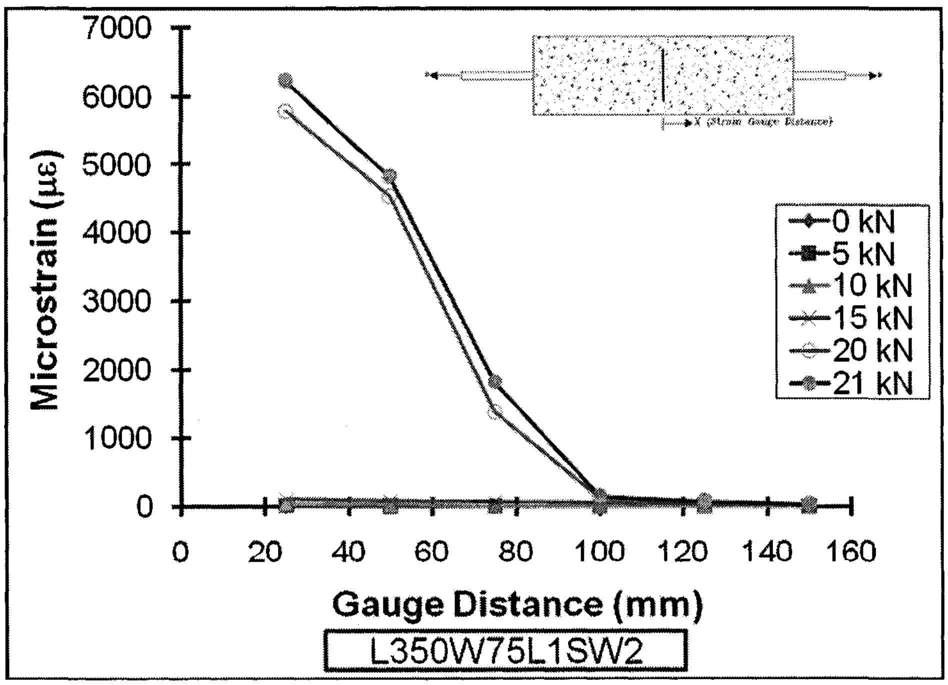
7000
6000
5000
4000
3000
2000
1000
0
Microstrain (με)
X (Strain Gauge Distance)
0 kN
5 kN
10 kN
15 kN
20 kN
21 kN
0 20 40 60 80 100 120 140 160
Gauge Distance (mm)
L350W75L1SW2

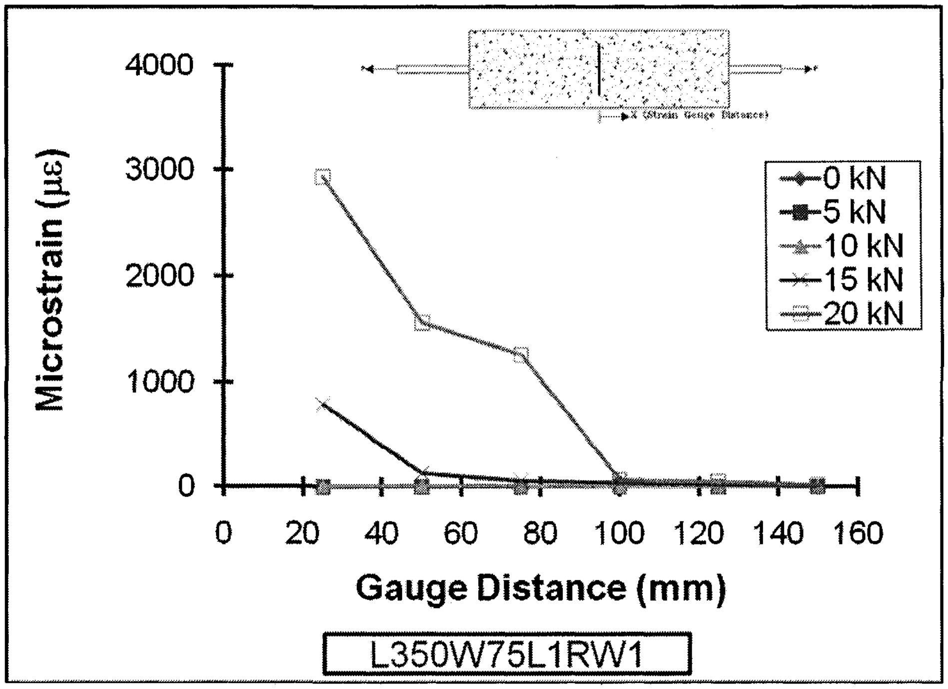

Microstrain (με)
4000
3000
2000
1000
0
0 20 40 60 80 100 120 140 160
Gauge Distance (mm)
0 kN
5 kN
10 kN
15 kN
20 kN
L350W75L1RW1

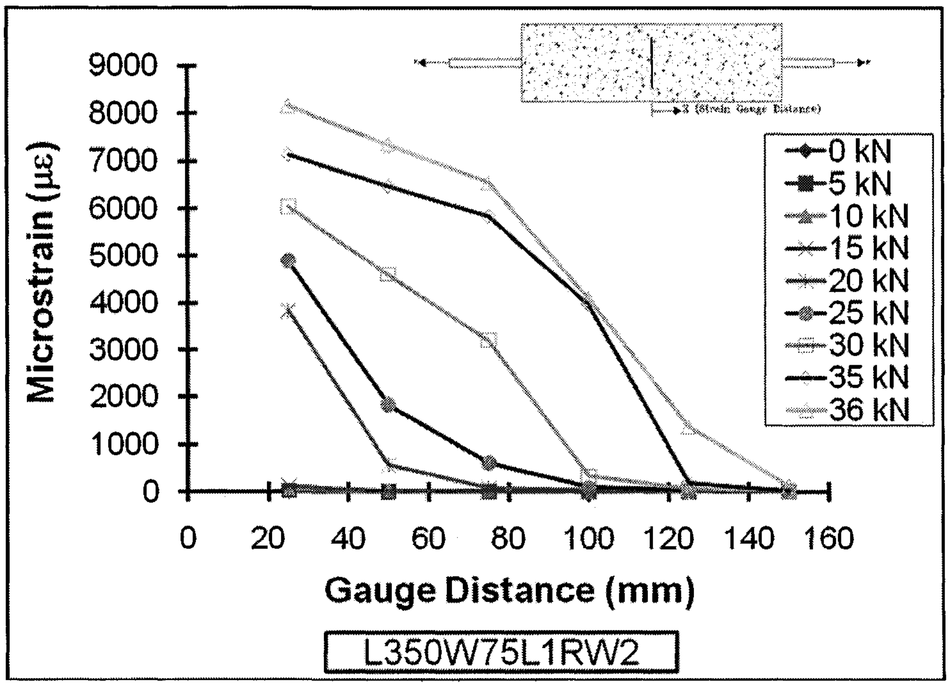

Microstrain (με)
9000
8000
7000
6000
5000
4000
3000
2000
1000
0
0 20 40 60 80 100 120 140 160
Gauge Distance (mm)
0 kN
5 kN
10 kN
15 kN
20 kN
25 kN
30 kN
35 kN
36 kN
L350W75L1RW2

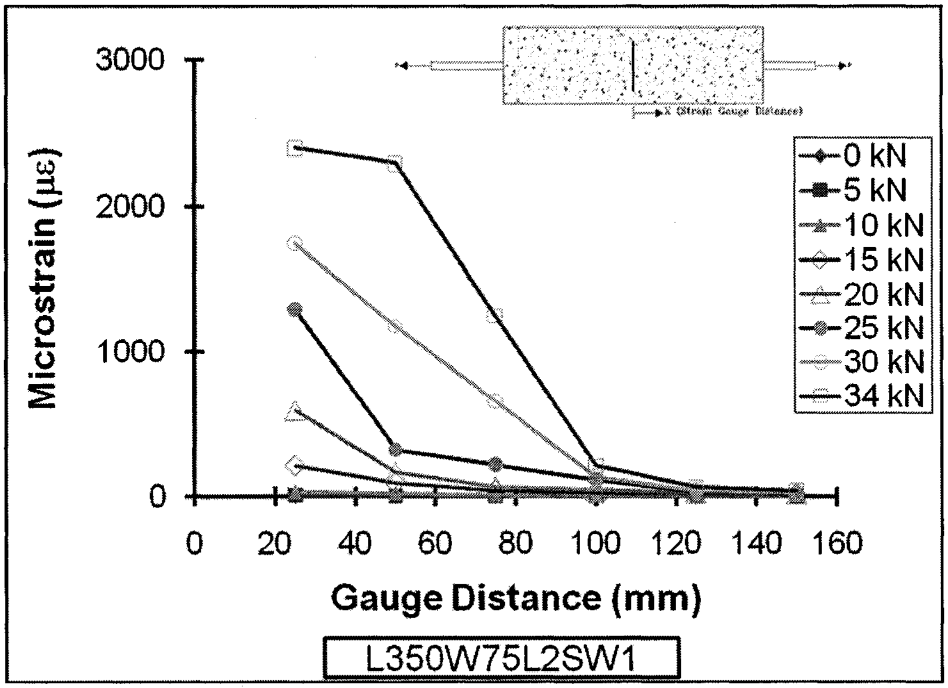
3000
2000
1000
0
Microstrain (με)
X (Strain Gauge Distance)
0 kN
5 kN
10 kN
15 kN
20 kN
25 kN
30 kN
34 kN
0 20 40 60 80 100 120 140 160
Gauge Distance (mm)
L350W75L2SW1

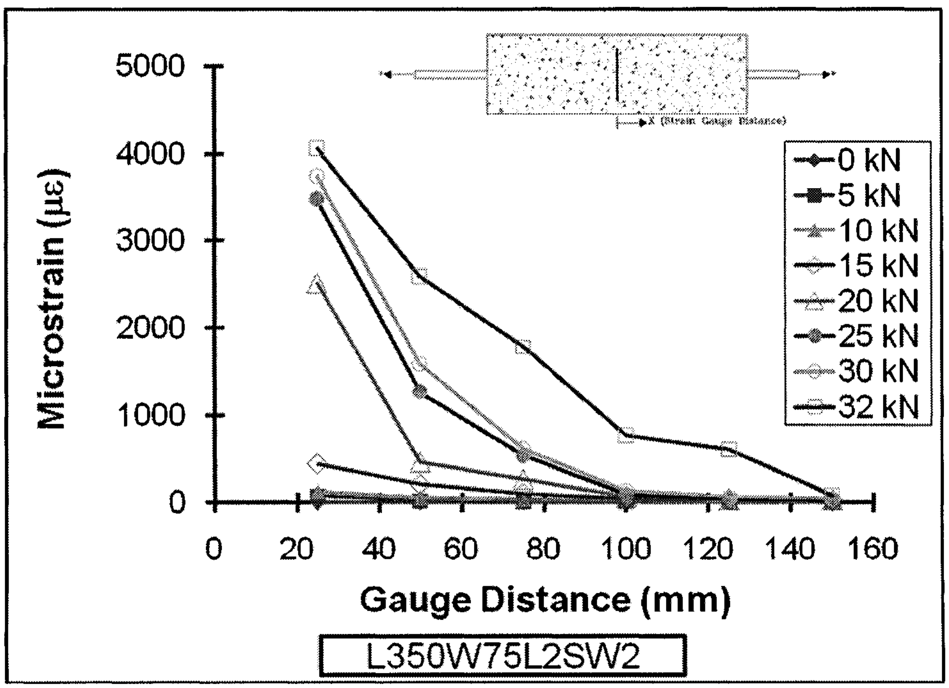
5000
4000
3000
2000
1000
0
Microstrain (με)
X (Strain Gauge Distance)
0 kN
5 kN
10 kN
15 kN
20 kN
25 kN
30 kN
32 kN
0 20 40 60 80 100 120 140 160
Gauge Distance (mm)
L350W75L2SW2

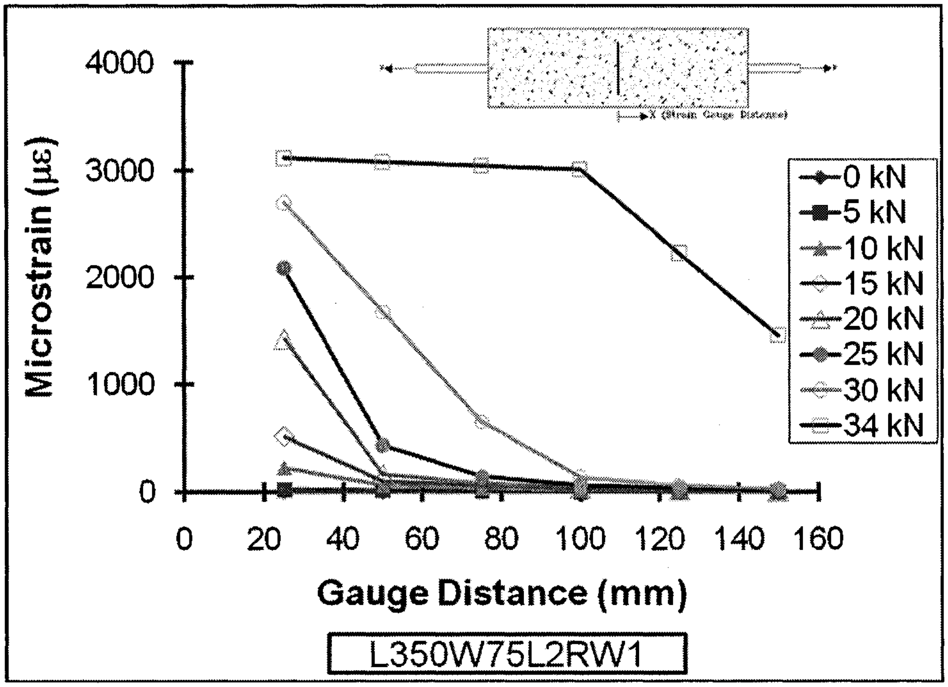

X (Strain Gauge Distance)
4000
3000
2000
1000
0
Microstrain (με)
0
20
40
60
80
100
120
140
160
Gauge Distance (mm)
0 kN
5 kN
10 kN
15 kN
20 kN
25 kN
30 kN
34 kN
L350W75L2RW1

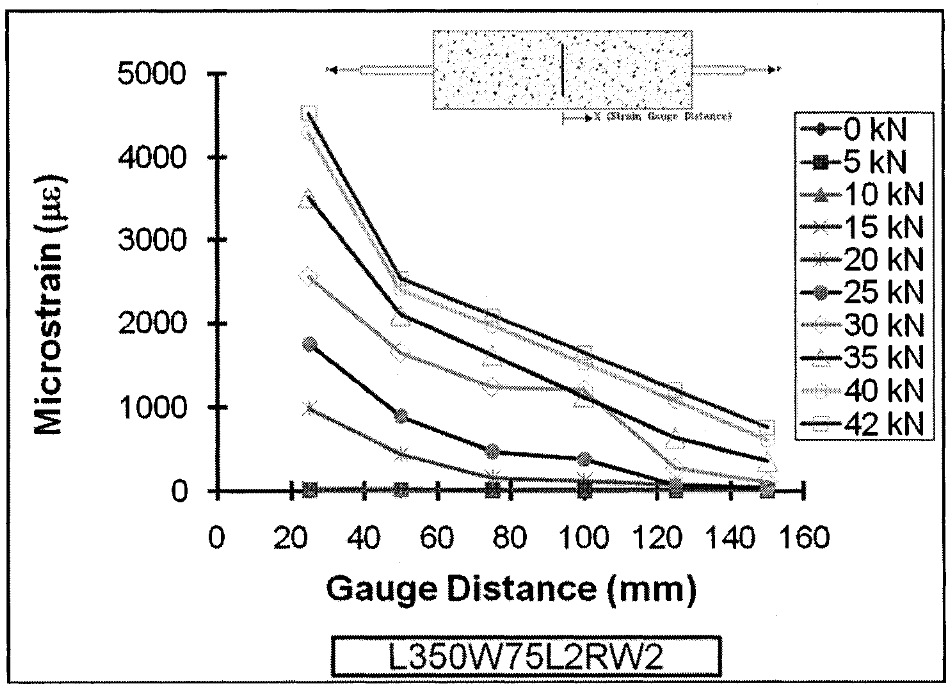

X (Strain Gauge Distance)
5000
4000
3000
2000
1000
0
Microstrain (με)
0
20
40
60
80
100
120
140
160
Gauge Distance (mm)
0 kN
5 kN
10 kN
15 kN
20 kN
25 kN
30 kN
35 kN
40 kN
42 kN
L350W75L2RW2

APPENDIX B

TRANSVERSE STRAIN VERSUS GAUGE DISTANCE

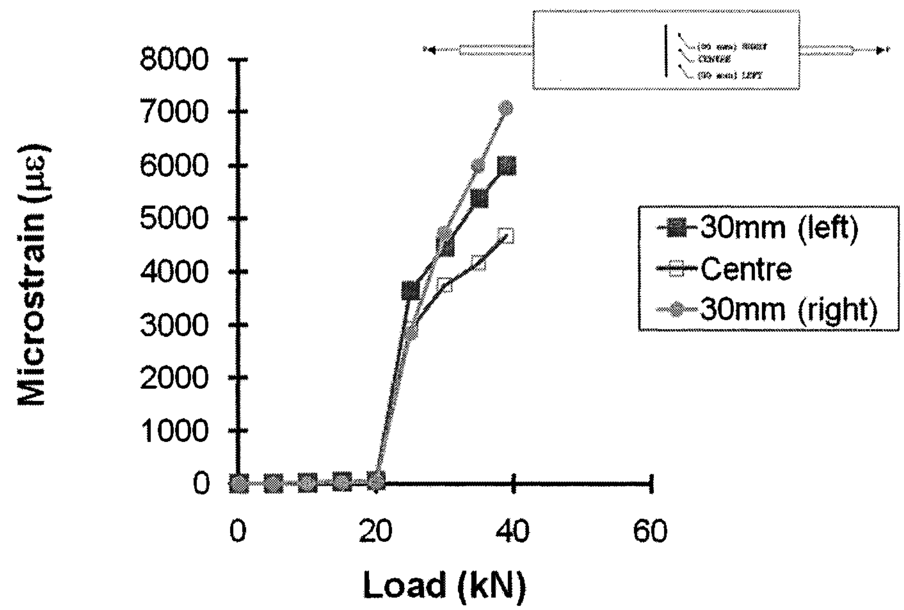

L450W100L1SW2

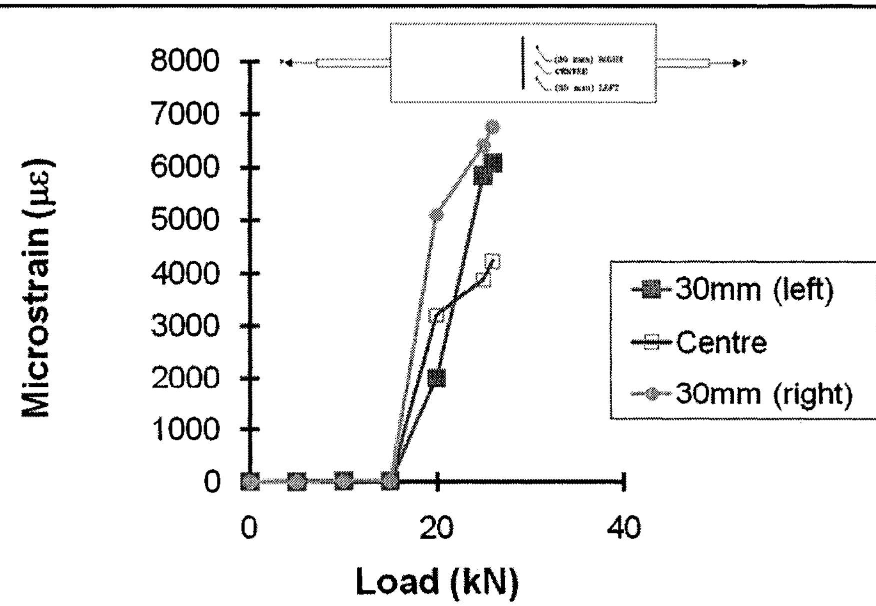

L450W75L1SW2

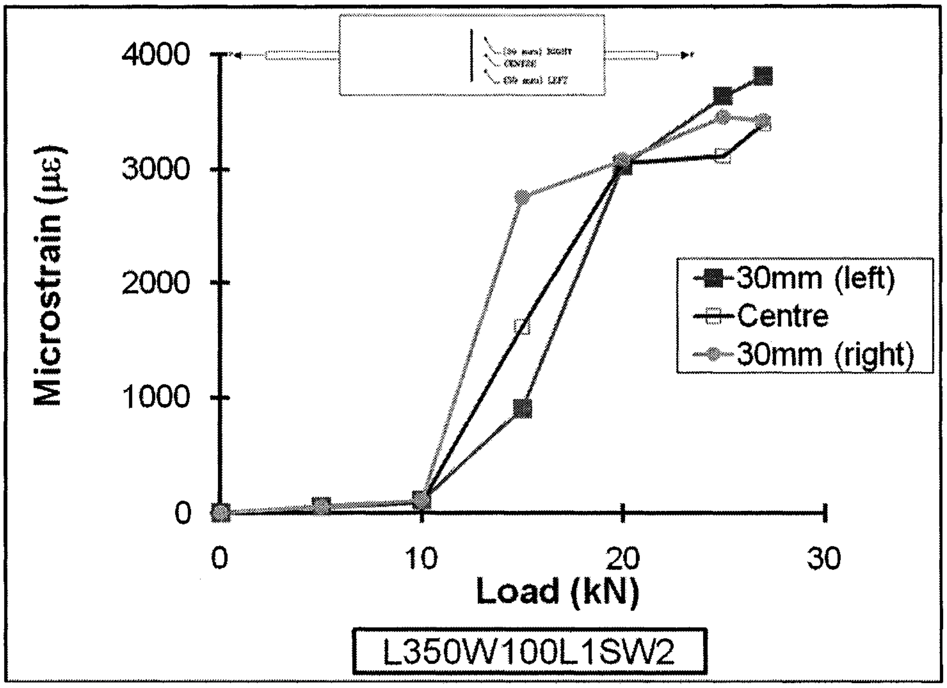

4000
3000
2000
1000
0
Microstrain (με)
0
10
20
30
Load (kN)
30mm (left)
Centre
30mm (right)
L350W100L1SW2

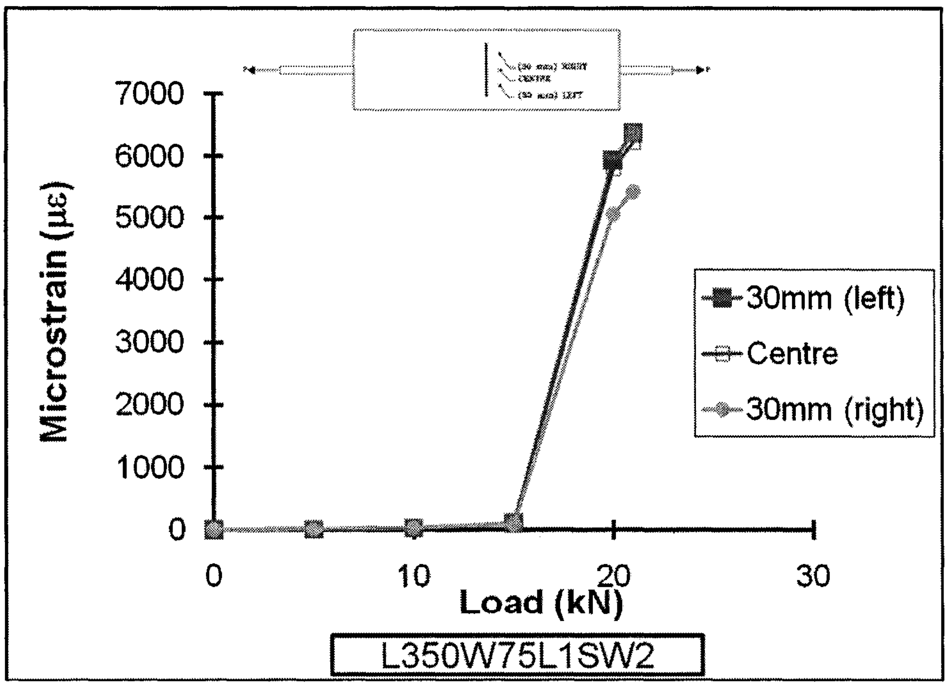

7000
6000
5000
4000
3000
2000
1000
0
Microstrain (με)
0
10
20
30
Load (kN)
30mm (left)
Centre
30mm (right)
L350W75L1SW2

APPENDIX C
LOAD VERSUS DISPLACEMENT

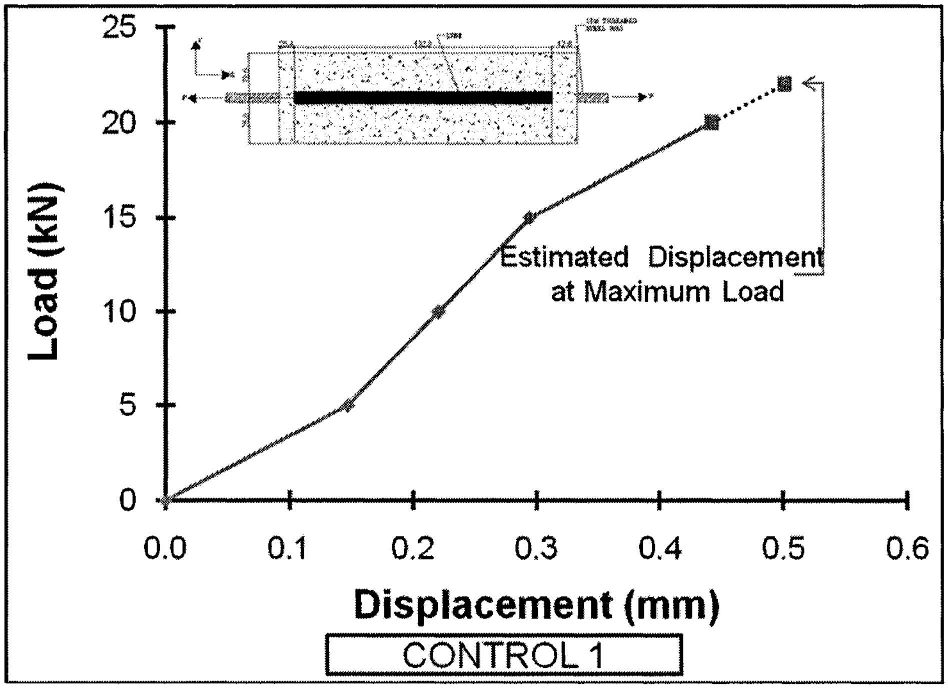

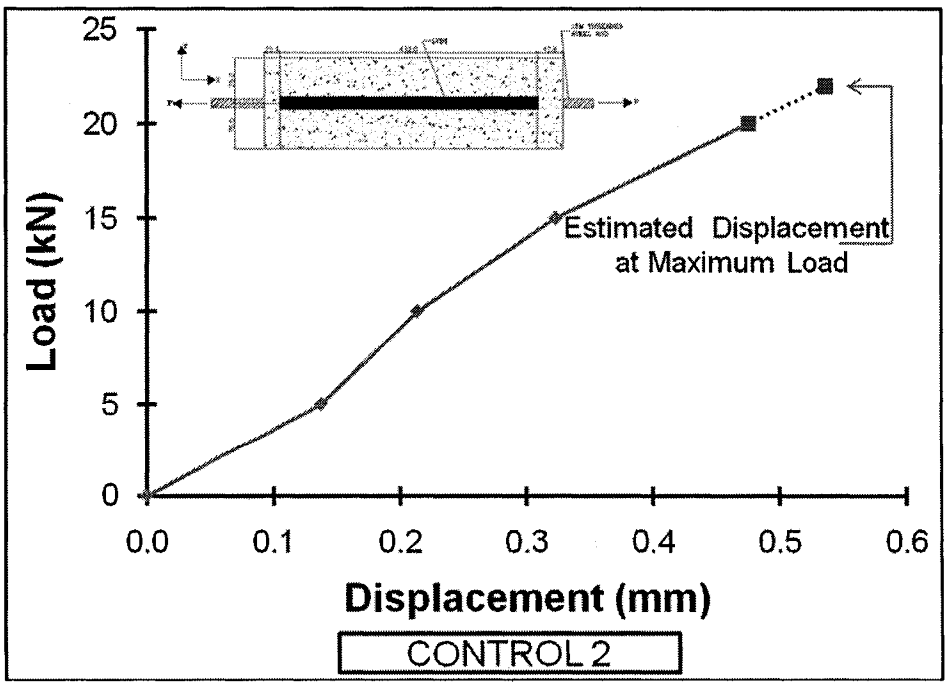

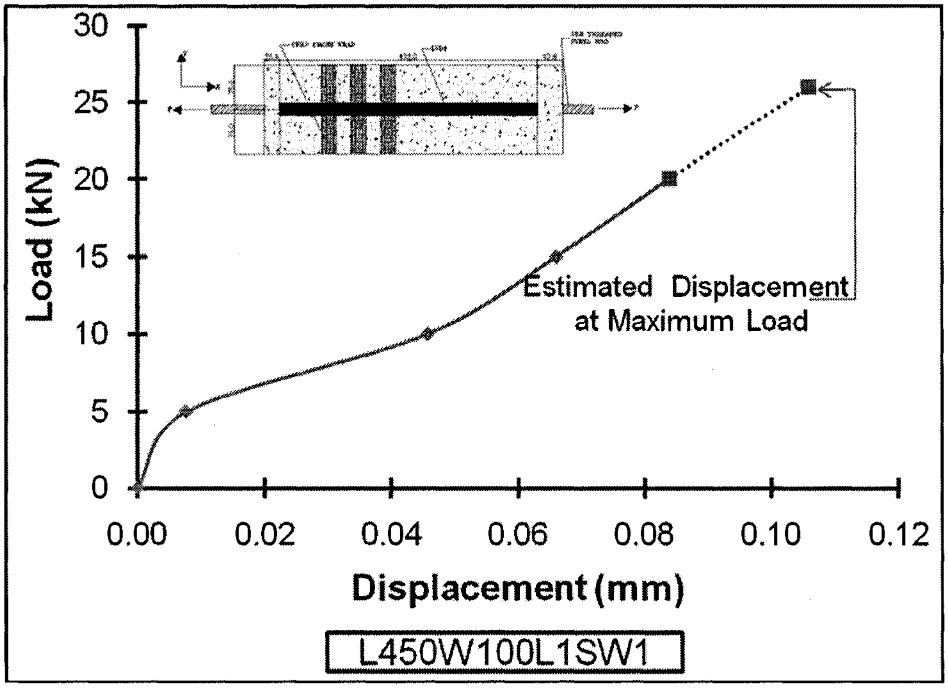

Load (kN)
Displacement (mm)
Estimated Displacement at Maximum Load
L450W100L1SW1

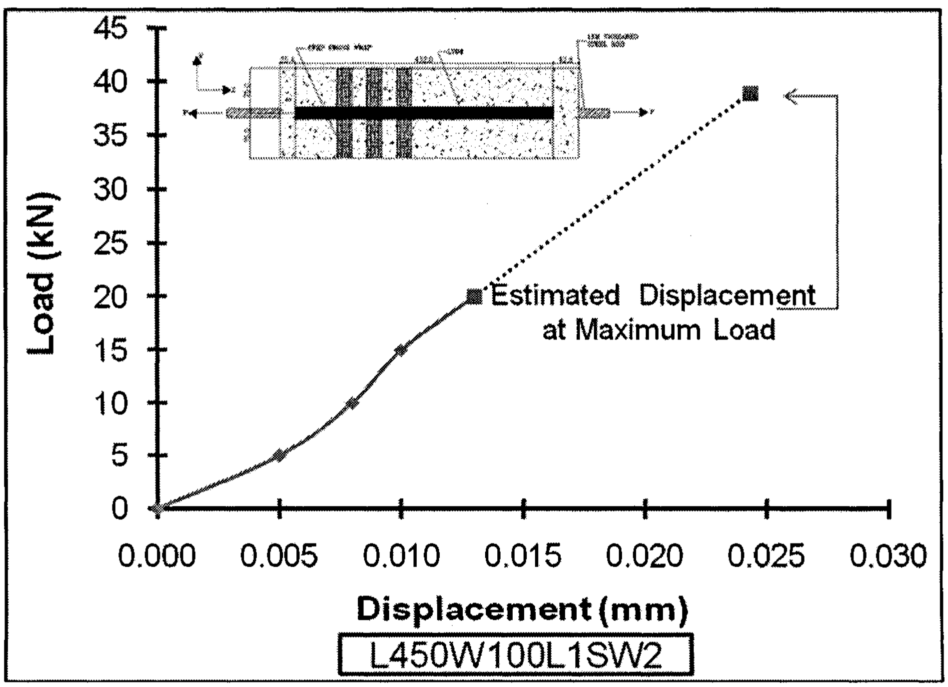

Load (kN)
Displacement (mm)
Estimated Displacement at Maximum Load
L450W100L1SW2

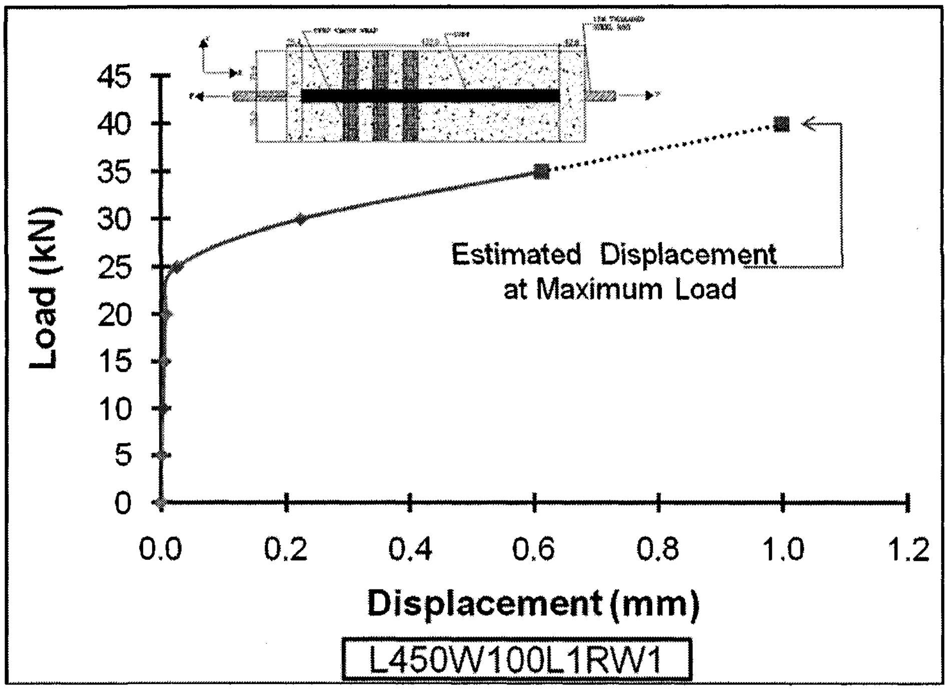
45
40
35
30
25
20
15
10
5
0
Load (kN)
0.0
0.2
0.4
0.6
0.8
1.0
1.2
Displacement (mm)
Estimated Displacement
at Maximum Load
L450W100L1RW1

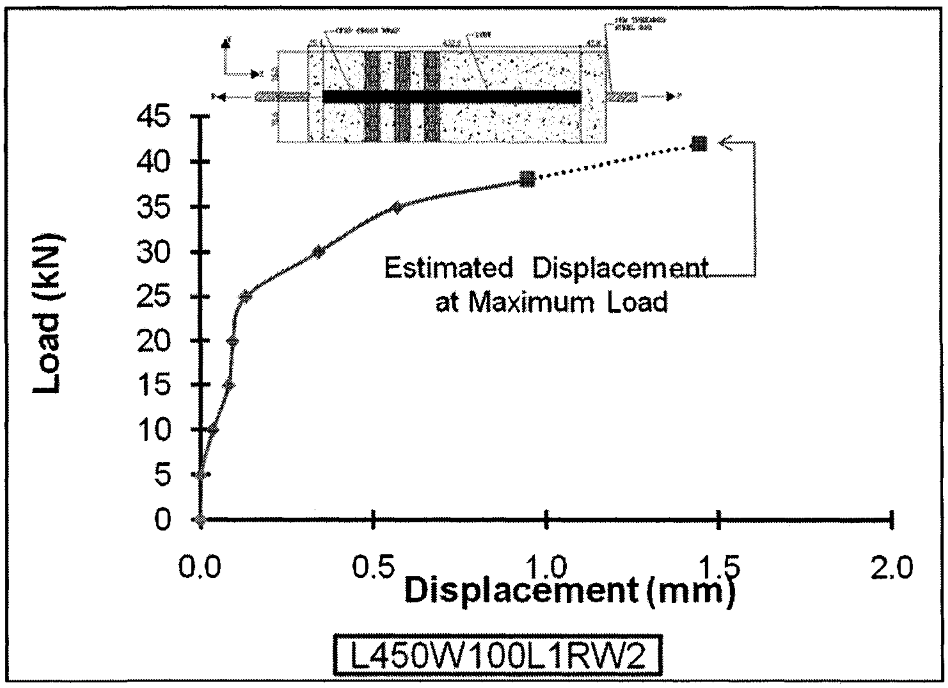
45
40
35
30
25
20
15
10
5
0
Load (kN)
0.0
0.5
1.0
1.5
2.0
Displacement (mm)
Estimated Displacement
at Maximum Load
L450W100L1RW2

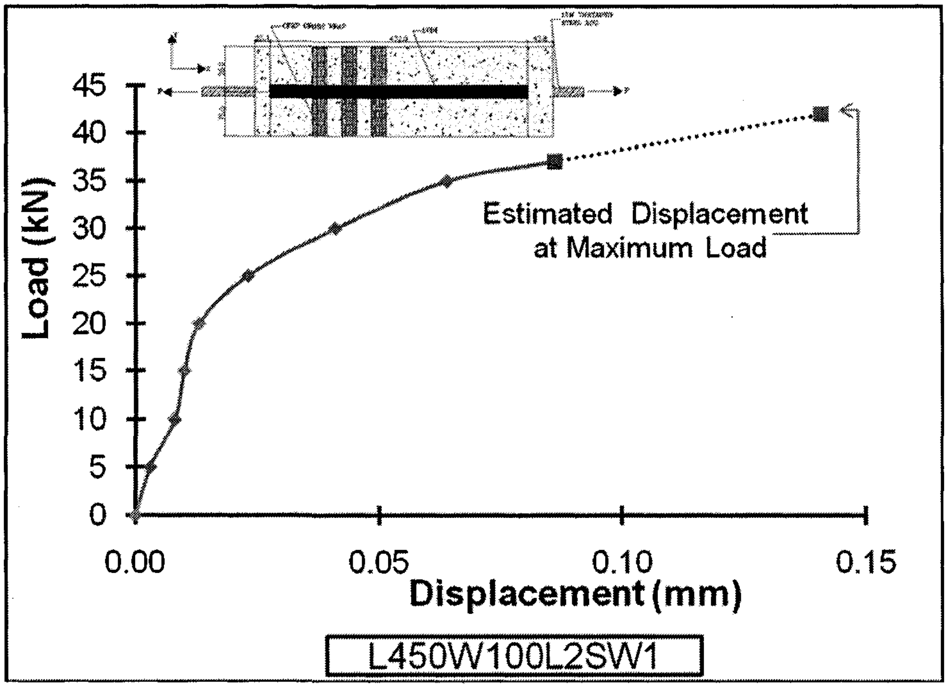

Load (kN)
Displacement (mm)
Estimated Displacement at Maximum Load
L450W100L2SW1

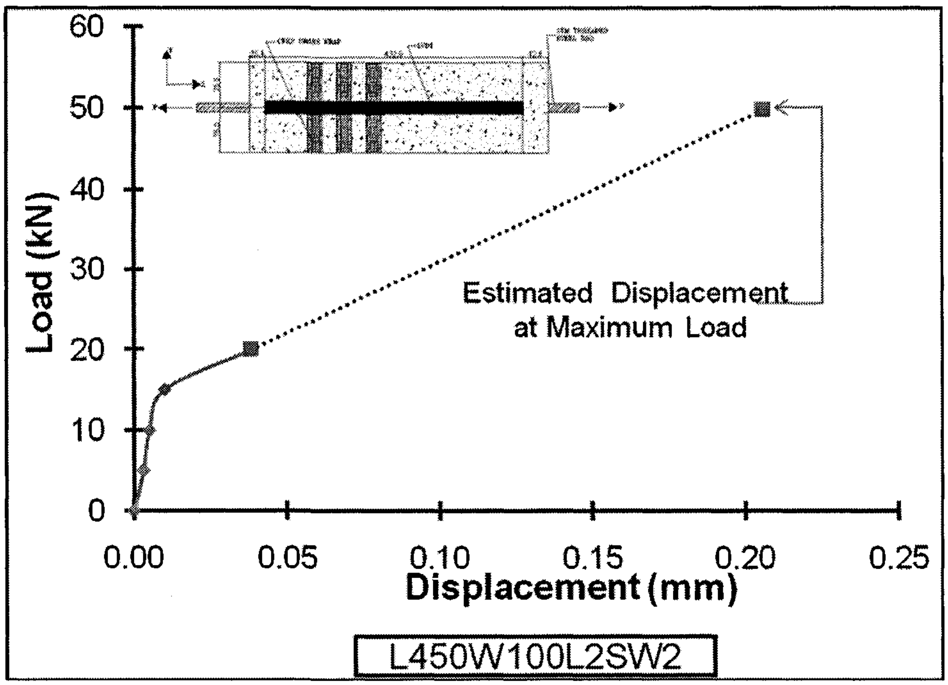

Load (kN)
Displacement (mm)
Estimated Displacement at Maximum Load
L450W100L2SW2

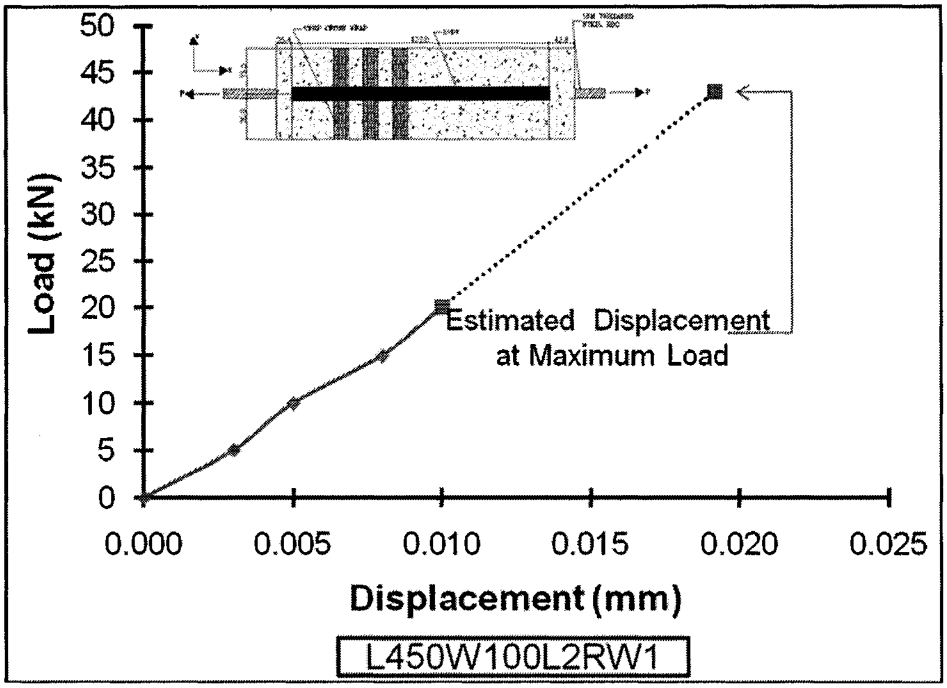
Load (kN)
Displacement (mm)
Estimated Displacement
at Maximum Load
L450W100L2RW1

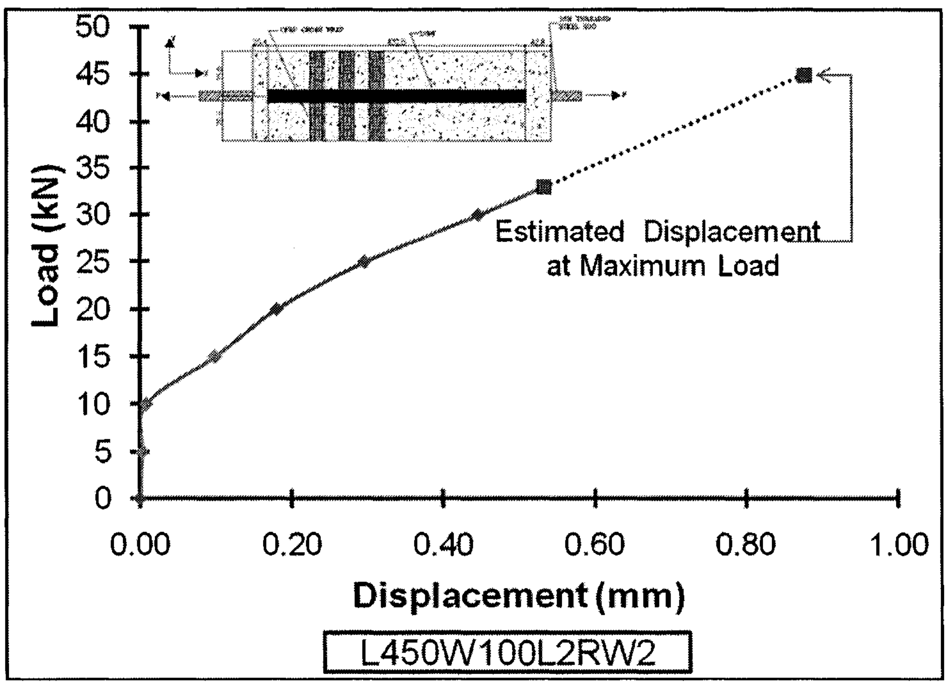
Load (kN)
Displacement (mm)
Estimated Displacement
at Maximum Load
L450W100L2RW2

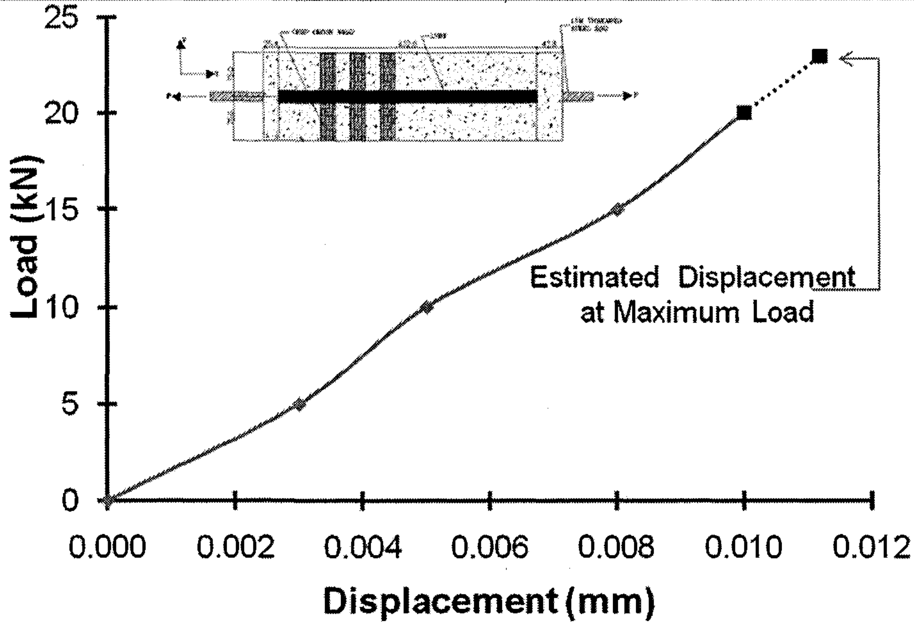

L450W75L1SW1

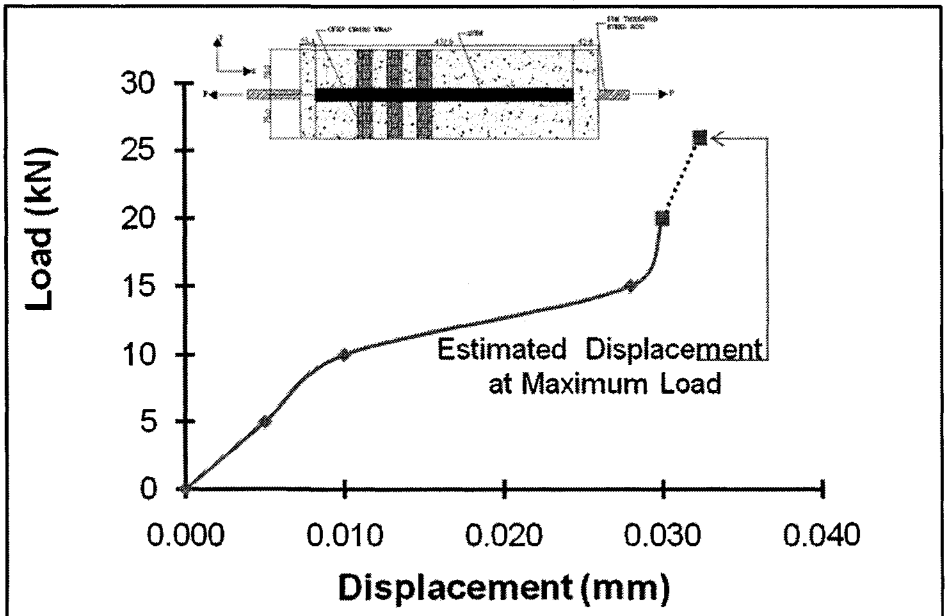

L450W75L1SW2

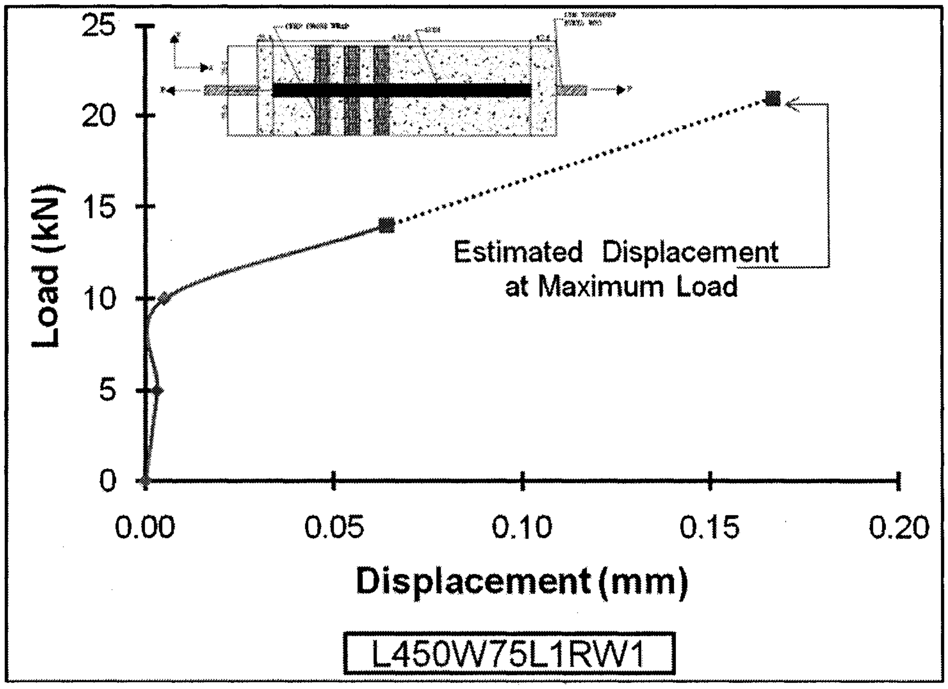
Load (kN)
Displacement (mm)
Estimated Displacement at Maximum Load
L450W75L1RW1

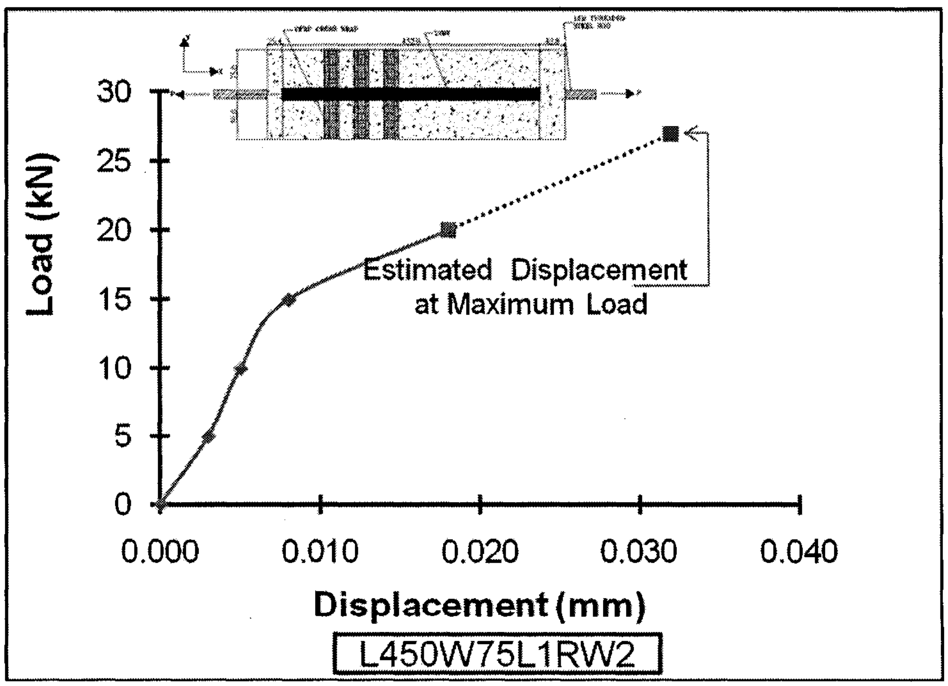
Load (kN)
Displacement (mm)
Estimated Displacement at Maximum Load
L450W75L1RW2

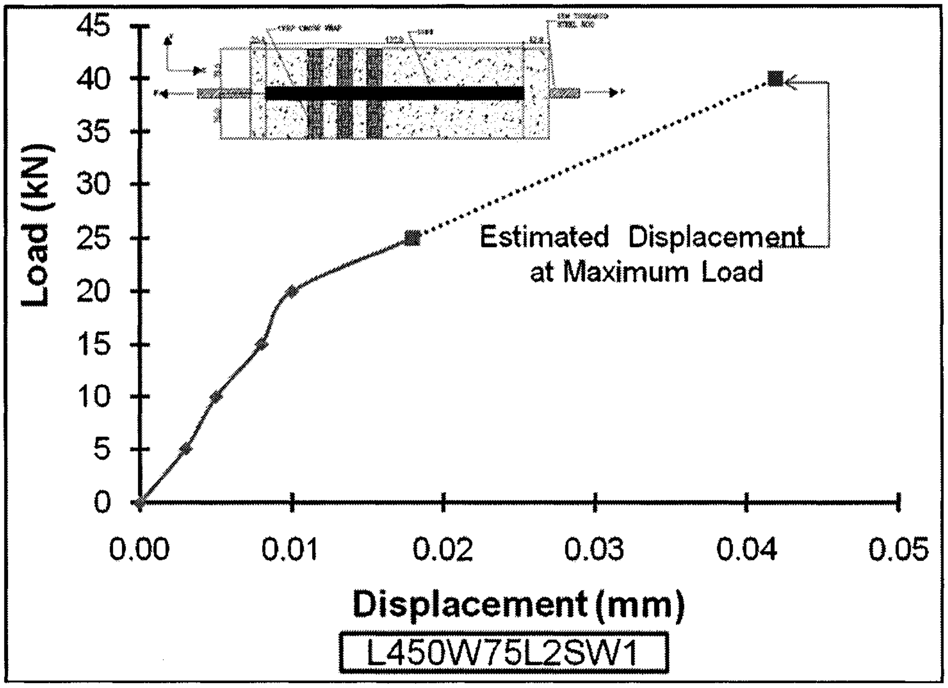
45
40
35
30
25
20
15
10
5
0
Load (kN)
0.00
0.01
0.02
0.03
0.04
0.05
Displacement (mm)
Estimated Displacement
at Maximum Load
L450W75L2SW1

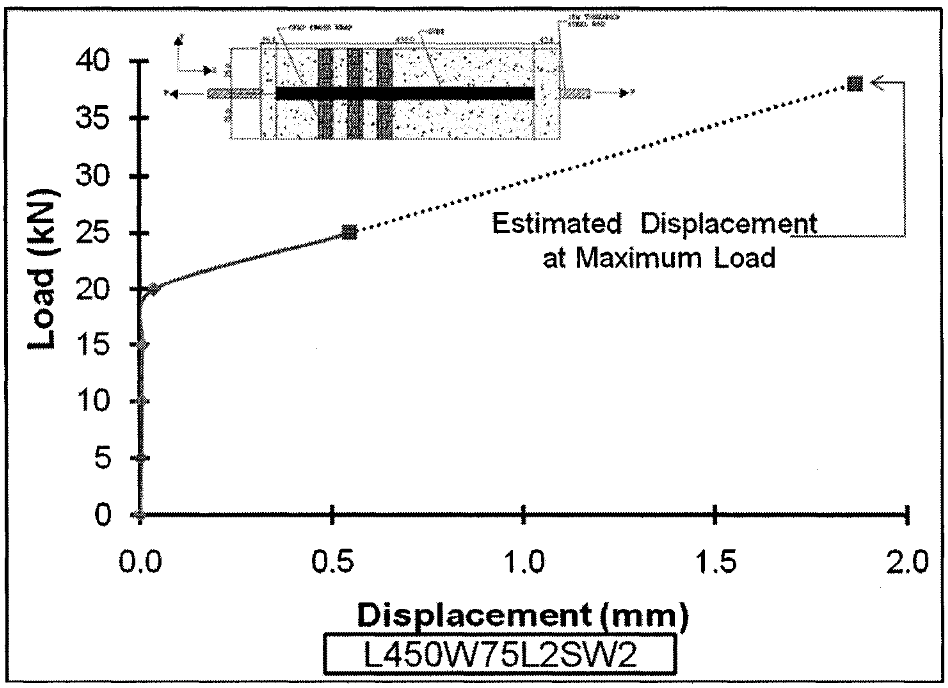
40
35
30
25
20
15
10
5
0
Load (kN)
0.0
0.5
1.0
1.5
2.0
Displacement (mm)
Estimated Displacement
at Maximum Load
L450W75L2SW2

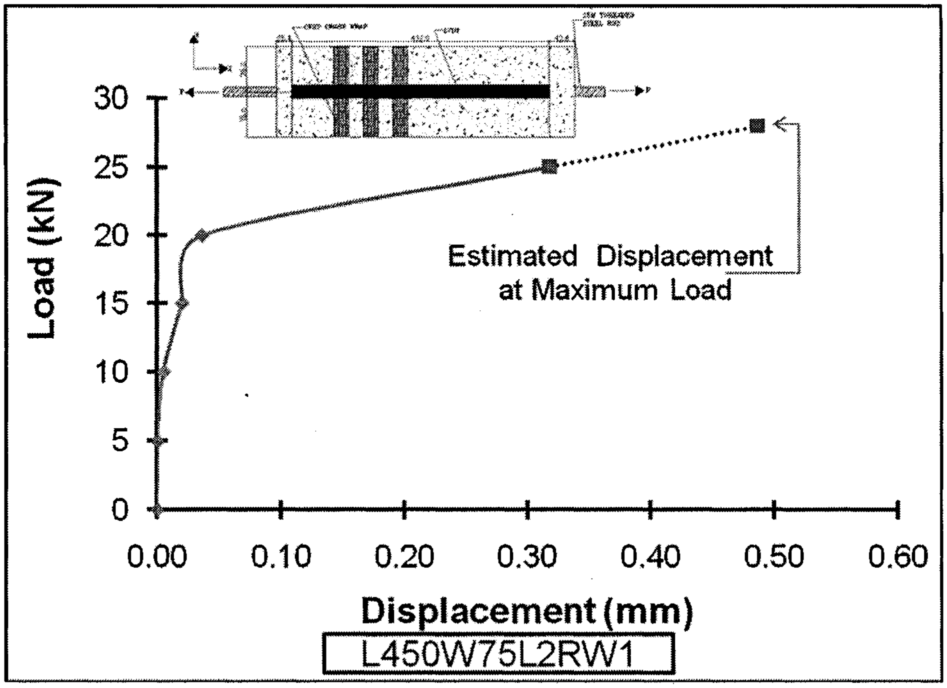

30
25
20
15
10
5
0
Load (kN)
0.00
0.10
0.20
0.30
0.40
0.50
0.60
Displacement (mm)
Estimated Displacement
at Maximum Load
L450W75L2RW1

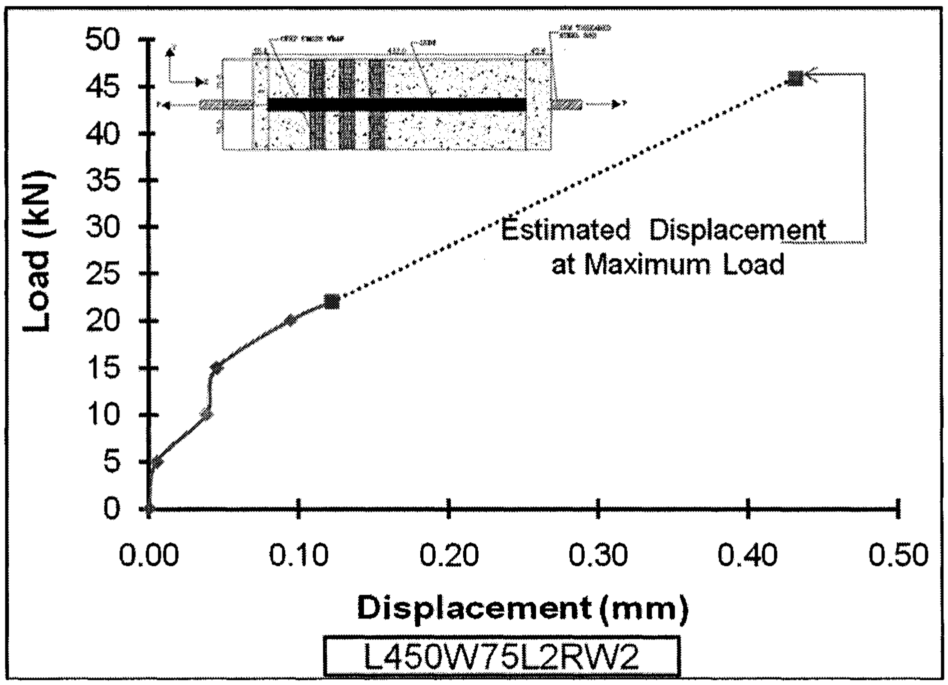

50
45
40
35
30
25
20
15
10
5
0
Load (kN)
0.00
0.10
0.20
0.30
0.40
0.50
Displacement (mm)
Estimated Displacement
at Maximum Load
L450W75L2RW2

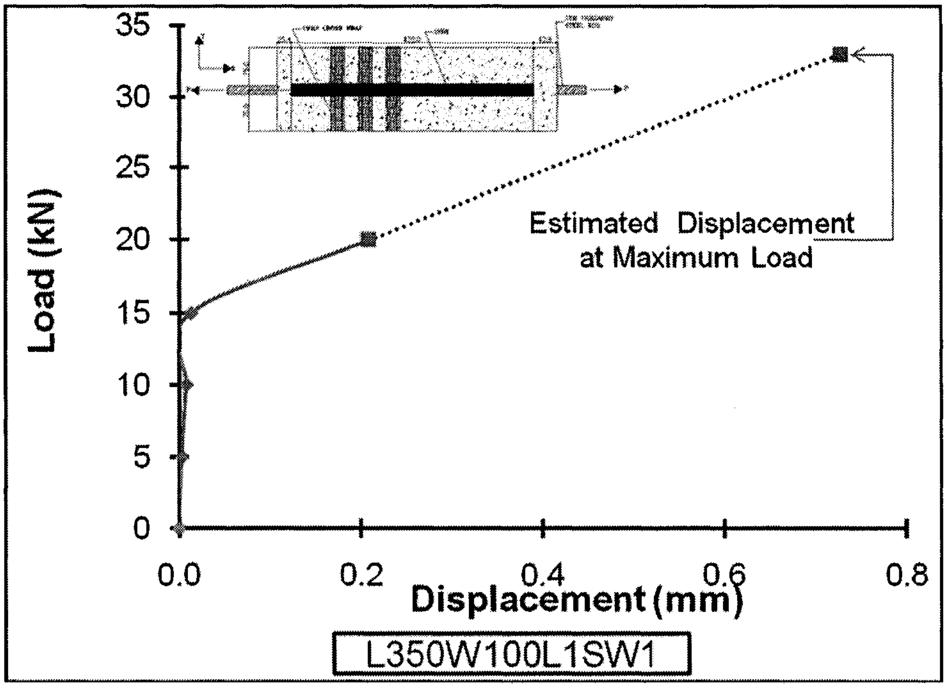

Load (kN)
35
30
25
20
15
10
5
0
0.0
0.2
0.4
0.6
0.8
Displacement (mm)
Estimated Displacement at Maximum Load
L350W100L1SW1

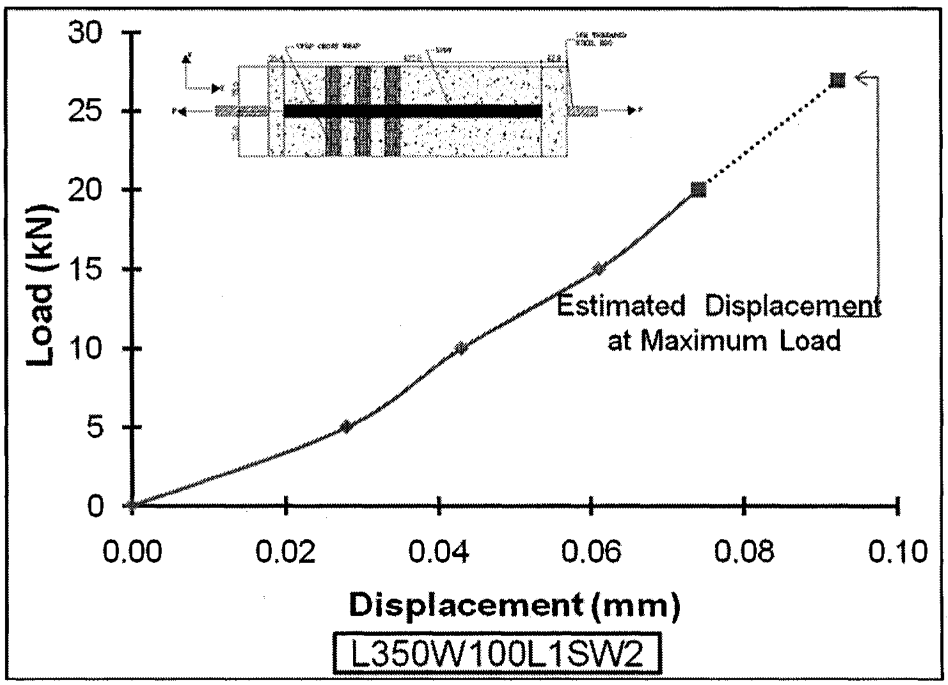

Load (kN)
30
25
20
15
10
5
0
0.00
0.02
0.04
0.06
0.08
0.10
Displacement (mm)
Estimated Displacement at Maximum Load
L350W100L1SW2

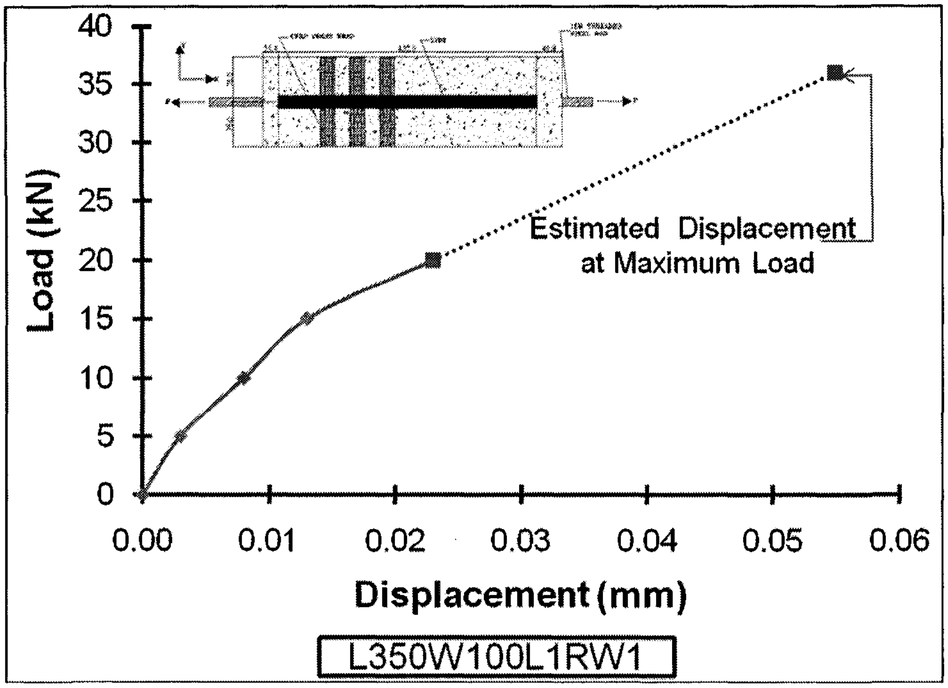
Load (kN)
Displacement (mm)
Estimated Displacement at Maximum Load
L350W100L1RW1

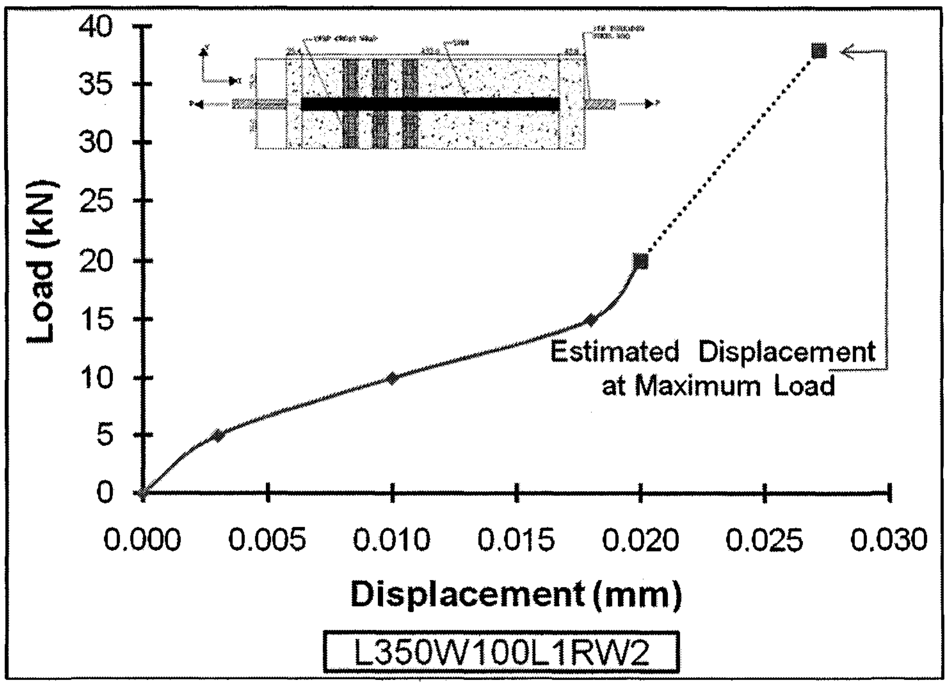
Load (kN)
Displacement (mm)
Estimated Displacement at Maximum Load
L350W100L1RW2

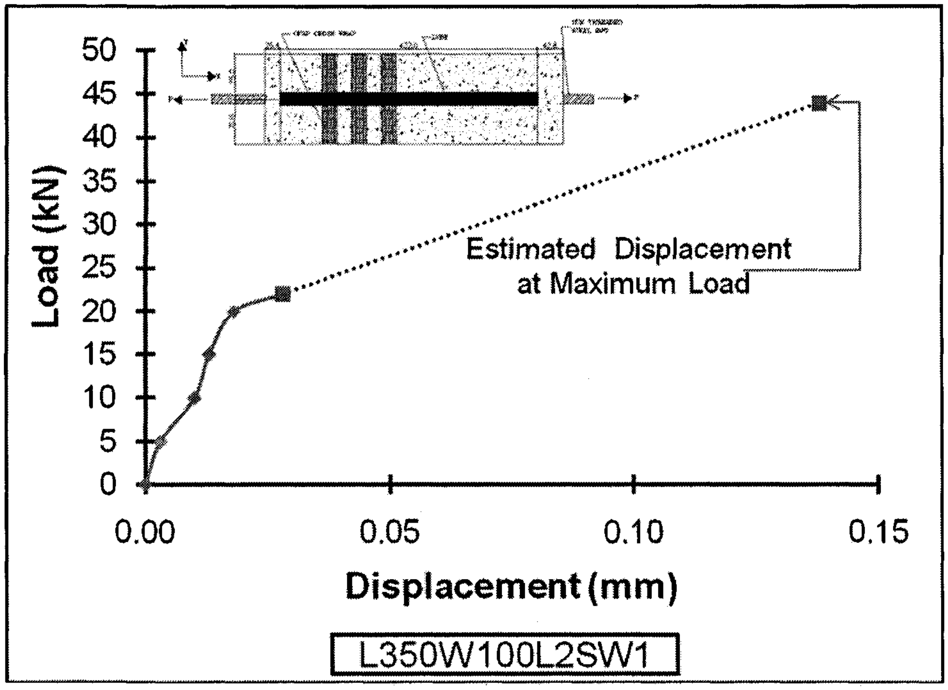

Load (kN)
Estimated Displacement at Maximum Load
Displacement (mm)
L350W100L2SW1

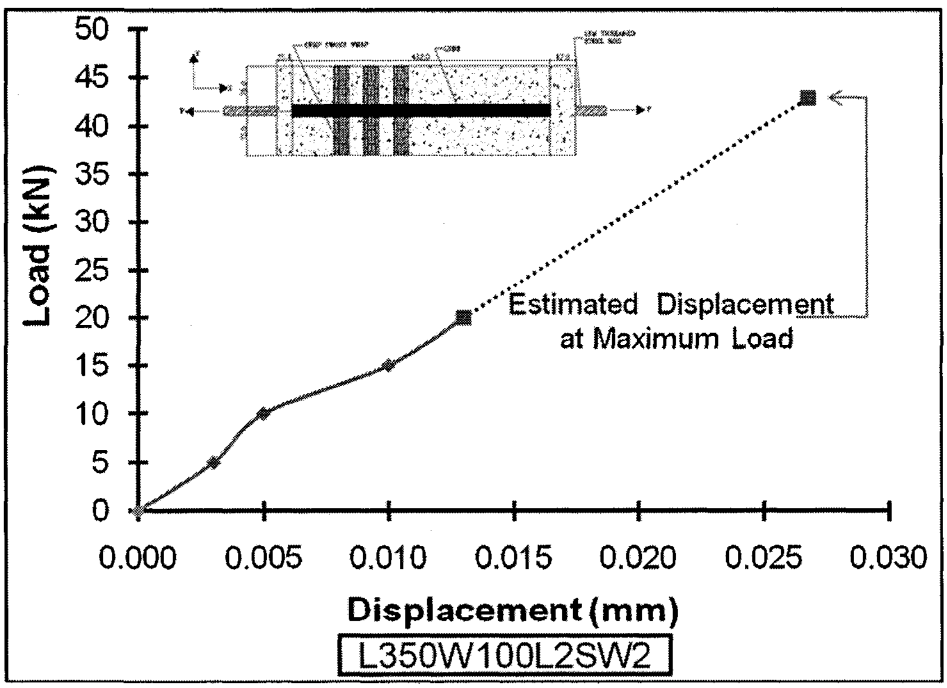

Load (kN)
Estimated Displacement at Maximum Load
Displacement (mm)
L350W100L2SW2

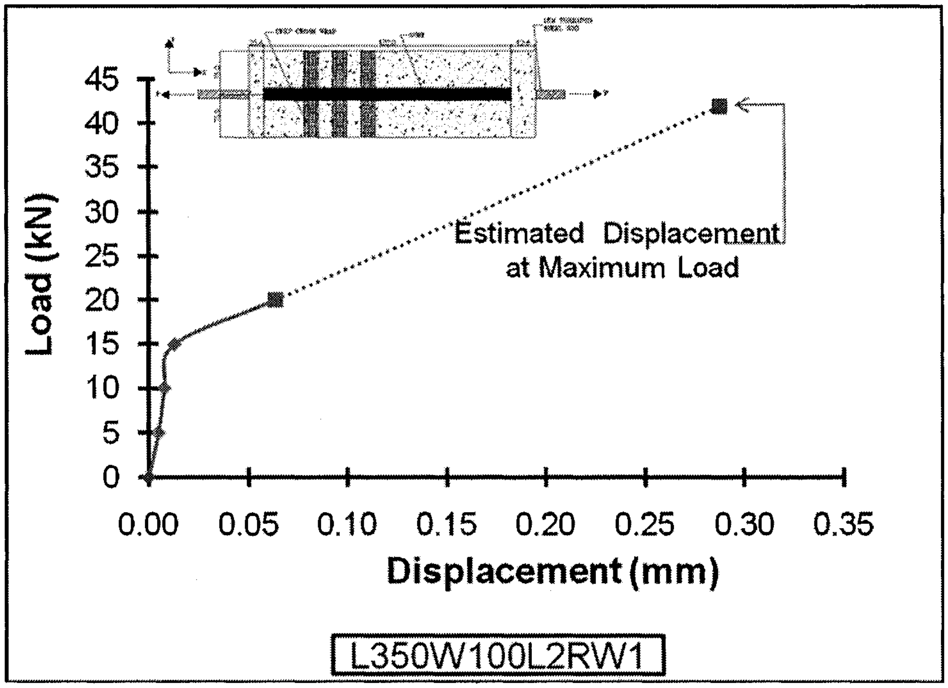
Load (kN)
0
5
10
15
20
25
30
35
40
45
0.00
0.05
0.10
0.15
0.20
0.25
0.30
0.35
Displacement (mm)
Estimated Displacement at Maximum Load
L350W100L2RW1

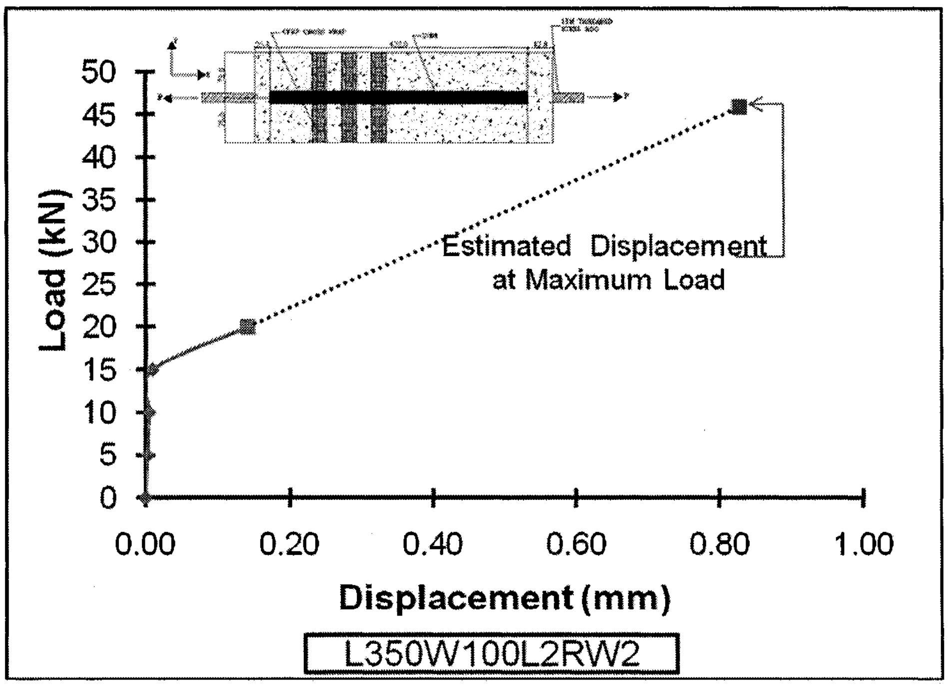
Load (kN)
0
5
10
15
20
25
30
35
40
45
50
0.00
0.20
0.40
0.60
0.80
1.00
Displacement (mm)
Estimated Displacement at Maximum Load
L350W100L2RW2

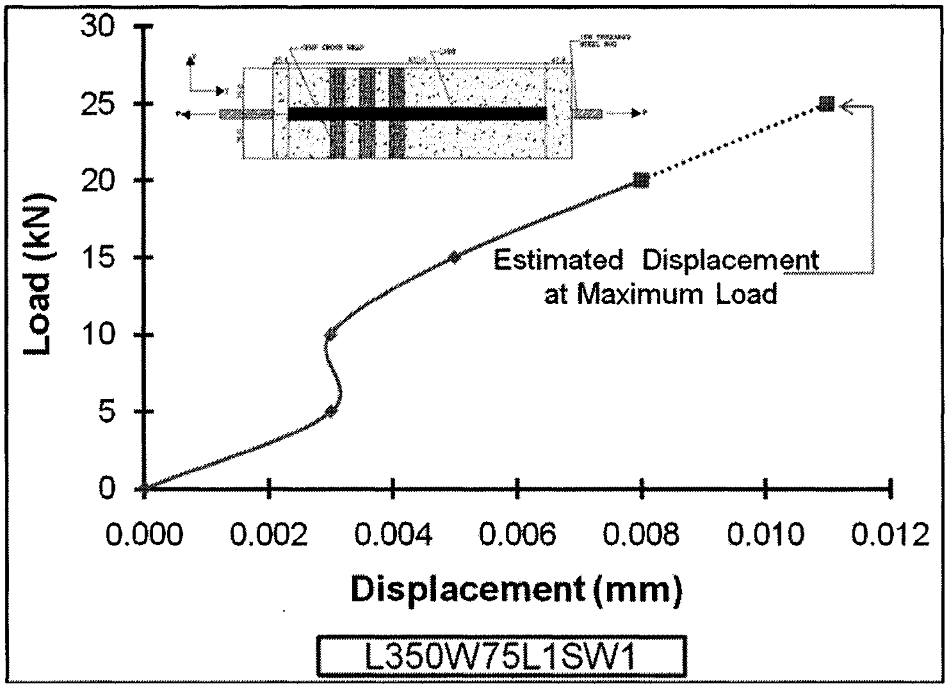

Load (kN)
Displacement (mm)
Estimated Displacement
at Maximum Load
L350W75L1SW1

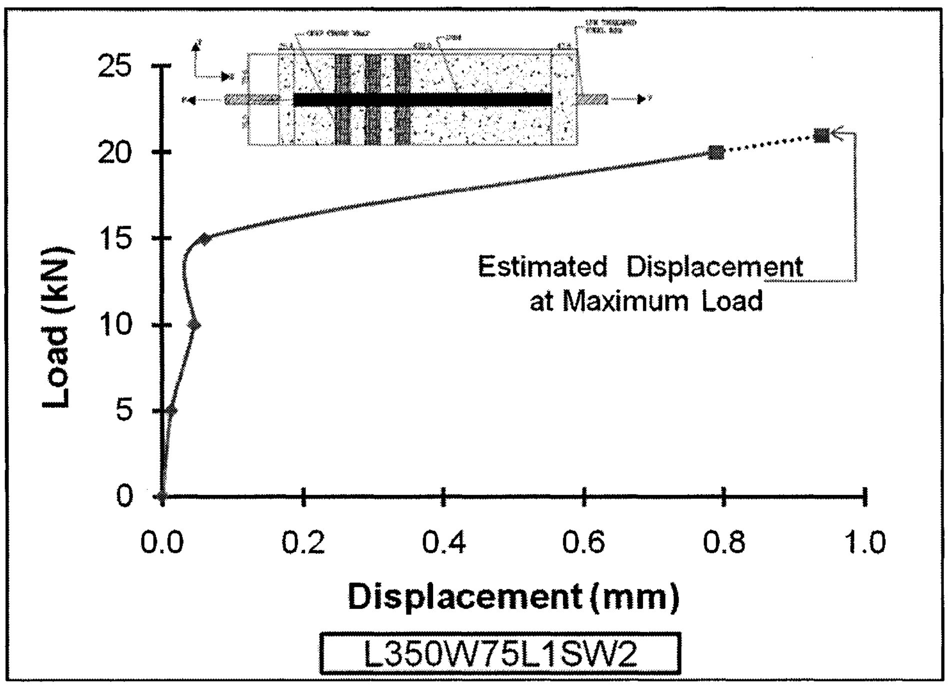

Load (kN)
Displacement (mm)
Estimated Displacement
at Maximum Load
L350W75L1SW2

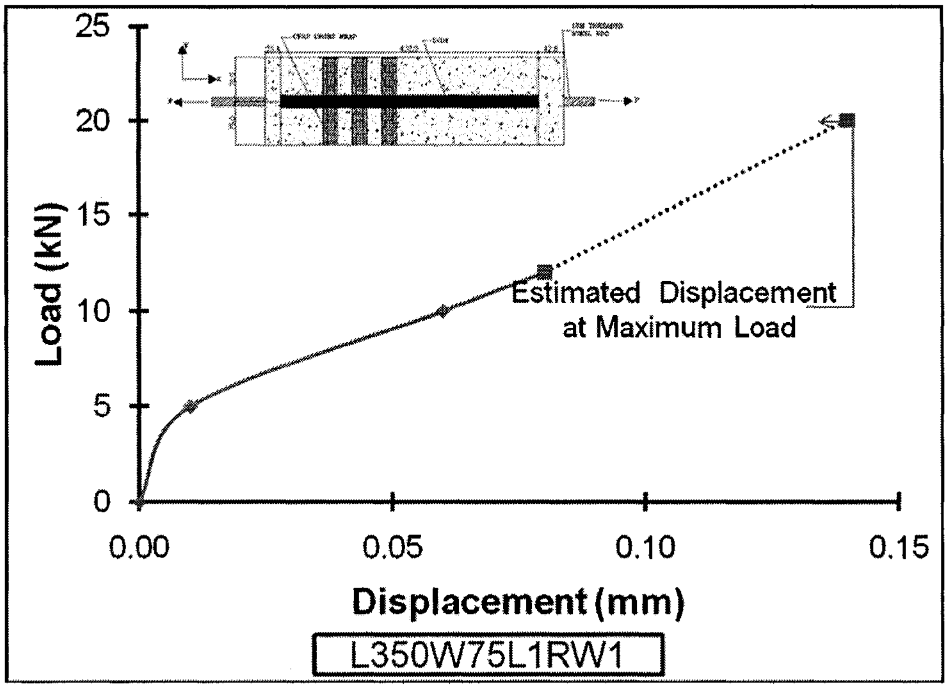

Load (kN)
Displacement (mm)
Estimated Displacement at Maximum Load
0
5
10
15
20
25
0.00
0.05
0.10
0.15
L350W75L1RW1

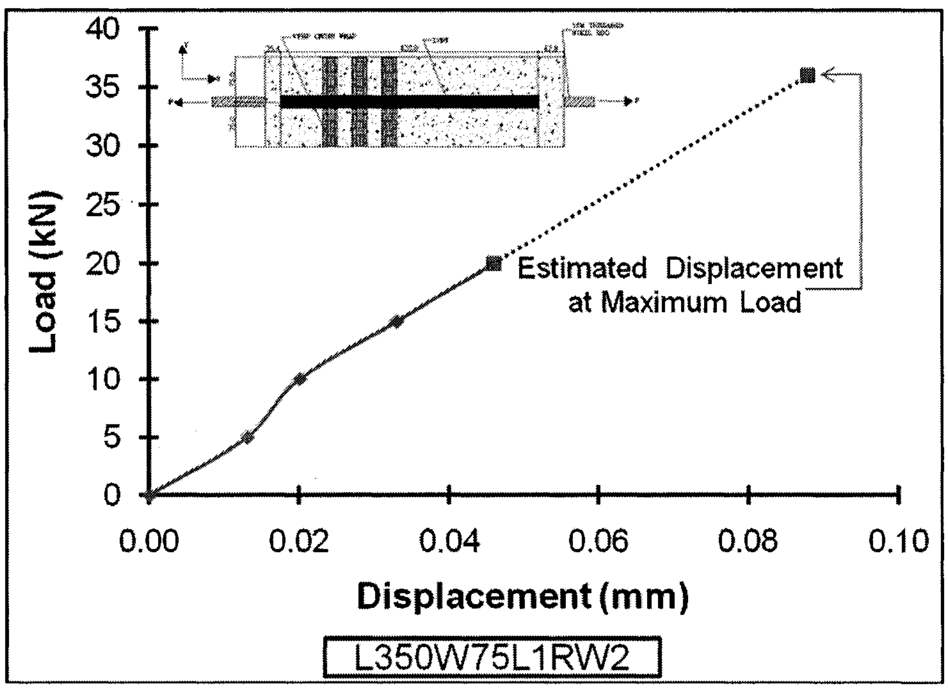

Load (kN)
Displacement (mm)
Estimated Displacement at Maximum Load
0
5
10
15
20
25
30
35
40
0.00
0.02
0.04
0.06
0.08
0.10
L350W75L1RW2

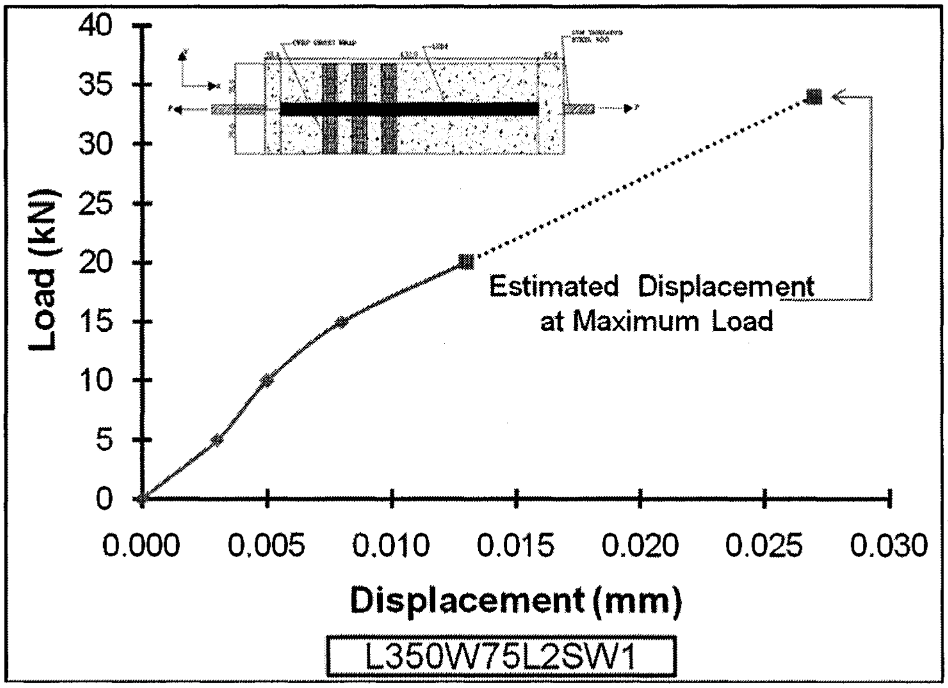

Load (kN)
Estimated Displacement at Maximum Load
Displacement (mm)
L350W75L2SW1

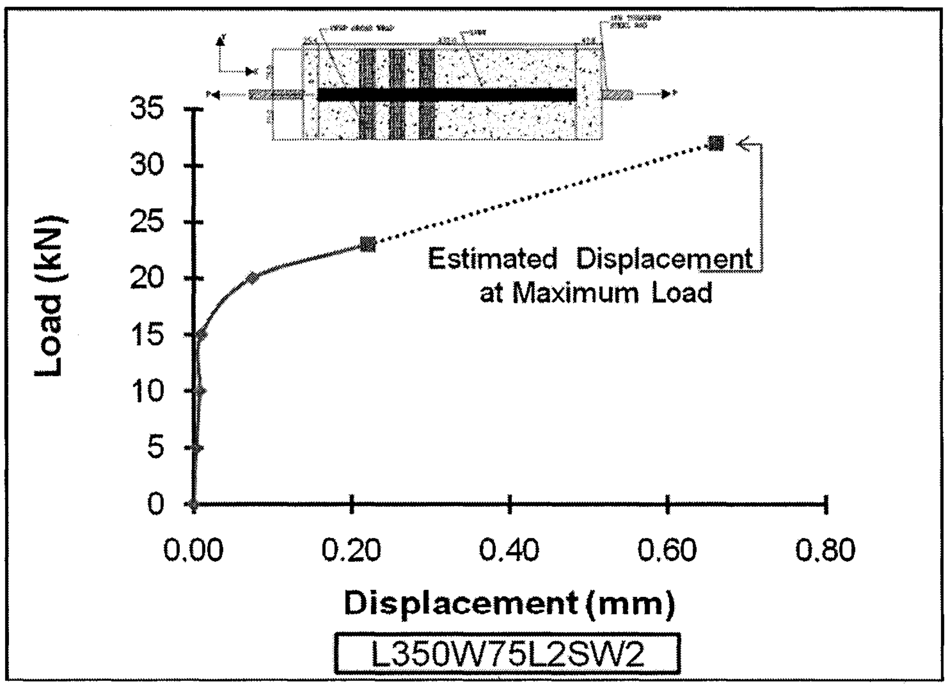

Load (kN)
Estimated Displacement at Maximum Load
Displacement (mm)
L350W75L2SW2

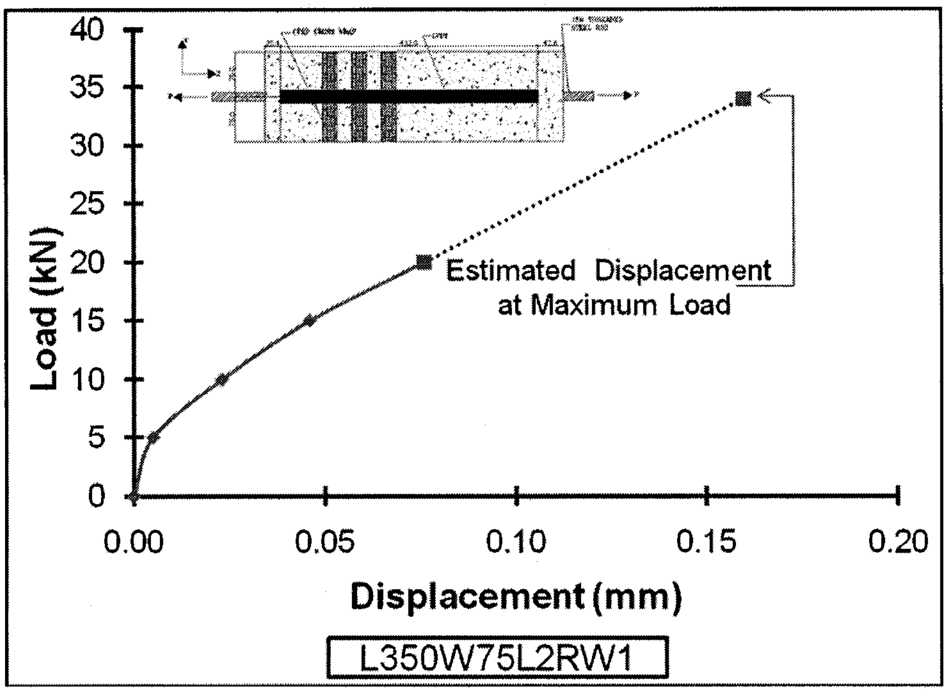

Load (kN)
Displacement (mm)
Estimated Displacement at Maximum Load
L350W75L2RW1

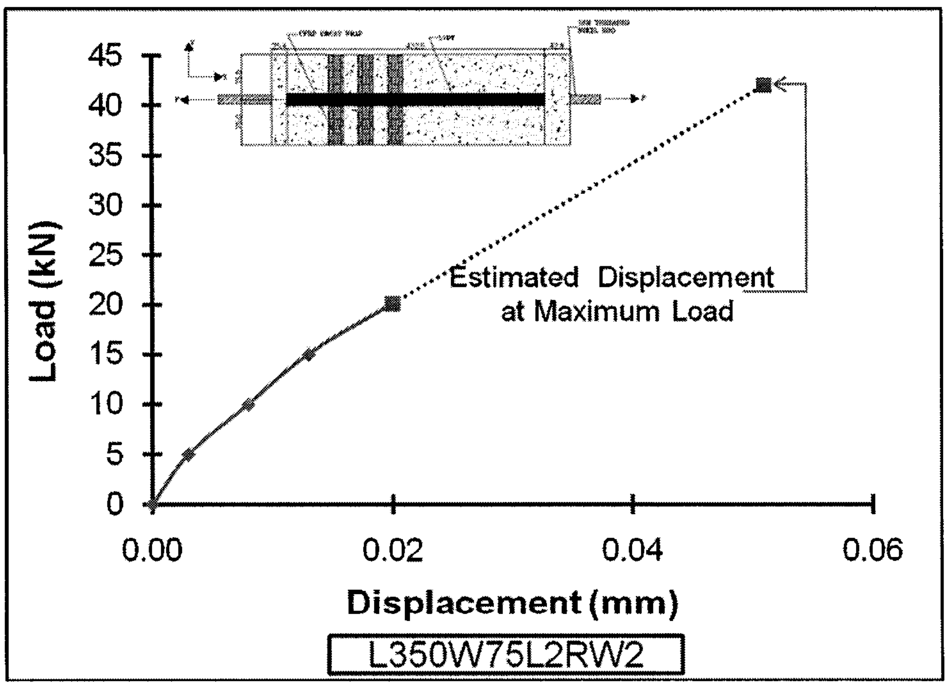

Load (kN)
Displacement (mm)
Estimated Displacement at Maximum Load
L350W75L2RW2

APPENDIX D
AVERAGE STRESS VERSUS AVERAGE SLIP

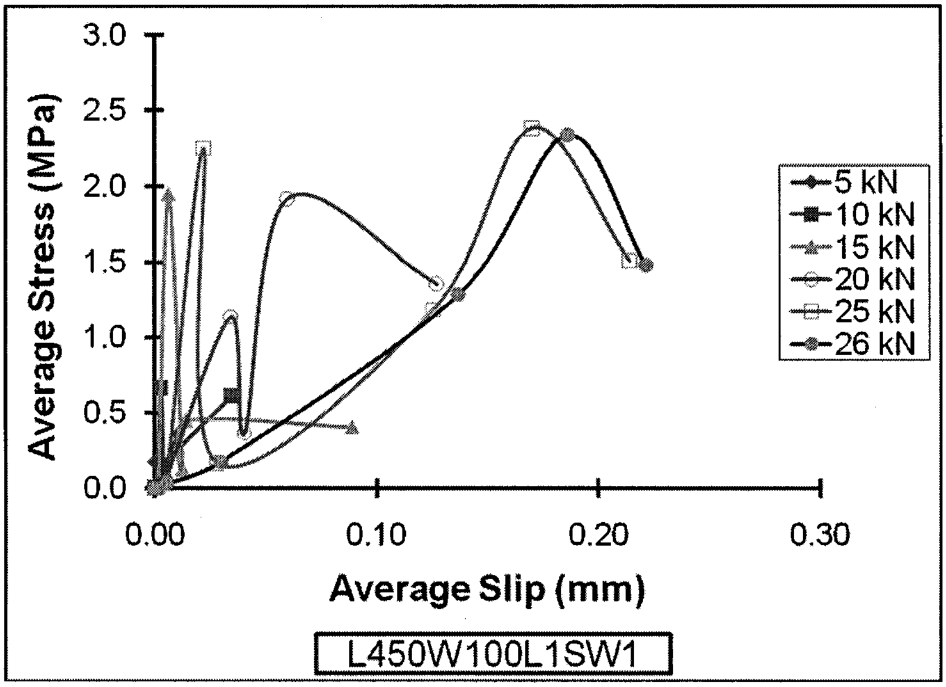

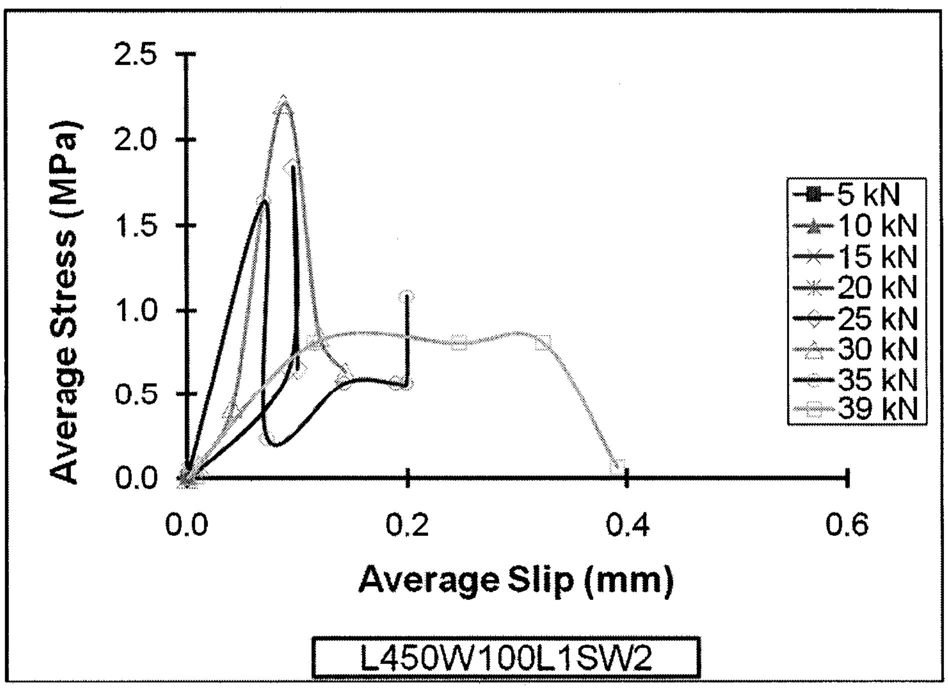

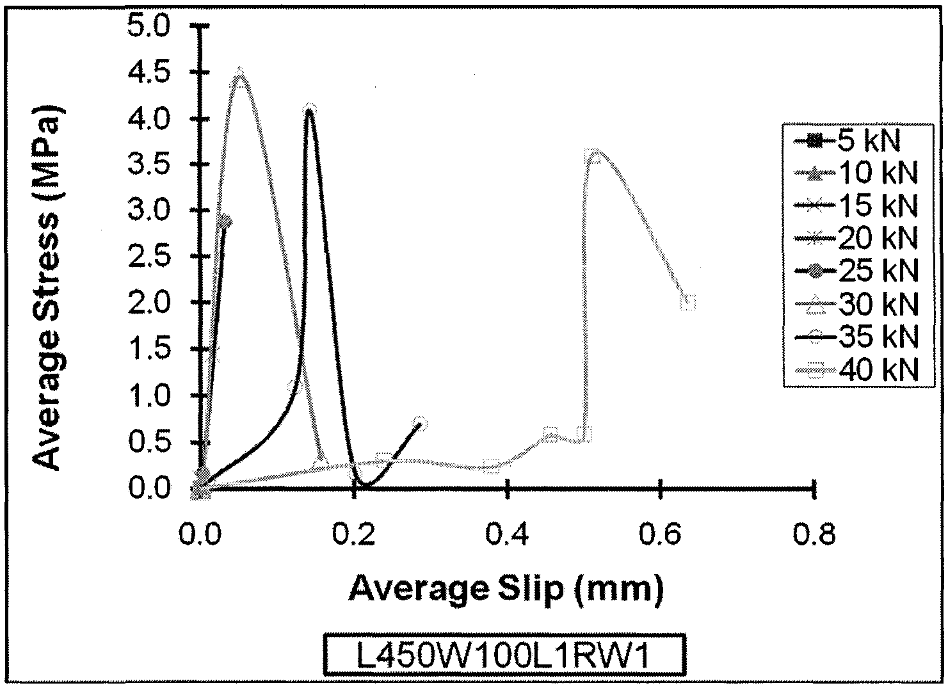

Average Stress (MPa)
5.0
4.5
4.0
3.5
3.0
2.5
2.0
1.5
1.0
0.5
0.0
0.0
0.2
0.4
0.6
0.8
Average Slip (mm)
5 kN
10 kN
15 kN
20 kN
25 kN
30 kN
35 kN
40 kN
L450W100L1RW1

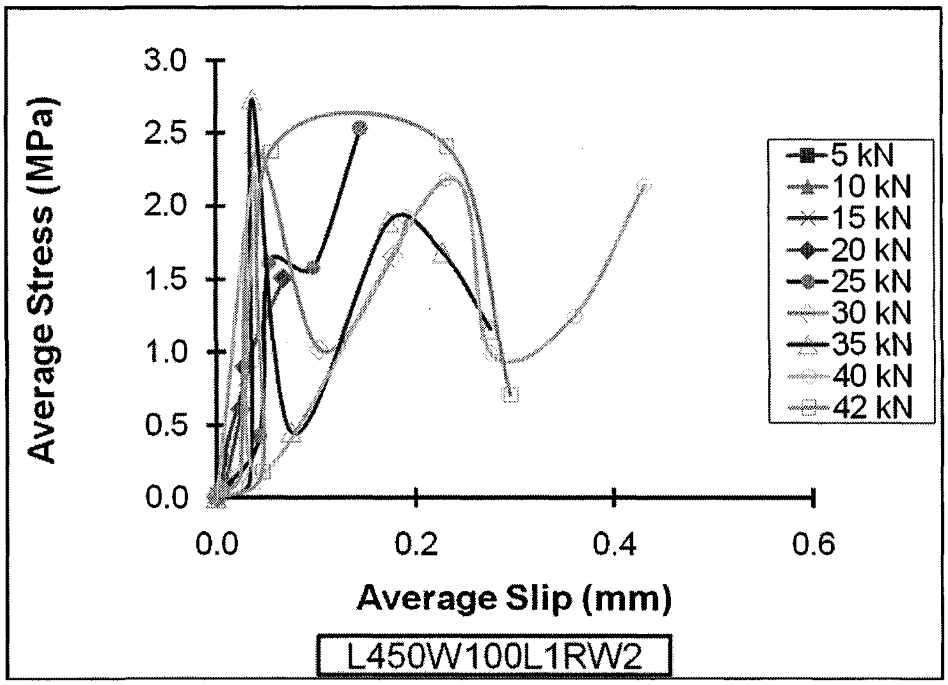

Average Stress (MPa)
3.0
2.5
2.0
1.5
1.0
0.5
0.0
0.0
0.2
0.4
0.6
Average Slip (mm)
5 kN
10 kN
15 kN
20 kN
25 kN
30 kN
35 kN
40 kN
42 kN
L450W100L1RW2

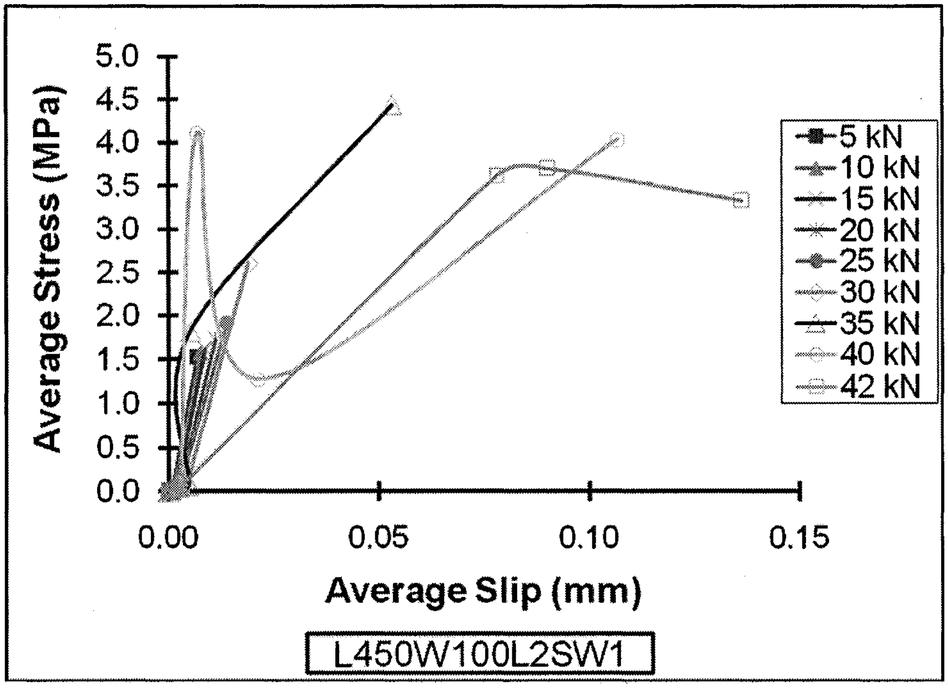

5.0
4.5
4.0
3.5
3.0
2.5
2.0
1.5
1.0
0.5
0.0
Average Stress (MPa)
0.00
0.05
0.10
0.15
Average Slip (mm)
5 kN
10 kN
15 kN
20 kN
25 kN
30 kN
35 kN
40 kN
42 kN
L450W100L2SW1

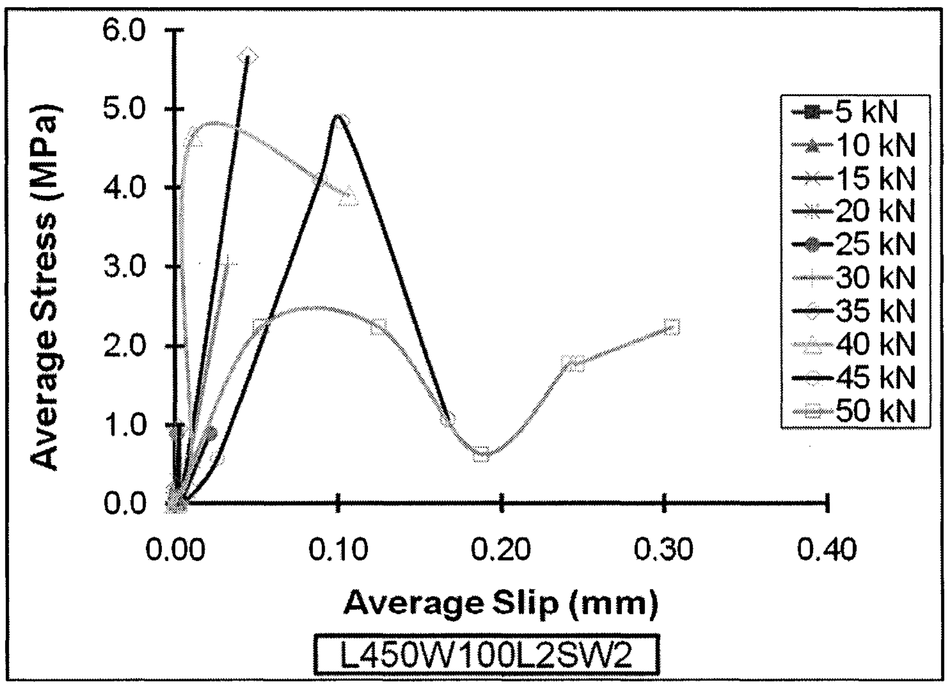

6.0
5.0
4.0
3.0
2.0
1.0
0.0
Average Stress (MPa)
0.00
0.10
0.20
0.30
0.40
Average Slip (mm)
5 kN
10 kN
15 kN
20 kN
25 kN
30 kN
35 kN
40 kN
45 kN
50 kN
L450W100L2SW2

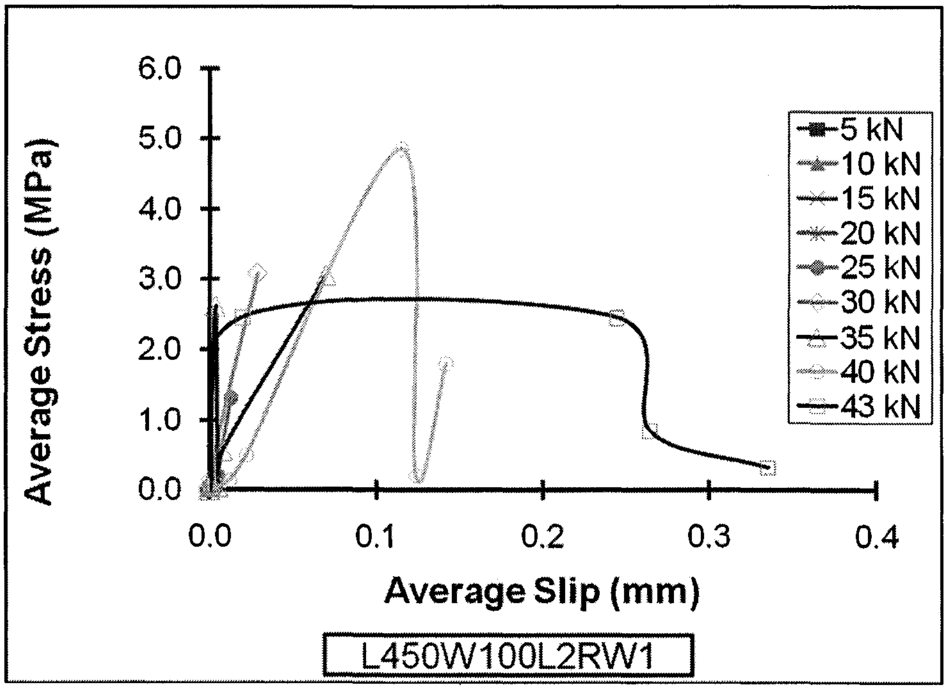
Average Stress (MPa)
Average Slip (mm)
5 kN
10 kN
15 kN
20 kN
25 kN
30 kN
35 kN
40 kN
43 kN
L450W100L2RW1

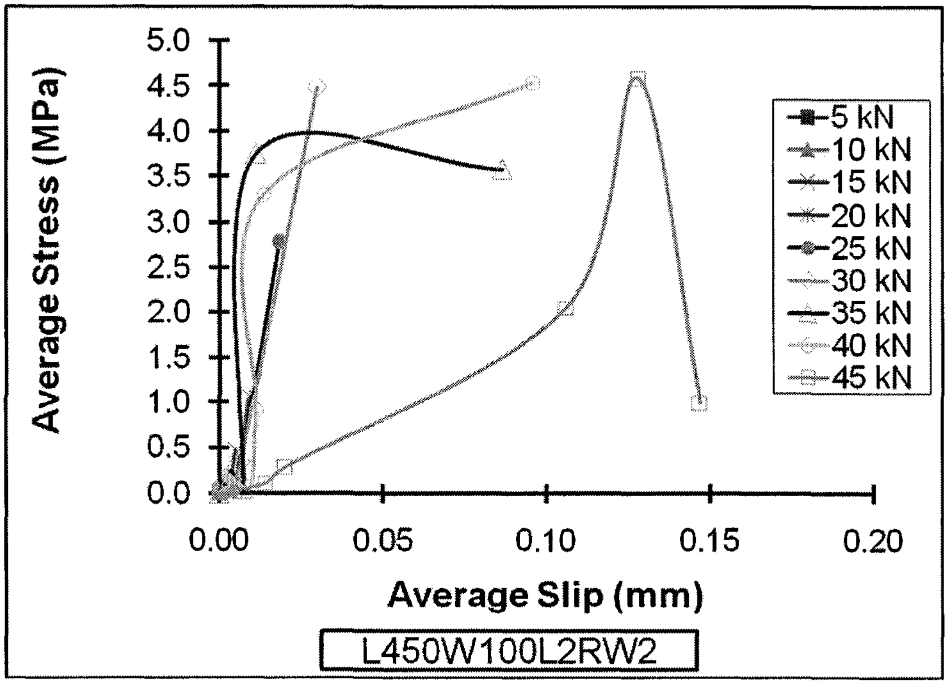
Average Stress (MPa)
Average Slip (mm)
5 kN
10 kN
15 kN
20 kN
25 kN
30 kN
35 kN
40 kN
45 kN
L450W100L2RW2

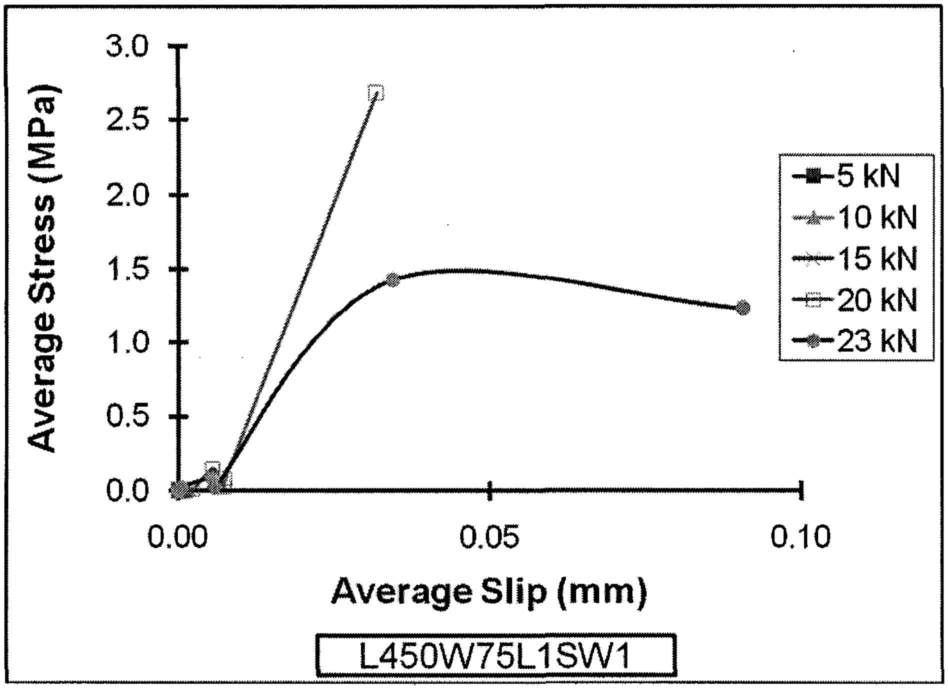
3.0
2.5
2.0
1.5
1.0
0.5
0.0
Average Stress (MPa)
0.00
0.05
0.10
Average Slip (mm)
5 kN
10 kN
15 kN
20 kN
23 kN
L450W75L1SW1

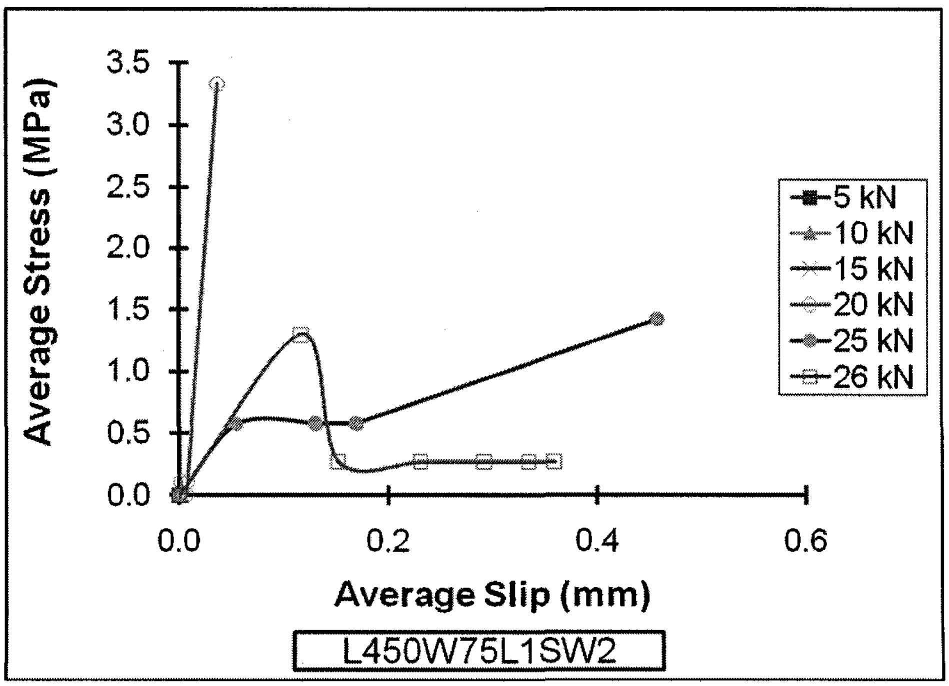
3.5
3.0
2.5
2.0
1.5
1.0
0.5
0.0
Average Stress (MPa)
0.0
0.2
0.4
0.6
Average Slip (mm)
5 kN
10 kN
15 kN
20 kN
25 kN
26 kN
L450W75L1SW2

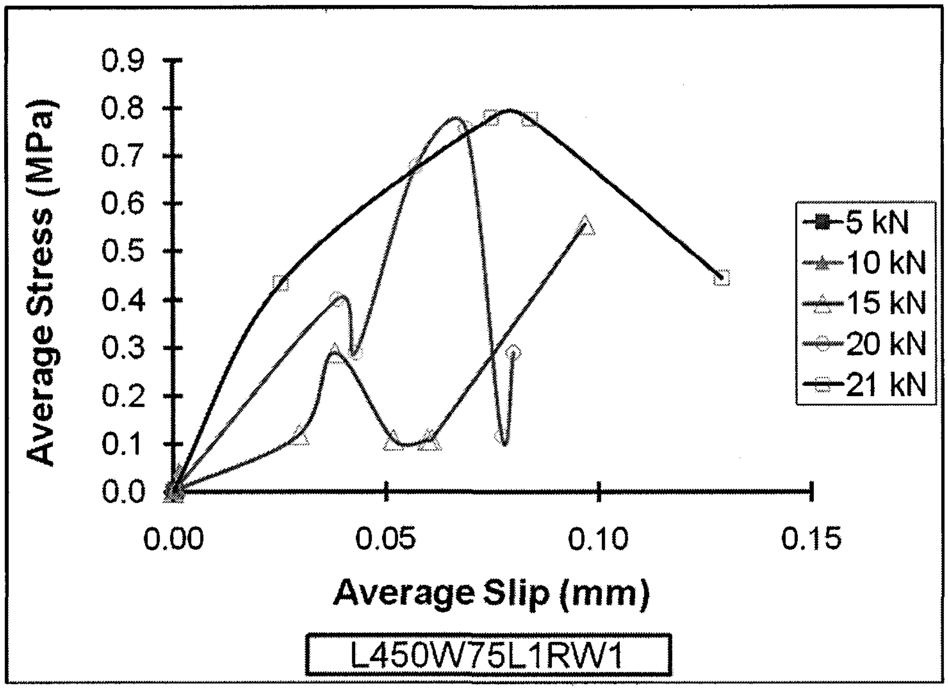

Average Stress (MPa)
Average Slip (mm)
5 kN
10 kN
15 kN
20 kN
21 kN
L450W75L1RW1

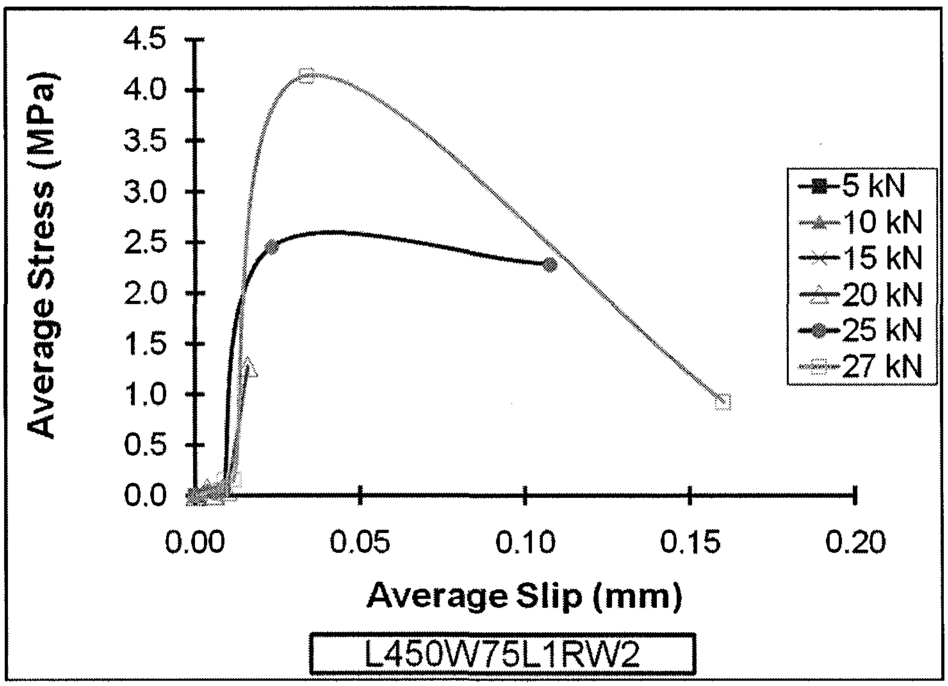

Average Stress (MPa)
Average Slip (mm)
5 kN
10 kN
15 kN
20 kN
25 kN
27 kN
L450W75L1RW2

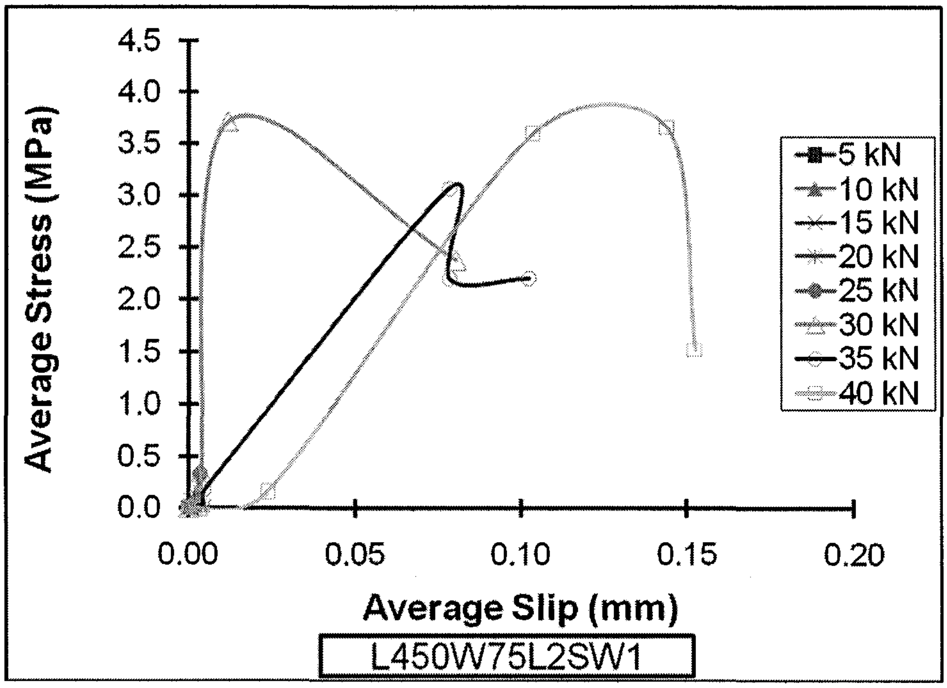
Average Stress (MPa)
4.5
4.0
3.5
3.0
2.5
2.0
1.5
1.0
0.5
0.0
0.00
0.05
0.10
0.15
0.20
Average Slip (mm)
L450W75L2SW1
5 kN
10 kN
15 kN
20 kN
25 kN
30 kN
35 kN
40 kN

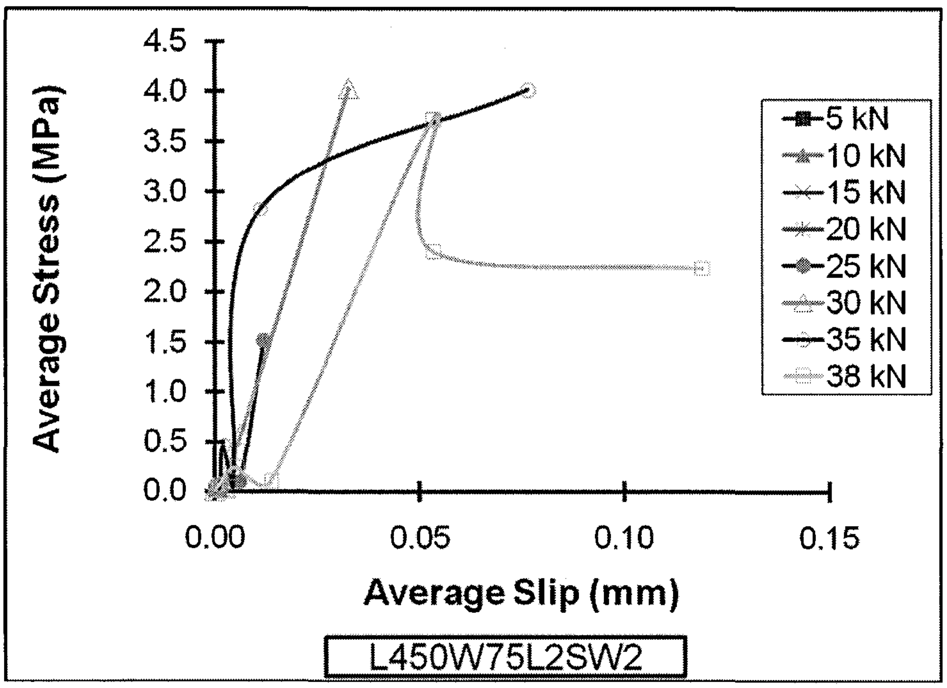
Average Stress (MPa)
4.5
4.0
3.5
3.0
2.5
2.0
1.5
1.0
0.5
0.0
0.00
0.05
0.10
0.15
Average Slip (mm)
L450W75L2SW2
5 kN
10 kN
15 kN
20 kN
25 kN
30 kN
35 kN
38 kN

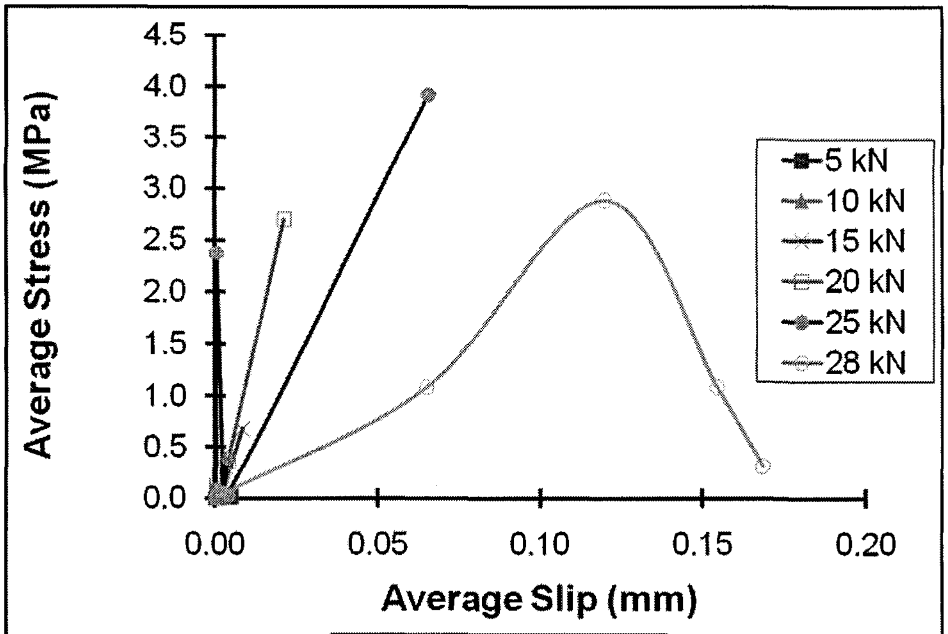

L450W75L2RW1

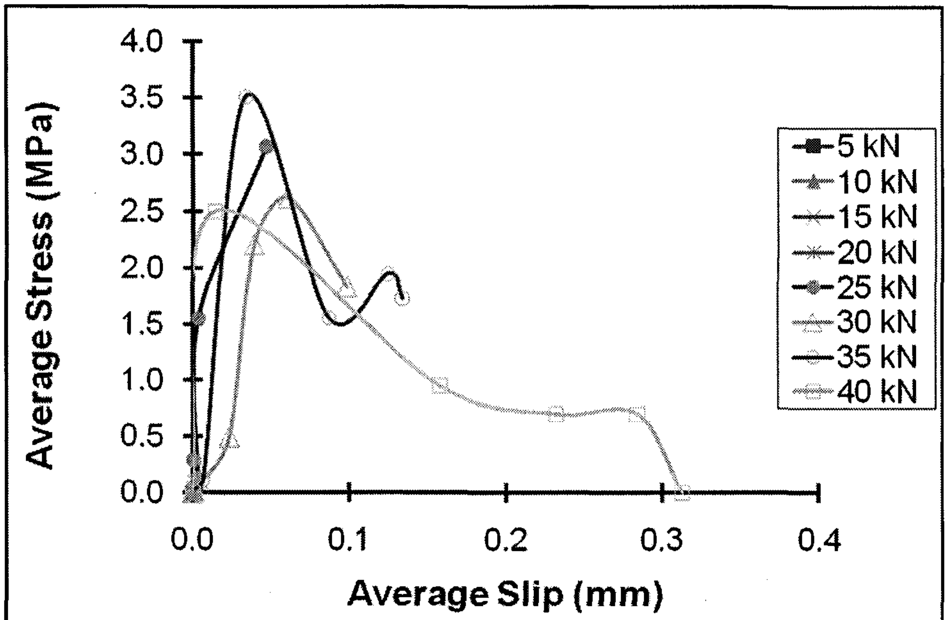

L450W75L2RW2

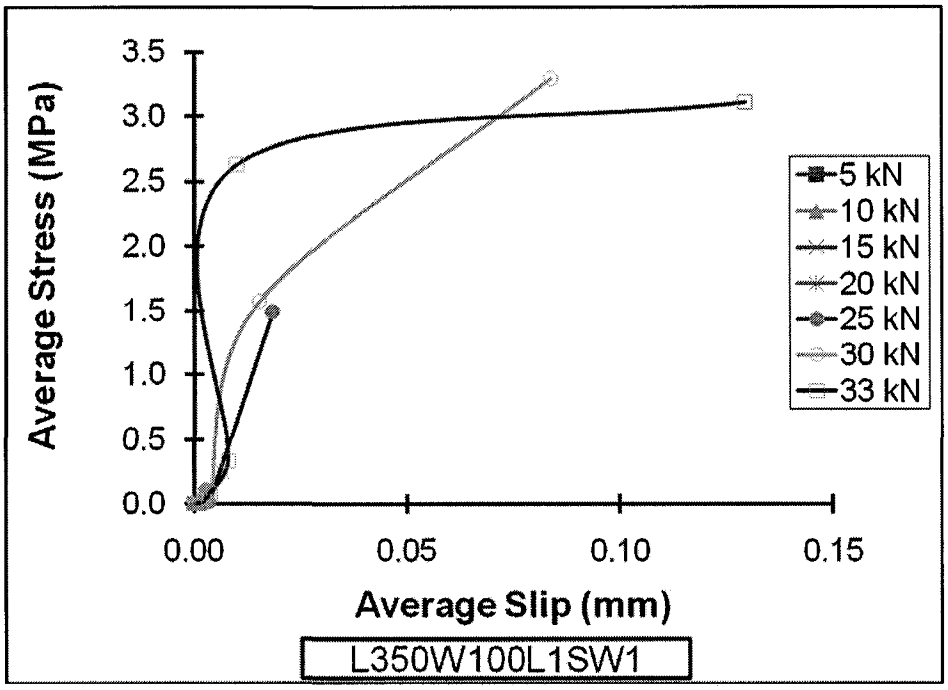
3.5
3.0
2.5
2.0
1.5
1.0
0.5
0.0
0.00
0.05
0.10
0.15
Average Stress (MPa)
Average Slip (mm)
5 kN
10 kN
15 kN
20 kN
25 kN
30 kN
33 kN
L350W100L1SW1

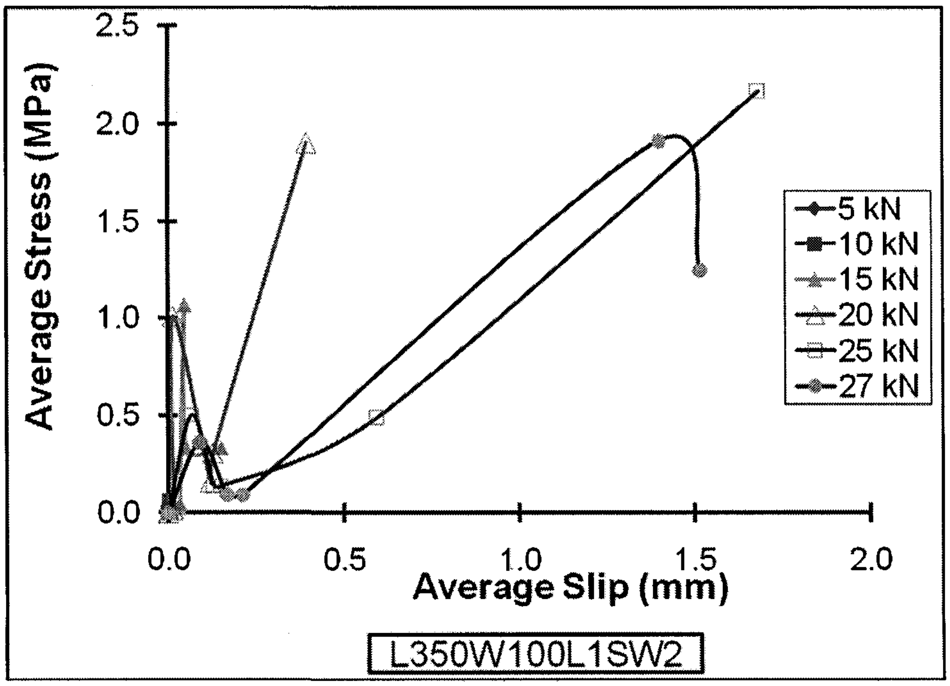
2.5
2.0
1.5
1.0
0.5
0.0
0.0
0.5
1.0
1.5
2.0
Average Stress (MPa)
Average Slip (mm)
5 kN
10 kN
15 kN
20 kN
25 kN
27 kN
L350W100L1SW2

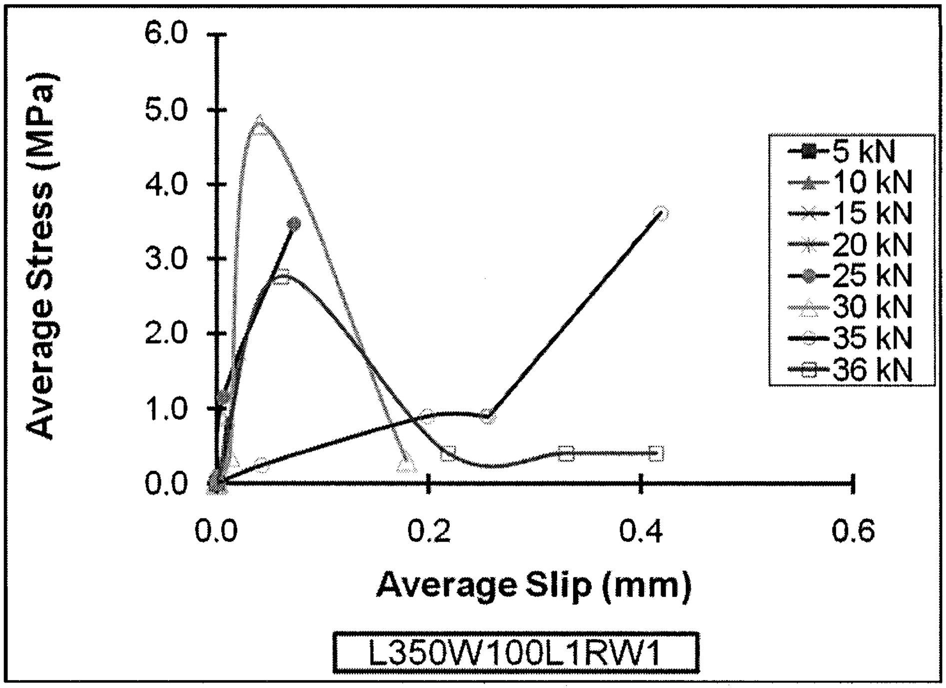

Average Stress (MPa)
6.0
5.0
4.0
3.0
2.0
1.0
0.0
0.0
0.2
0.4
0.6
Average Slip (mm)
5 kN
10 kN
15 kN
20 kN
25 kN
30 kN
35 kN
36 kN
L350W100L1RW1

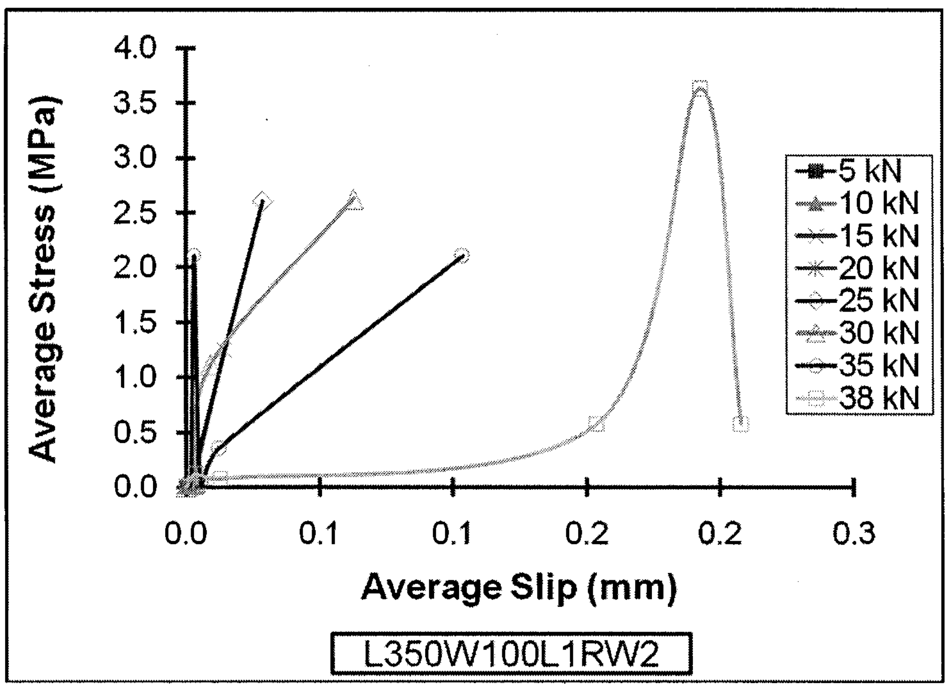

Average Stress (MPa)
4.0
3.5
3.0
2.5
2.0
1.5
1.0
0.5
0.0
0.0
0.1
0.1
0.2
0.2
0.3
Average Slip (mm)
5 kN
10 kN
15 kN
20 kN
25 kN
30 kN
35 kN
38 kN
L350W100L1RW2

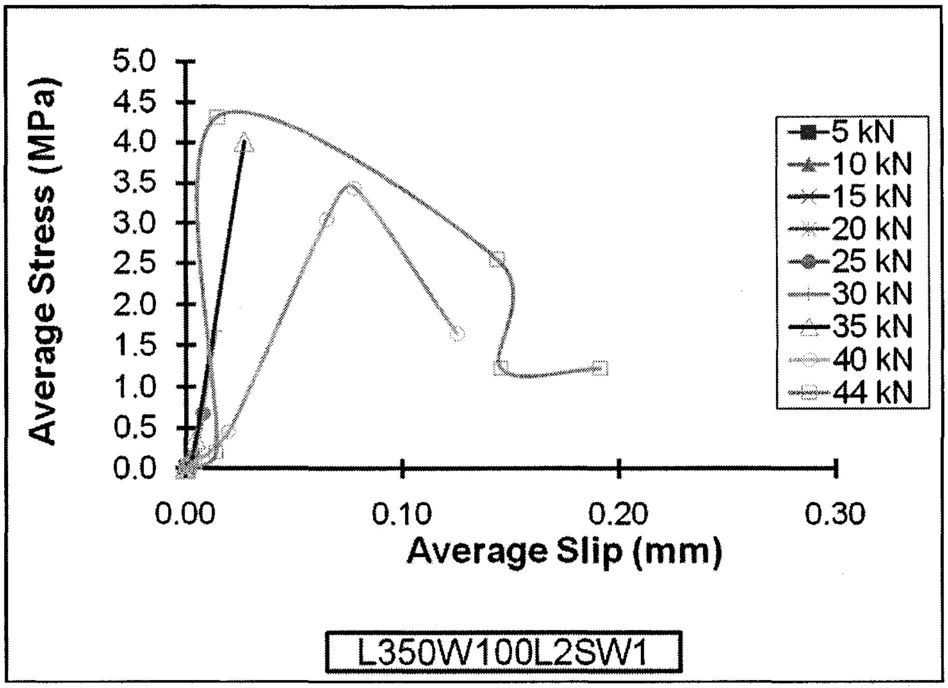

5.0
4.5
4.0
3.5
3.0
2.5
2.0
1.5
1.0
0.5
0.0
Average Stress (MPa)
0.00
0.10
0.20
0.30
Average Slip (mm)
5 kN
10 kN
15 kN
20 kN
25 kN
30 kN
35 kN
40 kN
44 kN
L350W100L2SW1

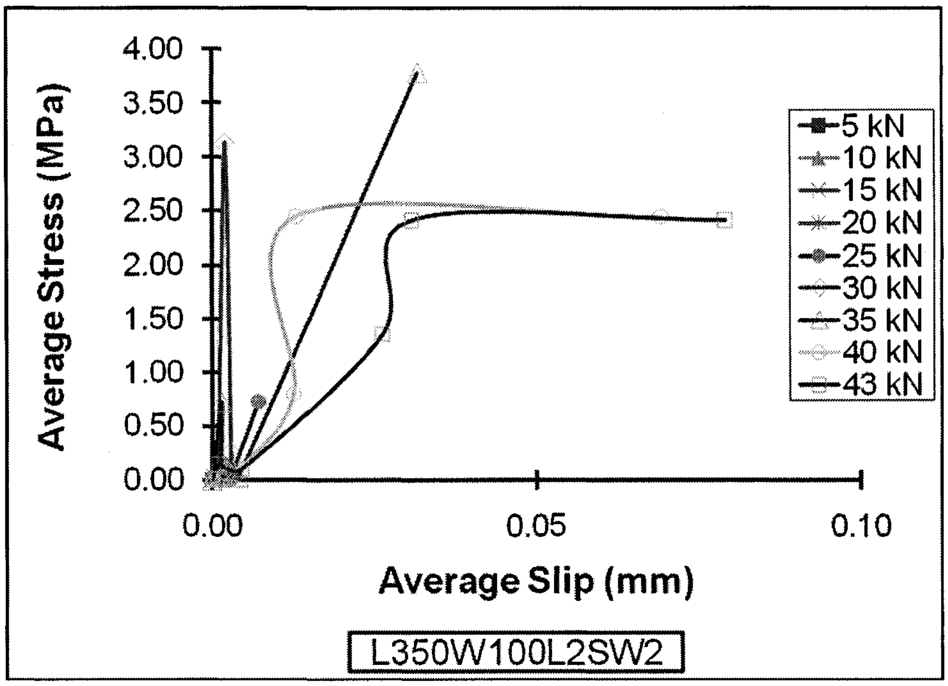

4.00
3.50
3.00
2.50
2.00
1.50
1.00
0.50
0.00
Average Stress (MPa)
0.00
0.05
0.10
Average Slip (mm)
5 kN
10 kN
15 kN
20 kN
25 kN
30 kN
35 kN
40 kN
43 kN
L350W100L2SW2

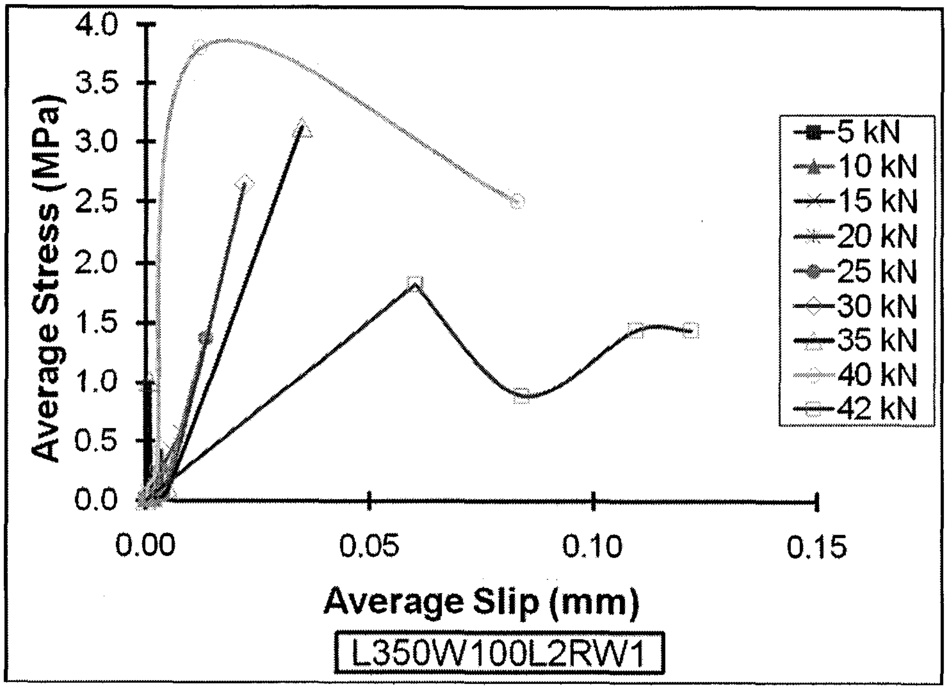
Average Stress (MPa)
4.0
3.5
3.0
2.5
2.0
1.5
1.0
0.5
0.0
0.00
0.05
0.10
0.15
Average Slip (mm)
L350W100L2RW1
5 kN
10 kN
15 kN
20 kN
25 kN
30 kN
35 kN
40 kN
42 kN

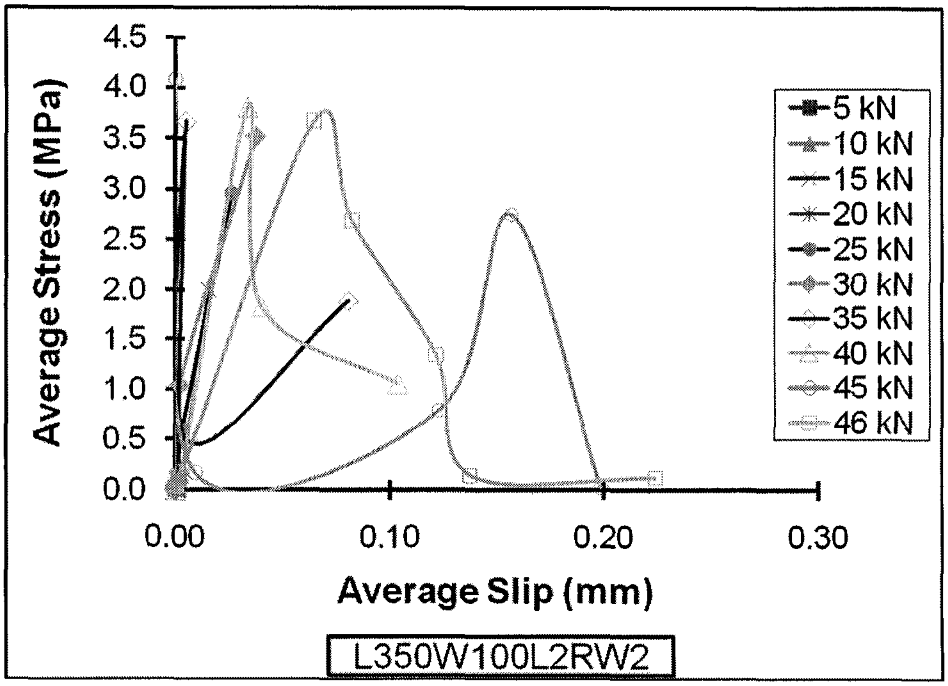
Average Stress (MPa)
4.5
4.0
3.5
3.0
2.5
2.0
1.5
1.0
0.5
0.0
0.00
0.10
0.20
0.30
Average Slip (mm)
L350W100L2RW2
5 kN
10 kN
15 kN
20 kN
25 kN
30 kN
35 kN
40 kN
45 kN
46 kN

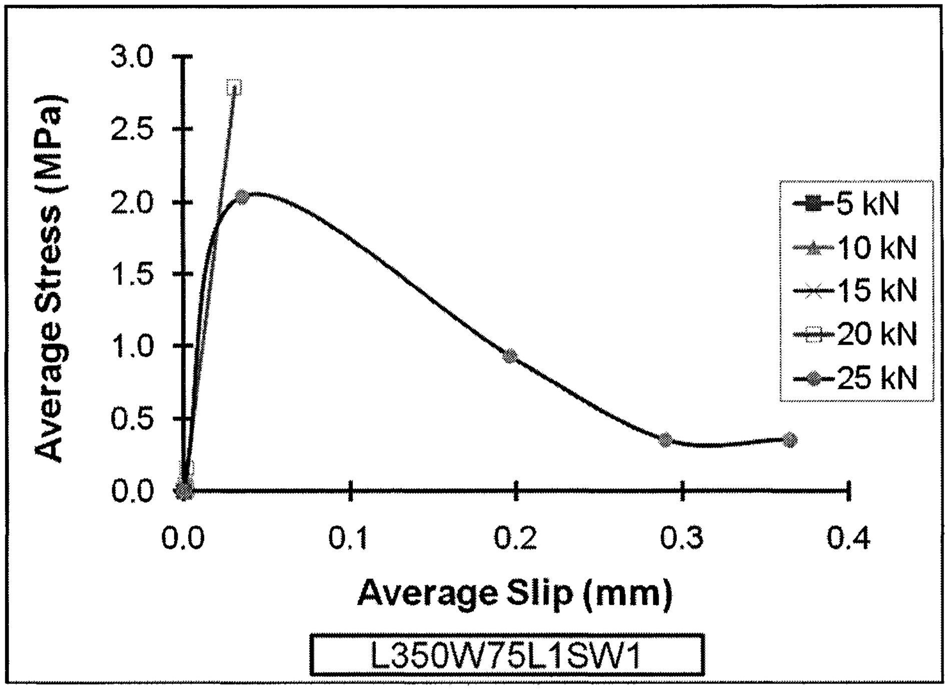

3.0
2.5
2.0
1.5
1.0
0.5
0.0
Average Stress (MPa)
0.0
0.1
0.2
0.3
0.4
Average Slip (mm)
5 kN
10 kN
15 kN
20 kN
25 kN
L350W75L1SW1

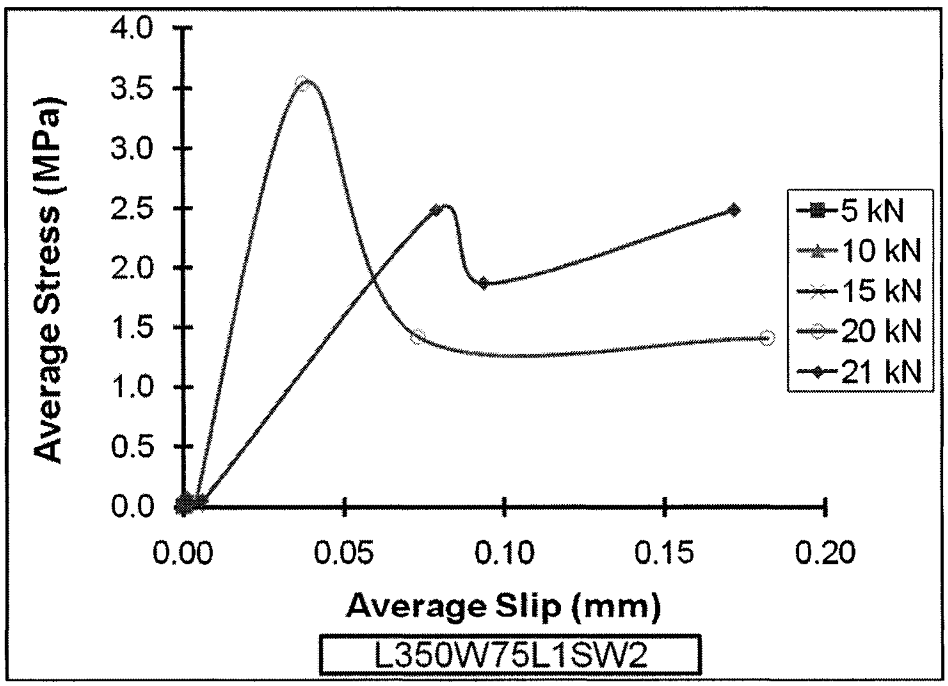

4.0
3.5
3.0
2.5
2.0
1.5
1.0
0.5
0.0
Average Stress (MPa)
0.00
0.05
0.10
0.15
0.20
Average Slip (mm)
5 kN
10 kN
15 kN
20 kN
21 kN
L350W75L1SW2

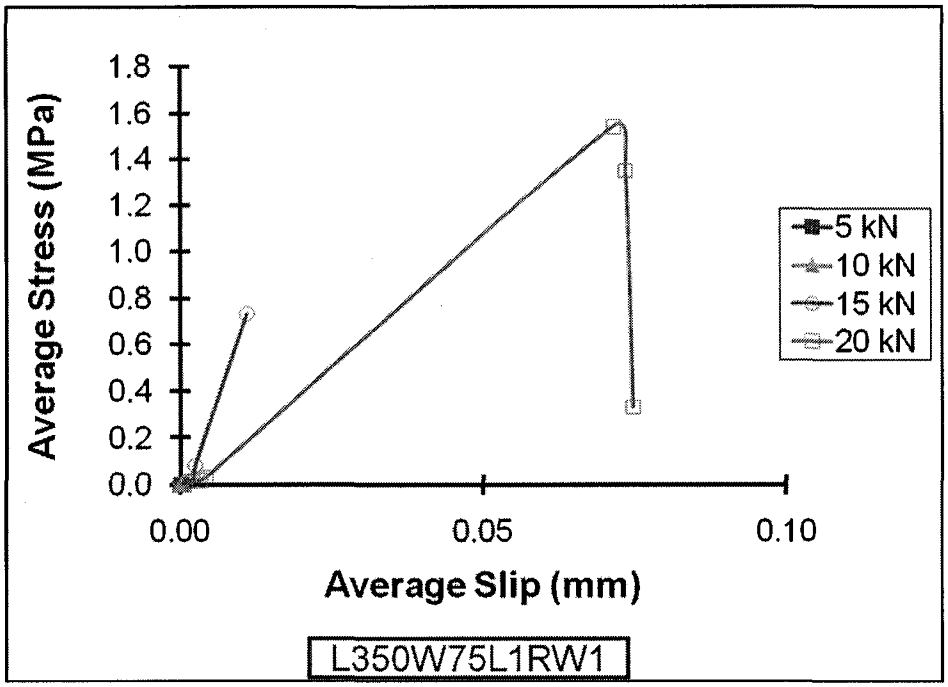
1.8
1.6
1.4
1.2
1.0
0.8
0.6
0.4
0.2
0.0
Average Stress (MPa)
0.00
0.05
0.10
Average Slip (mm)
5 kN
10 kN
15 kN
20 kN
L350W75L1RW1

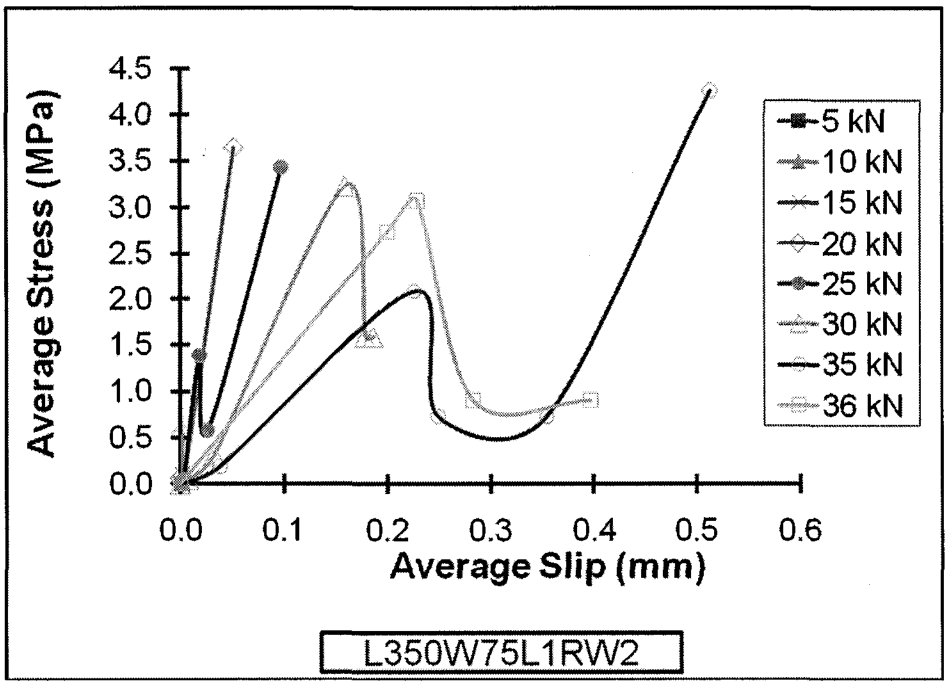
4.5
4.0
3.5
3.0
2.5
2.0
1.5
1.0
0.5
0.0
Average Stress (MPa)
0.0
0.1
0.2
0.3
0.4
0.5
0.6
Average Slip (mm)
5 kN
10 kN
15 kN
20 kN
25 kN
30 kN
35 kN
36 kN
L350W75L1RW2

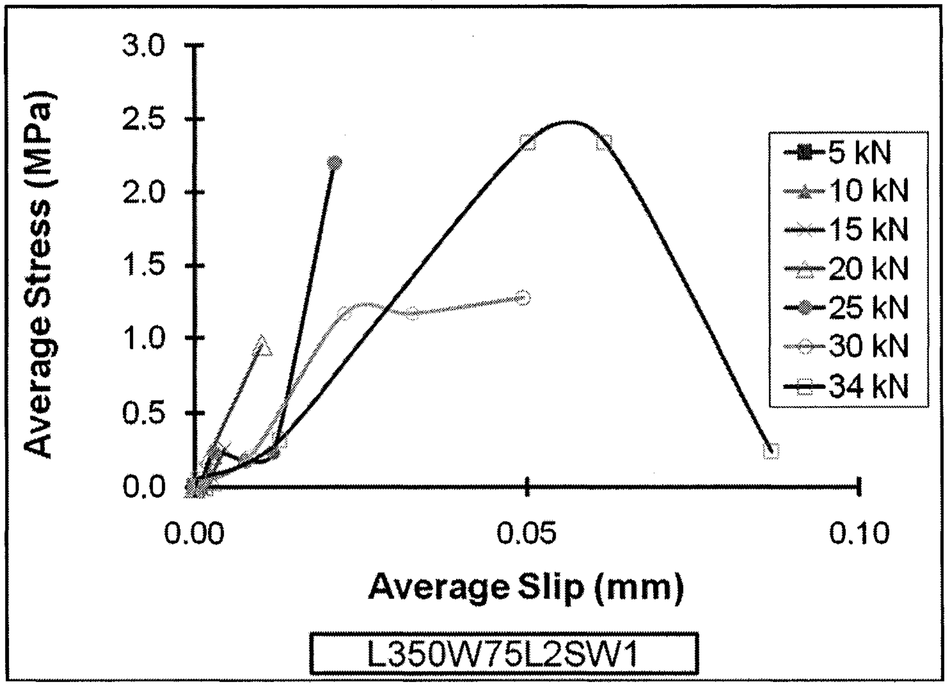
Average Stress (MPa)
3.0
2.5
2.0
1.5
1.0
0.5
0.0
0.00
0.05
0.10
Average Slip (mm)
5 kN
10 kN
15 kN
20 kN
25 kN
30 kN
34 kN
L350W75L2SW1

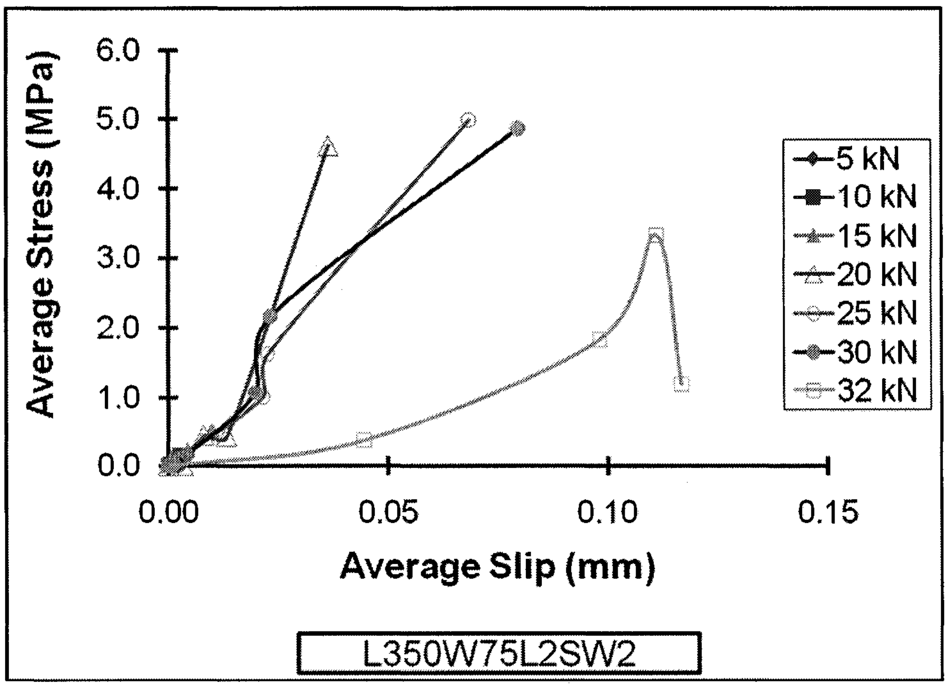
Average Stress (MPa)
6.0
5.0
4.0
3.0
2.0
1.0
0.0
0.00
0.05
0.10
0.15
Average Slip (mm)
5 kN
10 kN
15 kN
20 kN
25 kN
30 kN
32 kN
L350W75L2SW2

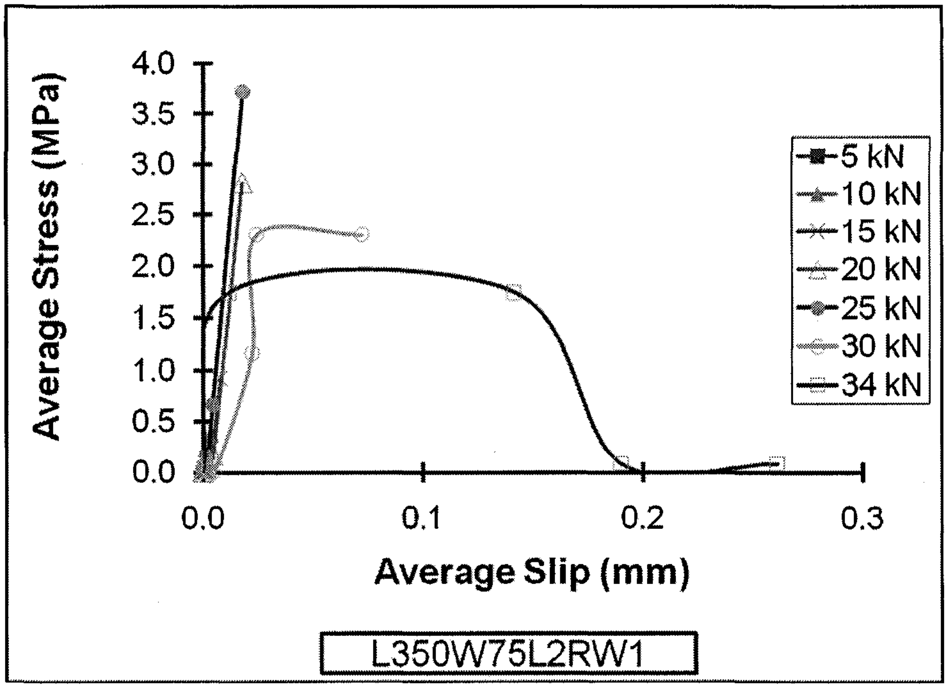

Average Stress (MPa)
4.0
3.5
3.0
2.5
2.0
1.5
1.0
0.5
0.0
0.0
0.1
0.2
0.3
Average Slip (mm)
5 kN
10 kN
15 kN
20 kN
25 kN
30 kN
34 kN
L350W75L2RW1

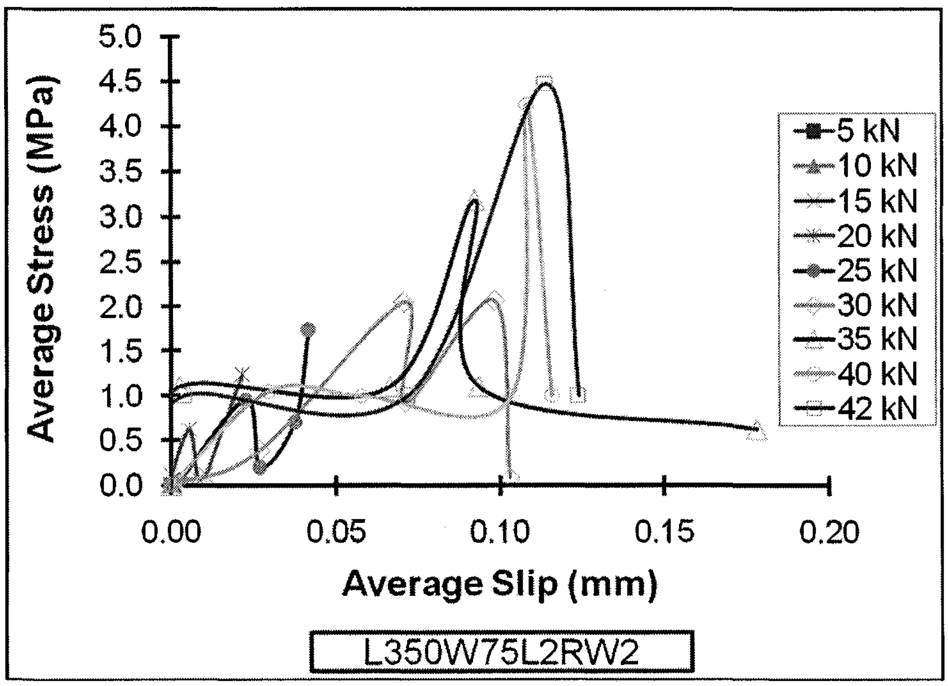

Average Stress (MPa)
5.0
4.5
4.0
3.5
3.0
2.5
2.0
1.5
1.0
0.5
0.0
0.00
0.05
0.10
0.15
0.20
Average Slip (mm)
5 kN
10 kN
15 kN
20 kN
25 kN
30 kN
35 kN
40 kN
42 kN
L350W75L2RW2

APPENDIX E
AVERAGE STRESS VERSUS RELATIVE LOAD

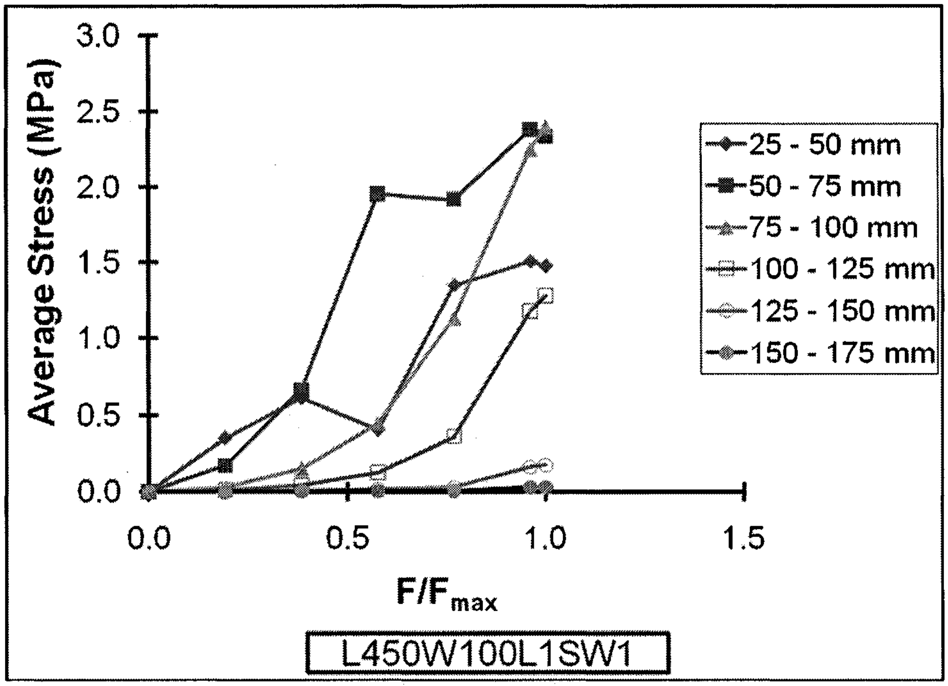

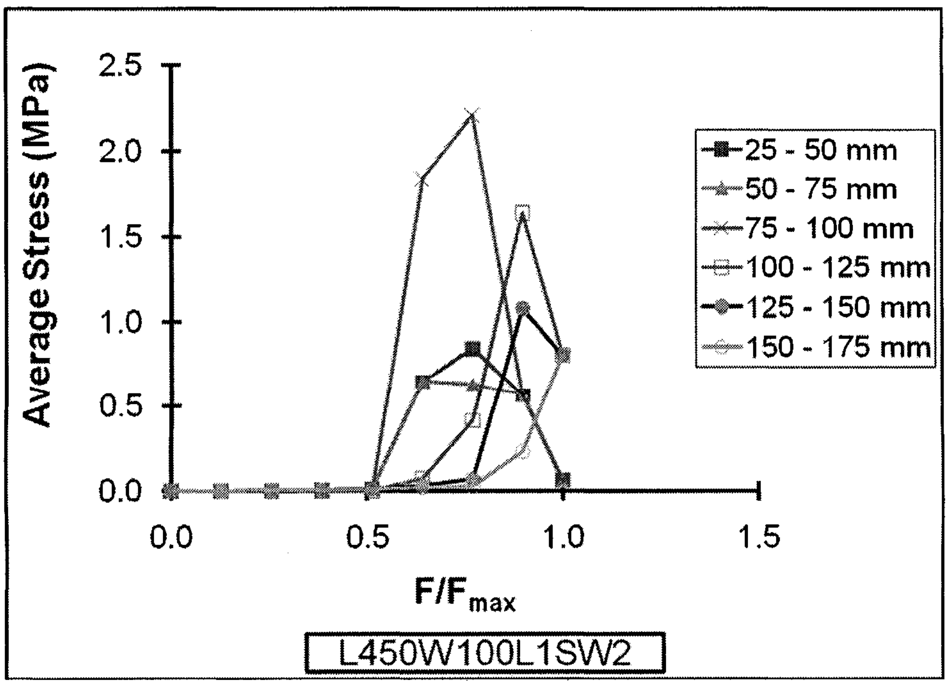

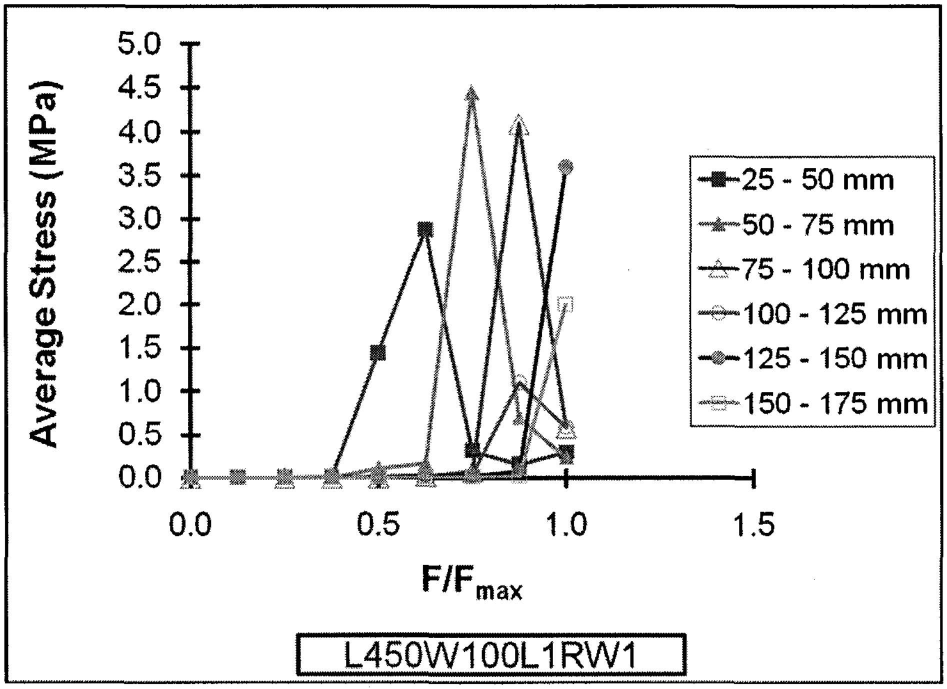

Average Stress (MPa)
5.0
4.5
4.0
3.5
3.0
2.5
2.0
1.5
1.0
0.5
0.0
0.0
0.5
1.0
1.5
F/F$_{max}$
25 - 50 mm
50 - 75 mm
75 - 100 mm
100 - 125 mm
125 - 150 mm
150 - 175 mm
L450W100L1RW1

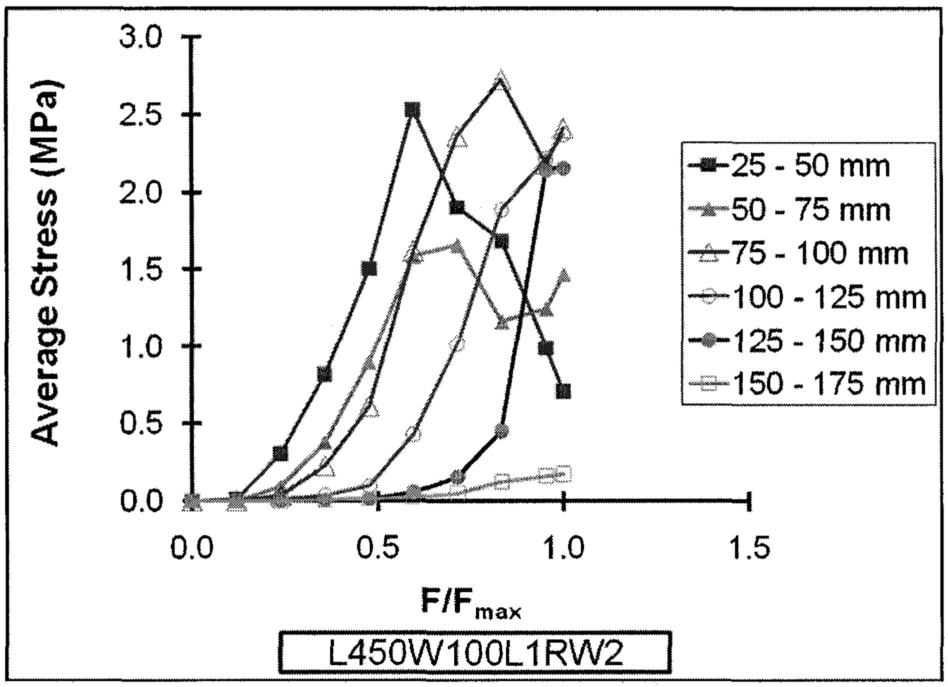

Average Stress (MPa)
3.0
2.5
2.0
1.5
1.0
0.5
0.0
0.0
0.5
1.0
1.5
F/F$_{max}$
25 - 50 mm
50 - 75 mm
75 - 100 mm
100 - 125 mm
125 - 150 mm
150 - 175 mm
L450W100L1RW2

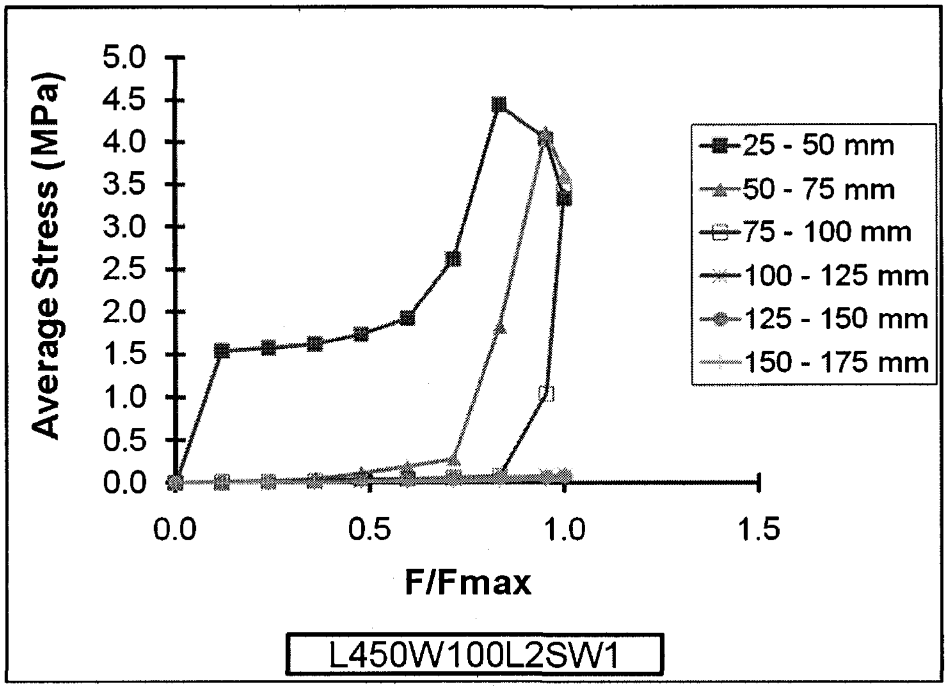

Average Stress (MPa)
5.0
4.5
4.0
3.5
3.0
2.5
2.0
1.5
1.0
0.5
0.0
0.0
0.5
1.0
1.5
F/Fmax
25 - 50 mm
50 - 75 mm
75 - 100 mm
100 - 125 mm
125 - 150 mm
150 - 175 mm
L450W100L2SW1

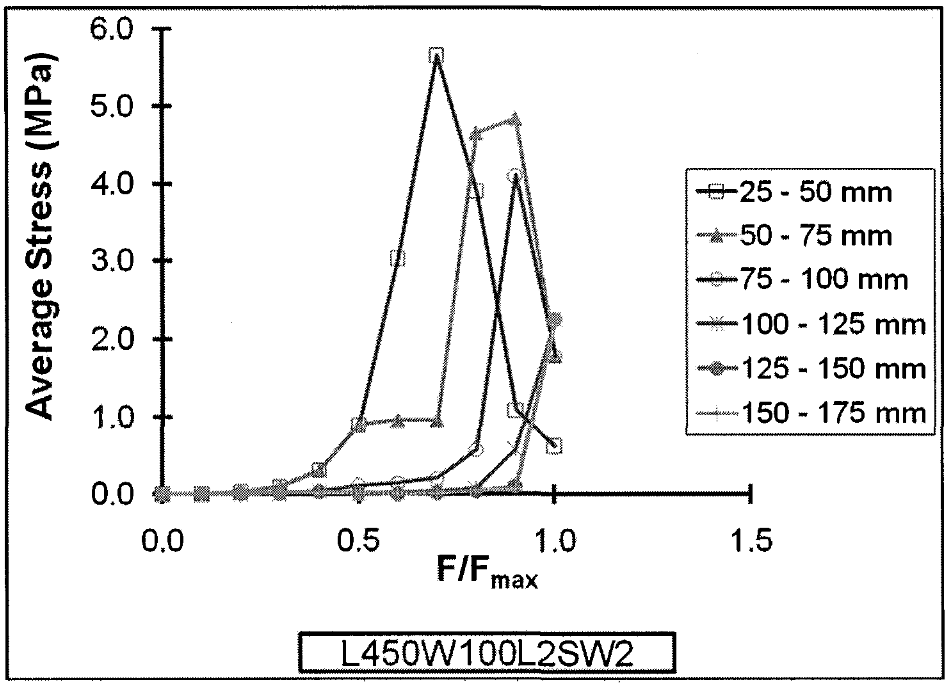

Average Stress (MPa)
6.0
5.0
4.0
3.0
2.0
1.0
0.0
0.0
0.5
1.0
1.5
F/Fmax
25 - 50 mm
50 - 75 mm
75 - 100 mm
100 - 125 mm
125 - 150 mm
150 - 175 mm
L450W100L2SW2

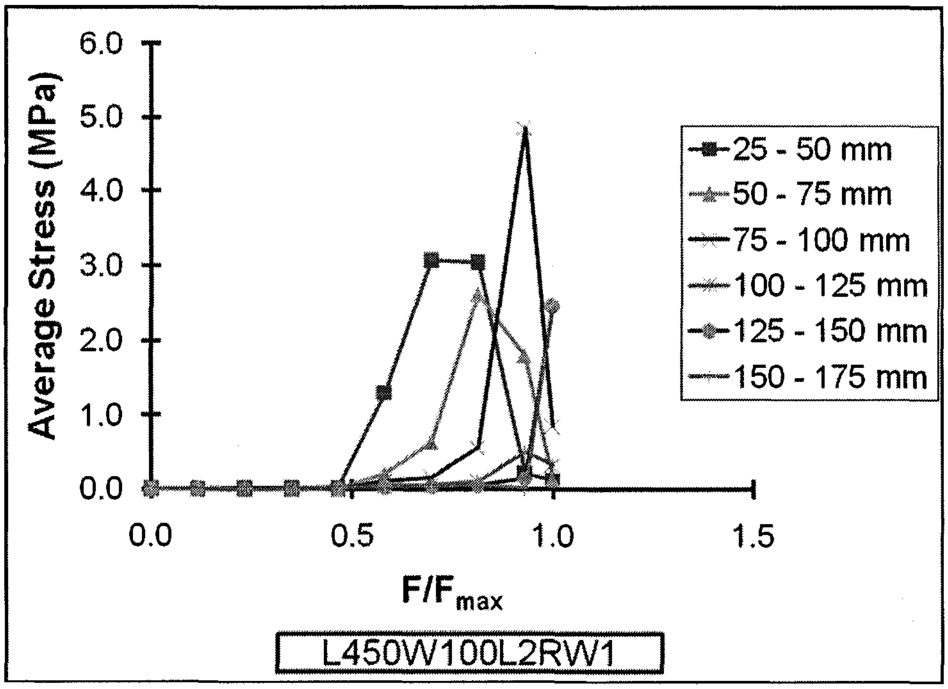
Average Stress (MPa)
6.0
5.0
4.0
3.0
2.0
1.0
0.0
0.0
0.5
1.0
1.5
F/Fmax
25 - 50 mm
50 - 75 mm
75 - 100 mm
100 - 125 mm
125 - 150 mm
150 - 175 mm
L450W100L2RW1

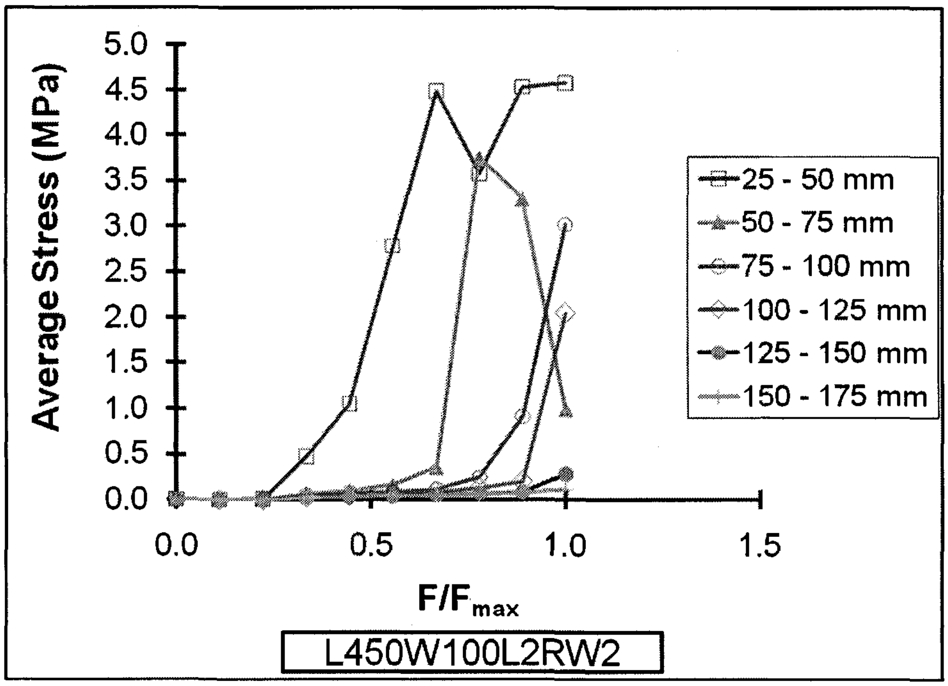
Average Stress (MPa)
5.0
4.5
4.0
3.5
3.0
2.5
2.0
1.5
1.0
0.5
0.0
0.0
0.5
1.0
1.5
F/Fmax
25 - 50 mm
50 - 75 mm
75 - 100 mm
100 - 125 mm
125 - 150 mm
150 - 175 mm
L450W100L2RW2

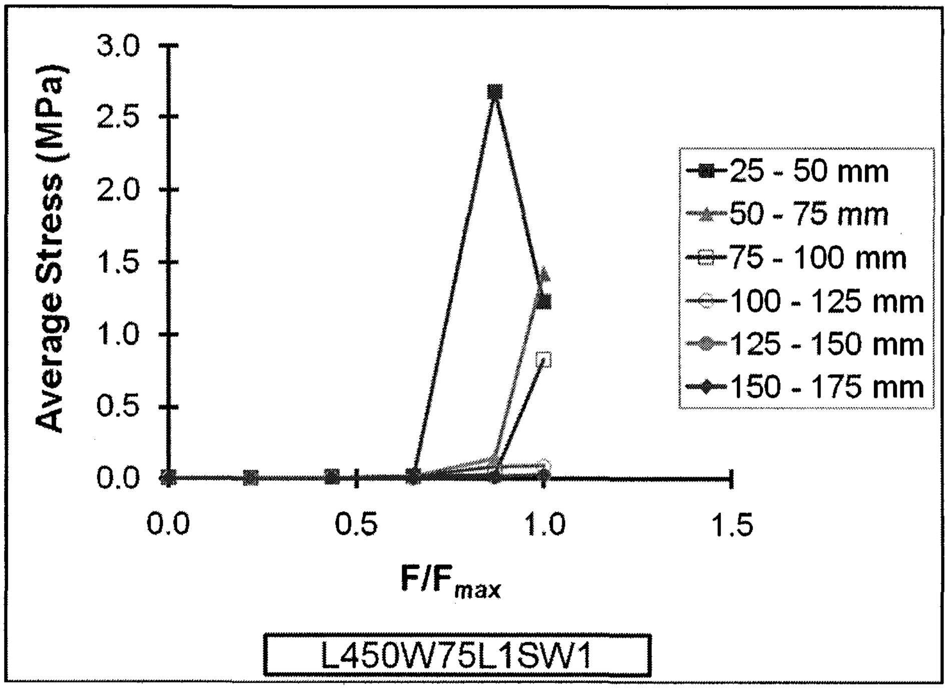

Average Stress (MPa)
3.0
2.5
2.0
1.5
1.0
0.5
0.0
0.0
0.5
1.0
1.5
F/F_{max}
25 - 50 mm
50 - 75 mm
75 - 100 mm
100 - 125 mm
125 - 150 mm
150 - 175 mm
L450W75L1SW1

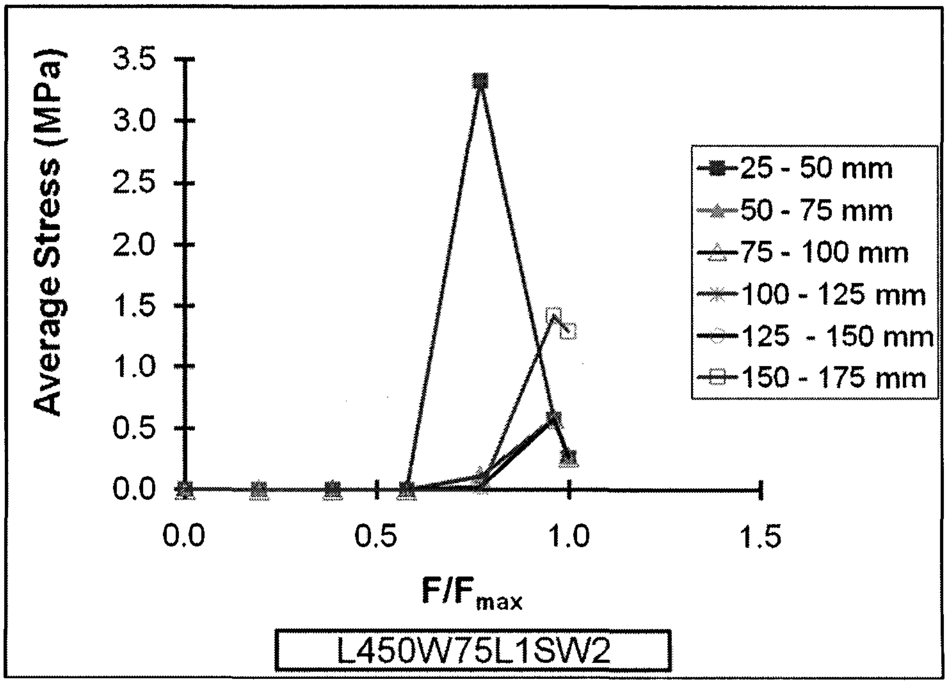

Average Stress (MPa)
3.5
3.0
2.5
2.0
1.5
1.0
0.5
0.0
0.0
0.5
1.0
1.5
F/F_{max}
25 - 50 mm
50 - 75 mm
75 - 100 mm
100 - 125 mm
125 - 150 mm
150 - 175 mm
L450W75L1SW2

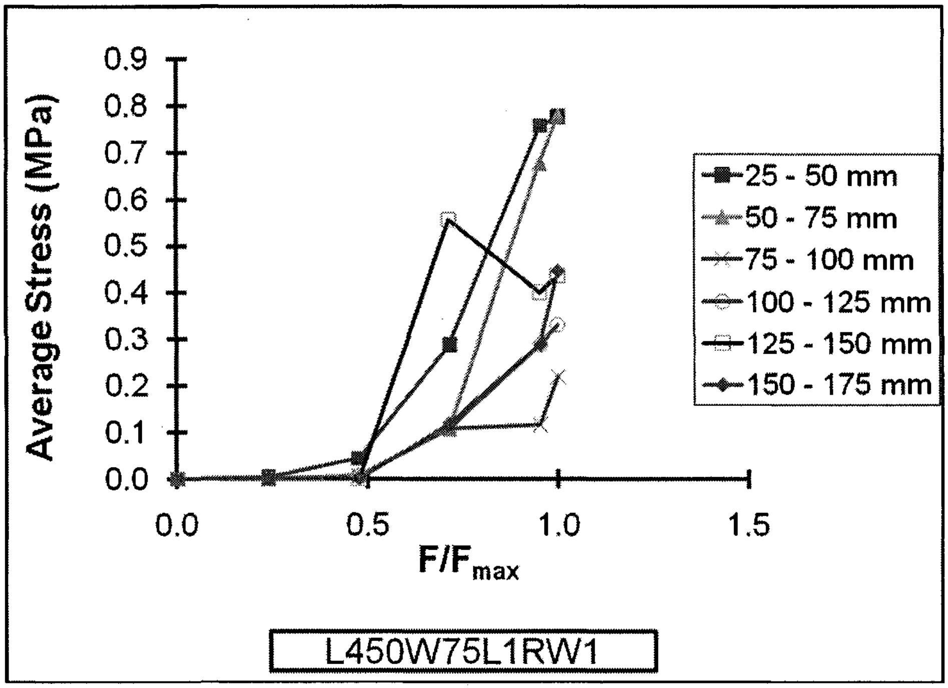

Average Stress (MPa)
0.9
0.8
0.7
0.6
0.5
0.4
0.3
0.2
0.1
0.0
0.0
0.5
1.0
1.5
F/F max
25 - 50 mm
50 - 75 mm
75 - 100 mm
100 - 125 mm
125 - 150 mm
150 - 175 mm
L450W75L1RW1

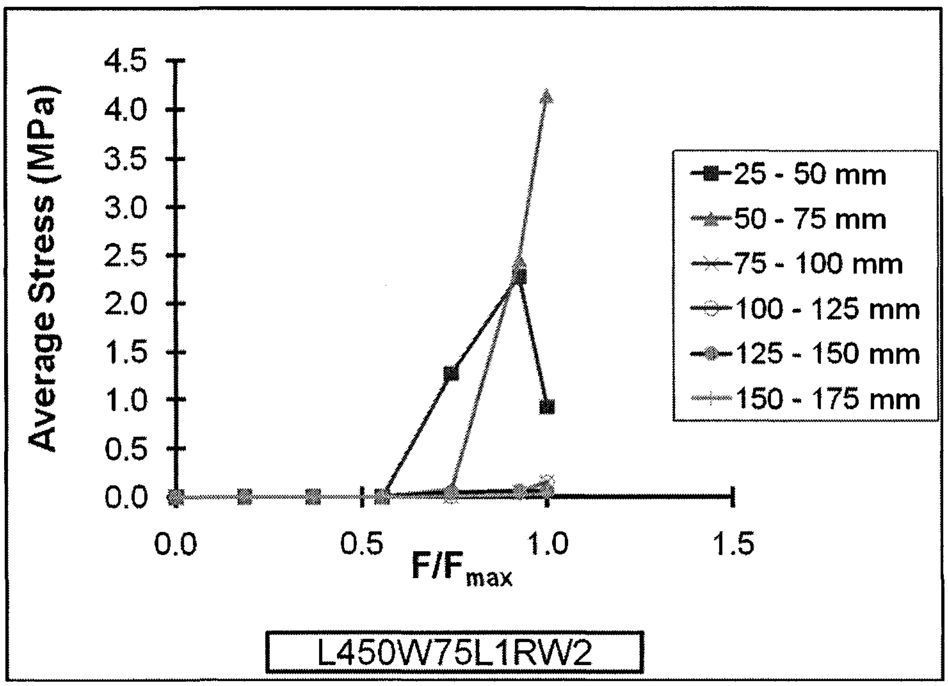

Average Stress (MPa)
4.5
4.0
3.5
3.0
2.5
2.0
1.5
1.0
0.5
0.0
0.0
0.5
1.0
1.5
F/F max
25 - 50 mm
50 - 75 mm
75 - 100 mm
100 - 125 mm
125 - 150 mm
150 - 175 mm
L450W75L1RW2

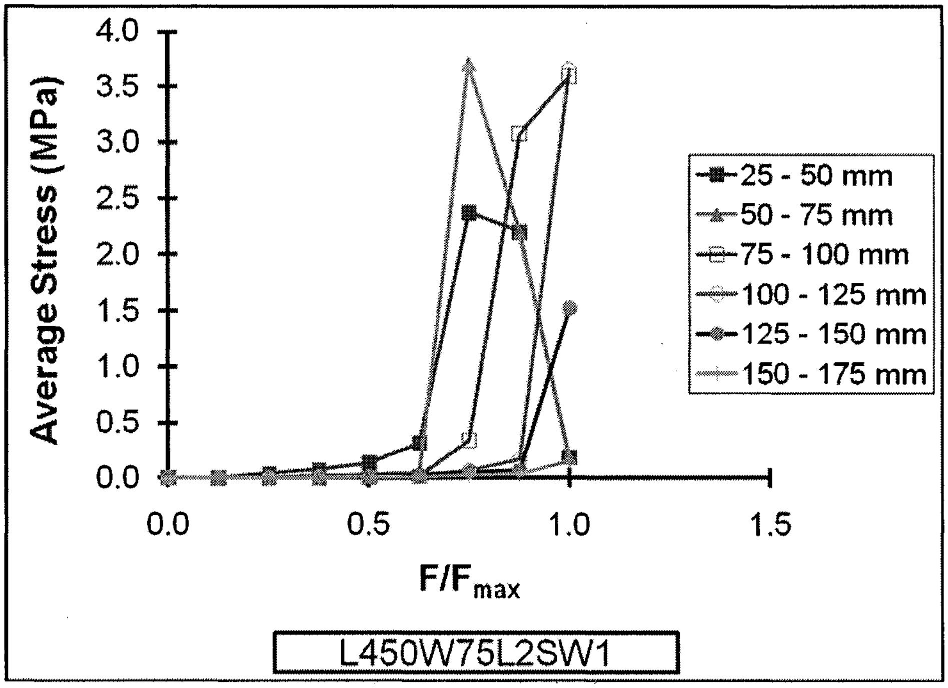
4.0
3.5
3.0
2.5
2.0
1.5
1.0
0.5
0.0
Average Stress (MPa)
0.0
0.5
1.0
1.5
F/F$_{max}$
25 - 50 mm
50 - 75 mm
75 - 100 mm
100 - 125 mm
125 - 150 mm
150 - 175 mm
L450W75L2SW1

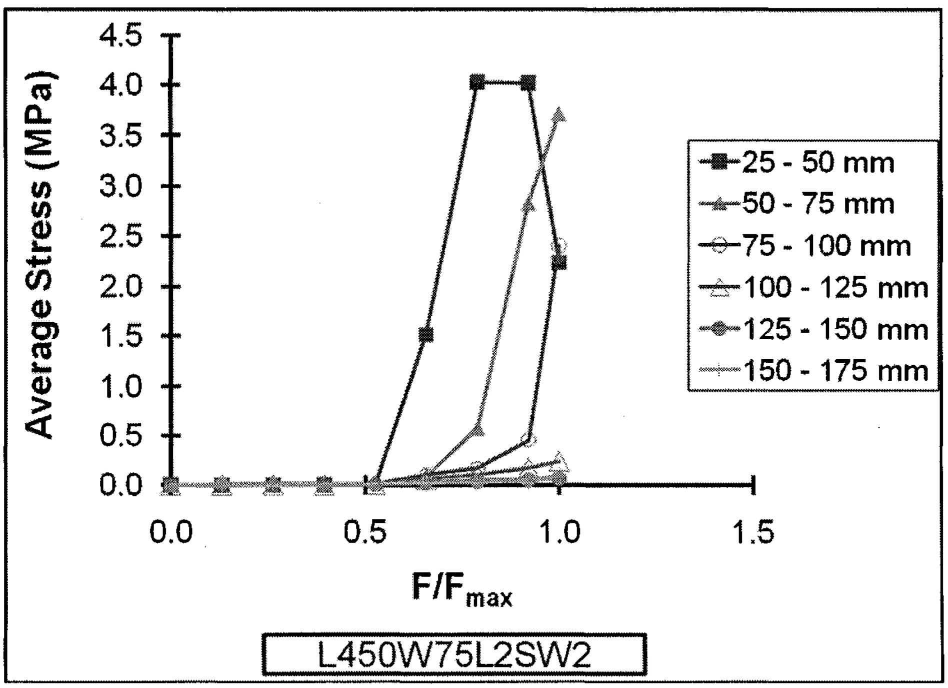
4.5
4.0
3.5
3.0
2.5
2.0
1.5
1.0
0.5
0.0
Average Stress (MPa)
0.0
0.5
1.0
1.5
F/F$_{max}$
25 - 50 mm
50 - 75 mm
75 - 100 mm
100 - 125 mm
125 - 150 mm
150 - 175 mm
L450W75L2SW2

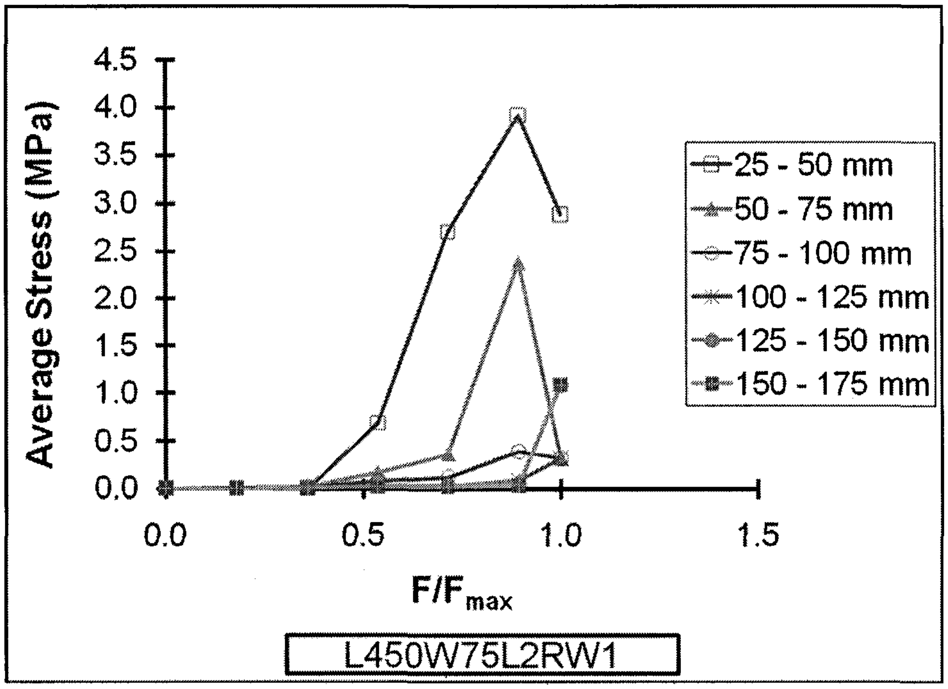
Average Stress (MPa)
4.5
4.0
3.5
3.0
2.5
2.0
1.5
1.0
0.5
0.0
0.0
0.5
1.0
1.5
F/F$_{max}$
25 - 50 mm
50 - 75 mm
75 - 100 mm
100 - 125 mm
125 - 150 mm
150 - 175 mm
L450W75L2RW1

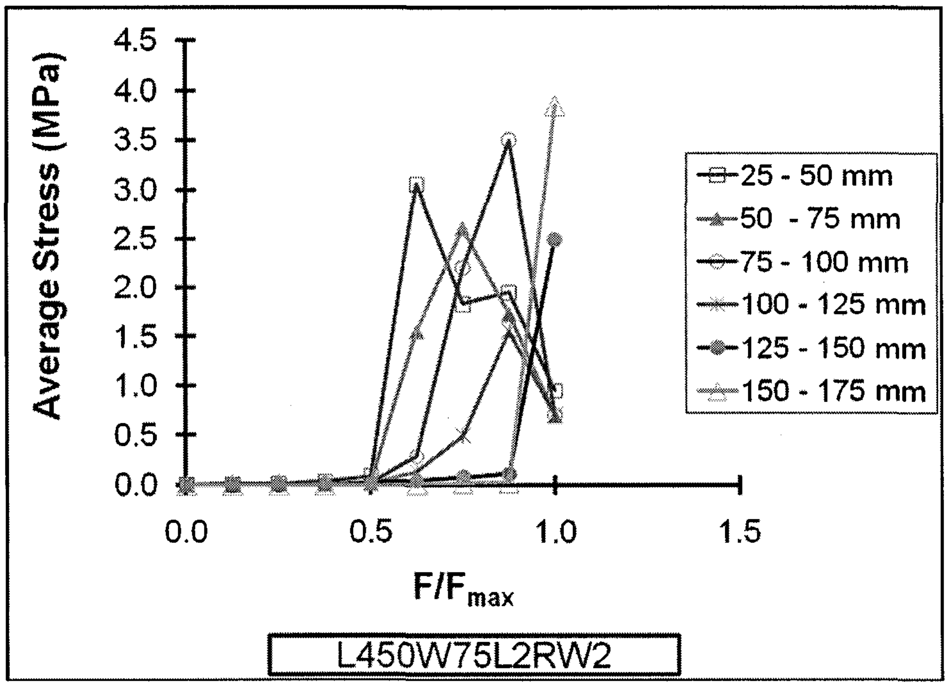
Average Stress (MPa)
4.5
4.0
3.5
3.0
2.5
2.0
1.5
1.0
0.5
0.0
0.0
0.5
1.0
1.5
F/F$_{max}$
25 - 50 mm
50 - 75 mm
75 - 100 mm
100 - 125 mm
125 - 150 mm
150 - 175 mm
L450W75L2RW2

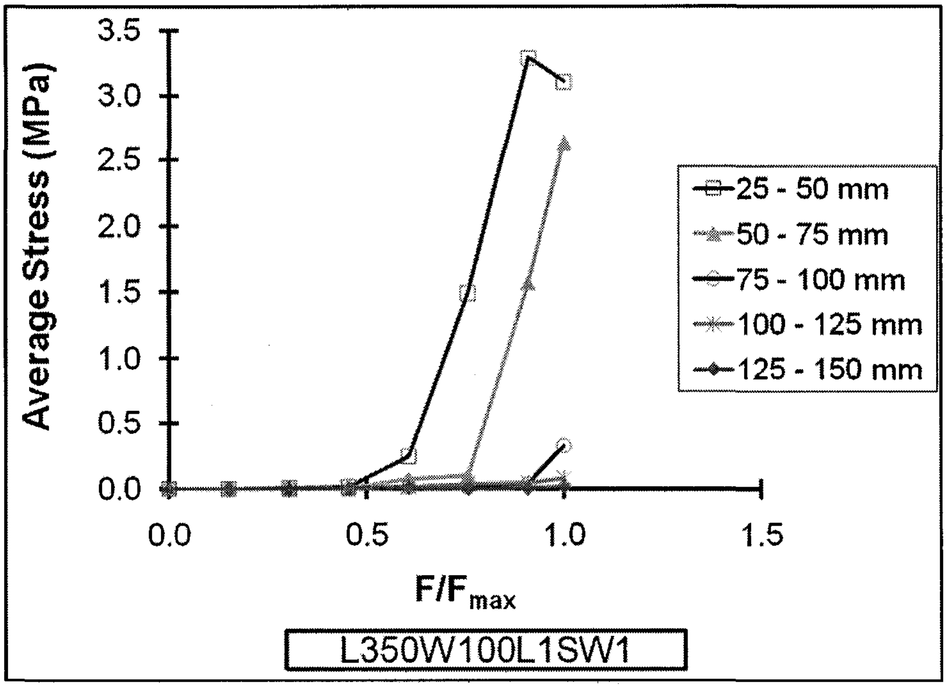

Average Stress (MPa)
3.5
3.0
2.5
2.0
1.5
1.0
0.5
0.0
0.0
0.5
1.0
1.5
F/Fmax
25 - 50 mm
50 - 75 mm
75 - 100 mm
100 - 125 mm
125 - 150 mm
L350W100L1SW1

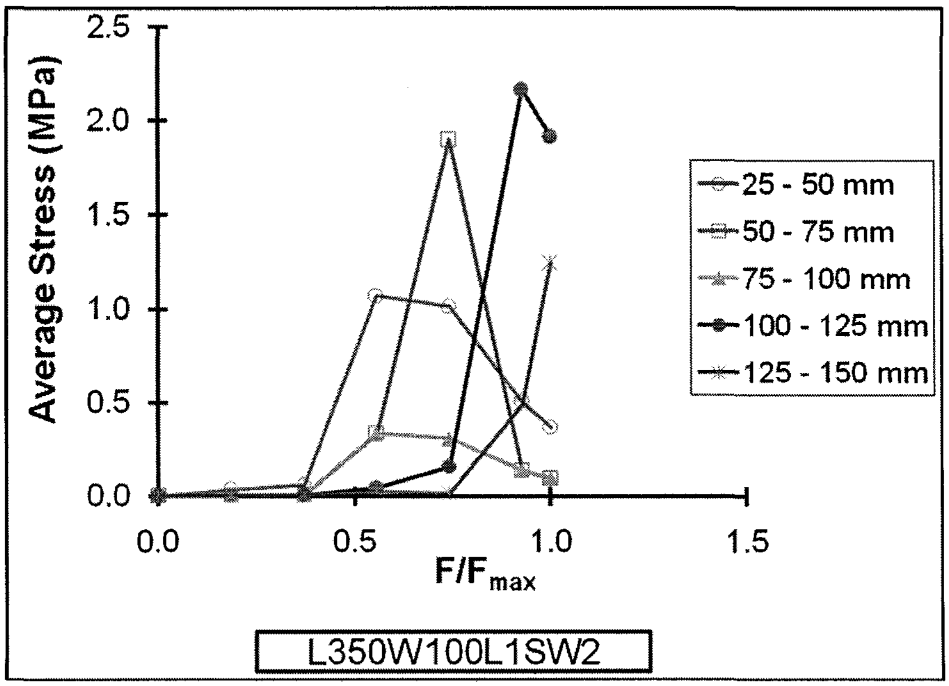

Average Stress (MPa)
2.5
2.0
1.5
1.0
0.5
0.0
0.0
0.5
1.0
1.5
F/Fmax
25 - 50 mm
50 - 75 mm
75 - 100 mm
100 - 125 mm
125 - 150 mm
L350W100L1SW2

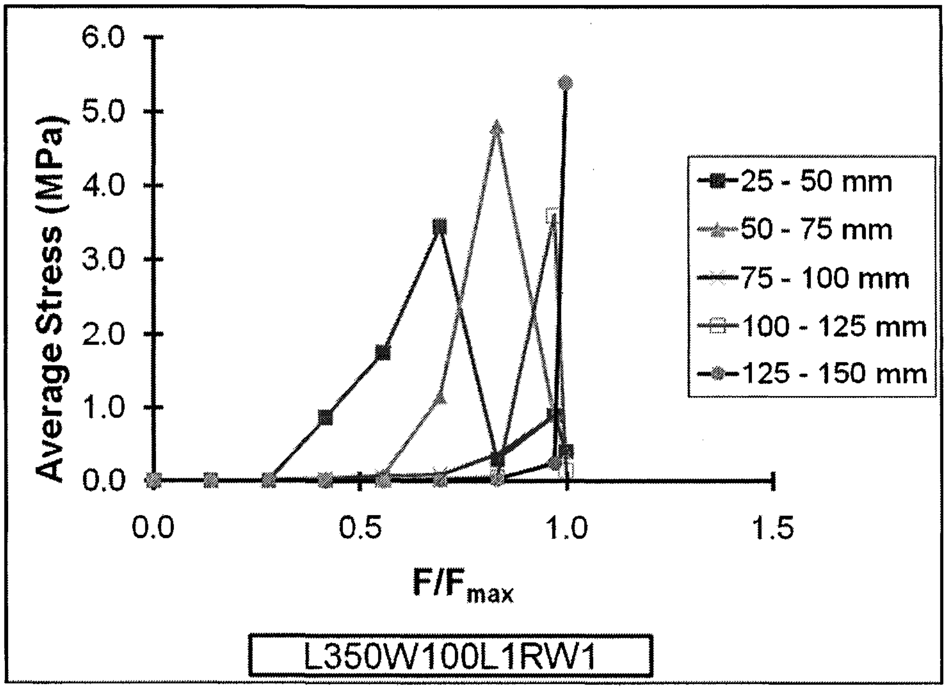
6.0
5.0
4.0
3.0
2.0
1.0
0.0
Average Stress (MPa)
0.0
0.5
1.0
1.5
F/F$_{max}$
25 - 50 mm
50 - 75 mm
75 - 100 mm
100 - 125 mm
125 - 150 mm
L350W100L1RW1

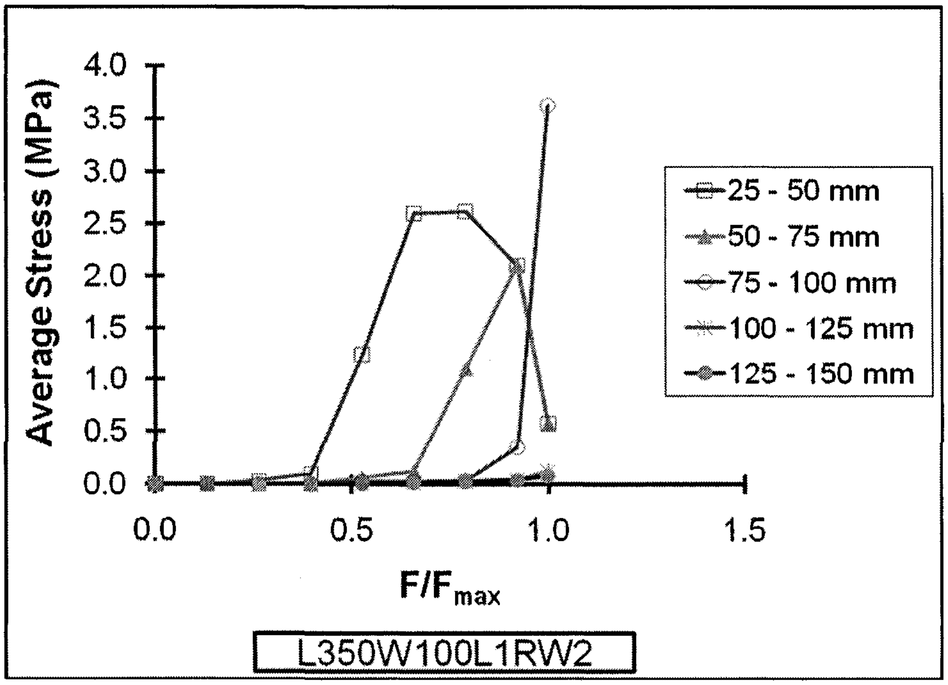
4.0
3.5
3.0
2.5
2.0
1.5
1.0
0.5
0.0
Average Stress (MPa)
0.0
0.5
1.0
1.5
F/F$_{max}$
25 - 50 mm
50 - 75 mm
75 - 100 mm
100 - 125 mm
125 - 150 mm
L350W100L1RW2

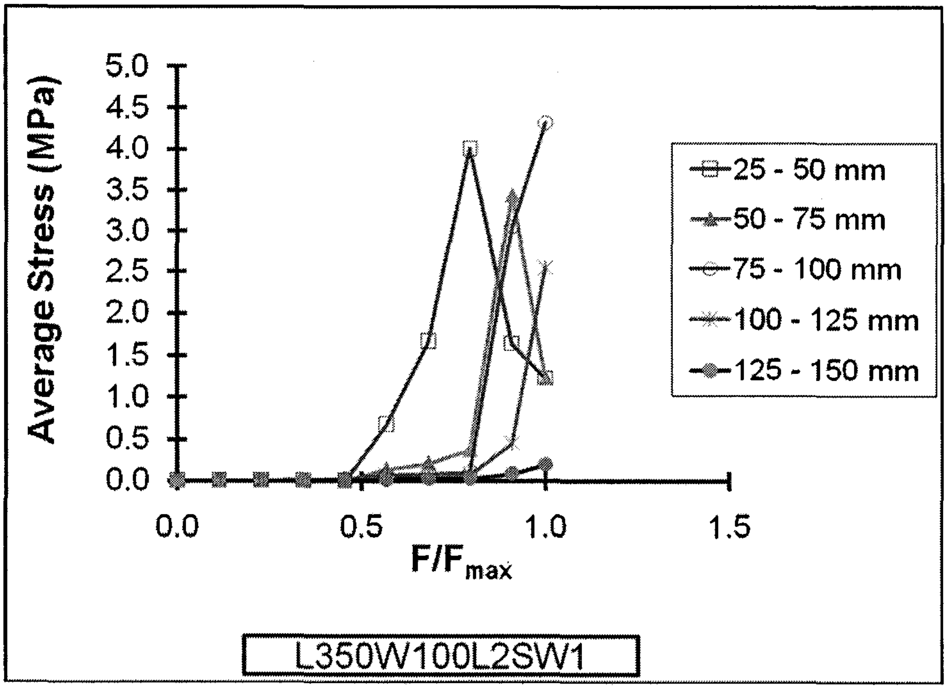
Average Stress (MPa)
5.0
4.5
4.0
3.5
3.0
2.5
2.0
1.5
1.0
0.5
0.0
0.0
0.5
1.0
1.5
F/F max
25 - 50 mm
50 - 75 mm
75 - 100 mm
100 - 125 mm
125 - 150 mm
L350W100L2SW1

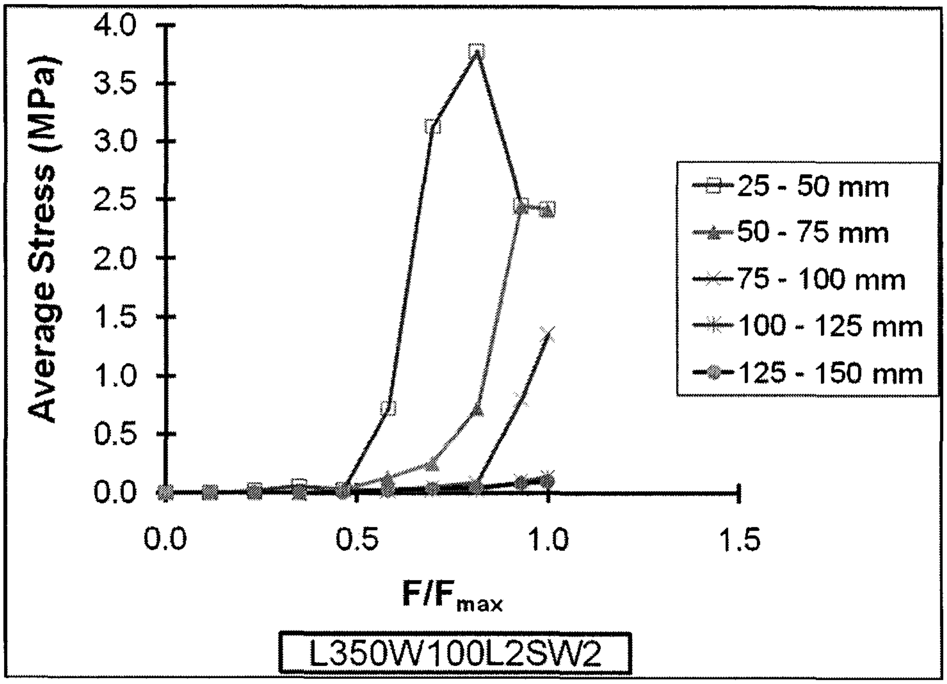
Average Stress (MPa)
4.0
3.5
3.0
2.5
2.0
1.5
1.0
0.5
0.0
0.0
0.5
1.0
1.5
F/F max
25 - 50 mm
50 - 75 mm
75 - 100 mm
100 - 125 mm
125 - 150 mm
L350W100L2SW2

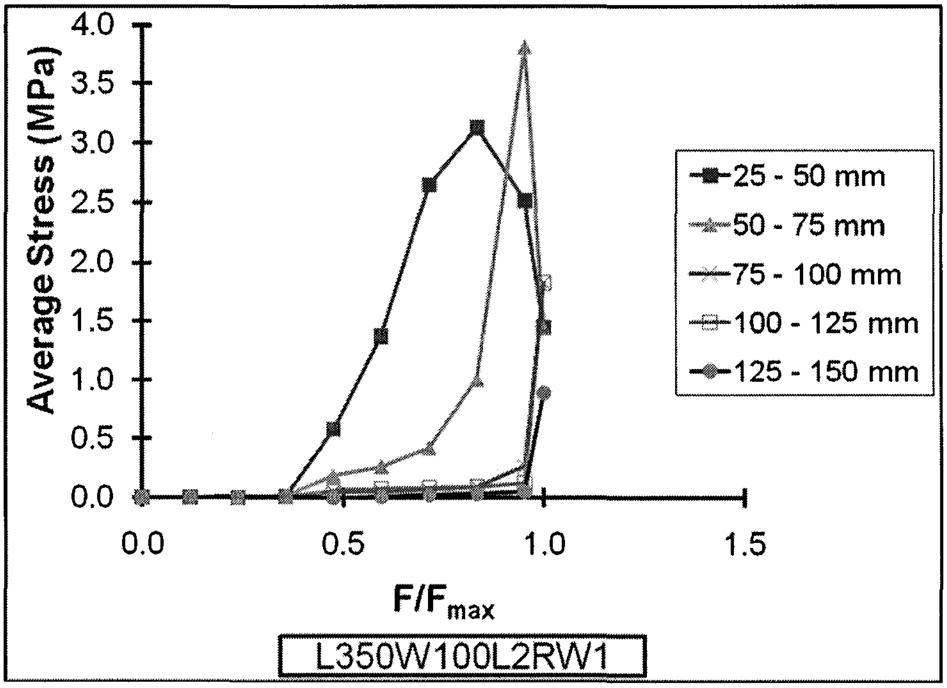
Average Stress (MPa)
F/F_max
25 - 50 mm
50 - 75 mm
75 - 100 mm
100 - 125 mm
125 - 150 mm
L350W100L2RW1

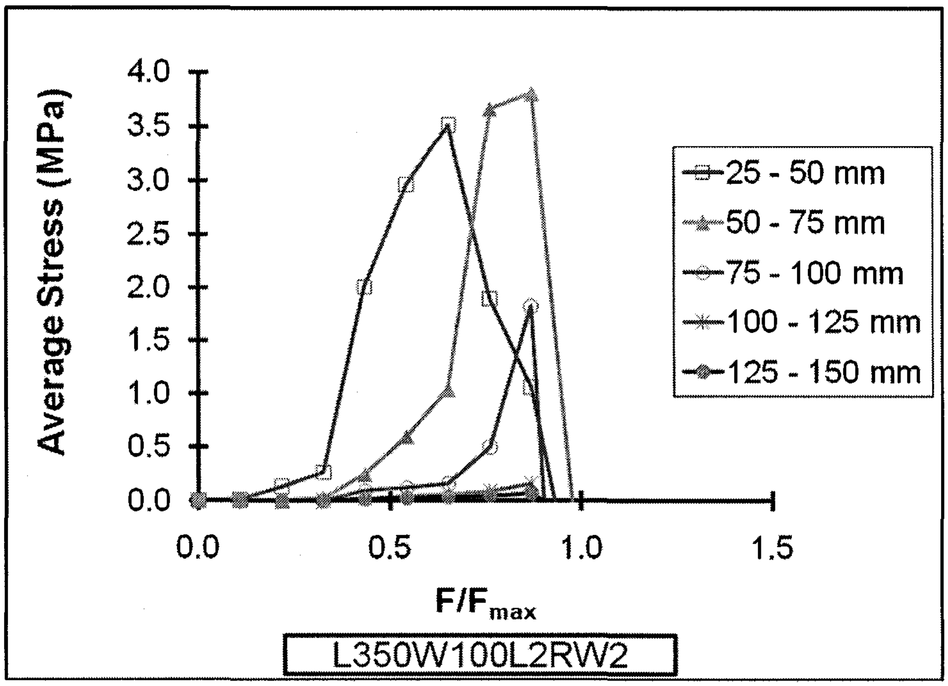
Average Stress (MPa)
F/F_max
25 - 50 mm
50 - 75 mm
75 - 100 mm
100 - 125 mm
125 - 150 mm
L350W100L2RW2

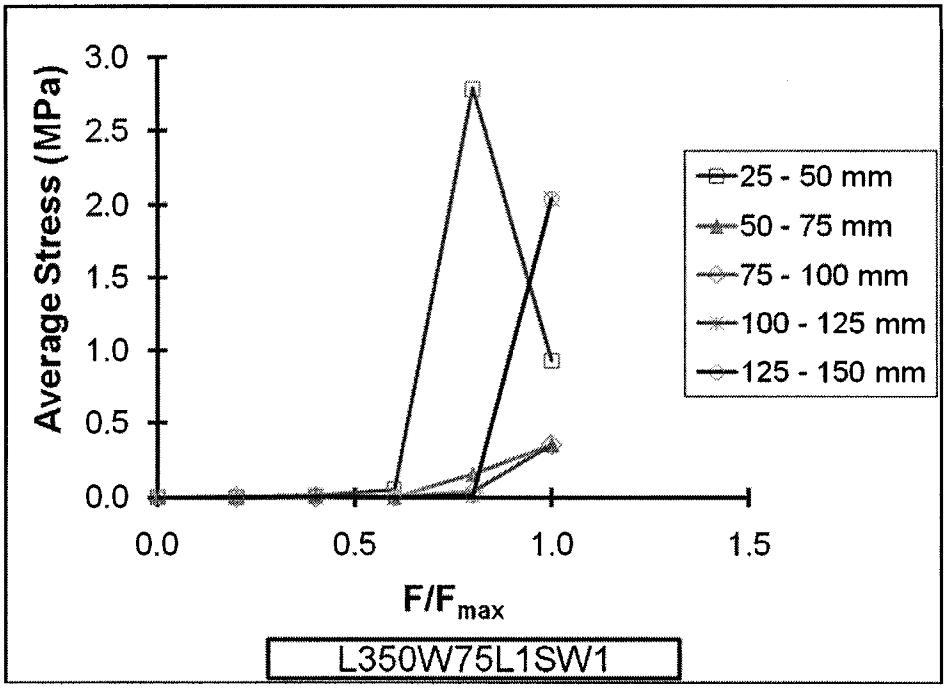
Average Stress (MPa)
3.0
2.5
2.0
1.5
1.0
0.5
0.0
0.0
0.5
1.0
1.5
F/Fmax
25 - 50 mm
50 - 75 mm
75 - 100 mm
100 - 125 mm
125 - 150 mm
L350W75L1SW1

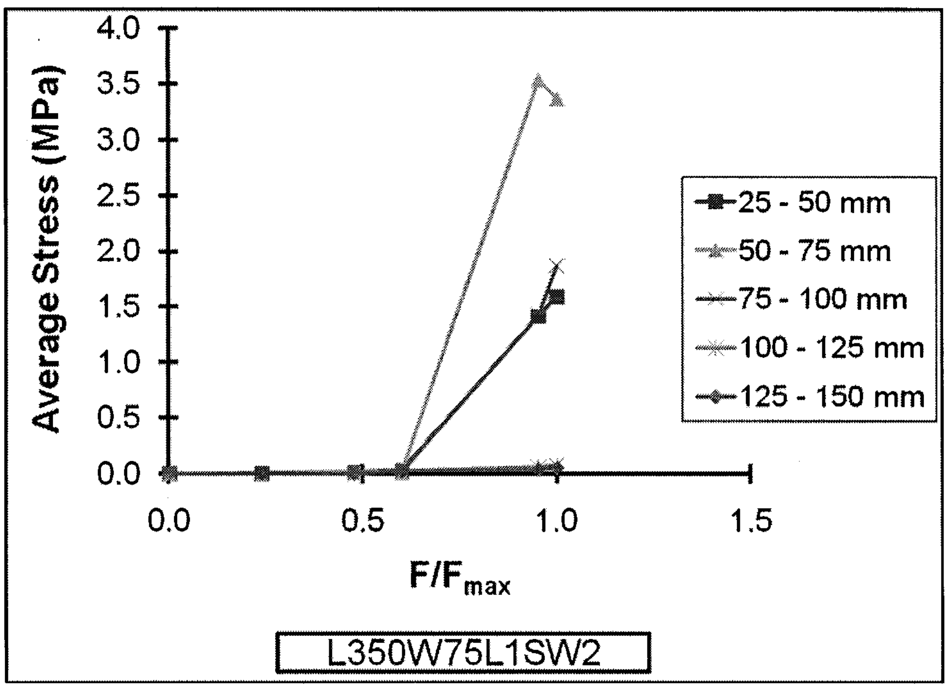
Average Stress (MPa)
4.0
3.5
3.0
2.5
2.0
1.5
1.0
0.5
0.0
0.0
0.5
1.0
1.5
F/Fmax
25 - 50 mm
50 - 75 mm
75 - 100 mm
100 - 125 mm
125 - 150 mm
L350W75L1SW2

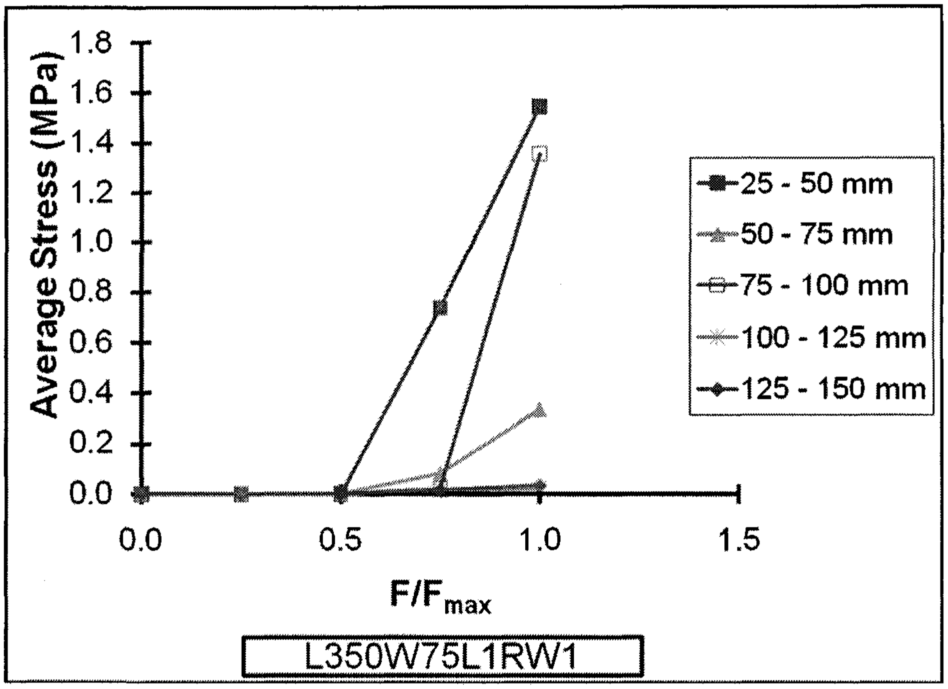

Average Stress (MPa)
1.8
1.6
1.4
1.2
1.0
0.8
0.6
0.4
0.2
0.0
0.0
0.5
1.0
1.5
F/F$_{max}$
25 - 50 mm
50 - 75 mm
75 - 100 mm
100 - 125 mm
125 - 150 mm
L350W75L1RW1

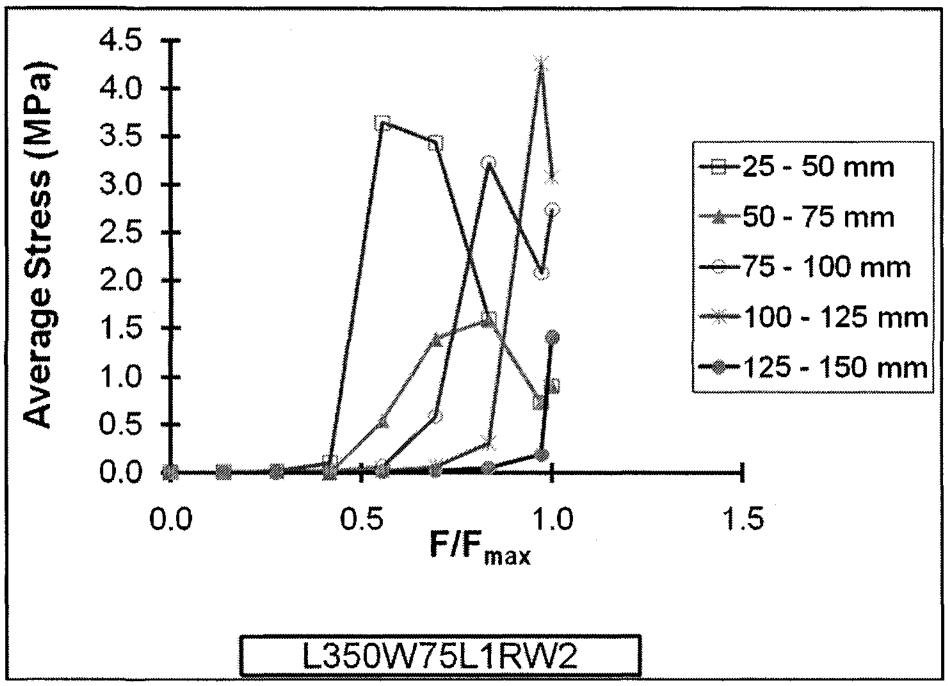

Average Stress (MPa)
4.5
4.0
3.5
3.0
2.5
2.0
1.5
1.0
0.5
0.0
0.0
0.5
1.0
1.5
F/F$_{max}$
25 - 50 mm
50 - 75 mm
75 - 100 mm
100 - 125 mm
125 - 150 mm
L350W75L1RW2

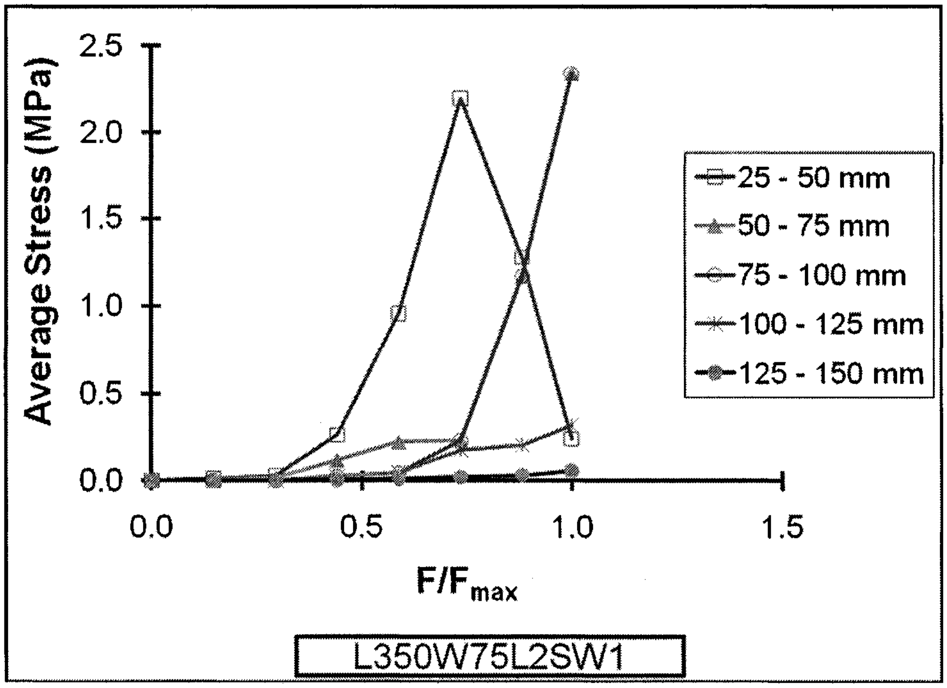
Average Stress (MPa)
2.5
2.0
1.5
1.0
0.5
0.0
0.0
0.5
1.0
1.5
F/F$_{max}$
25 - 50 mm
50 - 75 mm
75 - 100 mm
100 - 125 mm
125 - 150 mm
L350W75L2SW1

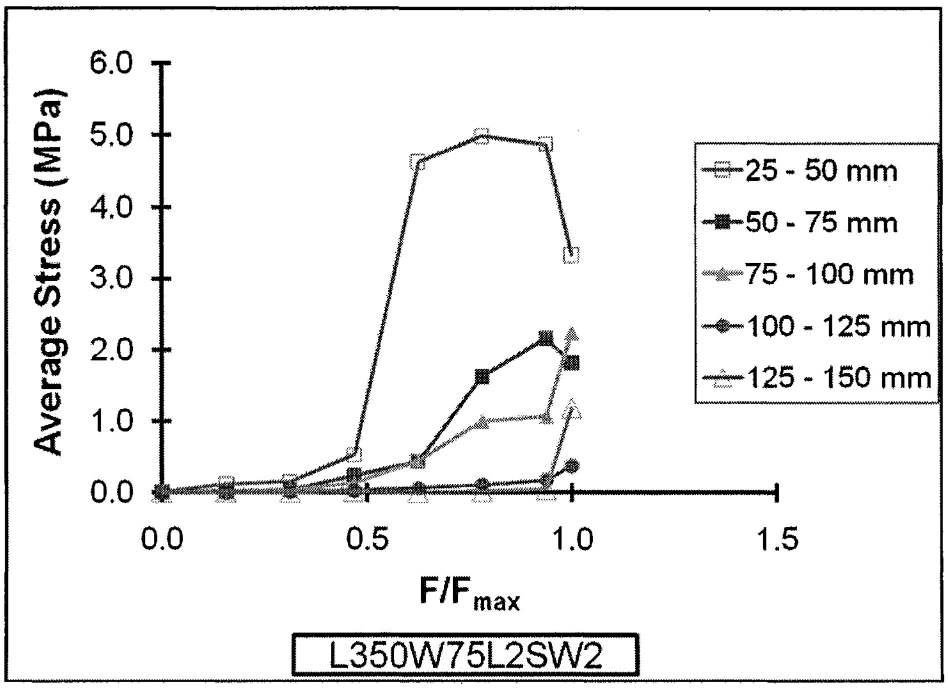
Average Stress (MPa)
6.0
5.0
4.0
3.0
2.0
1.0
0.0
0.0
0.5
1.0
1.5
F/F$_{max}$
25 - 50 mm
50 - 75 mm
75 - 100 mm
100 - 125 mm
125 - 150 mm
L350W75L2SW2

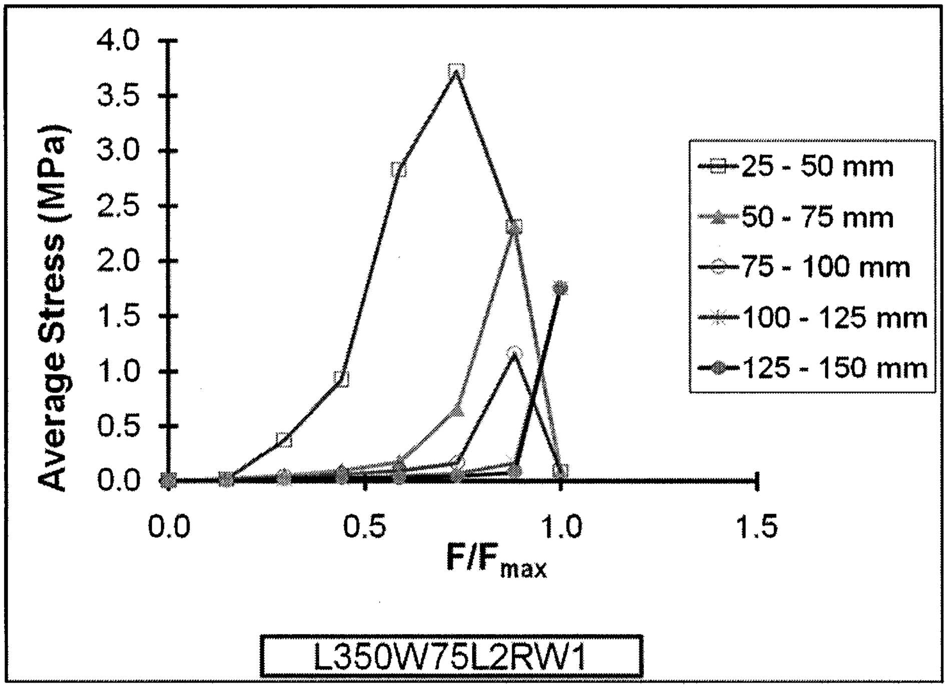

4.0
3.5
3.0
2.5
2.0
1.5
1.0
0.5
0.0
Average Stress (MPa)
0.0
0.5
1.0
1.5
F/F max
25 - 50 mm
50 - 75 mm
75 - 100 mm
100 - 125 mm
125 - 150 mm
L350W75L2RW1

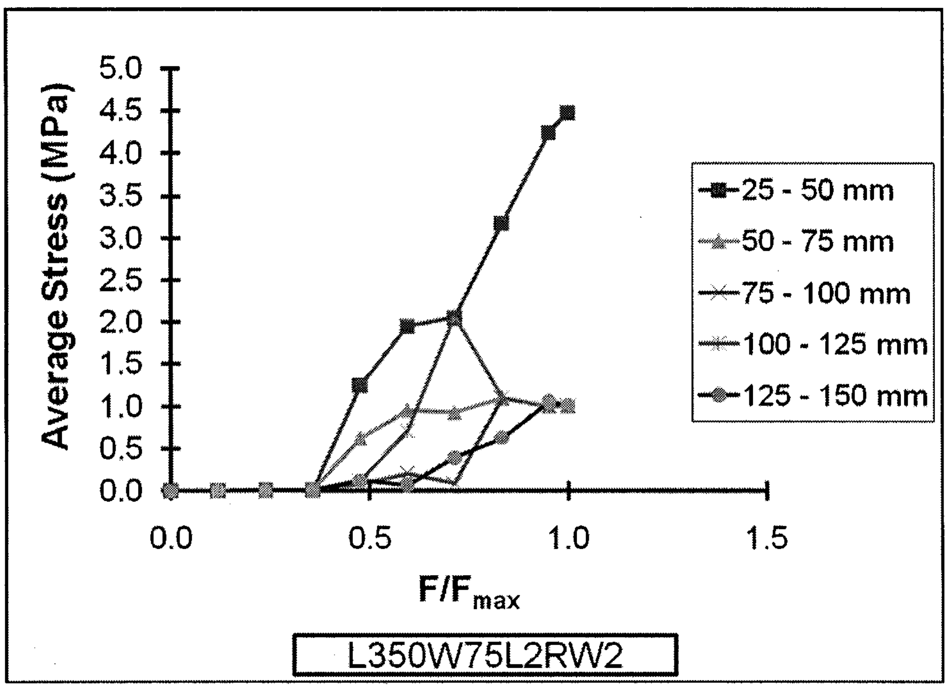

5.0
4.5
4.0
3.5
3.0
2.5
2.0
1.5
1.0
0.5
0.0
Average Stress (MPa)
0.0
0.5
1.0
1.5
F/F max
25 - 50 mm
50 - 75 mm
75 - 100 mm
100 - 125 mm
125 - 150 mm
L350W75L2RW2

APPENDIX F
AVERAGE STRESS VERSUS GAUGE DISTANCE

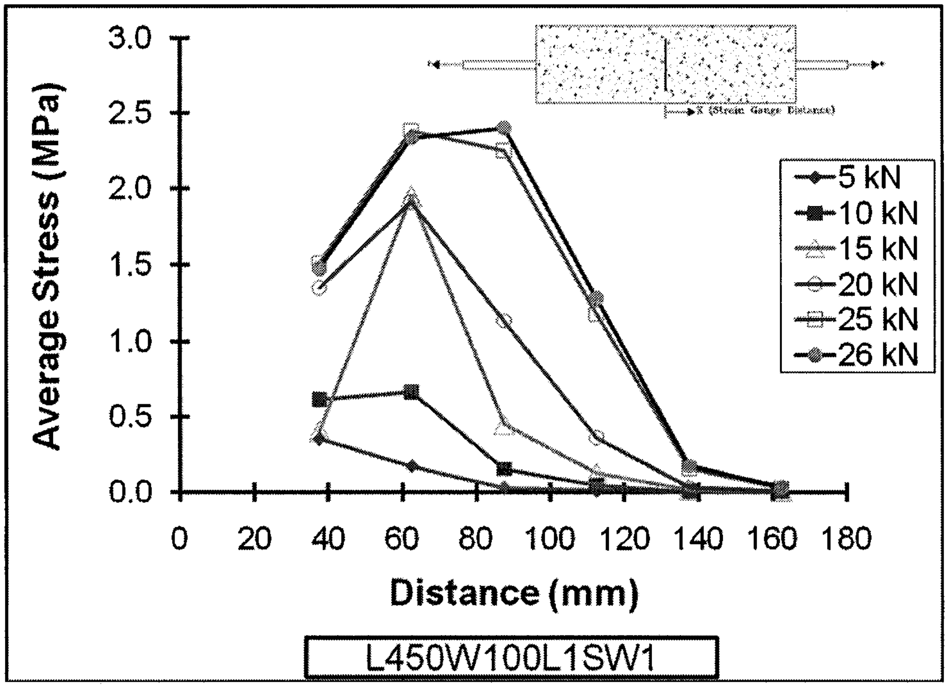

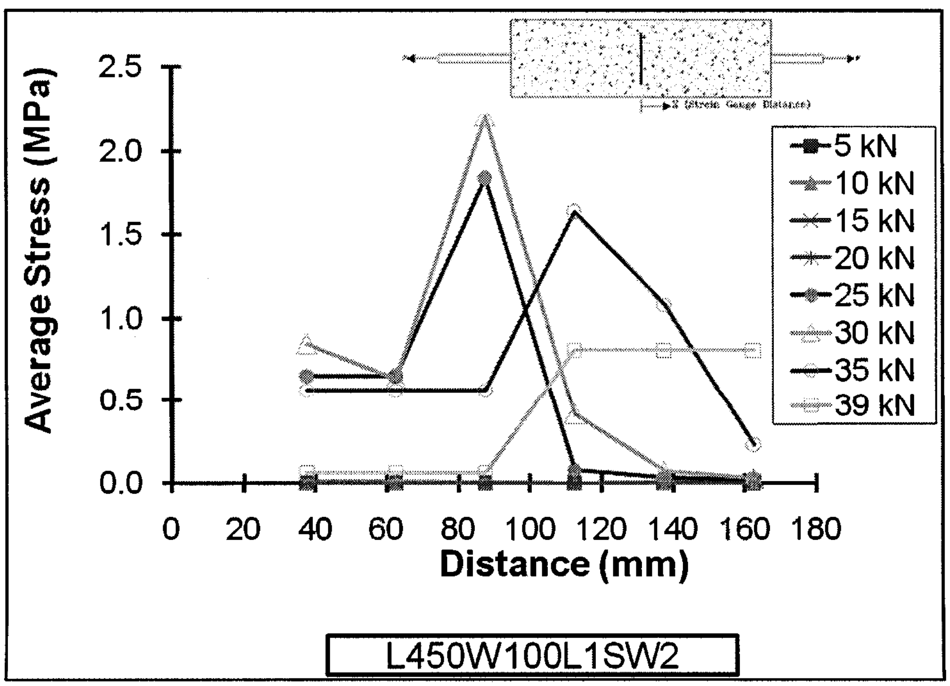

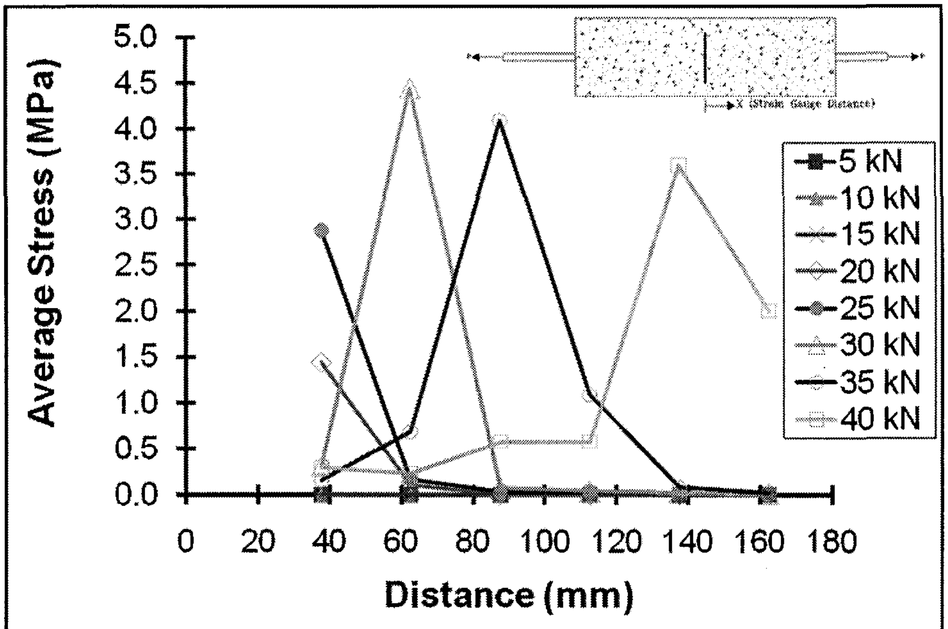

L450W100L1RW1

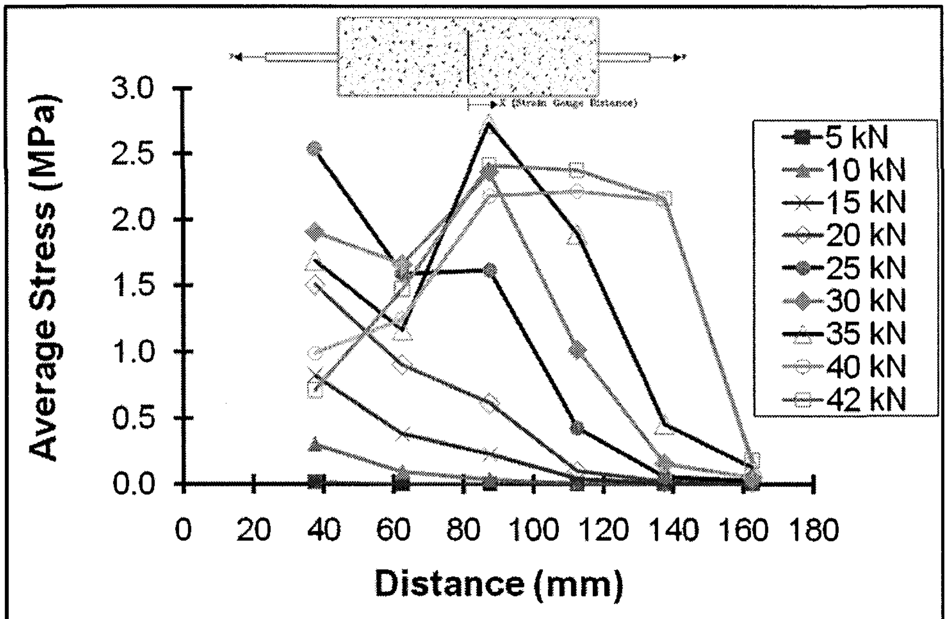

L450W100L1RW2

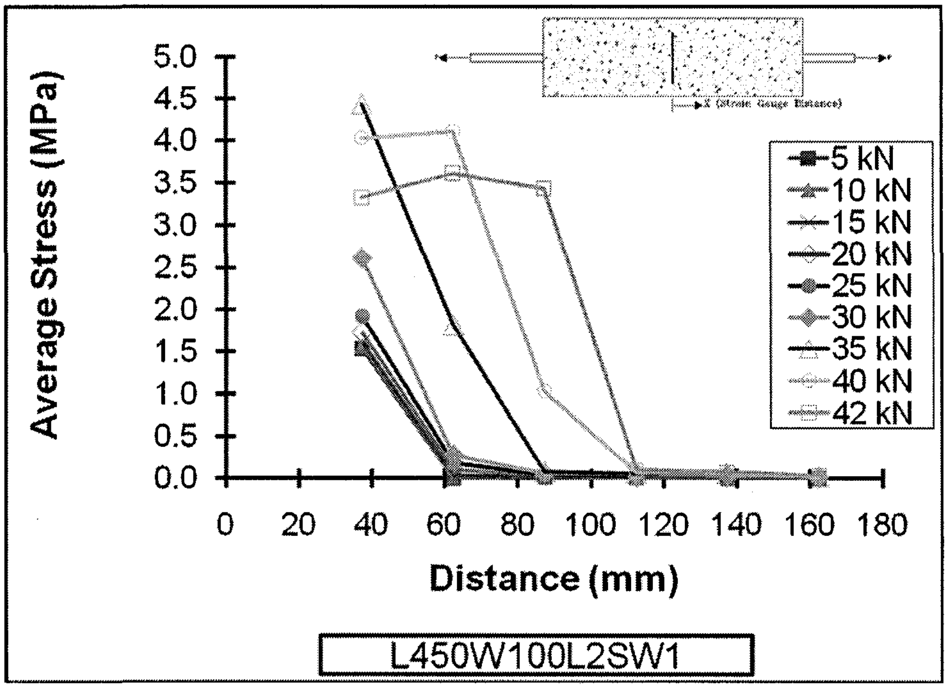

Average Stress (MPa)
5.0
4.5
4.0
3.5
3.0
2.5
2.0
1.5
1.0
0.5
0.0
0
20
40
60
80
100
120
140
160
180
Distance (mm)
5 kN
10 kN
15 kN
20 kN
25 kN
30 kN
35 kN
40 kN
42 kN
L450W100L2SW1

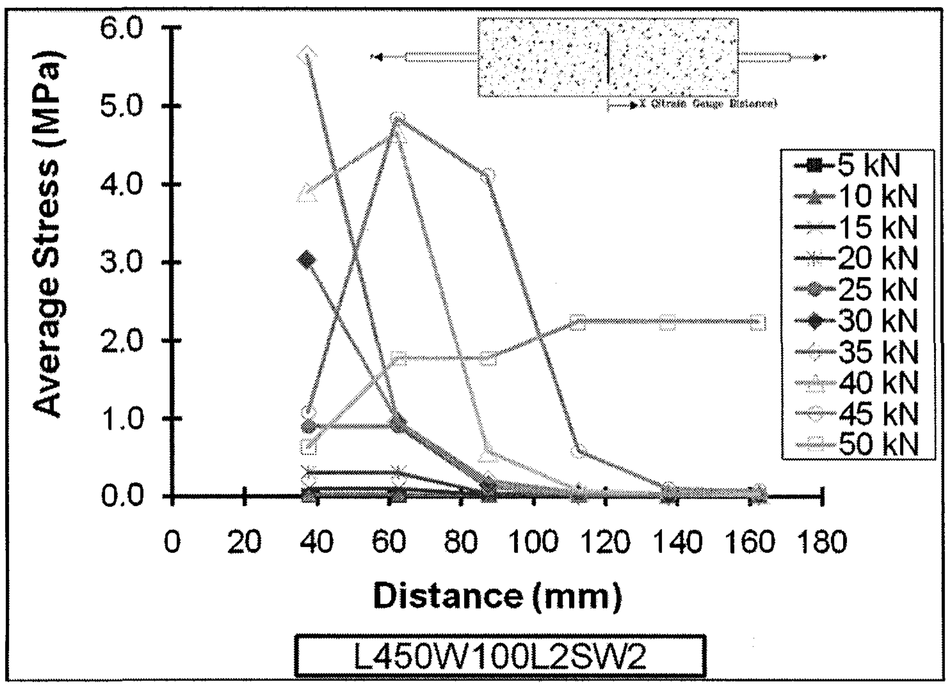

Average Stress (MPa)
6.0
5.0
4.0
3.0
2.0
1.0
0.0
0
20
40
60
80
100
120
140
160
180
Distance (mm)
5 kN
10 kN
15 kN
20 kN
25 kN
30 kN
35 kN
40 kN
45 kN
50 kN
L450W100L2SW2

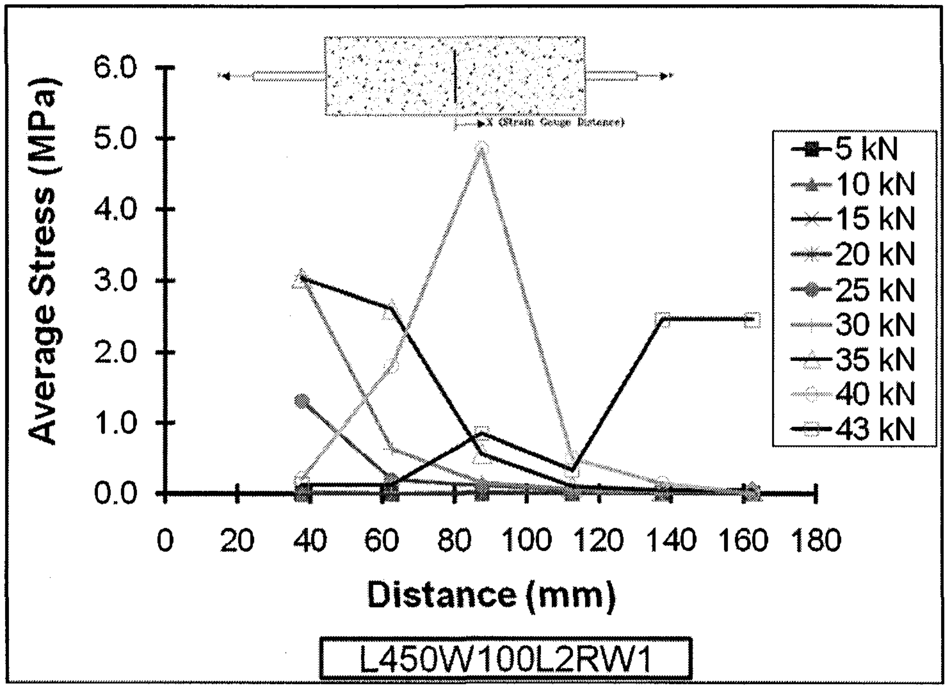

X (Strain Gauge Distance)
Average Stress (MPa)
6.0
5.0
4.0
3.0
2.0
1.0
0.0
0
20
40
60
80
100
120
140
160
180
Distance (mm)
5 kN
10 kN
15 kN
20 kN
25 kN
30 kN
35 kN
40 kN
43 kN
L450W100L2RW1

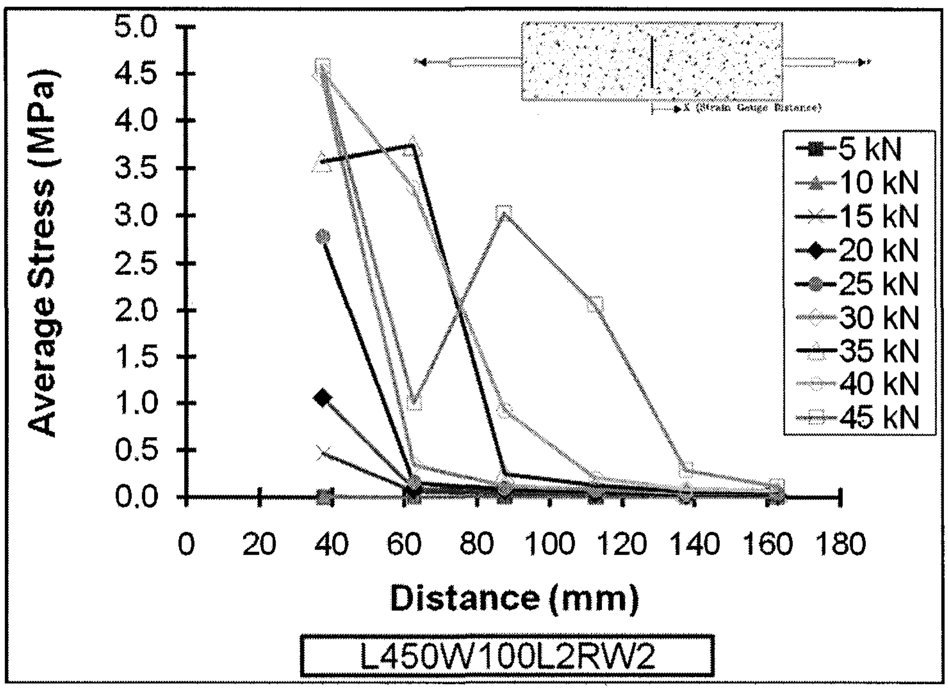

X (Strain Gauge Distance)
Average Stress (MPa)
5.0
4.5
4.0
3.5
3.0
2.5
2.0
1.5
1.0
0.5
0.0
0
20
40
60
80
100
120
140
160
180
Distance (mm)
5 kN
10 kN
15 kN
20 kN
25 kN
30 kN
35 kN
40 kN
45 kN
L450W100L2RW2

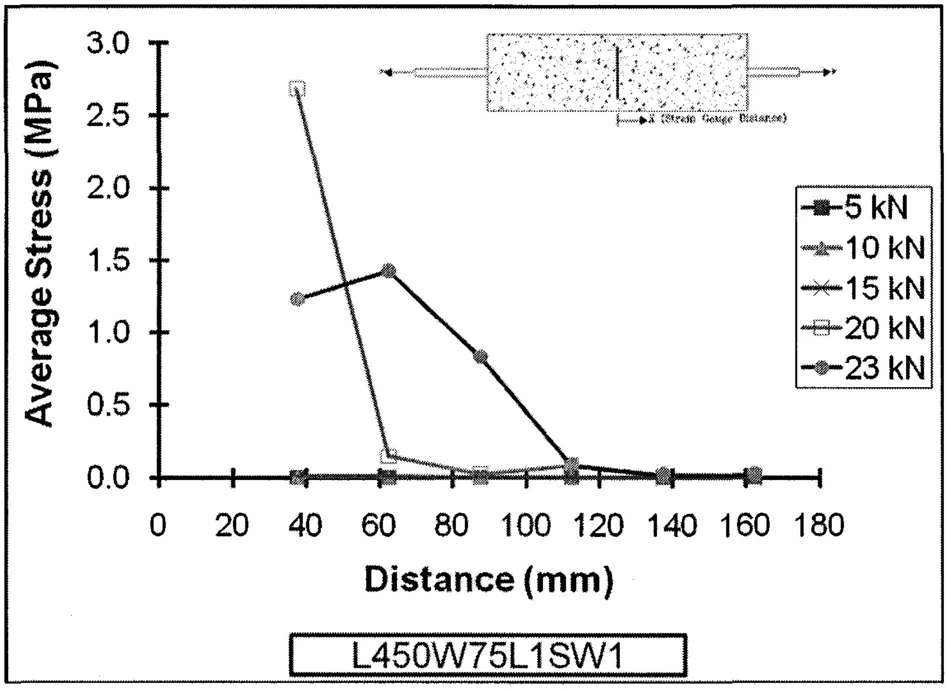
Average Stress (MPa)
3.0
2.5
2.0
1.5
1.0
0.5
0.0
0
20
40
60
80
100
120
140
160
180
Distance (mm)
5 kN
10 kN
15 kN
20 kN
23 kN
L450W75L1SW1

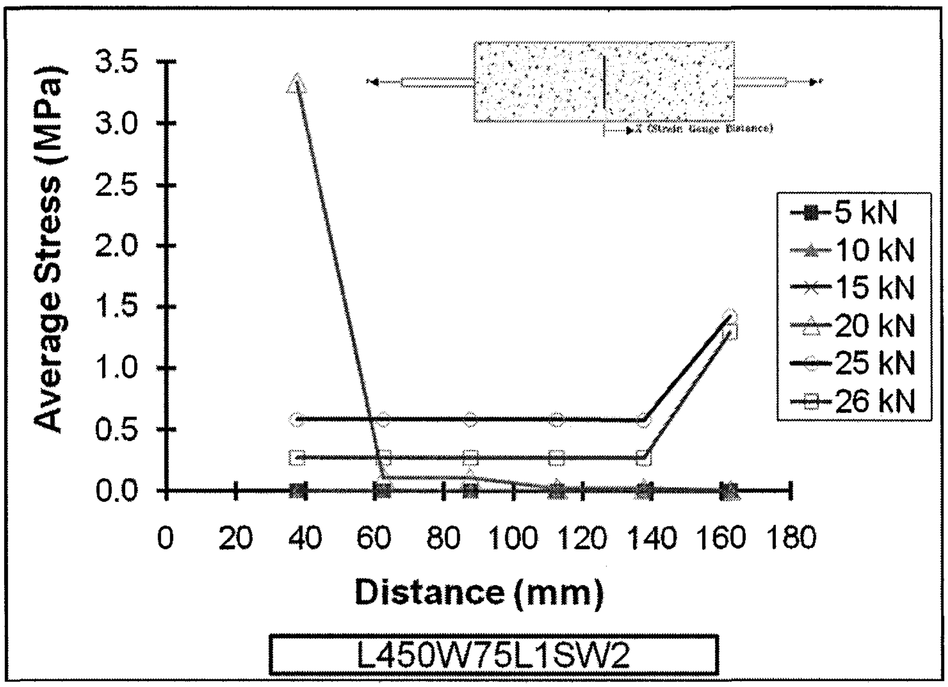
Average Stress (MPa)
3.5
3.0
2.5
2.0
1.5
1.0
0.5
0.0
0
20
40
60
80
100
120
140
160
180
Distance (mm)
5 kN
10 kN
15 kN
20 kN
25 kN
26 kN
L450W75L1SW2

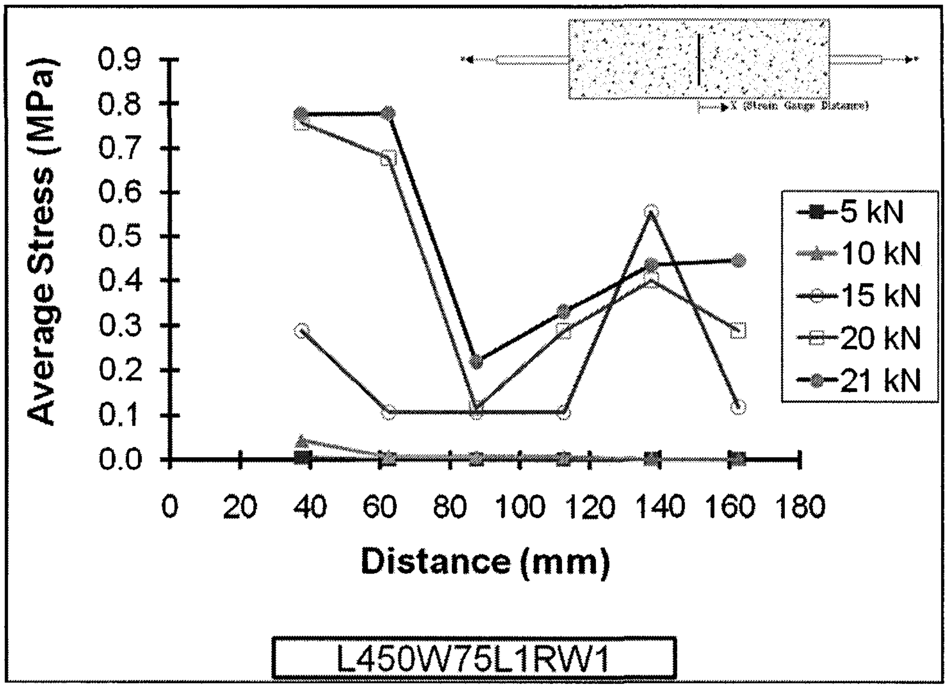

Average Stress (MPa)
0.9
0.8
0.7
0.6
0.5
0.4
0.3
0.2
0.1
0.0
0
20
40
60
80
100
120
140
160
180
Distance (mm)
5 kN
10 kN
15 kN
20 kN
21 kN
X (Strain Gauge Distance)
L450W75L1RW1

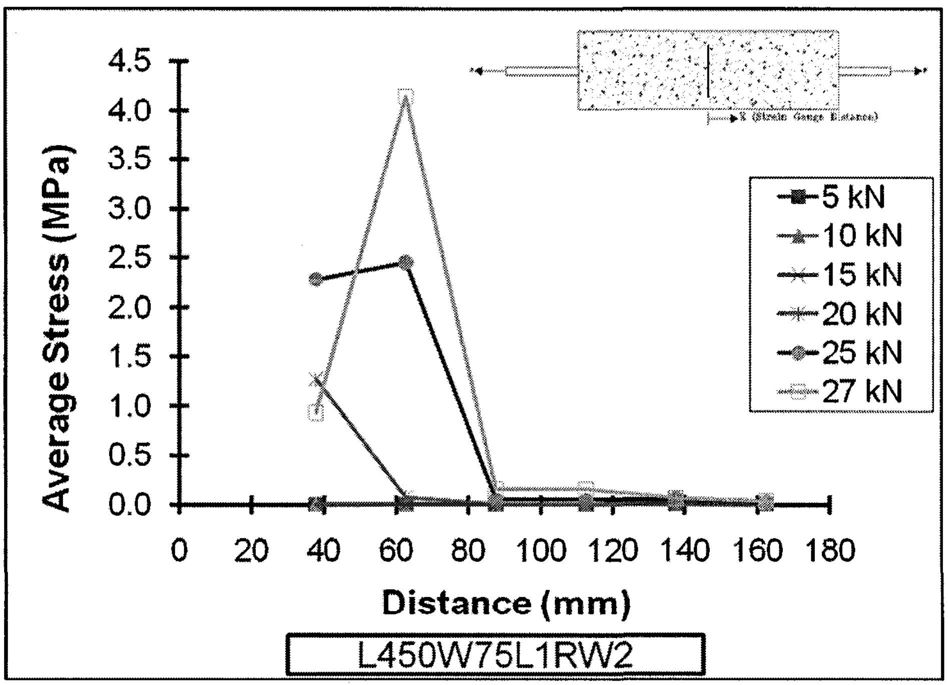

Average Stress (MPa)
4.5
4.0
3.5
3.0
2.5
2.0
1.5
1.0
0.5
0.0
0
20
40
60
80
100
120
140
160
180
Distance (mm)
5 kN
10 kN
15 kN
20 kN
25 kN
27 kN
X (Strain Gauge Distance)
L450W75L1RW2

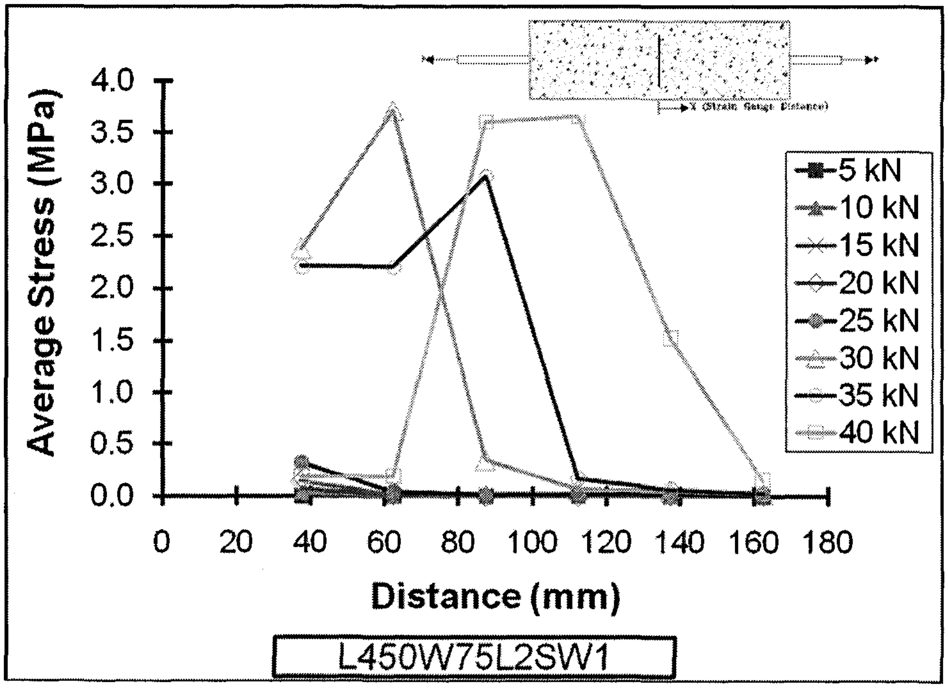
Average Stress (MPa)
4.0
3.5
3.0
2.5
2.0
1.5
1.0
0.5
0.0
0
20
40
60
80
100
120
140
160
180
Distance (mm)
5 kN
10 kN
15 kN
20 kN
25 kN
30 kN
35 kN
40 kN
X (Strain Gauge Distance)
L450W75L2SW1

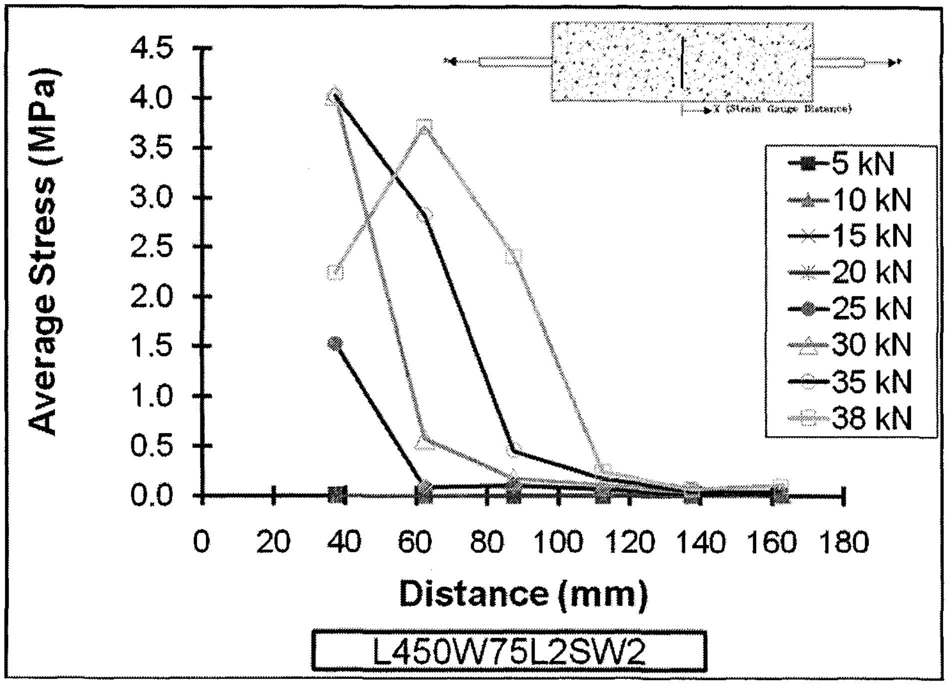
Average Stress (MPa)
4.5
4.0
3.5
3.0
2.5
2.0
1.5
1.0
0.5
0.0
0
20
40
60
80
100
120
140
160
180
Distance (mm)
5 kN
10 kN
15 kN
20 kN
25 kN
30 kN
35 kN
38 kN
X (Strain Gauge Distance)
L450W75L2SW2

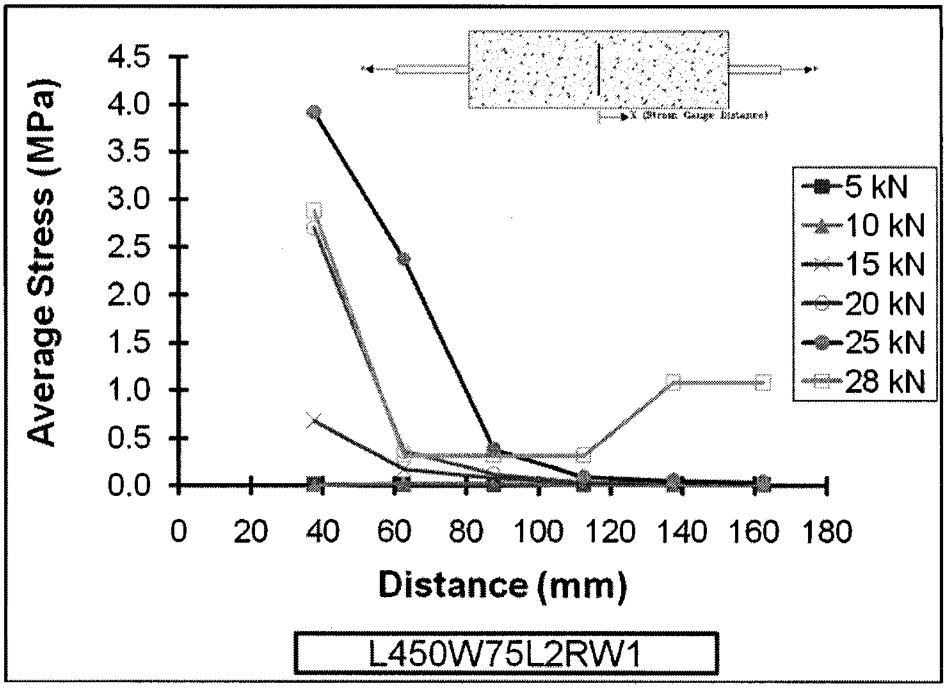
Average Stress (MPa)
4.5
4.0
3.5
3.0
2.5
2.0
1.5
1.0
0.5
0.0
0
20
40
60
80
100
120
140
160
180
Distance (mm)
5 kN
10 kN
15 kN
20 kN
25 kN
28 kN
L450W75L2RW1

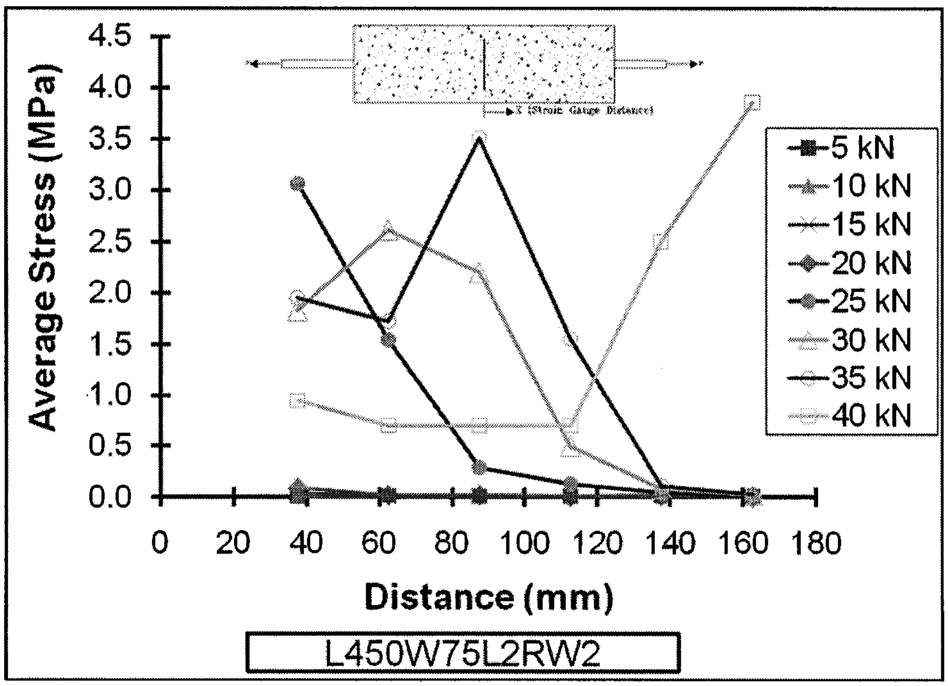
Average Stress (MPa)
4.5
4.0
3.5
3.0
2.5
2.0
1.5
1.0
0.5
0.0
0
20
40
60
80
100
120
140
160
180
Distance (mm)
5 kN
10 kN
15 kN
20 kN
25 kN
30 kN
35 kN
40 kN
L450W75L2RW2

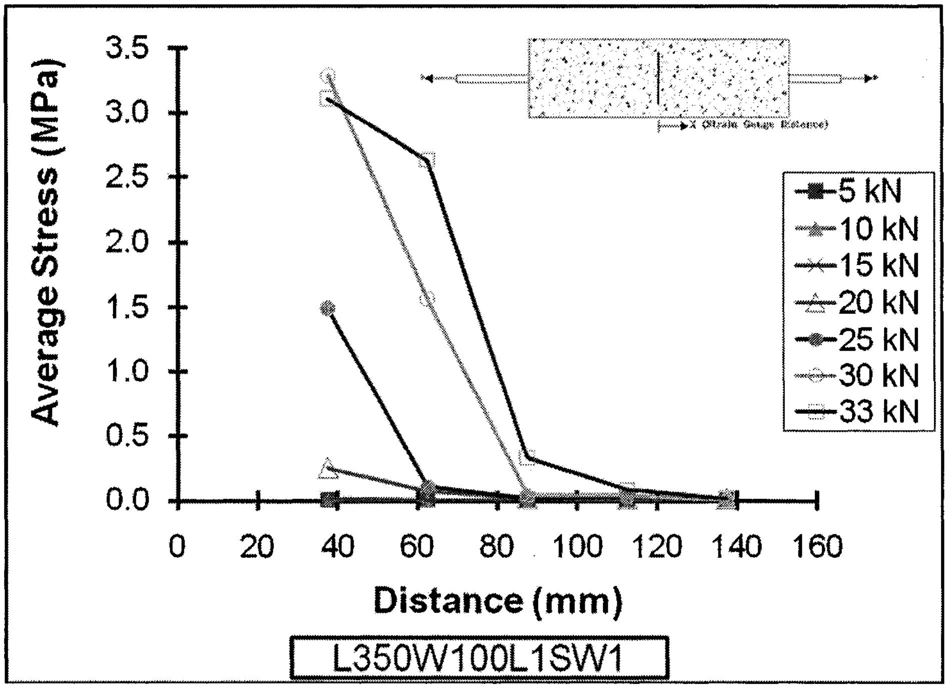

Average Stress (MPa)
3.5
3.0
2.5
2.0
1.5
1.0
0.5
0.0
0
20
40
60
80
100
120
140
160
Distance (mm)
5 kN
10 kN
15 kN
20 kN
25 kN
30 kN
33 kN
L350W100L1SW1

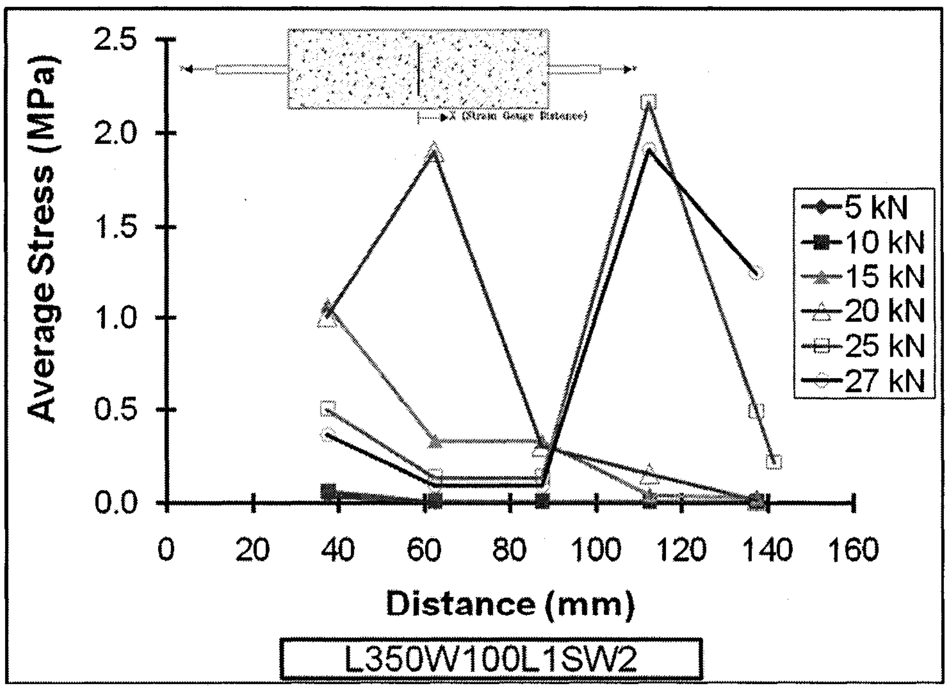

Average Stress (MPa)
2.5
2.0
1.5
1.0
0.5
0.0
0
20
40
60
80
100
120
140
160
Distance (mm)
5 kN
10 kN
15 kN
20 kN
25 kN
27 kN
L350W100L1SW2

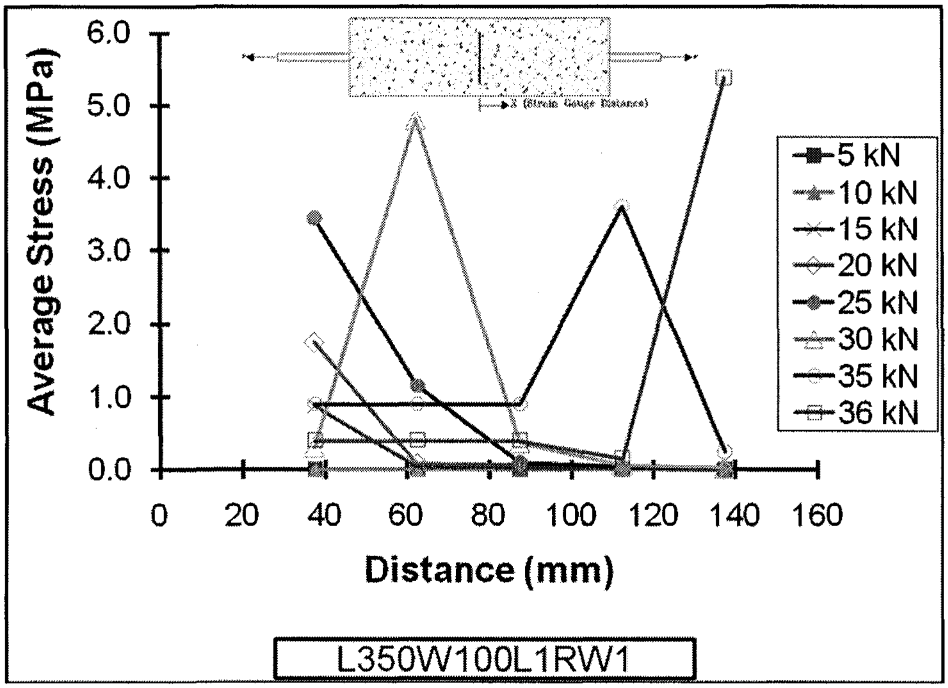
Average Stress (MPa)
6.0
5.0
4.0
3.0
2.0
1.0
0.0
0
20
40
60
80
100
120
140
160
Distance (mm)
5 kN
10 kN
15 kN
20 kN
25 kN
30 kN
35 kN
36 kN
L350W100L1RW1

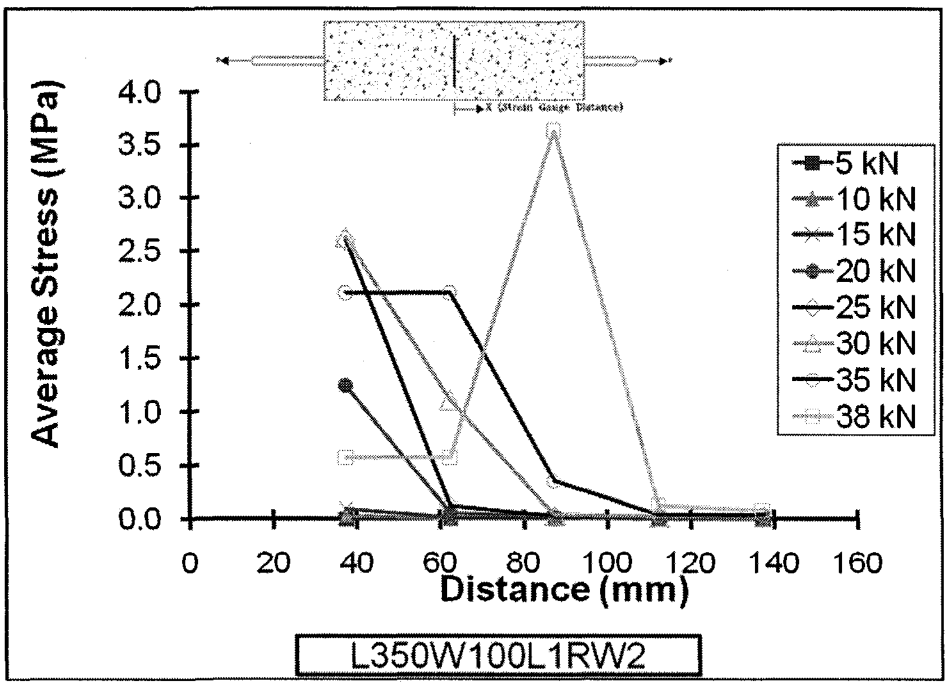
Average Stress (MPa)
4.0
3.5
3.0
2.5
2.0
1.5
1.0
0.5
0.0
0
20
40
60
80
100
120
140
160
Distance (mm)
5 kN
10 kN
15 kN
20 kN
25 kN
30 kN
35 kN
38 kN
L350W100L1RW2

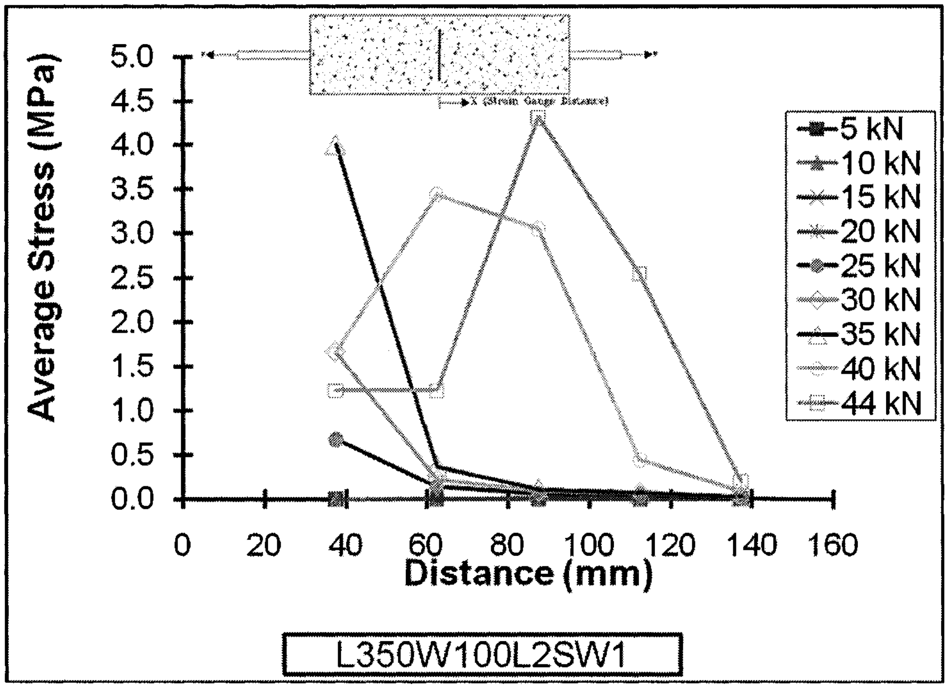

Average Stress (MPa)
5.0
4.5
4.0
3.5
3.0
2.5
2.0
1.5
1.0
0.5
0.0
0
20
40
60
80
100
120
140
160
Distance (mm)
5 kN
10 kN
15 kN
20 kN
25 kN
30 kN
35 kN
40 kN
44 kN
L350W100L2SW1

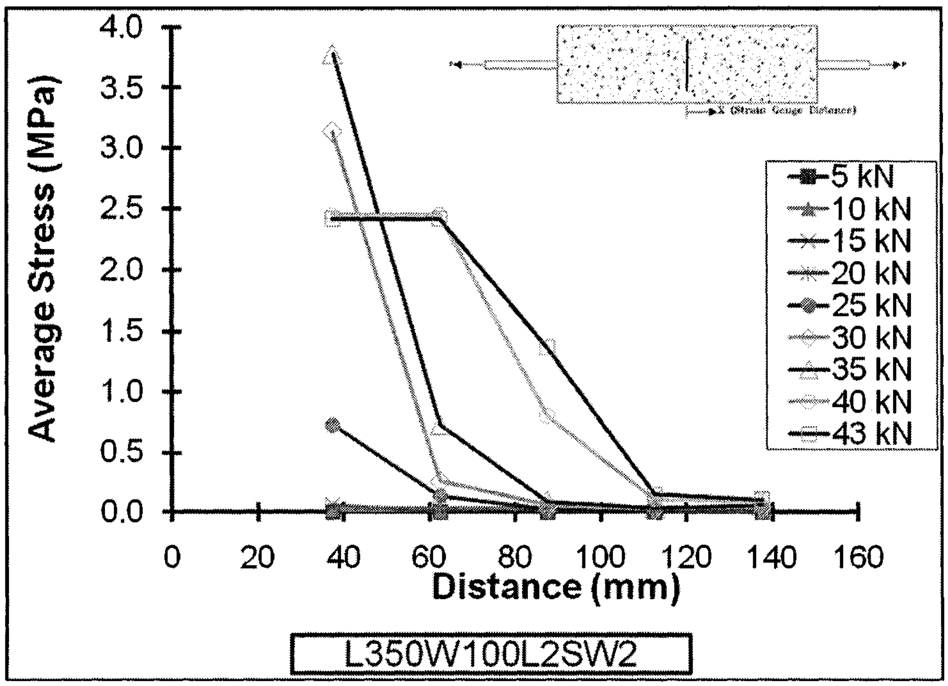

Average Stress (MPa)
4.0
3.5
3.0
2.5
2.0
1.5
1.0
0.5
0.0
0
20
40
60
80
100
120
140
160
Distance (mm)
5 kN
10 kN
15 kN
20 kN
25 kN
30 kN
35 kN
40 kN
43 kN
L350W100L2SW2

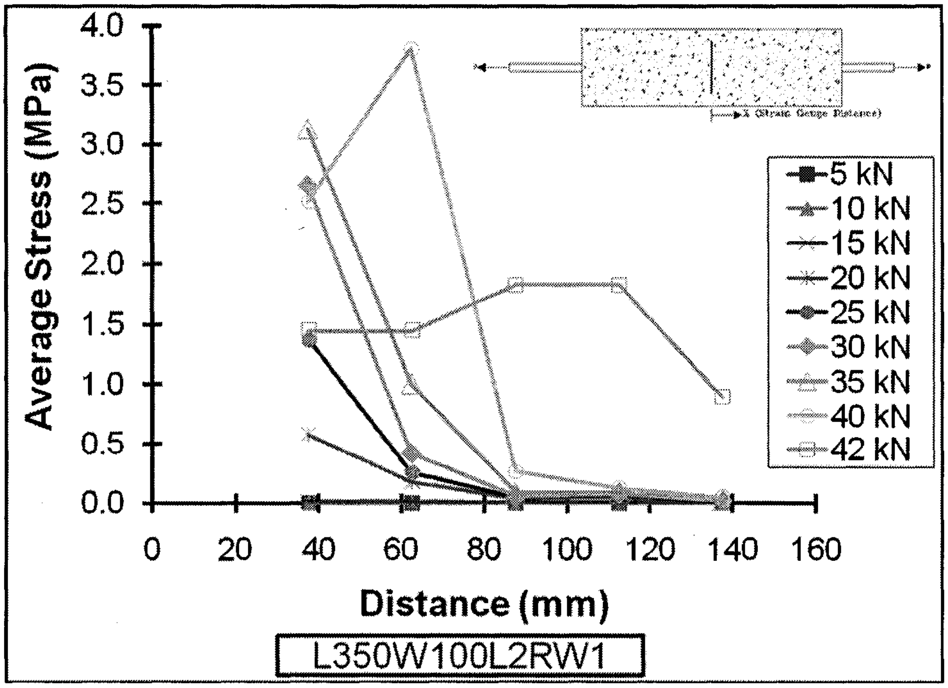

X (Strain Gauge Distance)
Average Stress (MPa)
4.0
3.5
3.0
2.5
2.0
1.5
1.0
0.5
0.0
0
20
40
60
80
100
120
140
160
Distance (mm)
5 kN
10 kN
15 kN
20 kN
25 kN
30 kN
35 kN
40 kN
42 kN
L350W100L2RW1

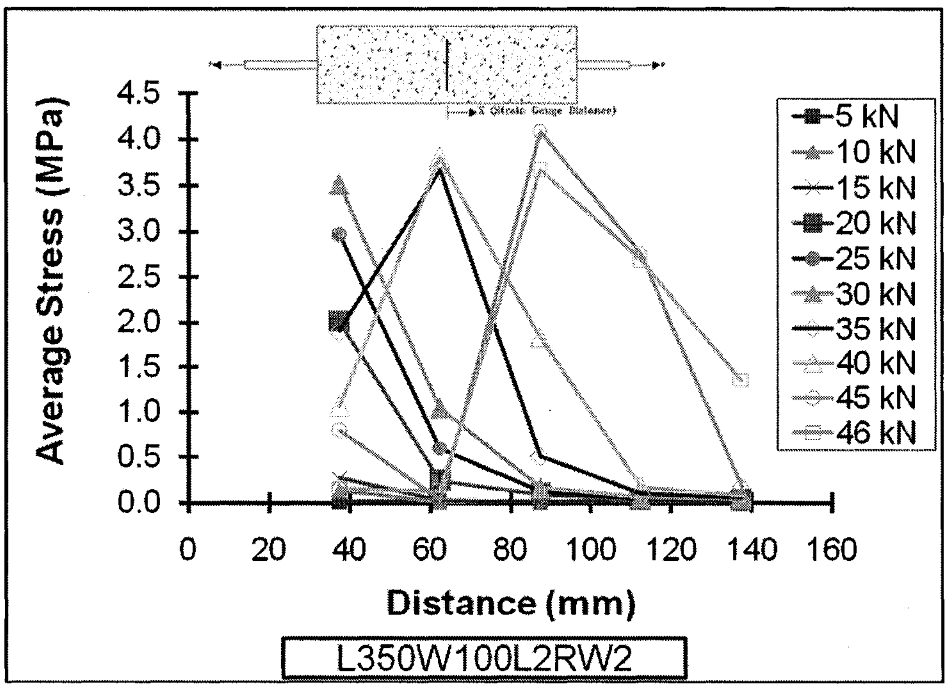

X (Strain Gauge Distance)
Average Stress (MPa)
4.5
4.0
3.5
3.0
2.5
2.0
1.5
1.0
0.5
0.0
0
20
40
60
80
100
120
140
160
Distance (mm)
5 kN
10 kN
15 kN
20 kN
25 kN
30 kN
35 kN
40 kN
45 kN
46 kN
L350W100L2RW2

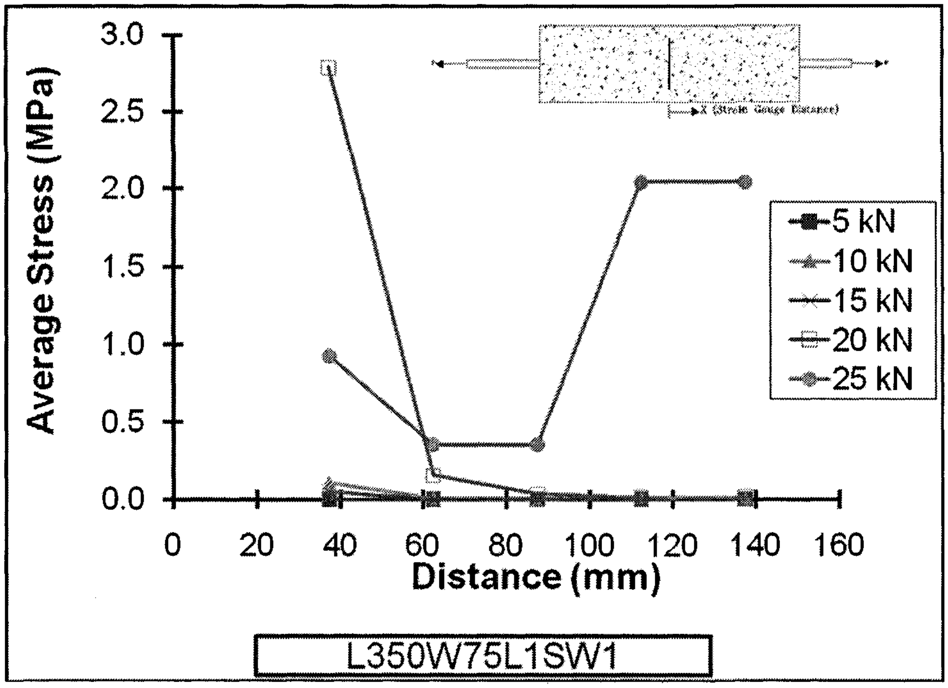
Average Stress (MPa)
Distance (mm)
X (Strain Gauge Distance)
5 kN
10 kN
15 kN
20 kN
25 kN
L350W75L1SW1

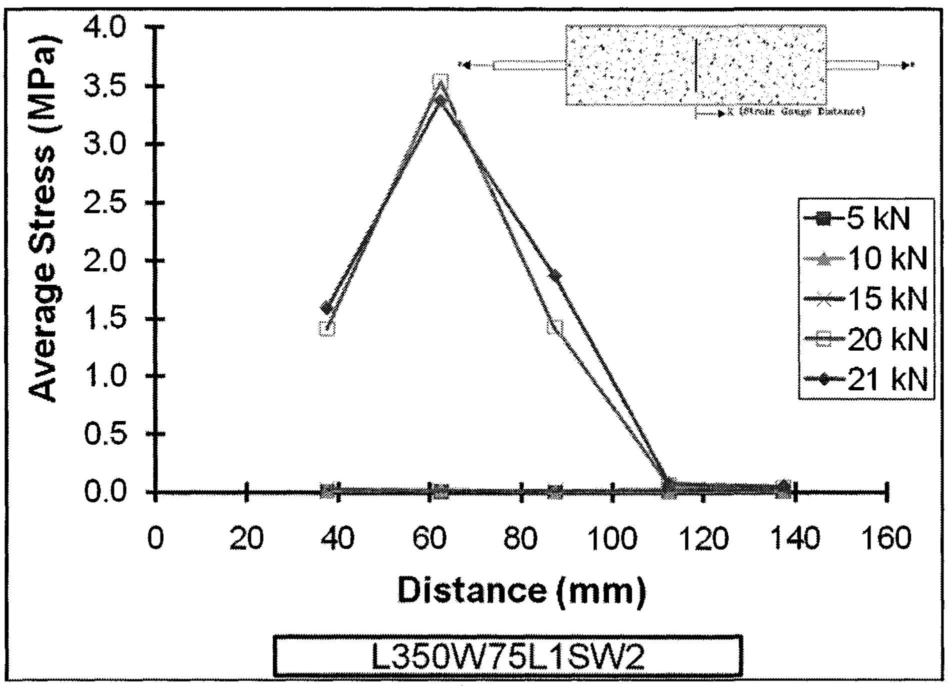
Average Stress (MPa)
Distance (mm)
X (Strain Gauge Distance)
5 kN
10 kN
15 kN
20 kN
21 kN
L350W75L1SW2

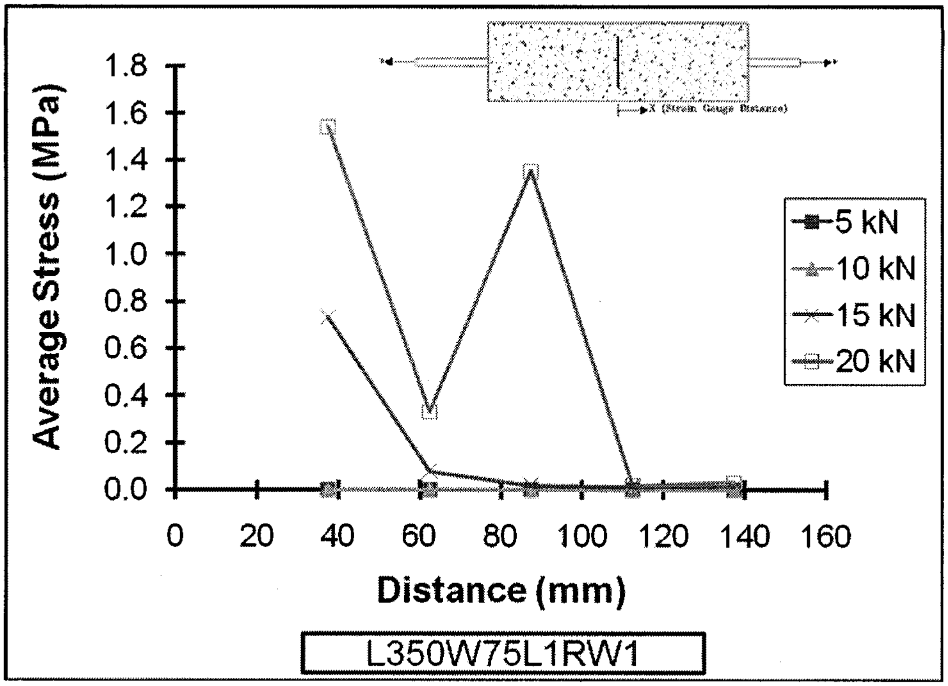
X (Strain Gauge Distance)
1.8
1.6
1.4
1.2
1.0
0.8
0.6
0.4
0.2
0.0
Average Stress (MPa)
0
20
40
60
80
100
120
140
160
Distance (mm)
5 kN
10 kN
15 kN
20 kN
L350W75L1RW1

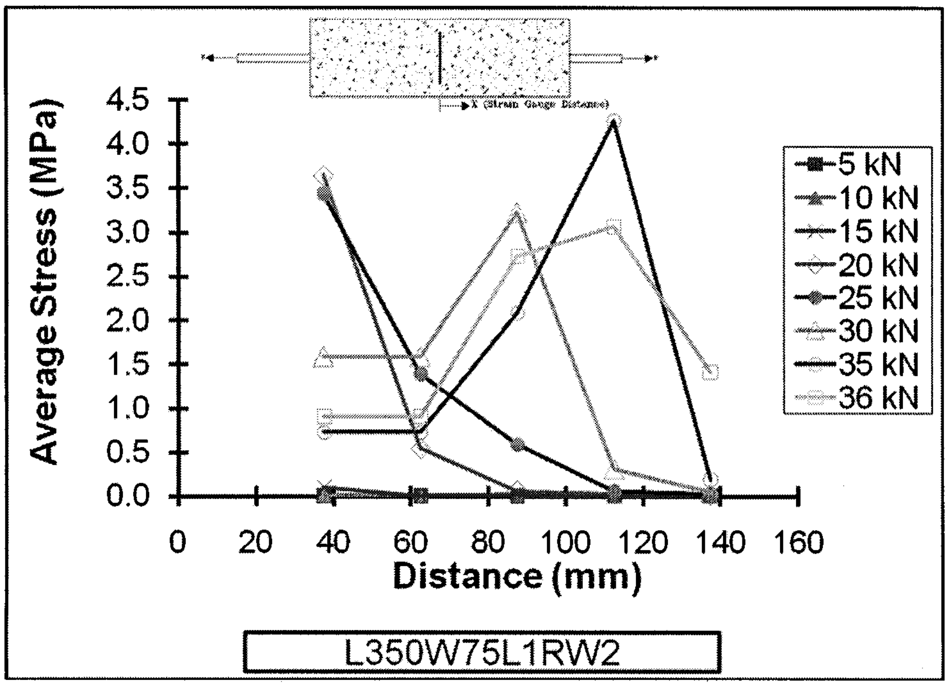
X (Strain Gauge Distance)
4.5
4.0
3.5
3.0
2.5
2.0
1.5
1.0
0.5
0.0
Average Stress (MPa)
0
20
40
60
80
100
120
140
160
Distance (mm)
5 kN
10 kN
15 kN
20 kN
25 kN
30 kN
35 kN
36 kN
L350W75L1RW2

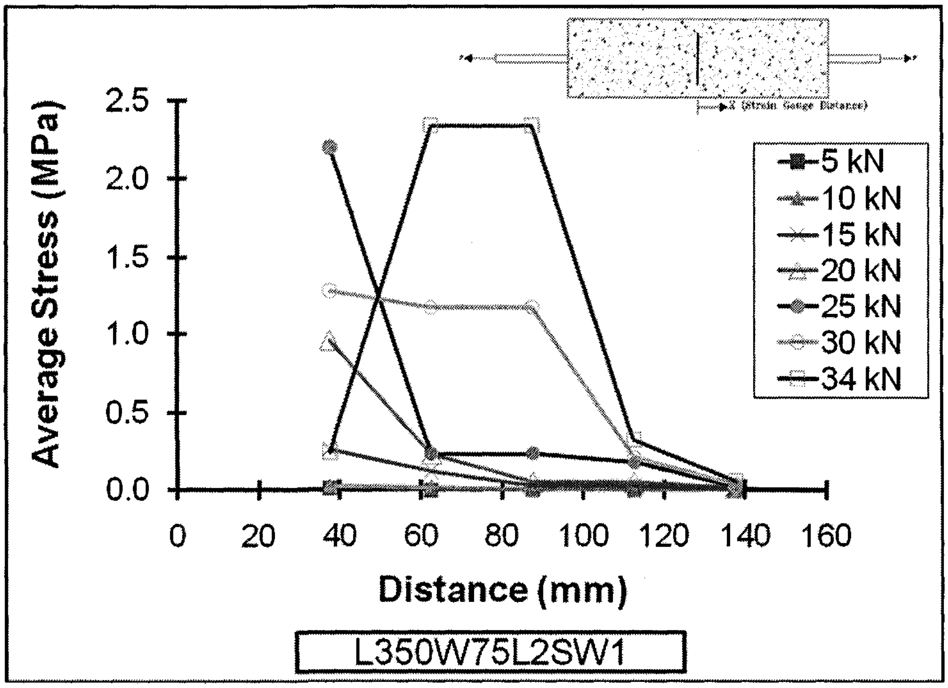
x (Strain Gauge Distance)
2.5
2.0
1.5
1.0
0.5
0.0
Average Stress (MPa)
5 kN
10 kN
15 kN
20 kN
25 kN
30 kN
34 kN
0
20
40
60
80
100
120
140
160
Distance (mm)
L350W75L2SW1

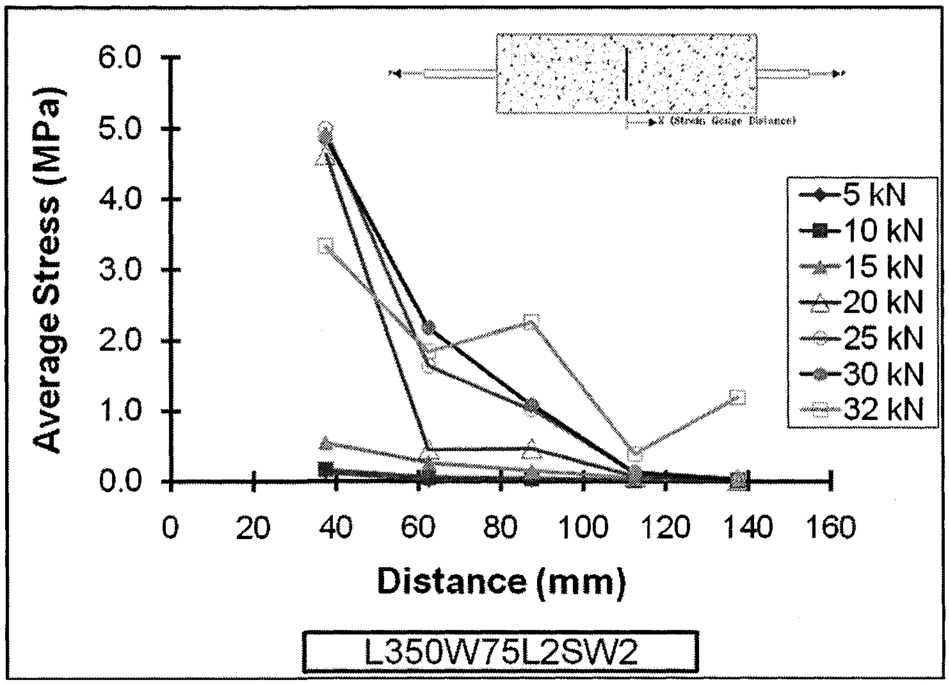
x (Strain Gauge Distance)
6.0
5.0
4.0
3.0
2.0
1.0
0.0
Average Stress (MPa)
5 kN
10 kN
15 kN
20 kN
25 kN
30 kN
32 kN
0
20
40
60
80
100
120
140
160
Distance (mm)
L350W75L2SW2

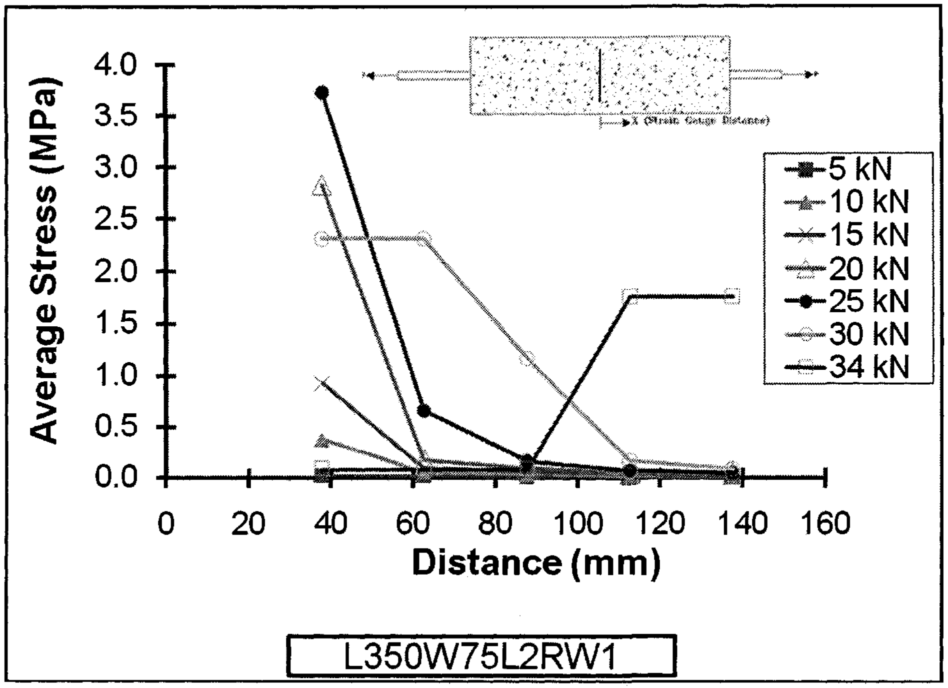

Average Stress (MPa)
4.0
3.5
3.0
2.5
2.0
1.5
1.0
0.5
0.0
0
20
40
60
80
100
120
140
160
Distance (mm)
5 kN
10 kN
15 kN
20 kN
25 kN
30 kN
34 kN
L350W75L2RW1

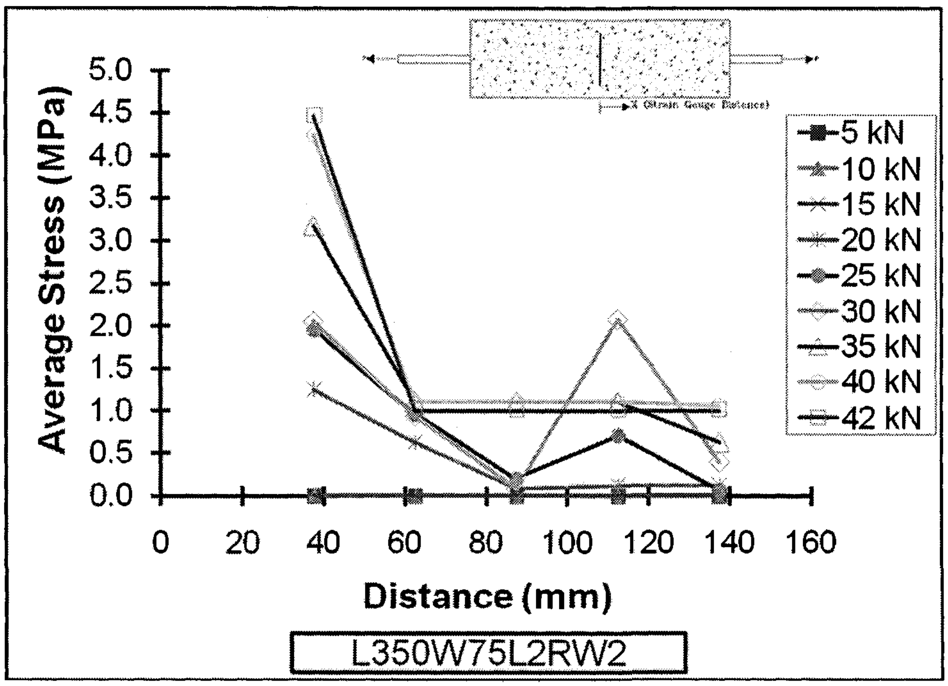

Average Stress (MPa)
5.0
4.5
4.0
3.5
3.0
2.5
2.0
1.5
1.0
0.5
0.0
0
20
40
60
80
100
120
140
160
Distance (mm)
5 kN
10 kN
15 kN
20 kN
25 kN
30 kN
35 kN
40 kN
42 kN
L350W75L2RW2